National Library of Canada

Acquisitions and Bibliographic Services Branch

395 Wellington Street
Ottawa, Ontario
K1A 0N4

Bibliothèque nationale du Canada

Direction des acquisitions et des services bibliographiques

395, rue Wellington
Ottawa (Ontario)
K1A 0N4

Your file Votre référence

Our file Notre référence

NOTICE

The quality of this microform is heavily dependent upon the quality of the original thesis submitted for microfilming. Every effort has been made to ensure the highest quality of reproduction possible.

If pages are missing, contact the university which granted the degree.

Some pages may have indistinct print especially if the original pages were typed with a poor typewriter ribbon or if the university sent us an inferior photocopy.

AVIS

La qualité de cette microforme dépend grandement de la qualité de la thèse soumise au microfilmage. Nous avons tout fait pour assurer une qualité supérieure de reproduction.

S'il manque des pages, veuillez communiquer avec l'université qui a conféré le grade.

La qualité d'impression de certaines pages peut laisser à désirer, surtout si les pages originales ont été dactylographiées à l'aide d'un ruban usé ou si l'université nous a fait parvenir une photocopie de qualité inférieure.

Canada

ISBN 0-612-04964-7

Canada

UNIVERSITÉ D'OTTAWA
UNIVERSITY OF OTTAWA

TABLE OF CONTENTS

ABSTRACT

Infrared and Solid State NMR spectroscopies have been used to study the reactions of PMe_nCl_{3-n} (n=0 to 2) with silica, the reactions of $P(OMe)_3$ and related compounds with alumina, as well as the adsorption of PMe_3 on a variety of oxides. Several reagents have been used in a study of the chlorination of silica. A short theoretical discussion of an interesting class of solid state NMR experiments is presented.

PMe_3 interacts with silica activated at moderate temperatures via hydrogen bonding or physisorption only. When the silica is activated at temperatures above 1000°C a Lewis acid-base complex can be detected. PMe_3 also adsorbs on Al_2O_3 by hydrogen bonding and Lewis acid-base interactions. In this case the observation of scalar coupling between phosphorus and aluminium in the ^{31}P MASNMR spectrum provides a very direct demonstration of the surface atom to adsorbate bond. The ^{31}P MASNMR spectra of PMe_3 adsorbed on titania and zirconia shows that several distinct types of Lewis acid site are present on the surfaces of both oxides. Under favourable conditions ^{31}P MASNMR of adsorbed PMe_3 can be used to quantify the Brønsted and Lewis acidity present on catalyst surfaces. This has been attempted for fluoride doped Al_2O_3, as well as sulfated titania and zirconia. If the ^{31}P T_1 is not too long, meaningful measurements of the quantities of strongly acidic surface sites can be made. The steric requirements of the probe molecule and the occurrence of chemical exchange hinder the quantification of weakly acidic sites. The infrared spectra of hydrogen bonded, coordinated and protonated PMe_3 are resolvable, and allow the detection of these species on surfaces.

PCl_3 interacts with silica at room temperature via a weak hydrogen bonding interaction. Previous assignments in the literature of two kinds of hydrogen bonded complex are shown to be in error. $OPCl_3$, often present as an impurity in PCl_3, is shown to be

responsible for the infrared peaks that had previously been incorrectly assigned to a second type of adsorbed PCl_3. Prolonged room temperature reaction led to the formation of small amounts of $\equiv Si\text{-}O\text{-}PCl_2$, $(\equiv SiO)_2P(H)=O$, $\equiv SiOP(H)OH$, and another unidentified product.

The formation of some of the above products requires the extraction of oxygen from the silica surface and its replacement by chlorine. This was difficult to verify in the case of PCl_3 chemisorption, where the extent of reaction is always small.

PMe_2Cl was much more reactive. It reacts to form $\equiv Si\text{-}O\text{-}P(O)Me_2$, removing most of the surface silanol groups in the process. The identity of this species could be verified by both IR and NMR. IR spectra of a thin film of ^{18}O exchanged silica showed that this compound definitely does extract oxygen from the silica surface.

$PMeCl_2$ shows intermediate reactivity towards silica. Most of the surface silanol groups are consumed after four or five hours reaction time. The dominant phosphorus containing surface species is $\equiv Si\text{-}O\text{-}P(O)(H)Me$. Commercially obtained $PMeCl_2$ always contains several mole per cent PCl_3. This reacts with the chemisorption products of $PMeCl_2$, artificially complicating the reaction system.

Silica can be totally dehydroxylated by reactions at temperatures greater than 300°C with many reagents, including $SiCl_4$, $SOCl_2$, $OPCl_3$, Cl_2, CCl_4 etc. This always gives rise to two new infrared bands, at 710 and 635 cm^{-1}. In spite of its unusually high frequency, the 710 cm^{-1} band is assigned to surface $\equiv SiCl$ species. This identification is aided by newly available infrared and Raman data for appropriate model compounds. It is shown that the 635 cm^{-1} band is probably due to $=SiCl_2$ groups.

The above mentioned bands are observed when both PMe_2Cl and $PMeCl_2$ react with silica, indicating that these compounds chlorinate silica at room temperature.

Dimethyl methylphosphonate (DMMP) reacts with Al_2O_3 by losing its methoxy groups in a sequential manner. For room temperature interaction molecular DMMP, either hydrogen bonded to the surface or coordinated to Lewis acidic aluminium atoms, is the predominant species. After reaction at 100°C most of the DMMP molecules have lost one methoxy group. After 300°C reaction all of the DMMP has lost both of its methoxy groups. The infrared spectra are quite complicated, and indicate the presence of multiple species under most of the conditions studied. Dimethyl phosphite (DMP) reacts in a similar manner to DMMP, although some P-Me groups form during the reaction, indicating that Al_2O_3 can cleave the P-H bond of dialkyl phosphites. Trimethyl phosphite reacts with Al_2O_3 to give all of the products observed in the reactions of DMMP and DMP with Al_2O_3. No chemisorbed trivalent phosphorus species are observed to form during the interaction of $P(OMe)_3$ with Al_2O_3.

Many of the magic-angle-spinning NMR spectra presented in this thesis were acquired with pulse sequences that result in the Total Suppression of Sidebands (TOSS). Exact mathematical expressions for the pulse and acquisition times for TOSS sequences are presented. It is shown that all potentially useful four-pulse TOSS sequences have already been discovered. For completeness, a similar mathematical treatment of pulse sequences that produce Phase Adjusted Spinning Sidebands (PASS) is also presented. Two interesting new pulse sequences that produce Hahn echoes in rotating samples are demonstrated.

ACKNOWLEDGEMENTS

I am indebted to my supervisor, Dr. Barry Morrow, for his inspiration, guidance and good company. I am also indebted to Dr. Ian Gay, both for extensive use of his facilities and for actually succeeding in making me understand a little about solid state NMR.

Thanks to Andy McFarlan for showing me the ropes, and to my colleages, Wang, Dave and Bruce, for being such pleasant and helpful coworkers.

Thanks to my best friends in the chemistry department, Rashmi, Bob and John, for all the good times.

Thanks especially to my parents, for everything.

To Manon and Kristina: I love you.

CHAPTER 1

Introduction

The surface chemistry of oxide-based materials is of tremendous technological and economic importance. Catalysis, in all its forms, has been estimated to be responsible for on the order of one trillion dollars in economic output in the United States in 1989.[1] Perhaps the easiest example to cite is catalysis by zeolites.[2,3] The position of zeolites as the premier cracking catalysts in the petroleum industry has led to them becoming among the most extensively studied materials in heterogeneous catalysis. Due to increasing environmental concern, hydrotreating catalysts for NO_x and SO_x abatement have undergone extensive development and study.[4] Many other examples of the benefits of oxide catalysts and supported catalysts to society could easily be given.[5]

Apart from catalytic applications, the surface chemistry of oxides is important in other diverse areas. Silane coupling agents for example, are routinely used to modify surfaces, to improve adhesion properties or corrosion resistance,[6,7] or to manufacture high performance chromatographic materials.[8] The interaction of soil with environmental pollutants, such as pesticides, fertilizers or even chemical weapons, is yet another area of study worthy of mention.

A common feature of the materials relevant to the above examples is that generally

they are not amenable to the methods of surface science. Many techniques of surface science require either fairly large crystals to be obtained, or can only be applied to electrically conducting materials. The use of techniques involving electron beams (eg. Low Energy Electron Diffraction or Electron Energy Loss Spectroscopy) requires ultra high vacuum conditions. This rules out study of the material in the presence of a reactant gas. Sometimes this limitation is quite severe.

In cases where the elegant techniques of the surface scientist are not applicable, transmission infrared spectroscopy can almost always be fruitfully applied. In the transmission infrared method, sensitivity to surface must be achieved by using microcrystalline materials. (Using high surface area materials that are made up of large particles of high porosity is sometimes impossible, since scattering losses of infrared radiation increase with particle size.) With microcrystalline samples the surface to volume ratio is relatively high, and signal from the surface is detectable in the presence of signal from the bulk phase. Thus, fortuitously, infrared spectroscopy is precisely the tool to use in an important case where more elaborate surface science techniques fail to be applicable, the study of microcrystalline materials. Several monographs, some rather old and some very recent, attest to the longevity and ongoing utility of infrared spectroscopy as a technique for the study of surfaces.[9-13]

In recent times, powerful NMR spectroscopic techniques applicable to surfaces have become much more commonly available.[14] In common with infrared spectroscopy, NMR

can be used with microcrystalline non-conducting materials, in the presence of nearly any desired atmosphere. NMR has many advantages over other spectroscopies, including quantitativity, characterization of mobility, and the use of internuclear couplings to establish molecular connectivity. In time it can be anticipated that, as in many other areas of chemistry, the contribution of NMR to problem solving in surface chemistry will far surpass those of any other technique.

The objective of this thesis was to investigate what contributions could be made to surface chemistry using the combination of infrared and NMR spectroscopic methods. All of the studies in this thesis centre on the surface chemistry of phosphorus. The practical reason for this is that the ^{31}P nucleus has such favourable properties for surface NMR studies. (100% natural abundance spin-½, with magnetogyric ratio γ large enough to provide sensitivity but not so large as to necessitate special techniques for suppression of the homonuclear dipolar interaction). What is again fortuitous is that there are many aspects of phosphorus surface chemistry that are of scientific interest. As will be seen in later chapters, sometimes the goal of an experiment will be the catalytic destruction of an objectionable gas phase molecule. Other times a volatile organophosphorus compound is in fact used as a dopant to manufacture a catalyst. In still other instances phosphorus compounds will be used as probe molecules, in an attempt to learn something about materials that are of intrinsic interest in themselves, by studying their interaction with compounds of known chemistry. Each of these endeavors will be made possible by the fact that there already exists an enormous amount of empirical knowledge of the infrared and NMR properties of phosphorus compounds.

This thesis is divided into three parts. The first deals with the surface reactions of the methylchlorophosphines (Me_nPCl_{3-n} n=0 to 3). PMe_3 is now being routinely used in at least four research labs as an NMR probe of the acidic properties of solids. In Chapter 3 this rewarding type of work is extended, and infrared spectra-structure correlations for chemisorbed PMe_3 species are examined in detail for the first time.

In Chapter 4 the reaction of PCl_3 with silica is reexamined, and some inconsistencies in the literature are corrected.

Chapter 5 involves a necessary digression. The chemistry of the interaction of methylchlorophosphines with silica cannot be satisfactorily explained unless it is assumed that these compounds extract oxygen from the silica surface and replace it with chlorine. This seemed a surprising result, in view of the fact that Si-O bonds are quite strong. In order to substantiate this result, infrared criteria for the chlorination of silica had to be developed. Silica was chlorinated with a variety of reagents, and infrared bands common to all the derivatized silicas were identified with surface Si-Cl species.

Chapter 6 is about the chemistry of silica and PMe_2Cl, and Chapter 7 is about the reactions of silica and $PMeCl_2$. These chapters are somewhat arbitrarily arranged in order of increasing complexity.

The second major part of this thesis concerns reactions of $P(OMe)_3$ and related compounds with Al_2O_3. Al_2O_3 is much more versatile in the types of reactions it can undergo or catalyze than silica, and there are still obscure aspects of the chemistry of interaction with $P(OMe)_3$. Chapter 8 is a somewhat long chapter, in which hopefully the more important aspects of the chemistry have been explained.

Chapter 9 is a small contribution to the theory of NMR experiments. The 'TOSS' (Total Suppression of Sidebands) experiment fascinated this author when he first encountered it. It seemed unsatisfactory that no exact expressions for the pulse times in this experiment had yet been presented. Such expressions were not very difficult to develop, and a by-product of their derivation was a proof that there were no potentially useful 4-pulse TOSS sequences remaining to be discovered. Hahn-echoes and PASS (Phase Adjusted Spinning Sidebands) are two less common experiments proposed by the originator of the TOSS sequence. These experiments are analyzed in a similar fashion to the TOSS sequence.

Most of the background information required by the reader is given as needed in later chapters. In order to help the reader better understand the conditions under which spectra are obtained, a few spectroscopic properties of the relevant oxides are summarized here. No attempt is made at a complete review of all spectroscopic results on these materials. These sections are only intended as an introduction to the most prominent features of the spectra, for the benefit of those not already familiar with them.

The Infrared Properties of Silica

The infrared absorbance spectra of a self-supporting disk of SiO_2 degassed at increasing temperatures are presented in Fig. 1-1. In Fig. 1-1A the sample has been degassed at 150°C. Under these conditions there are several bands in the region of the spectrum associated with surface SiOH groups.[15,16] These are differentiated from each other by the extent to which they participate in hydrogen bonding. At about 3746 cm^{-1} there is a relatively

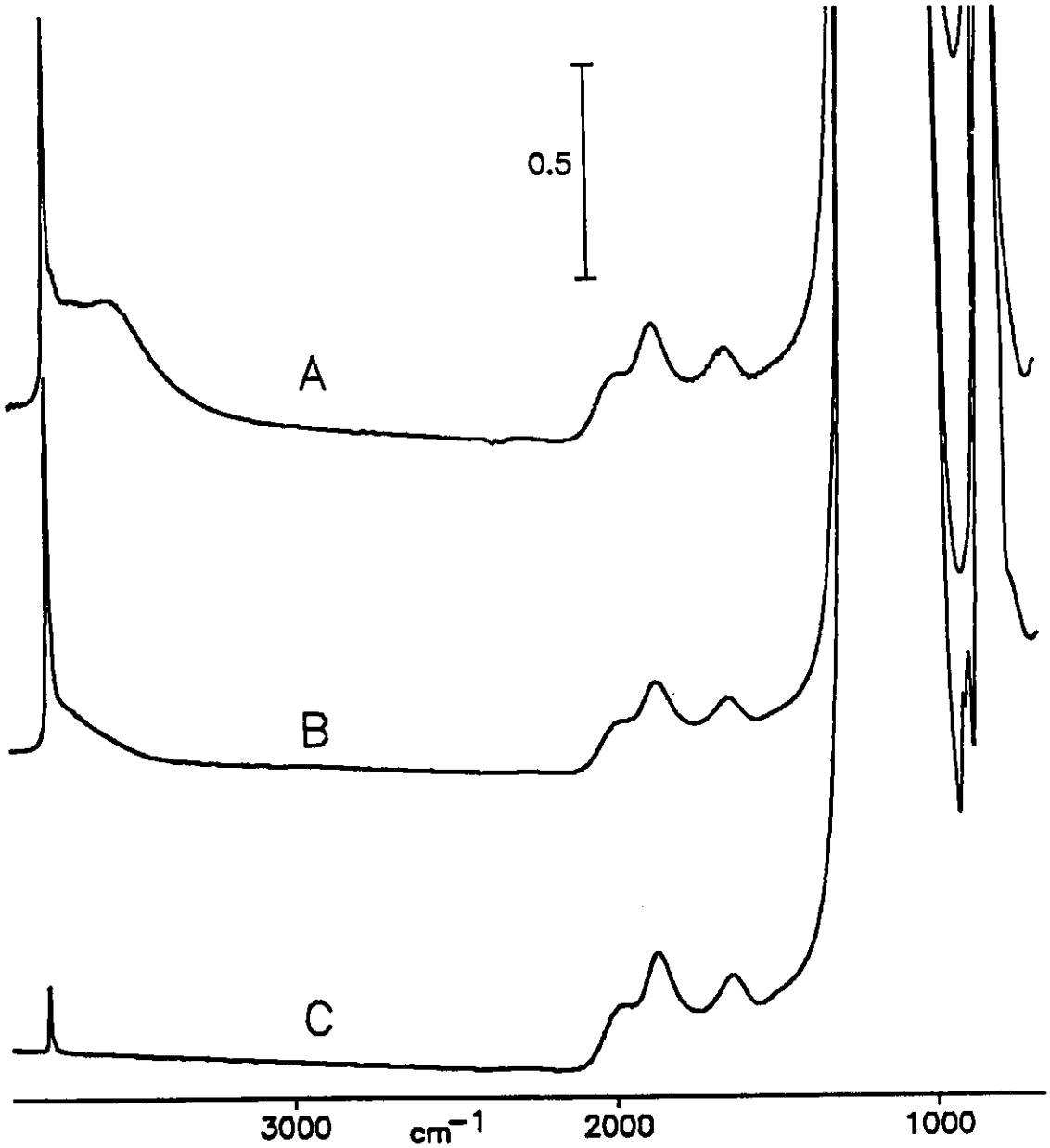

Fig. 1-1: Infrared Absorbance Spectra of a 10 mg/cm^2 SiO_2 Disk

A- Evacuated at 150°C.

B- Evacuated at 450°C.

C- Evacuated at 1150°C.

sharp band due to isolated SiOH groups. This band has a broader shoulder near 3720 cm^{-1}, which along with the even broader band near 3520 cm^{-1}, are thought to belong to H-bonded pairs. The SiOH species responsible for the 3520 cm^{-1} are thought to be due to the proton donor, while the band at 3720 cm^{-1} is thought to be due to SiOH groups that behave as proton acceptors:

$$\nu(O\text{-}H)=3520\ cm^{-1} \rightarrow \quad \begin{matrix} O\text{-}H \cdots O\text{-}H \\ | \qquad\quad | \\ Si \qquad Si \end{matrix} \quad \leftarrow \nu(O\text{-}H)= 3720\ cm^{-1}$$

In addition to the features of the hydrogen bonded pairs schematized above, there is also an inflection visible at about 3650 cm^{-1} in Fig 1.-1A. This band is said to be due to inaccessible SiOH groups, since it does not disappear even when silica is in contact with very reactive gases.(eg. $ZnMe_2$ BCl_3 etc.)[16]

The weak broad features between 2000 and 1300 cm^{-1} in Fig. 1-1A are due to overtones or combination bands of modes belonging to bulk phase SiO_2. They are not affected by adsorption of any compound, and are therefore not modes due to surface species. They can be used to quantify the disk thickness if this is desired.

Self-supporting disks of silica are always opaque to infrared radiation between about 1300 and 1000 cm^{-1}. After this there is a window region of partial transmission between about 1000 and 850 cm^{-1}. Another silica bulk mode appears at about 800 cm^{-1}. In the spectra shown, this band is also effectively totally absorbing. For silica disks of thickness below about 4 mg/cm^2 this region can be accessed, as the absorbance due to this feature is only about 1.5. (The thinnest self-supporting disks made in this laboratory have a mass per unit

area of about 2 mg/cm^2.) From about 750 to 600 cm^{-1} there is another window of partial transmission. Below this there is another very strong bulk mode centred at about 450 cm^{-1}. The combination of the presence of this band, and the fact that the spectrometer is rapidly losing sensitivity with decreasing wavenumber in this region, make obtaining data below about 600 cm^{-1} very difficult.

The spectrum in Fig. 1-1B has been taken after the silica was degassed at 450°C. As might be expected, the intensity of the features due to hydrogen bonded SiOH groups decreases substantially compared to those observed for activation at 150°C. The isolated SiOH peak at 3746 cm^{-1} has gained intensity. Other changes in the spectrum are rather more subtle, and not apparent on this absorbance scale until the sample is degassed at even higher temperature.

In Fig. 1-1C it is evident that even after activation at 1150°C there are still some residual isolated SiOH groups remaining, as there is still a very distinct narrow peak in the appropriate region. High temperature activation causes this band to shift to about 3750cm^{-1} . New bands at 908 and 888 cm^{-1}, assigned to Lewis acidic surface defects [17-19], are now observed in the 'window region' of the spectrum. These defects will be discussed further in Chapter 3.

The Infrared Properties of Al_2O_3

Fig. 1-2 shows the infrared spectra of Al_2O_3 (provided by Degussa Corp.) after activation at increasing temperatures. In fig. 1-2A there are two shoulders, due to different types isolated AlOH groups, near 3730 and 3680 cm^{-1}. When the Al_2O_3 is activated at only 150°C these bands are almost completely overwhelmed by an enormous, broad asymmetric band peaked at about 3530 cm^{-1}. This band is due to both hydrogen bonded AlOH groups and coordinated molecular water. After degassing at 450°C the water and H-bonded AlOH groups are eliminated. Several strongly overlapped peaks due to different types of isolated AlOH groups remain. Two weak sharp peaks marked at 1561 and 1481 cm^{-1} in Fig. 1-2B are assigned to a small amount of surface carbonate impurity. When it is desired these can be eliminated by heating the sample in excess (eg. 50 Torr) oxygen at 450°C. These bands were also present in Fig. 1-1A, but in this case the 1561 cm-1 carbonate band is overlapped by a broad band centred at about 1620 cm^{-1}, which is due to the bending mode of molecular water. After activation at 900°C there are virtually no AlOH groups left. Note that below 1000 cm^{-1} the absorbance of Al_2O_3 rises steeply, and by 950 cm^{-1} the Al_2O_3 is opaque.

It is customary to heat Al_2O_3 samples in air before use, in order to remove any potential organic impurities. With Degussa Al_2O_3, significant changes occur in the spectrum of the isolated AlOH groups occur when this is done, as illustrated in Fig. 1-3. The spectrum of the calcined sample reported in Fig. 1-3A shows different relative intensities compared to the uncalcined, as received sample shown in Fig. 1-3B. Even more noticeable is the greatly enhanced intensity and resolution of the two bands at 3790 and 3775 cm^{-1} in

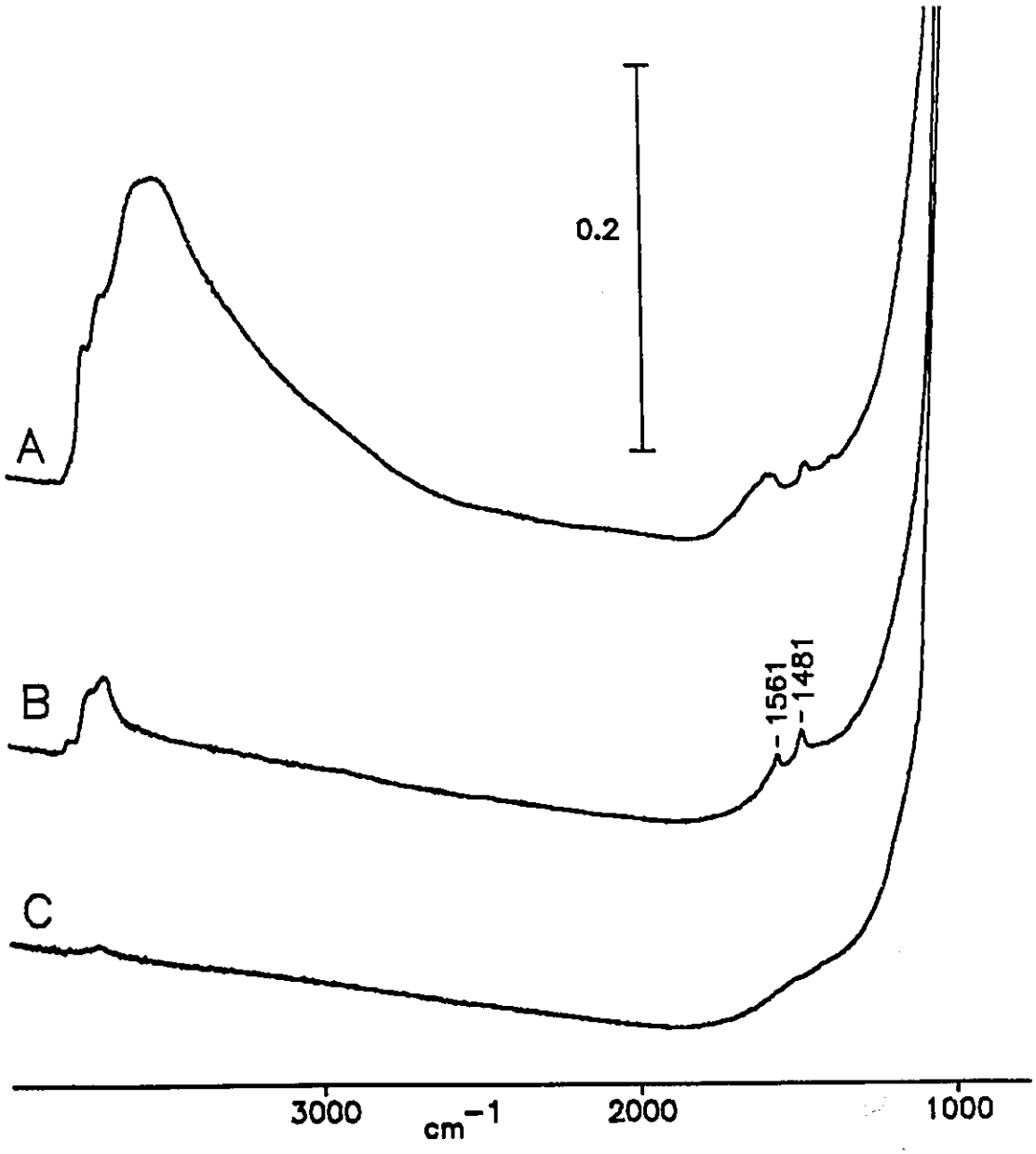

Fig. 1-2: Infrared Absorbance Spectra of a 6 mg/cm^2 Al_2O_3 Disk

A- Activated at 150°C

B- Activated at 450°C

C- Activated at 900°C

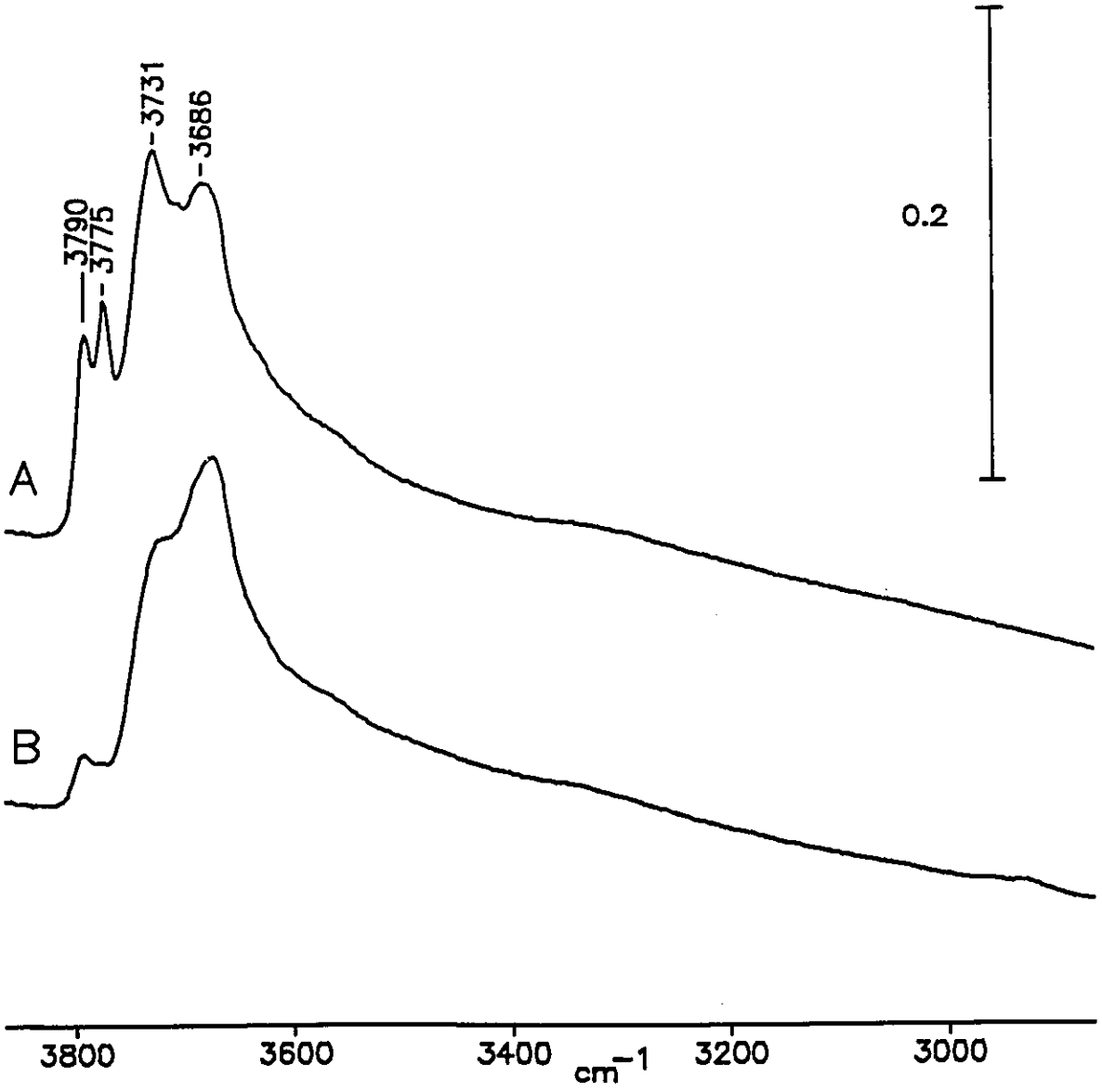

Fig. 1-3: Infrared Absorbance Spectra of Al_2O_3

A- A sample heated for 24 hours in air at 500°C, allowed to rehydrate in air, then mounted in the infrared cell at degassed at 450°C

B- A sample of as received Al_2O_3 activated at 450°C

Fig.1-3A. The spectrum after calcination shown in Fig. 1-3A resembles literature spectra of the aluminas actually used in catalytic applications[23] more closely than that of the as received material shown in Fig. 1-3B. The differences are related to the preparation method used for Degussa Al_2O_3. This material is produced by flame hydrolysis of $AlCl_3$, which involves very high temperatures. This leads to Degussa Al_2O_3 being mainly δ phase Al_2O_3[20]. The δ phase usually the predominates only after treatment of the Al_2O_3 at temperatures above 850°C.[21] As just discussed, Al_2O_3 is largely dehydroxylated under such conditions. 'Real' Al_2O_3 samples, usually prepared using precipitation methods, always show a distinct band near 3775 cm^{-1}. The appearance of this band is not thermally reversible.[22] By this it is meant that this band appears on 'virgin' samples, but once it has been removed by high temperature evacuation, it can't be restored by room temperature rehydration. It can be restored by heating in water vapour at T > 400°C.[22] Thus Degussa Al_2O_3 should probably be calcined before use in order to maintain as much relevance as possible to practical catalysts.

A simple scheme has been proposed by Knözinger [23] for the interpretation of the infrared peaks shown in Fig. 1-3A. In this spectrum four peaks are readily distinguished, at 3790, 3775, 3731 and 3686 cm^{-1}. Sometimes a shoulder on the 3731 cm^{-1} band at about 3740 cm^{-1} can also be distinguished, giving a total of five bands to be accounted for. By considering the likely terminations of the crystal planes of catalytically active Al_2O_3 phases, it could be demonstrated that there are five most likely configurations for surface AlOH groups. These are enumerated in Table 1-1. In this table the Roman numeral gives the coordination number of the OH group. The subscript 'a' or 'b' is an arbitrary label that tells whether the

coordinating Al atoms originate from octahedral or tetrahedral sites of the Al_2O_3 lattice. This information is given in separate columns of Table 1-1 for clarity. The assignments are then made on the basis of rather simple assumptions. An acidic OH group is assumed to have a weak O-H bond and hence a low ν(O-H). Conversely, this frequency is assumed to increase with increasing basicity of the OH group. The basicity is then assumed to increase with increasing formal negative charge of the hydroxyl group. If it is assumed that the Al atoms distribute their three units of positive charge evenly among all of its bonds to oxygen, a formal charge on a hydroxyl group may be calculated as:

$$Q = \tfrac{1}{2}N_o + \tfrac{3}{4}N_t - 1 \qquad [1.1]$$

where N_o is the number of octahedral Al atoms that the OH group is coordinated by, and N_t the number of tetrahedral Al atoms to which the OH group is coordinated. The frequency is assumed to decrease steadily as the hydroxyl group charge increases, as shown in Table 1-1.

Table 1-1: Assignments of AlOH Frequencies

Type of OH	N_o	N_t	Q	ν(O-H)cm^{-1}
I_b	1	0	-½	3790
I_a	0	1	-¼	3773
II_b	2	0	0	3740
II_a	1	1	-¼	3731
III	3	0	½	3686

N_o=number of octahedral neighbours, N_t= number of tetrahedral neighbours
Q=formal charge given by Eq.[1.1]

This scheme has been criticized for a number of reasons. It has often been observed that the acidity of an OH group and its stretching frequency are unrelated.[24] Furthermore, the experimental fact is that in materials such as $AlPO_4$ and some inverse spinels, where there is only tetrahedrally coordinated aluminum, the OH frequencies are always greater than 3750 cm^{-1}. In α-Al_2O_3 and normal spinels, where there is only octahedrally coordinated aluminum, the OH frequencies are less than 3750 cm^{-1}.[25,26] These observations are inconsistent with some of the attributions given in Table 1-1. The question of the attribution of the AlOH bands in the infrared spectrum of Al_2O_3 is not yet definitively answered.

The view held in [23], and in most of the infrared literature, is that the coordination number of the OH group should have a very strong influence on ν(O-H), with higher coordination numbers giving lower frequencies. Consider for example the SiOH frequency of 3746 cm^{-1} on silica, where the OH group is certainly bonded to a single silicon atom. When such an OH group is then coordinated by an aluminium atom, forming the type of bridging OH group present in all zeolites, ν(O-H) is invariably lowered. There is a band at about 3650 cm^{-1} due to bridging OH groups in the infrared spectrum of zeolite HY.[9]

The author of [28] and [29] has recently challenged the idea that increasing coordination number of the OH group always leads to such large shifts to low wavenumber. The attribution of the ν(O-H) bands present in the infrared spectra of oxides remains a rather speculative and controversial matter.

Infrared Spectra of Some Other Oxides

Infrared spectra of the other oxides studied in this thesis are presented in Fig. 1-4. Spectra are shown for typical pretreatment conditions before any adsorption experiments. Recent references to the spectra of these samples may be found in [27] for TiO_2, [28] for ZrO_2, and [29] for MgO. It is simply noted here that under appropriate conditions each oxide has multiple OH species. TiO_2 is somewhat unique in that it retains molecular water up to quite high temperatures. At activation temperatures lower than 400°C spectra always show a fairly intense band at 1620 cm^{-1} due to the bending mode of molecular water.

Note also that for self-supporting disks, spectral data can be acquired above 1000 cm^{-1} for TiO_2, 850 cm^{-1} for ZrO_2, and above about 750 cm^{-1} for MgO.

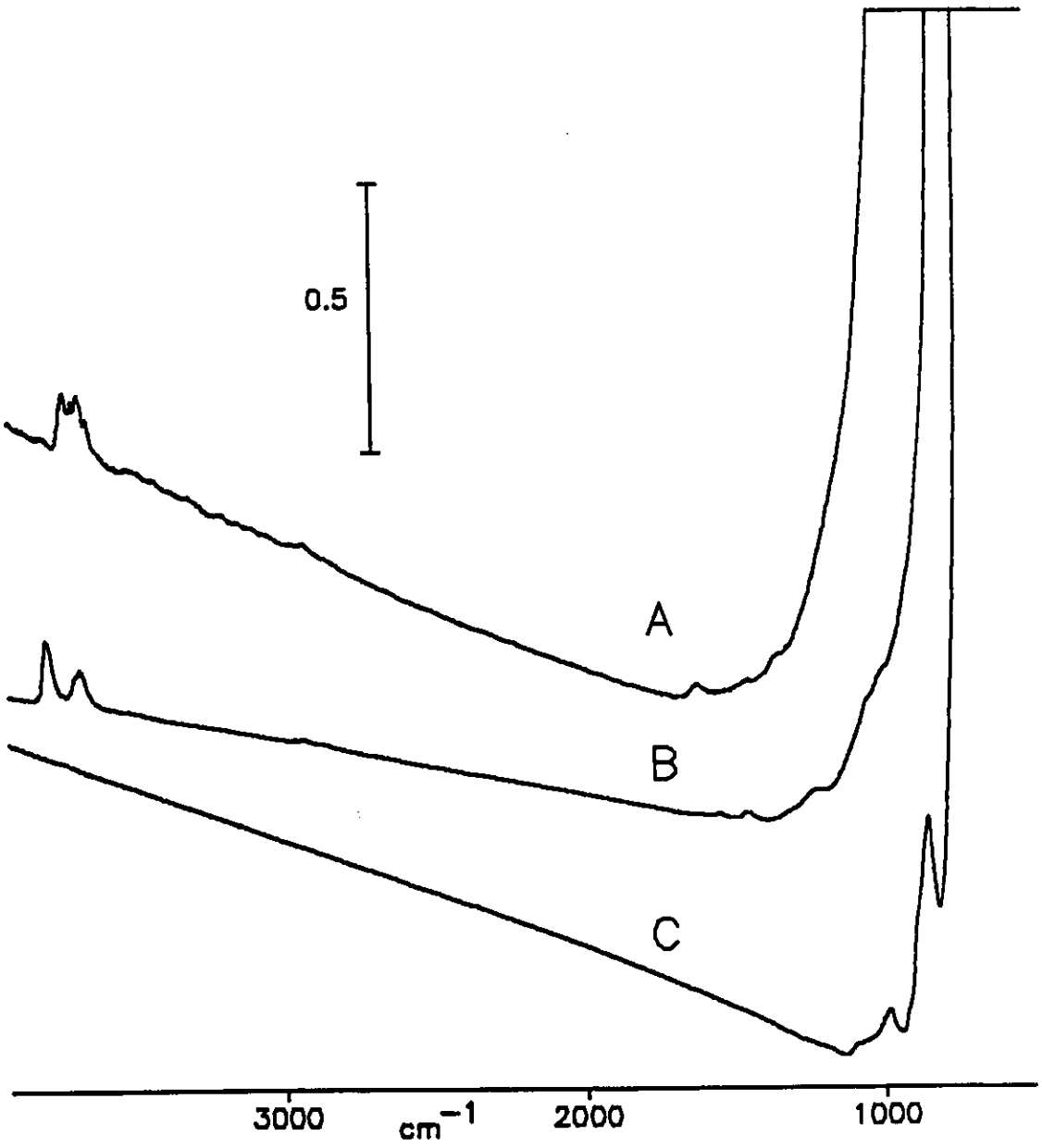

Fig. 1-4: Infrared Absorbance Spectra of Three Oxides

A- A 20 mg/cm^2 TiO_2 sample degassed at 400°C

B- A 20 mg/cm^2 ZrO_2 sample degassed at 450°C

C- A 15 mg/cm^2 MgO sample degassed at 1000°C

CHAPTER 2

General Experimental

The Infrared Spectrometers

The Fourier transform infrared (FTIR) spectra recorded during these studies were obtained with either a Bomem DA3.02 or a Bomem MB100 spectrometer. Both instruments were equipped with KBr beam-splitters, limiting their useful range to the mid infrared region, about 5000 to 450 cm^{-1}. Most of the spectra presented in this thesis were acquired with the MB100, which was equipped with a deuterium triglycine sulfate (DTGS) detector. Obtaining a routine spectrum involved signal averaging 25 scans at 4 cm^{-1} resolution, leading to an acquisition time of about 70 seconds. Spectra recorded on the DA3.02 were obtained using a faster scanning mercury cadmium telluride (MCT) detector. Acquiring 100 scans for signal averaging at 4 cm^{-1} resolution required about 34 seconds. Higher resolutions were used only occasionally when narrow peaks were encountered. The maximum resolutions available were 0.02 cm^{-1} for the DA3.02 and 1 cm^{-1} for the MB100. All spectra were processed using Spectra Calc software on an IBM compatible personal computer. All infrared spectra are presented as absorbance against wavenumber. ($\log_{10}(I_0/I)$ vs cm^{-1})

Solid State NMR Measurements

NMR spectra were recorded at Simon Fraser University using a home-built probe[73]

and a field strength of either 1.4 T or 3.5 T. This gave ^{31}P resonance frequencies of 24.3 MHz and 60.5 MHz respectively. All spectra were recorded at room temperature. The 90° degree pulse length varied from 4 to 6 μs. Decoupling fields were between 45 and 60 kHz. Sealed samples were spun at the magic angle at speeds between 2 and 3 kHz. ^{31}P chemical shifts are reported relative to 85% H_3PO_4, and positive chemical shifts are to low field. For quantitative measurements a relaxation delay of at least $5T_1$ was placed between successive scans during signal averaging. (T_1 is a time constant which characterizes the rate at which M_z, the component of magnetization parallel to the constant magnetic field B_0, attains its thermal equilibrium value (M_0).

$$\frac{dM_z}{dt} = \frac{(M_0-M_z)}{T_1}$$

For samples containing species with different T_1's it is necessary to wait at least 5 times the slowest T_1 value between scans in order to ensure that observed peak areas are proportional to the species' populations.) Delayed decoupling was used to detect species that contained a direct P-H bond. If decoupling the protons was delayed by 70 μs prior to the start of data acquisition, signals due to species containing at least one direct P-H bond would disappear from the spectrum, while other signals would be only partially attenuated. This technique requires that the P-H containing species in question be immobile enough that a large direct dipolar coupling between phosphorus and hydrogen exists.

Infrared Cells

A standard cell of the type described by Morrow and Ramamurthy [30] has been used for most experiments. It is shown in Fig. 2-1. The cell bottom and sample holder are made

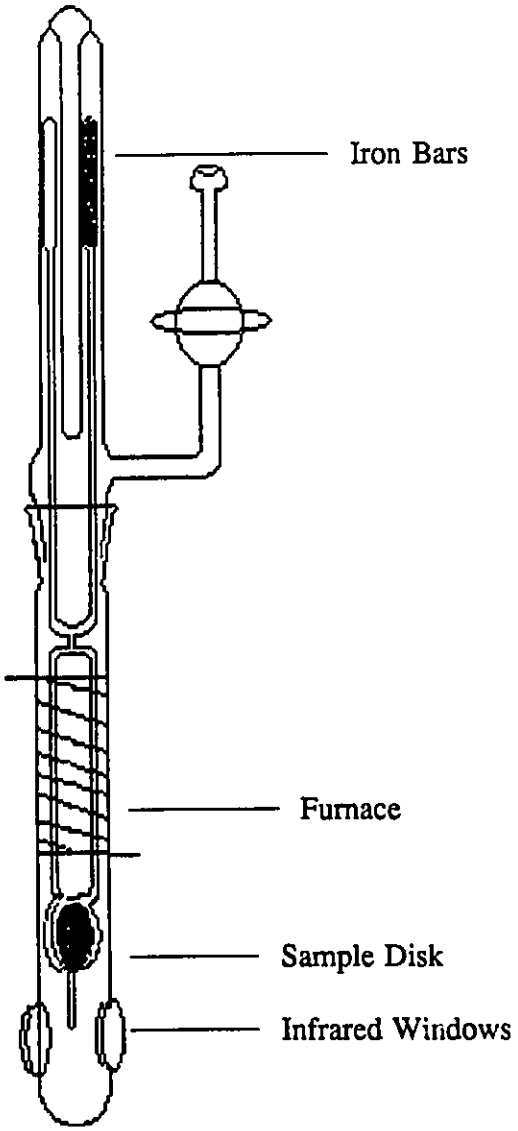

Fig. 2-1: The Standard Infrared Cell

of quartz, so that activation temperatures can be as high as 1200°C. Quoted activation temperatures were determined by means of a chromium-alumel thermocouple placed inside the insulation in the middle of the furnace. Magnets allowed the sample to be moved from the furnace to the window region without breaking vacuum. The top of the cell was made of pyrex. It was attached to the cell bottom by means of a taper joint and Apiezon H grease. The cell was connected to vacuum lines by a ball and socket ground glass joint and Apiezon N grease. The total cell volume was about 300 cm^3.

Some spectra were recorded with the sample close to liquid nitrogen temperature (-196°C) by means of the simple cell shown in Fig. 2-2. The quartz tube that constitutes the body of the cell can be either heated or cooled *in situ*. The cell is closed by placing a 50 mm window directly onto a glass flange that is lubricated with Apiezon H grease. The stopcock must extend far enough from the cell that it can be operated while the body of the cell is fixed in a purged sample compartment. This cell had about 100 cm^3 internal volume.

KBr windows were used for almost all of the experiments. Sometimes these were chemically incompatible with a reagent, and the more expensive ZnSe windows would have to be used.

The Vacuum Manifold

The vacuum apparatus used for sample treatment was a portable pyrex manifold equipped with 6 inlet taper joints. Each inlet is opened or closed by an 8 mm teflon stopcock. A 15 mm stopcock is used to isolate the main manifold from the pumps and trap. An oil diffusion pump backed by a two-stage rotary pump and protected from reactive gases

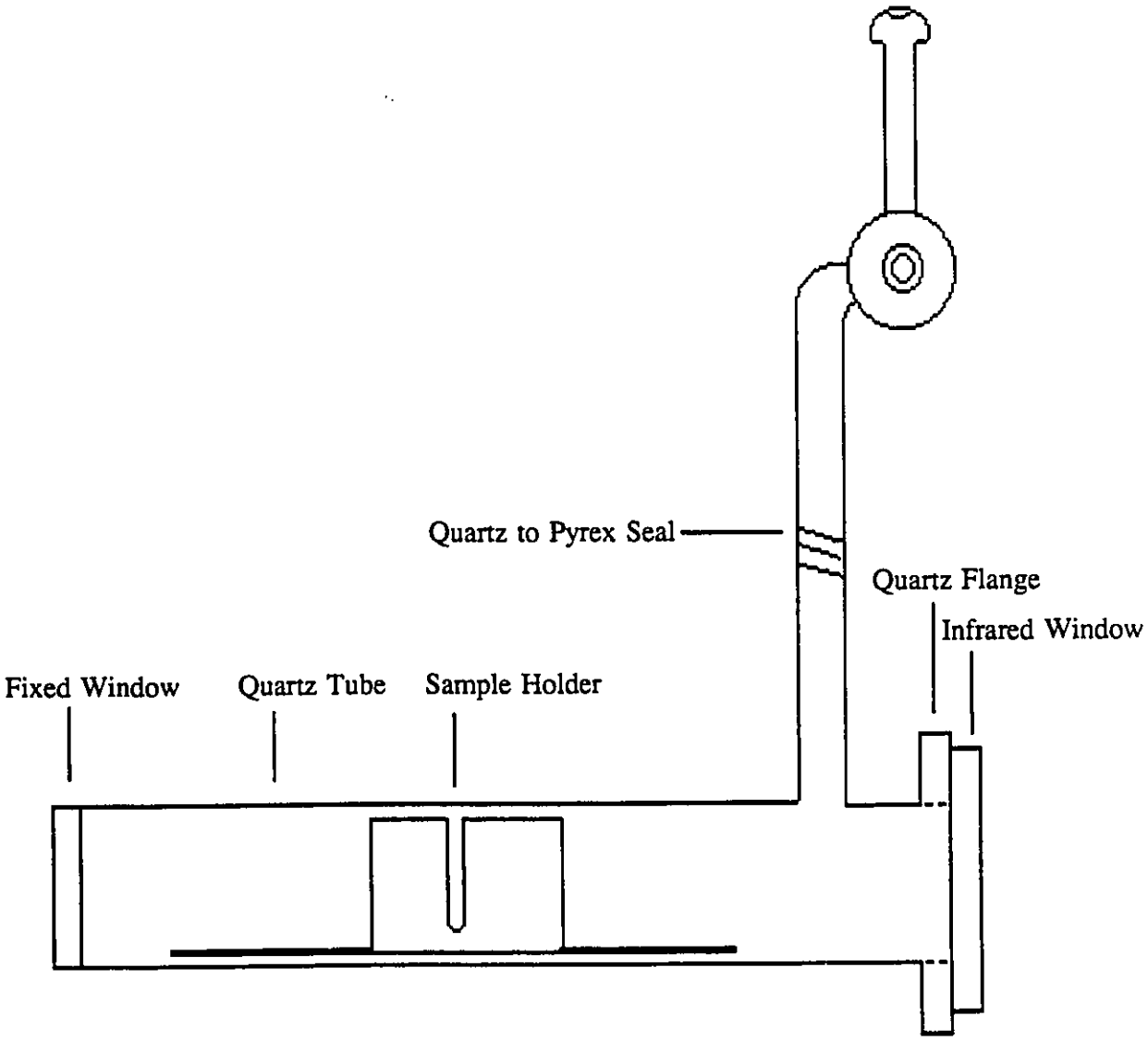

Fig. 2-2: Variable Temperature Infrared Cell

When the cell is mounted *in situ* the quartz tube that makes the up the cell body can be enclosed in either a furnace or a snugly fitting polystyrene liquid nitrogen reservoir.

by a liquid nitrogen trap provides a base pressure of about 10^{-6} Torr. Evacuating an infrared cell from atmospheric pressure for 1 hour generally gave residual pressures of about 10^{-5} Torr under standard working conditions.

Materials

Alumina, titania and zirconia were provided by Degussa A.G. Frankfurt. The Al_2O_3 (Aluminium Oxid C) was mainly in the δ form, and had a BET surface area of 105 m^2/g. The titania (P25) is said to be mainly anatase with about 15% rutile present [31]. Its surface area was 55 m^2/g. The zirconia was an experimental product. It was a nearly equal mixture of the monoclinic and tetragonal phases, and its area was 45 m^2/g.

The silica used was Cab-O-Sil HS5, supplied by Cabot Inc. Its surface area was 325 m^2/g.

Reagent grade MgO purchased from J. T. Baker Inc. was found to be quite suitable for infrared studies, provided the inevitable surface carbonates were removed by gradually heating self-supporting disks to 1000°C under vacuum.

Doped materials were prepared by slurrying an oxide to incipient wetness with an aqueous solution of appropriate concentration. For sulfated Al_2O_3, ZrO_2 and TiO_2 about 4 ml of solution was used per gram of oxide. This gave slurries that were quite homogeneous in appearance, and led to small, tolerable losses in surface area after the sample was dried at 110°C. TiO_2 sulfated with 200 μmols of H_2SO_4 per gram of oxide had a BET surface area of 45 m^2/g. This loss of about 10 m^2/g seems to be fairly typical for the technique, although the surface areas were not always measured. When Al_2O_3 was doped with NH_4F solutions about

10 ml of solution per gram of oxide was required to make a homogeneous appearing slurry. This material was calcined for 2 hours at 400 °C to remove NH_4^+ ions after drying. Al_2O_3 doped to a 2% F content by mass had a BET surface area of 91 m^2/g.

As a matter of convenience, a notation specifying the treatment of infrared samples in abbreviated form will often be used. The formula of the oxide will be given, followed in parentheses by an indication of any dopant that may be present, and the activation temperature. $ZrO_2(450)$ means zirconia heated under vacuum at 450°C. $Al_2O_3(2\%F,100)$ means alumina doped to 2 per cent fluoride by mass, then heated under vacuum at 100°C. $Al_2O_3(RT)$ will be used to indicate Al_2O_3 evacuated at room temperature. (22±1°C)

Chemical reagents were all obtained from standard chemical sources. Any special materials or procedures will be described where appropriate as they arise in later chapters.

It should be noted that $PMeCl_2$ has a lingering odour that is more offensive than can be appreciated without direct experience. A vacuum line with a trap that could be completely removed and placed in a fumehood was constructed especially for handling this substance. Once $PMeCl_2$ vapour is in contact with Apiezon grease it cannot be removed acceptably by evacuation. The large greased ground glass joints on vacuum infrared cells should only be opened in a fumehood after contact with $PMeCl_2$ vapour. The same warning applies to a lesser degree to PMe_3 and PMe_2Cl.

Sample Handling

For infrared studies weighed amounts of oxide were placed in a 1 inch diameter stainless steel die and pressed into self supporting disks. Al_2O_3, MgO, TiO_2 and ZrO_2 would

adhere to the die if pressed without camera lens papers between the oxide and the die face. These lens papers were easy to peel off of the oxide disk once they had been impregnated with the powder by pressing several disks. Pressures in the range 10^7 to 10^8 Pa were used to form the disks. Pressed disks were then mounted in the infrared cell where all further treatments would occur.

Observation of infrared spectra in regions of strong absorption by the bulk of the oxide is impossible if a self supporting disk is used. If such data seemed potentially useful, a thin film of the oxide was applied directly to a ZnSe infrared window using a smooth firm stroke with a spatula. The window was then mounted in the infrared cell and treated as if it was a self supporting disk.

For NMR studies weighed amounts of solid material were placed into a NMR tube that had been joined to a pyrex tube with a glass-blowing torch. This was usually attached to the vacuum manifold by means of an O-ring seal. A roughly 50 cm^3 portion of the vacuum line that included a gas buret was used to add known quantities of gas to the sample. When the sample treatment was complete a torch was used to detach the sealed NMR tube from the vacuum line. This could be done with the bottom of the tube cooled by liquid nitrogen if it was necessary to have a gas present in the sealed tube.

Sometimes the NMR tube was sealed to an approximately 100 cm^3 tube containing the catalyst powder. This somewhat larger 'reactor' volume was necessary during studies of $PMeCl_2$ adsorption, as it allowed the sample to be in contact with larger amounts of gas under conditions of reasonably good circulation. (If an amount of $PMeCl_2$ comparable to the number of hydroxyl groups present on the oxide was condensed into an approximately 0.75

cm^3 volume NMR tube, there would necessarily be liquid phase $PMeCl_2$ present during the reaction. This seemed to lead to more complicated chemistry, as reproducible spectra could not be obtained using samples prepared this way.)

CHAPTER 3

Adsorption of PMe_3 on Oxide Surfaces

Trimethylphosphine (PMe_3) is becoming an important probe molecule for the study of acidic surfaces. It has been used to obtain both qualitative and quantitative information on the acidity of zeolites.[47,53,66] Tailored catalysts prepared by chemical vapour deposition of silica layers on Al_2O_3 have been characterized.[35,67] Under certain circumstances information on the dynamics of the adsorbed PMe_3 may be obtained, or if immobile Me_3PH^+ ions are formed, the P-H bond length may be determined.[68,69] All of these applications are interesting and important, but for general conclusions relevant to catalysis to be drawn, studies will have to be extended to many other systems.

The studies mentioned above are all mainly NMR studies of the interaction of PMe_3 with surfaces. Only a few reports of infrared spectra have appeared in the literature.[52,53] These are restricted to zeolite Y, and really go no farther than stating that a P-H stretching band at 2490 cm^{-1} is observed when PMe_3 is adsorbed on zeolite HY.

In this chapter infrared spectra-structure correlations for PMe_3 interacting with a number of interesting surfaces will be developed. This study will always be supplemented by ^{31}P NMR experiments, in order to complement the infrared work and extend the data that already exists in the literature.

Several surfaces were chosen for study. Silica, because of its relative simplicity, will be examined first. Al_2O_3 and fluoride doped Al_2O_3 were studied next. These allow the

observation of different types of interaction than with silica, but still give simple spectra that allow correlations for later use to be developed.

A tremendous amount of literature is accumulating on the properties of 'super-acidic' materials prepared by treating oxides with sulfuric acid.[see 58, 62 and references therein] The last sections of this chapter will deal with the characterization of titania and zirconia, both as pure materials, and after modification with sulfuric acid.

Adsorption of PMe_3 on SiO_2

Since SiO_2 normally has no significant acidity or basicity [16], PMe_3 may be expected to interact with SiO_2 mainly via hydrogen-bonding. The infrared spectra shown in Fig. 3-1 confirm this expectation. In this experiment 32 Torr of PMe_3 has been allowed to equilibrate with $SiO_2(450)$ and spectra of the sample and gas were taken. The pressure was then reduced in steps for the recording of subsequent spectra. The most striking feature in this spectrum is the very sharply defined isosbestic point. This shows clearly that there is no chemical reaction between SiOH groups and PMe_3. When a silanol group (ν=3746 cm^{-1}) hydrogen-bonds with a PMe_3 molecule, its spectrum broadens and its frequency shifts to about 3250 cm^{-1}. No SiOH groups are lost through any other process.

In Fig. 3-2 attention is focused on the C-H stretching region of the spectrum of adsorbed PMe_3. This region will be found to be the most interesting part of the spectrum of adsorbed PMe_3 in this and in other systems. The dashed curve shows the spectrum of gas phase PMe_3. The C-H stretching region of the infrared spectrum of PMe_3 has been studied

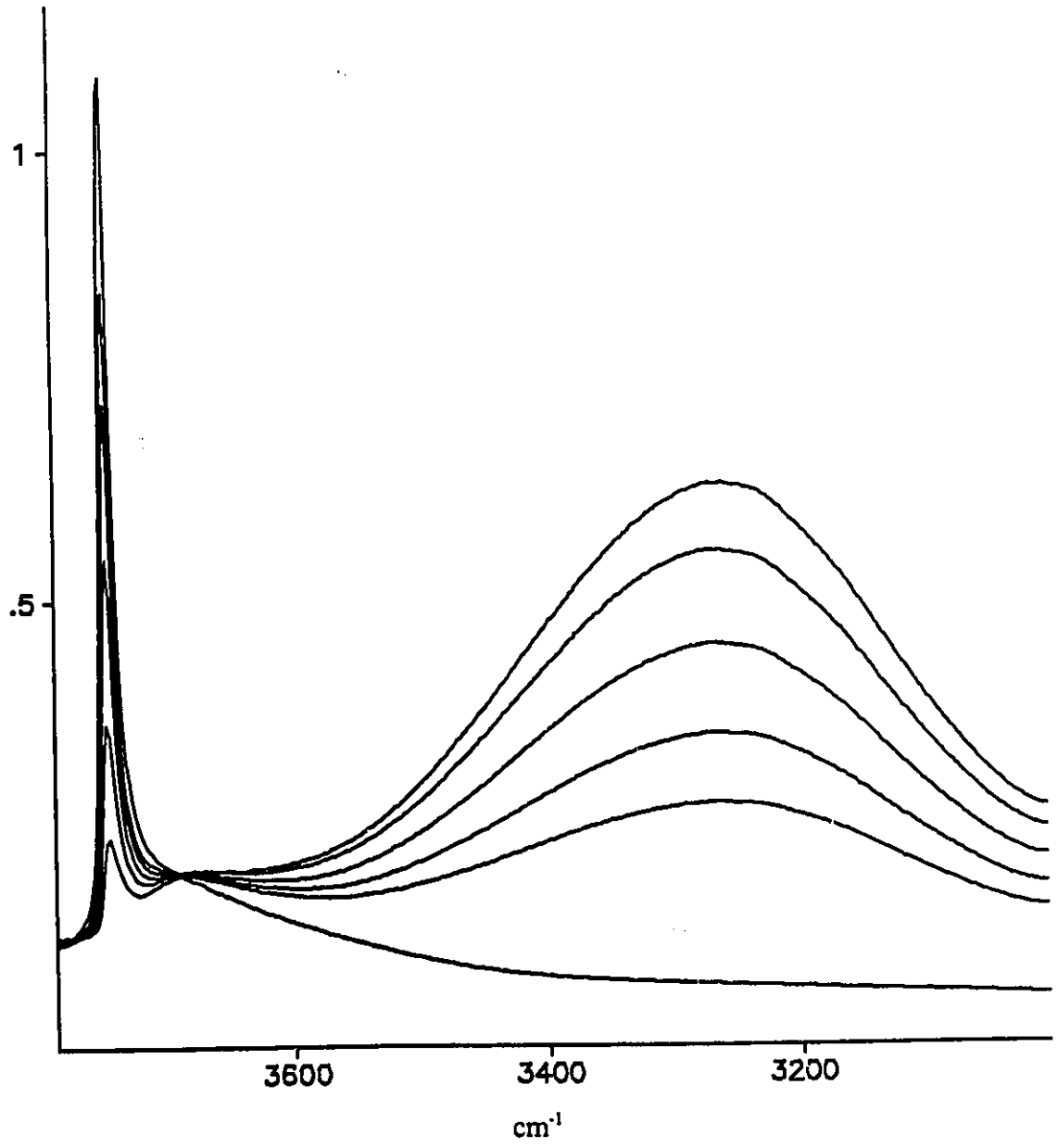

Fig. 3-1: Infrared Spectra of PMe_3 on SiO_2(450)

Gas pressures are 1.2, 2.7, 6.0, 13.7 and 32.0 torr. The gas phase has been subtracted from all spectra. The sharp feature at 3746 cm^{-1} decreases with gas increasing pressure, while the broad feature centred at about 3250 cm^{-1} grows with increasing gas pressure.

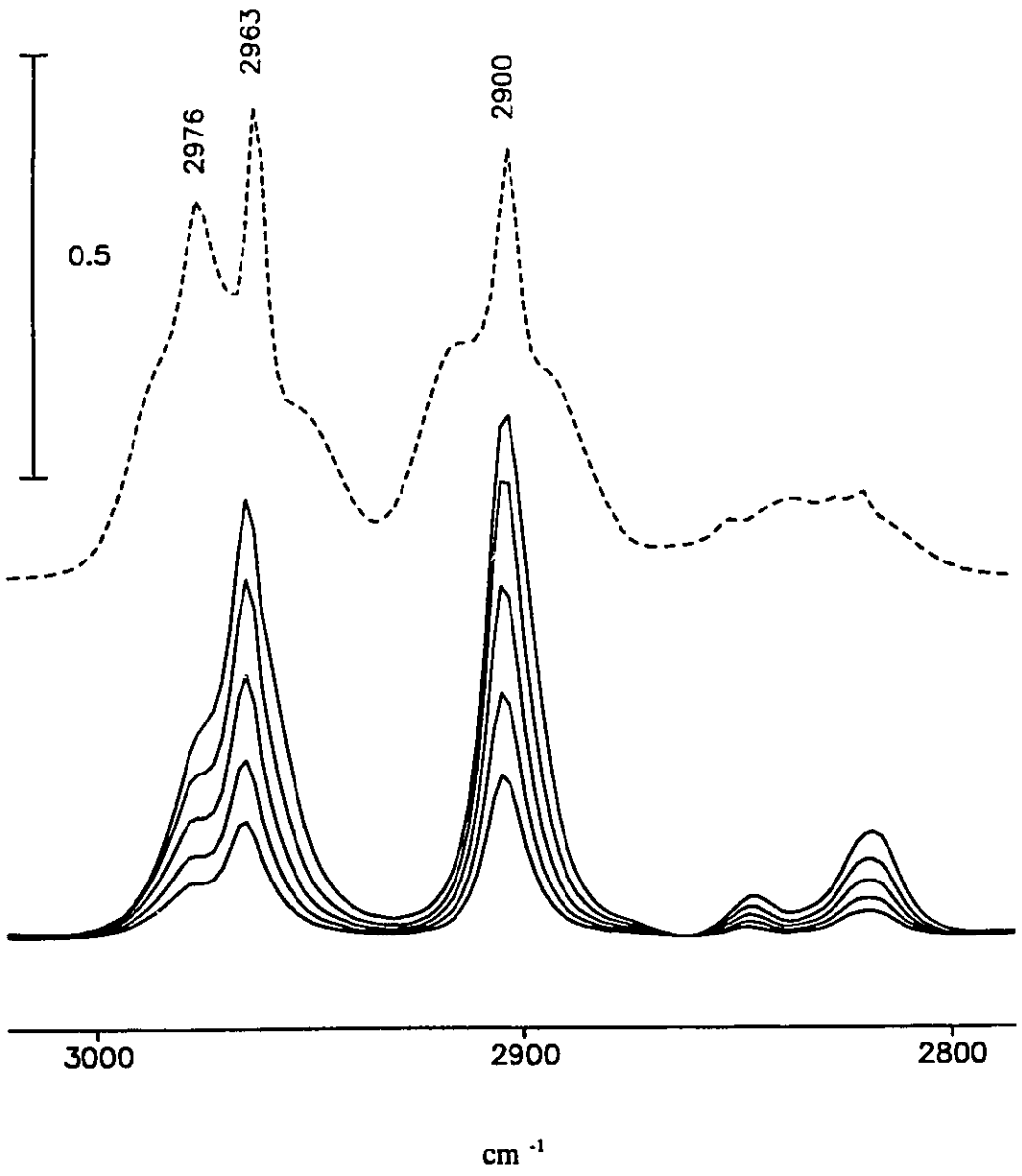

Fig. 3-2: PMe_3 on SiO_2(450)

Dashed Curve- gas phase PMe_3 (pressure 32 torr, path length 5 cm)

Solid Curves- Spectra of PMe_3 adsorbed at pressures of 1.2, 2.7, 6.0, 13.7 and 32.0 torr. Increasing intensity corresponds to increasing pressure. The gas phase has been subtracted from these spectra, and a 2 point baseline correction applied.

extensively by McKean *et. al.* [32]. They have shown that the spectrum is virtually independent of 'n' in the series $P(CH_3)_{3-n}(CD_3)_n$ when 'n' is less than three. This indicates that for the purpose of qualitative interpretation one can ignore any coupling effects between methyl groups, and interpret the spectrum as if only a single methyl group is present. In the case of a single methyl group with local three-fold symmetry, one expects two bands to appear in the C-H stretching region of the infrared spectrum. Both the non-degenerate symmetric mode and the doubly degenerate asymmetric stretching mode will be active in the infrared. McKean [33] has shown that in compounds that have non-bonded electron pairs, the C-H bonds that are trans to the lone pair are often inequivalent to the other C-H bonds, so that local three-fold symmetry doesn't apply, and the asymmetric mode is split into two bands. If methyl groups contain only one proton, as in the compound $P(CD_2H)_3$, vibrational coupling can cause only a negligible perturbation to the observed ν(C-H) frequencies. Such frequencies are termed "isolated", to indicate their relatively unperturbed nature. In the case of $P(CD_2H)_3$[34], a C-H bond trans to the lone pair is weaker than a C-H bond trans to a methyl group, and the isolated frequencies are 2919 and 2955 cm^{-1} respectively. Given this background information, the dashed curve in Fig. 3-2 is easily understood. In the region of $\nu_{as}(CH_3)$ there are two Q-branches, at 2976 and 2963 cm^{-1}, due to the splitting of ν_{as} by the symmetry lowering effect of the non-bonded electron pair. In the region of $\nu_s(CH_3)$ there is only a single Q-branch at 2900 cm^{-1}. The weaker bands below 2900 cm^{-1} are overtones of the CH_3 deformation bands. Since these bands are weak and have been found to be of little interpretive use, they will not be discussed further. The solid curves in Fig. 3-2 show that, except for the collapse of some gas phase rotational structure, the spectrum of PMe_3 does not

change on adsorption on SiO_2. All three C-H stretching bands are preserved on adsorption, although the 2976 cm^{-1} band only appears as a shoulder to high wavenumber of the 2965 cm^{-1} band. A linear fit of the baseline has been subtracted from these spectra to take away the non-constant slope in the background due to the growing 3250 cm^{-1} SiOH band. When this is done there is virtually no frequency shift or change in relative intensities in the C-H stretching bands with coverage. No evidence can be found for any species other than hydrogen-bonded PMe_3 in these spectra.

Other adsorbate bands that can be detected are those due to $\delta_{as}(CH_3)$ modes at 1440 and 1427 cm^{-1}, $\delta_s(CH_3)$ modes at 1314, 1302 and 1284 cm^{-1}, a massive band due to $\rho(CH_3)$ modes at 947 cm^{-1}, and $\nu_{as}(PC_3)$ at 717 cm^{-1}. These bands also correspond exactly to those of the parent molecule and are not shown.

When PMe_3 interacts with SiO_2 that has been activated at temperatures less than 450°C, similar results are obtained, but since there are several types of hydrogen-bonded SiOH group already present before adsorption [16], the spectrum in the SiOH region is more complex. As might be anticipated, no isosbestic point is observed. The ^{31}P MASNMR spectrum of PMe_3 adsorbed on SiO_2(RT) is shown in Fig. 3-3. In agreement with [35], a single line is seen at -59 ppm. Neat PMe_3 resonates at -62 ppm. The slight shift to high frequency on adsorption is consistent with a weak interaction with the surface via hydrogen-bonding. No signal could be obtained from this sample using cross polarization, showing that PMe_3 is very mobile on the SiO_2 surface.

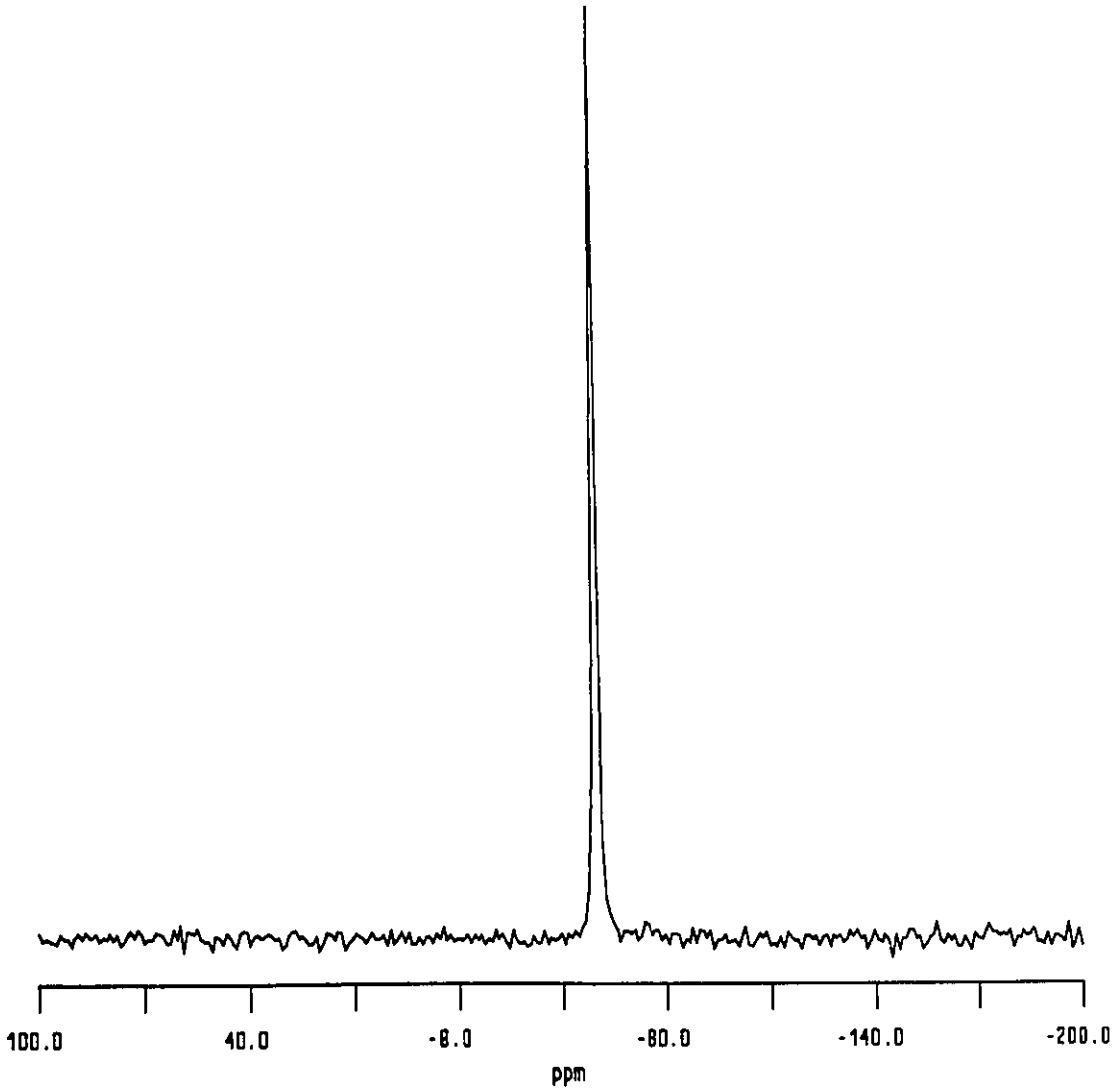

Fig. 3-3: ^{31}P MASNMR Spectrum of PMe_3 on SiO_2(RT)

The sample is in equilibrium with about 10 torr of PMe_3 in a sealed NMR tube. This spectrum was acquired in 90-degree pulse mode. No signal could be observed using cross-polarization.

Adsorption of PMe_3 on Highly Activated SiO_2

When SiO_2 is degassed at temperatures greater than 450°C, defect sites possessing Lewis acid properties are formed.[17-19] These sites are known to coordinate NMe_3 quite strongly [17]; degassing at 200°C was required to remove coordinated NMe_3. Spectra in the C-H stretching region after adsorption of PMe_3 on SiO_2(1150) are shown in Fig. 3-4. In Fig 3-4A narrow bands are seen at 2988 cm^{-1} and 2924 cm^{-1}, as well as broader bands centred near 2964 cm^{-1} and 2902 cm^{-1}. These latter bands are due to hydrogen bonded PMe_3 as has already been discussed. When this sample is evacuated for two minutes at room temperature, Fig 3-4B, the two bands due to H-bonded PMe_3 disappear, while the new pair of bands due to coordinated PMe_3 are only partially attenuated. The coordination complex between PMe_3 and the defect SiO_2 site is not as strong as that formed by NMe_3. Fig 3-4C, it is evident that the coordinated PMe_3 can be pumped away slowly at room temperature.

Two features of the new pair of bands require discussion. Firstly, $\nu_{as}(CH_3)$ is not split into two components as was the case for the free molecule and for hydrogen bonded PMe_3. This might indicate that withdrawal of electron density from phosphorus by the Lewis acid site has caused the strength of C-H bonds trans to the formerly non-bonded electron pair to become more similar to those trans to a methyl group, leading to a reduction in the splitting of $\nu_{as}(CH_3)$. While the local symmetry of the methyl group obviously cannot have increased on adsorption, so that a splitting of $\nu_{as}(CH_3)$ must still exist in principle, it can no longer be resolved in the infrared spectrum. It will be seen in subsequent sections that for Lewis bound PMe_3 on other oxides, sometimes a splitting of $\nu_{as}(CH_3)$ is observed, and sometimes no

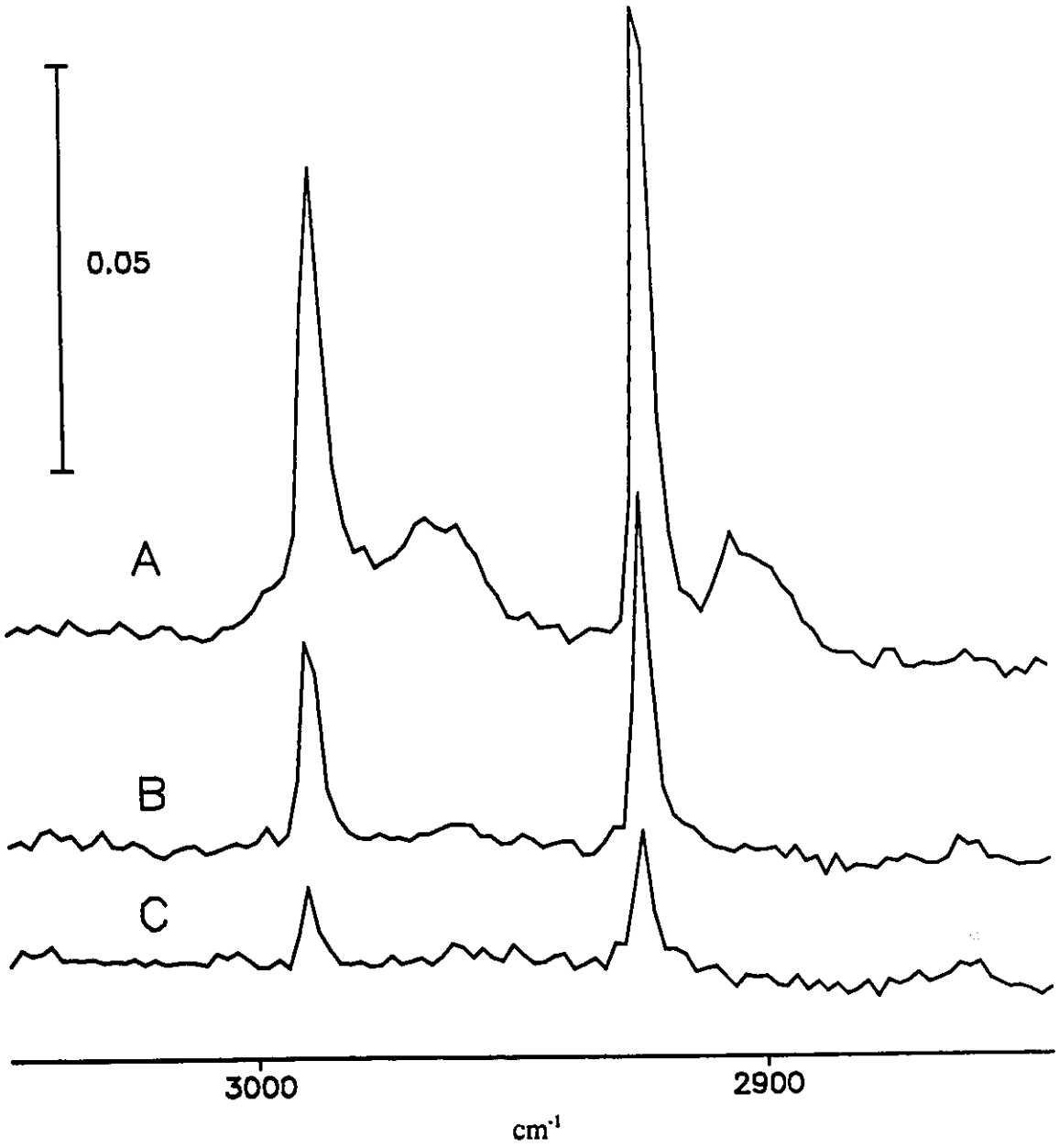

Fig. 3-4: PMe_3 on SiO_2(1150)

A: 0.8 torr PMe_3 in cell, gas phase subtracted

B: Evacuate 2 minutes.

C: Evacuate 30 minutes.

splitting can be resolved, even when the band is sharpened by cooling the sample to liquid nitrogen temperatures. Whether or not a splitting of $\nu_{as}(CH_3)$ is observed does not correlate with the strength of adsorption of PMe_3. There is no splitting at all on high temperature activated SiO_2, where the PMe_3 is relatively loosely bound.

At this point it may be of interest to note that in the chloride[36] and iodide[37] of $P(Me)_4^+$, where local threefold symmetry applies rigorously, no splitting of $\nu_{as}(CH_3)$ occurs. At least in a formal way, one may consider the PMe_4^+ ion as a Lewis acid-base adducts of PMe_3 and CH_3^+. If a splitting of $\nu_{as}(CH_3)$ occurred in these compounds, then the interpretation of the infrared spectra of PMe_3 given here would have to be discarded. The essential point to recognize is that interpreting the spectrum as if only a single methyl group is present is really only a convenient artifice. The vibrational dynamics of the entire molecule are really more complex. In the case of tetramethylphosphonium iodide for example, the infrared frequencies are 2975 and 2901 cm^{-1} , while the only peaks in this region in the Raman spectrum occur at 2966 and 2927 cm^{-1}. These latter peaks belong to different vibrational modes of different symmetry from those observed in the infrared. Nevertheless, considering only the modes of a single methyl group turns out to be the most useful way to rationalize the infrared spectra of adsorbed PMe_3.

A second difference between the bands of coordinated PMe_3 and the corresponding bands of gas phase or hydrogen-bonded PMe_3 is that they occur at higher wavenumber. Can one expect this to be the case generally? There are several factors affecting the frequencies of C-H stretching bands in methyl groups but the two most relevant ones appear to be the bond-weakening effect of the non-bonded pair and the H-C-H bond angle. Coordination,

protonation or oxidation of PMe_3 can all be expected to decrease the hyperconjugative weakening of the C-H bonds by the lone pair and lead to higher stretching frequencies, provided no other effect intervenes.

It has long been known [38] that in hydrocarbons the C-H stretching frequencies increase with the degree of *s* character in the C-H bond. When comparing oscillators containing single C-H groups, it is found that an aliphatic C-H group (sp^3 hybridization, bond angle near 109°) will absorb near 2900 cm^{-1} , an olefinic C-H group (sp^2 hybridization, bond angle near 120°) will absorb near 3100cm^{-1}, and an acetylenic C-H group (sp hybridization, bond angle 180°) will absorb near 3300cm^{-1}. Thus as the bond angle increases so does the degree of *s* character of the bond, and the vibrational frequencies increase. This trend even holds when comparing different methyl groups, where no such gross changes in hybridization state would be considered to occur. If vibrational coupling effects are excluded through the use of isolated ν(C-H) frequencies, an excellent linear correlation is observed between the H-C-H bond angle in methyl groups and the vibrational frequency.[33] As an indication of the range that might be expected for methyl group frequencies, note that the extremes in this correlation are neopentane, with bond angle 106° and isolated ν(C-H) frequency 2933 cm^{-1} , and iodomethane, with bond angle 111° and isolated ν(C-H) frequency 3035 cm^{-1}.

The above considerations lead to the conclusion that the C-H stretching frequencies of PMe_3 will normally be increased on coordination, but if the coordination site is sterically hindered in such a manner as to force the methyl groups to adopt smaller H-C-H bond angles, there will be a compensating effect. The frequencies may be scarcely changed or even decreased in some cases.

The high C-H stretching frequencies in Fig. 3-4 therefore imply that PMe_3 is interacting with an electron withdrawing site, and that the adsorption environment is not strongly hindered sterically. The bands are also quite narrow, which implies a surprising degree of homogeneity in the Lewis-acid defect sites.

In order to complete the discussion of the $\nu(CH_3)$ bands of coordinated PMe_3 for later sections, a few literature examples of Lewis acid complexes of PMe_3 should be discussed. It has been reported that in the series of boron trihalide adducts of PMe_3 the C-H frequencies increase in the order $BCl_3 > BBr_3 > BI_3$ [39]. (All of the adducts had higher $\nu(CH_3)$ frequencies than the free molecule). This order is opposite to that of increasing Lewis acidity[40], and can only be rationalized if the halogen size is assumed to be the dominant factor. BI_3 has the lowest frequencies in spite of being the strongest Lewis acid because the large radius of iodine forces the H-C-H bond angles to decrease. The proton magnetic resonance spectra of BX_3 adducts of PMe_3 have also been rationalized by invoking the halogen size as an important factor.[41]

PMe_3 forms a 1:1 adduct with CS_2. The infrared spectrum of this adduct shows that its $\nu(CH_3)$ bands are unshifted from those of the parent compound.[42] Slight shifts of the $\nu(CH_3)$ bands to lower wavenumber have been reported when PMe_3 is complexed by GaH_3[43], although a steric effect probably cannot be invoked in this case.

The $\nu(CH_3)$ frequencies of coordinated PMe_3 will thus reflect more factors than just the Lewis acidity of the coordinating entity, and the magnitudes of the shifts will not be useful as an empirical acidity scale.

Adsorption of PMe_3 on Al_2O_3 and Fluorided Al_2O_3

Fig. 3-5 shows the C-H stretching region of the infrared spectra of PMe_3 adsorbed on Al_2O_3 samples that have been activated different temperatures. Fig. 3-5A shows the spectrum of PMe_3 on Al_2O_3(150). There is a band at about 2902 cm^{-1} in this spectrum, which by analogy with the previous results for PMe_3 adsorption on silica may be attributed to $\nu_s(CH_3)$ of PMe_3 that is held to the surface via hydrogen-bonding. This band has a shoulder at about 2910 cm^{-1}, which is to be attributed to PMe_3 interacting with Lewis acid sites. The other bands in Fig 3-5A, at 2960 and about 2972 cm^{-1}, resemble those already discussed for $\nu_{as}(CH_3)$ of PMe_3 hydrogen-bonded to the surface, and the presence of any Lewis bound PMe_3 is not yet detectable by examination of this region.

Spectra in the AlOH region are not shown, but as must be the case when hydrogen-bonding is invoked, the isolated AlOH peaks lose intensity, and a broad asymmetric band peaked at about 3370 cm^{-1} appears. These changes are reversed by room temperature evacuation.

When the activation temperature is raised to 450°C as in Fig. 3-5B, the band due to $\nu_s(CH_3)$ near 2902 cm^{-1} is barely detectable as a shoulder to low wavenumber of the band at 2910 cm^{-1} due to $\nu_s(CH_3)$ of coordinated PMe_3. The 2960 cm^{-1} band due to $\nu_{as}(CH_3)$ of hydrogen-bonded PMe_3 is also much less intense, most of the infrared absorption at 2972 cm^{-1} is to be attributed to $\nu_{as}(CH_3)$ of coordinated PMe_3.

In Fig. 3-5C the sample has been activated at 900°C, and there are no surface AlOH groups left. A pair of bands due to coordinated PMe_3 at 2975 cm^{-1} and 2910 cm^{-1} is all that can be observed. No splitting of $\nu_{as}(CH_3)$ was detected, even when a similarly prepared sample was

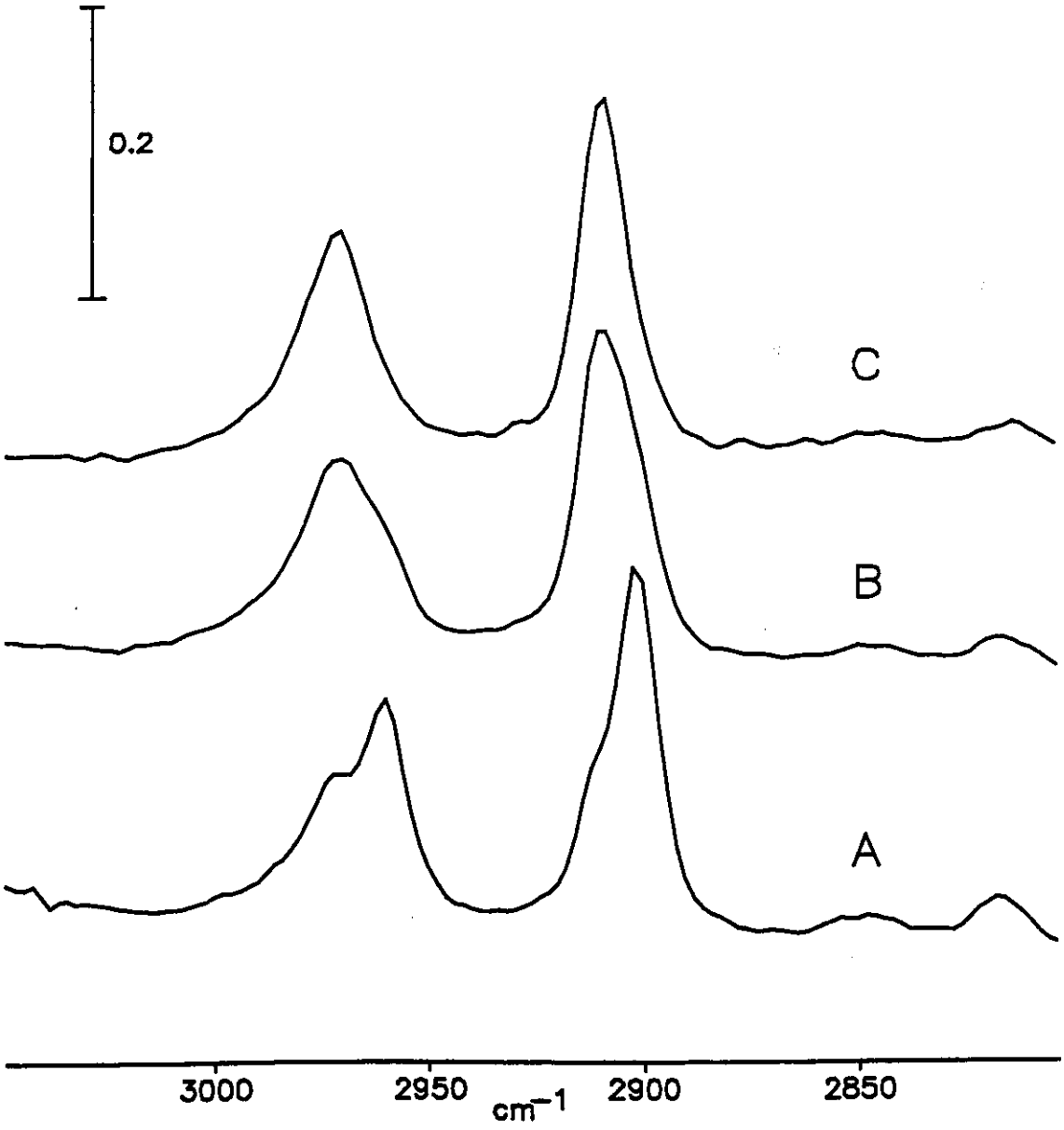

Fig. 3-5: PMe_3 Adsorption on Al_2O_3

A- PMe_3 on Al_2O_3(150)

B- PMe_3 on Al_2O_3(450)

C- PMe_3 on Al_2O_3(900)

About 2 Torr of gas is present in each experiment. It has been subtracted out of these spectra.

cooled to liquid nitrogen temperature.

^{31}P NMR spectra of PMe_3 adsorbed on Al_2O_3(RT) are shown in Fig. 3-6. Both spectra in this figure required long acquisition times, and were obtained by signal averaging overnight. As expected, the 90° pulse spectrum in Fig. 3-6A spectrum is dominated by resonance due to physisorbed and hydrogen bonded PMe_3 at -62 ppm. There is probably some interaction with weak Lewis acid sites, and possibly the spectrum is broadened by chemical exchange, as the width of this peak is more than eight times as broad as was observed for PMe_3 adsorbed on SiO_2(RT). In Fig 3-6B, there is a weak and very broad peak centred at about -50 ppm that can just be detected. This confirms the presence of weak Lewis acidity, and shows that there is a small fraction of the surface phosphorus that is held rigidly enough to be cross-polarized.

Fig. 3-7 shows the ^{31}P CPMAS NMR spectra of PMe_3 adsorbed on Al_2O_3(300). All of the curves in this figure are spectra of the same sample. In Fig 3-7A multiple local maxima are seen. These could be due to multiple surface sites, or reflect scalar coupling to surface aluminum atoms. ^{27}Al has 100% natural abundance and has nuclear spin 5/2, so that a sextet of peaks could be observed in the ^{31}P NMR spectrum of PMe_3 coordinated to aluminum, provided the ^{27}Al T_1 is not short compared to the inverse of the scalar coupling constant. Lunsford has shown that in the case of PMe_3 adducts with $AlCl_3$ a sextet of peaks separated by about 300 Hz is observed, and that the splitting is due to scalar coupling.[44] A theoretical analysis of the rather complicated behavior of the intensity distribution under magic-angle-spinning was also presented.[45] Fig. 3-7 shows spectra of the same sample that have been collected at two different field strengths, and provides evidence that scalar coupling is also observable when PMe_3 adsorbs on Al_2O_3. In curves A and B the x axis is ppm, and the spectrum appears much

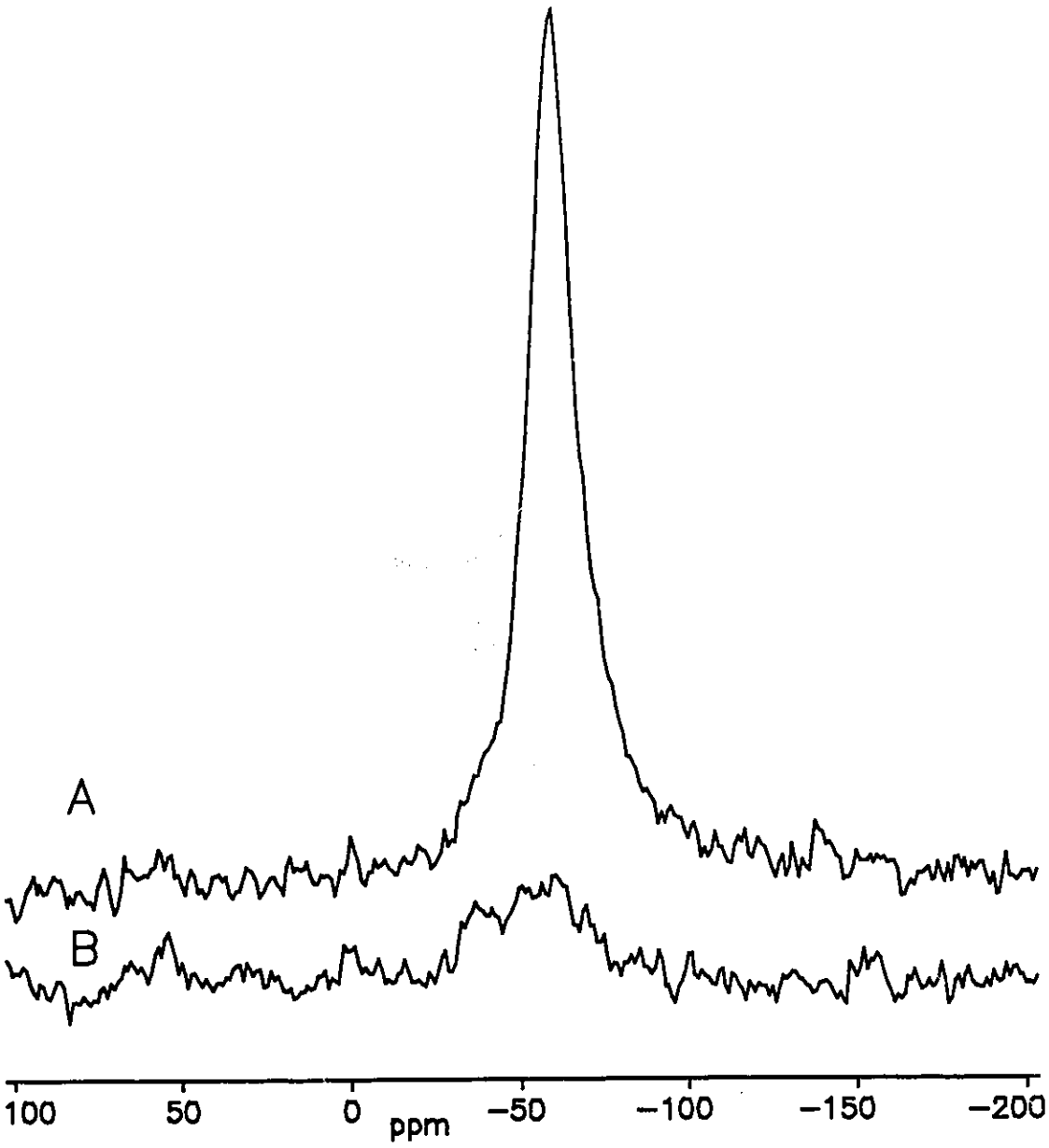

Fig. 3-6: ^{31}P MASNMR Spectra of PMe_3 on Al_2O_3(RT)

A- 90° pulse spectrum

B- CPMAS spectrum

About 27 μmols PMe_3 was frozen into the NMR tube with 0.2g Al_2O_3(RT).

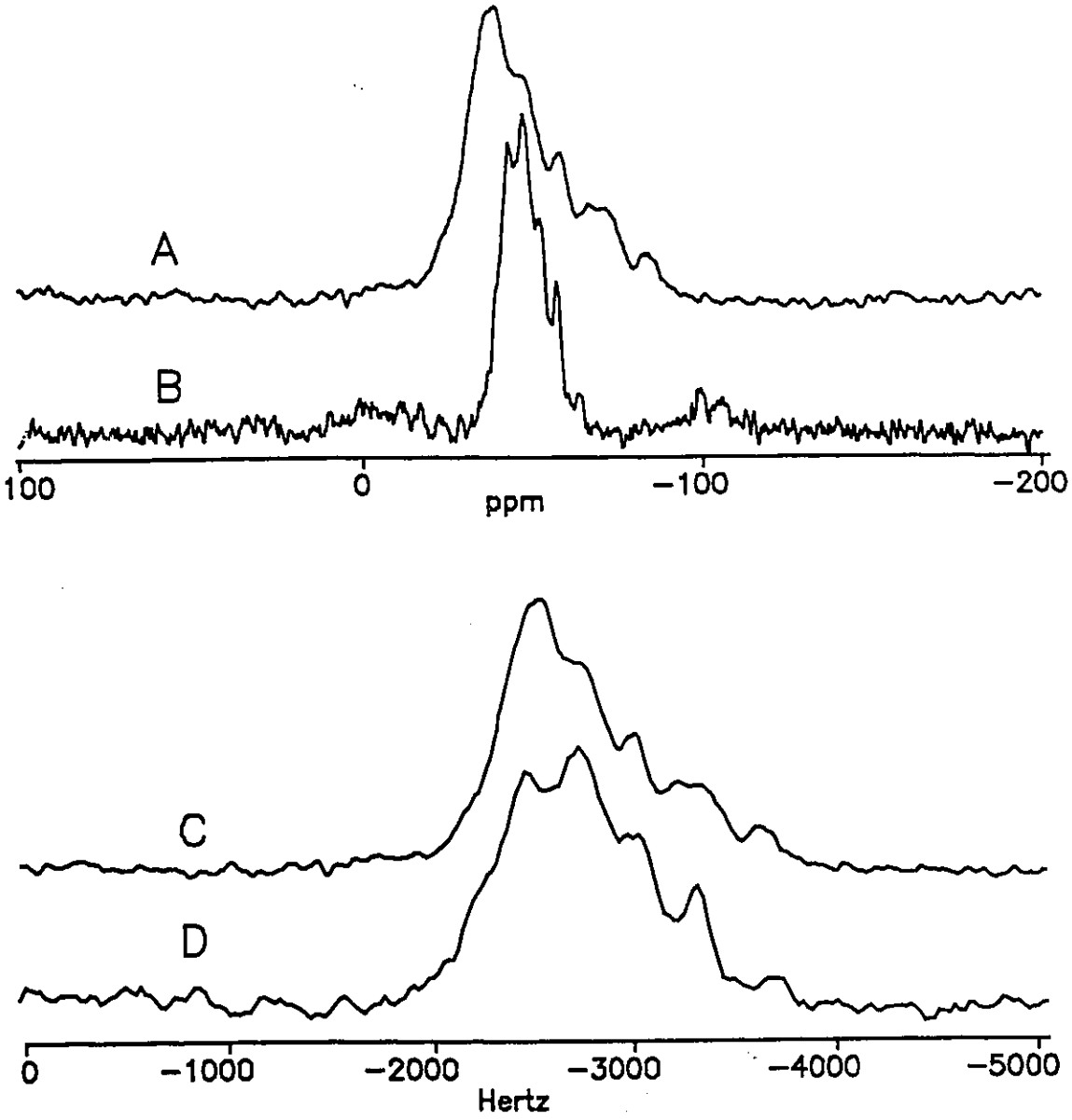

Fig. 3-7: ^{31}P CPMAS Spectra of PMe_3 on $Al_2O_3(300)$

About 17 μmols of PMe_3 was frozen into the NMR tube with 0.2g $Al_2O_3(300)$.

Spectra A and C were recorded at 24.3 MHz, curves B and D at 60.4 MHz.

narrower in curve B, the higher field spectrum. If the multiple maxima in Fig. 3-7 were due to distinct chemical species, their separation, and hence the width of the spectrum, would be constant when expressed in ppm. If the maxima are due to scalar coupling, a property of the sample and not the magnet, the peak separation and width of the spectrum would be constant in Hertz. In curves 1-7C and 1-7D it is apparent that width of the spectrum is approximately constant in Hertz.

The appearance of scalar coupling provides rather vivid evidence of phosphorus aluminum bonding and hence surface Lewis acidity. Unfortunately the large spectral width produced by the scalar coupling precludes any opportunity to observe distinct Lewis acid sites on Al_2O_3 by NMR of adsorbed PMe_3. Distinct families of adsorption sites on Al_2O_3 can be differentiated by infrared spectroscopy of adsorbed CO[22] and pyridine[46]. In this study neither infrared nor NMR spectroscopy of adsorbed PMe_3 were effective at demonstrating the multiple Lewis acid adsorption sites known to exist on Al_2O_3.

Brønsted acidity could not be detected on pure Al_2O_3. If such sites were present a peak near -3ppm would be observed in the ^{31}P spectrum of adsorbed PMe_3. The infrared signature of protonated PMe_3 will be discussed shortly. The authors of [47] have reported the presence of a very small amount of Me_3PH^+ when PMe_3 is adsorbed on Al_2O_3. One possible reason for the discrepancy may be the different Al_2O_3 samples used. During these studies it has been found that different Al_2O_3 samples can have very different amounts of surface carbonate impurities. Ripmeester has shown [48] that surface hydrogenocarbonate species on Al_2O_3 can protonate pyridine. No sites capable of protonating PMe_3 were found for pure Al_2O_3 in [35], but a small quantity of protonated PMe_3 was observed in similar experiments in [49]. It is evident that

different Al_2O_3 samples can have different surface properties. It should be emphasized that there is general agreement that Brønsted acidity is not a significant feature of the surface chemistry of alumina [23]. Whether or not a small amount of Me_3PH^+ is formed when PMe_3 is adsorbed by Al_2O_3 is not a matter worthy of controversy.

Fig. 3-8 shows the infrared spectrum of PMe_3 on $Al_2O_3(800)$. The spectrum shown is the difference between the spectra before and after adsorption of PMe_3, so that features that increase on adsorption point up, and features that decrease on adsorption point down. As has been mentioned, there is a decrease in the intensity of the peaks due to residual AlOH groups around 3700 cm^{-1}, and a very broad distribution of new absorbance due to hydrogen-bonded AlOH groups appears at lower wavenumber. The $\nu(CH_3)$ stretching peaks due to Lewis bound PMe_3 appear, as has already been discussed, and 2 doublets centred around 1430 cm^{-1} and 1300 cm^{-1} due to $\delta(CH_3)$ modes appear. In order to extend transmission to as low frequency as possible, this sample is as thin a self-supporting disk as can be made. When PMe_3 is adsorbed on this sample and the background subtracted, a negative peak appears centred at about 1040 cm^{-1}. This feature has been attributed to strong Lewis acid defect sites that are created when Al_2O_3 is activated at temperatures above 450°C.[50] It is really quite remarkable that a nearly symmetrical negative band appears when "defects" are relaxed by coordination of PMe_3.

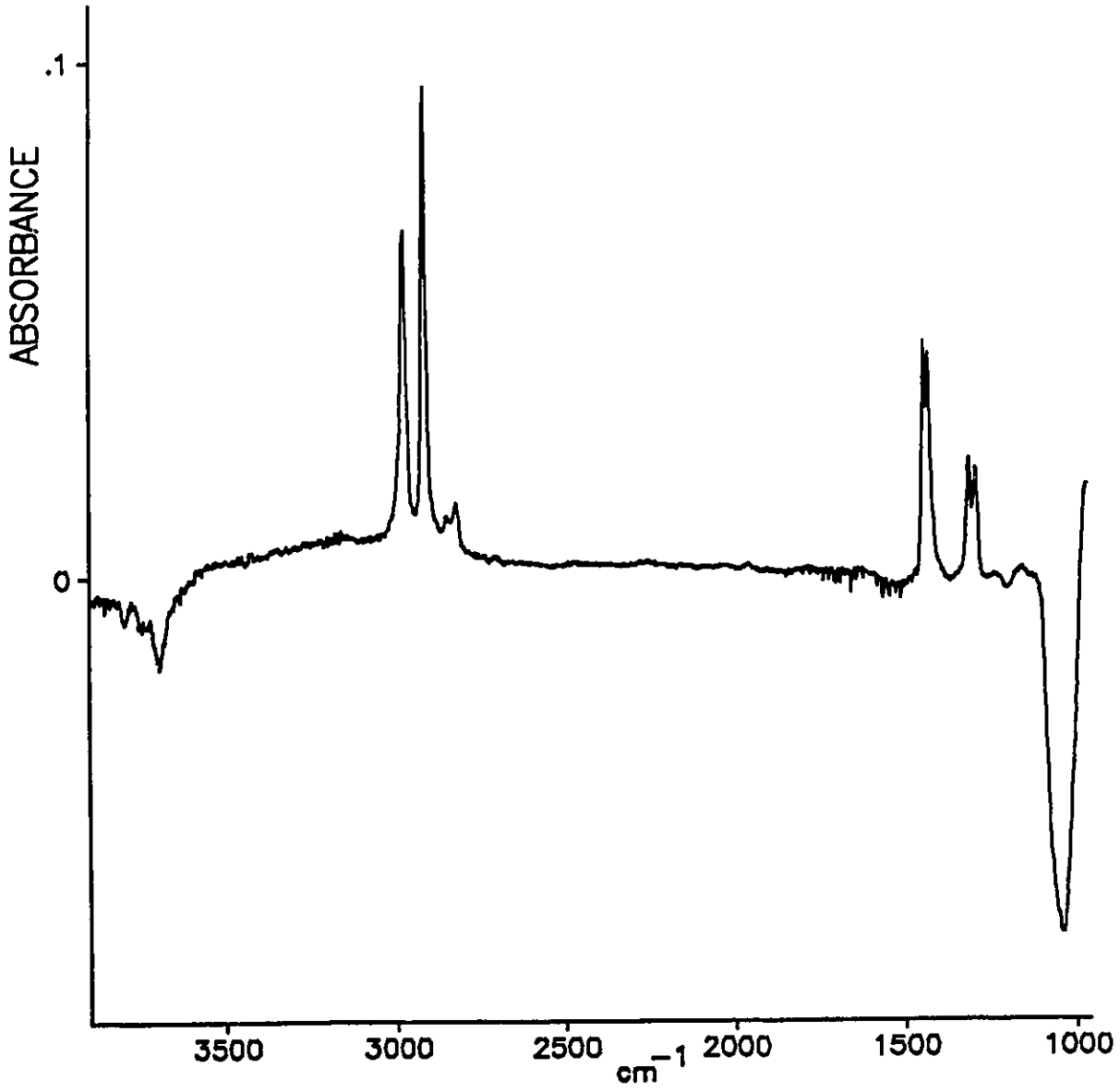

Fig. 3-8: Infrared Spectra of PMe_3 on Al_2O_3(900)

A thin (4mg/cm^2) self-supporting disk has been degassed at 800°C; allowed to interact with 1 Torr of PMe_3, and evacuated briefly. The curve shown is the difference between the spectra before and after adsorption.

Adsorption of PMe_3 on Fluorided Al_2O_3

Fluoride doped Al_2O_3 has long been known to show enhanced catalytic activity compared to pure Al_2O_3, and it is thought that this is due to the presence of strong Brønsted acid sites not found in pure Al_2O_3.[51] Fluorided Al_2O_3 thus offers the opportunity to study the interaction of PMe_3 with a Brønsted acidic surface.

Fig. 3-9A shows the infrared spectra observed after adsorption of PMe_3 on fluorided Al_2O_3. This sample has been doped with NH_4F so as to produce a sample that is nominally 2 weight percent fluoride after destruction of the NH_4^+ ions by calcination at 400°C. The sample was allowed to rehydrate by equilibration with ambient air and then degassed at 150°C. In Fig. 3-9A excess PMe_3 is present, and the most intense bands in the infrared spectrum are those due to hydrogen-bonded PMe_3 at 2904 and 2966 cm^{-1}. These bands decrease in intensity very quickly when the cell is evacuated. After 2 minutes evacuation, Fig. 3-9C, three bands can clearly be seen in the $\nu_s(CH_3)$ region, at 2904, 2918 and 2928 cm^{-1}. Three bands are also apparent in the $\nu_{as}(CH_3)$ region, at about 2966, 2978 and 3008 cm^{-1} respectively. It has been shown that the pair of bands at 2904 and 2966 cm^{-1} are due to H-bonded PMe_3, and the pair of bands at 2978 and 2918 cm^{-1} due to Lewis bound PMe_3. This leaves the bands at 3008 and 2928 cm^{-1} that might be attributable to protonated PMe_3. The presence of Me_3PH^+ in the sample is confirmed by the appearance of a weak band at 2475 cm^{-1}. This band does not appear if the sample is extensively deuterium exchanged prior to PMe_3 adsorption, but a new band then appears at about 1790 cm^{-1}. Thus the 2475 cm^{-1} band is likely the ν(P-H) mode of adsorbed Me_3PH^+. This frequency is close to the 2490 cm^{-1} frequency reported for the ν(P-H) band Me_3PH^+ formed by adsorption of

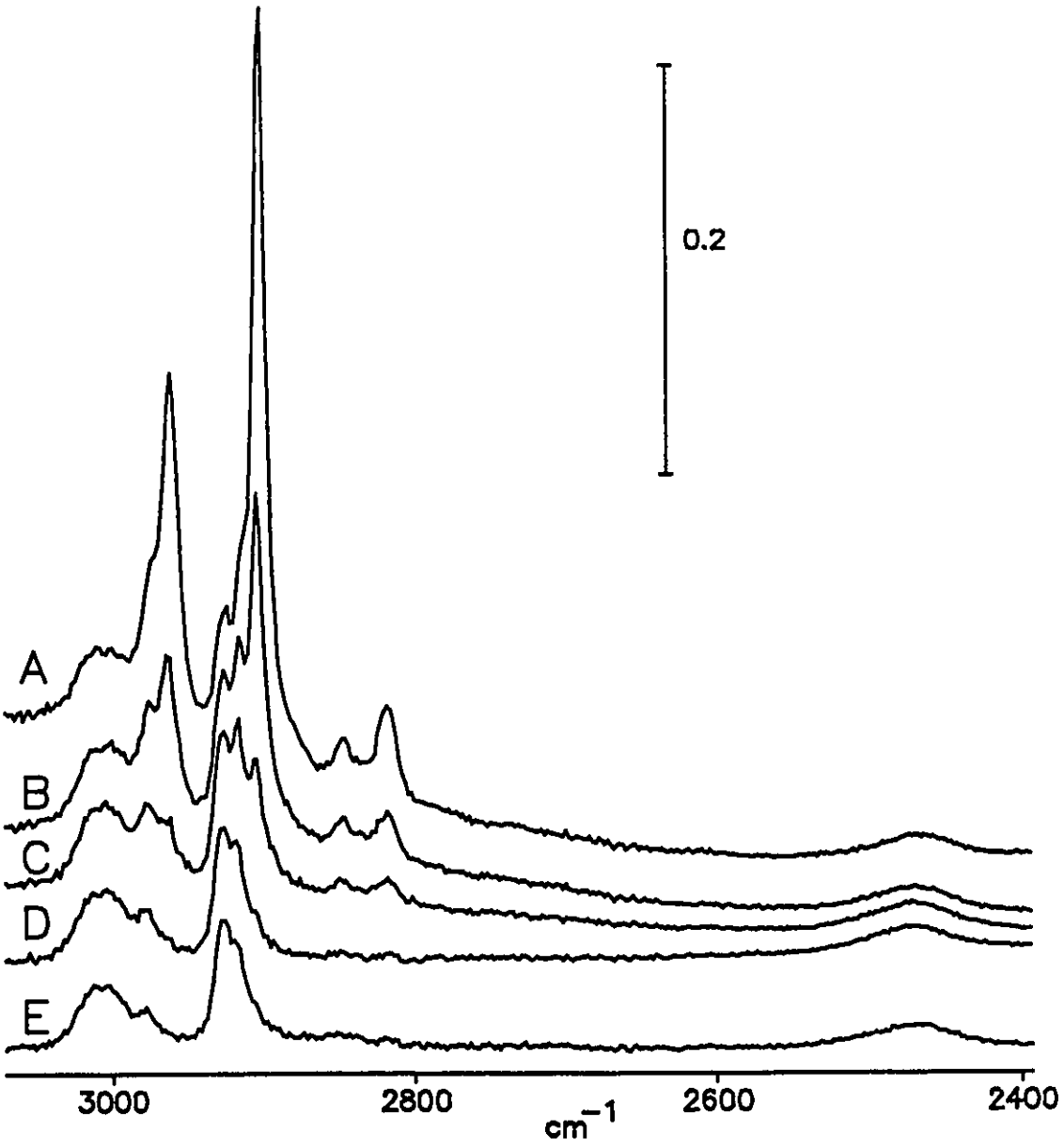

Fig. 3-9: PMe_3 Adsorption on Al_2O_3(2%F, 150)

A- 1.2 Torr of PMe_3 is present in the cell, but the gas phase spectrum has been subtracted out. Curves B through E are the infrared spectra after evacuation at room temperature for 30 seconds, 2 minutes, 15 minutes and 45 minutes respectively.

PMe_3 on zeolite HY [52,53]. A recent paper reported a range of frequencies for ν(P-H) of salts of Me_3PH^+ with different counterions, from 2424 cm^{-1} in the SbF_6^- salt, to 2484 cm^{-1} in the AsF_6^- salt.[54] This paper also showed that as expected, C-H stretching frequencies shift to higher wavenumber when PMe_3 is protonated. For example in the SbF_6^- salt two bands were seen in the C-H stretching region of the infrared spectrum, at 3014 and 2940 cm^{-1}.

In Fig. 3-9 it is evident that protonated PMe_3 is the most strongly held surface species in this system, since the bands due to other species all disappear slowly when the sample is evacuated at room temperature.

One can conclude that bands near 3008, 2920 and 2475 cm^{-1} might be useful as infrared criteria to establish the presence of adsorbed Me_3PH^+ on acidic solids. However, it is also possible that the high wavenumber ν(C-H) bands may actually be due to $Me_3P{=}O$. This compound in CS_2 solution has been reported to show two bands in the ν(CH_3) region of the infrared spectrum, at 2983 and 2912 cm^{-1}.[55] These bands may shift to higher wavenumber on surface complexation and be difficult to distinguish from those of Me_3PH^+. PMe_3 is a pyrophoric compound, and at low oxygen pressures avidly takes up oxygen to form $Me_3P{=}O$. Thus trimethylphosphine oxide can be expected to be present in any experiment where oxygen has not been excluded rigorously enough, and may also occur if there is any reducible surface species present. The only infrared criteria that can be used to distinguish $Me_3P{=}O$ from Me_3PH^+ are the P-H stretching band near 2480 cm^{-1}, and the P=O stretching band near 1160 cm^{-1} for $Me_3P{=}O$.[55] The P-H band is often quite weak, as seen in Fig. 3-9. For many of the materials of interest in this study the 1160 cm^{-1} region of the spectrum is either unavailable due to absorption by the bulk oxide, or cluttered with other absorptions; for example those due to

surface sulfate species. There will therefore be cases where infrared spectra do not provide an unambiguous determination of the surface species. Fortunately the ^{31}P resonances of surface species derived from $Me_3P=O$ are all above 30 ppm and hence well resolved from those of other surface species.[56]

In the Al_2O_3/PMe_3 and fluorided Al_2O_3/PMe_3 systems no absorbance in the 1150 cm^{-1} region was observed for room temperature absorption of PMe_3 under any conditions. When samples were degassed at temperatures greater than 200°C after PMe_3 adsorption, an intense broad band was usually seen in this region. Strongly adsorbed PMe_3 apparently does not desorb intact upon evacuation at elevated temperatures, but rather undergoes rather ill-defined oxidation and decomposition reactions, as was observed in [52] for desorption of PMe_3 on zeolite HY.

The ^{31}P MAS NMR spectrum of PMe_3 adsorbed on Al_2O_3(2%F, RT) is shown in Fig. 3-10. In agreement with the infrared results, no resonances above 0 ppm that might be attributed to oxidation products are observed. A weak peak is observed at -3 ppm due to protonated PMe_3. The intense peak at -61 ppm is due to H-bonded and physisorbed PMe_3. In an attempt to sample all of the Brønsted sites by neutralizing them with PMe_3, a large excess of PMe_3 was added to this sample. It has since been shown through studies of the coverage dependence of the ^{31}P NMR spectrum of adsorbed PMe_3 that chemical exchange between protonated and physisorbed PMe_3 can occur, and that this can lead to a loss of intensity in the -3 ppm peak.[35] If this fact is ignored the peak areas in Fig. 3-10 would lead to the conclusion that the sample contains 8.7 μmols of Me_3PH^+, or that under these conditions Al_2O_3(2%F, RT) contains 72 μmols per gram of Brønsted acid sites. This is a rather small number when considered in relation to the 1050 μmols per gram of fluoride ions with which the sample was doped. If the correction scheme

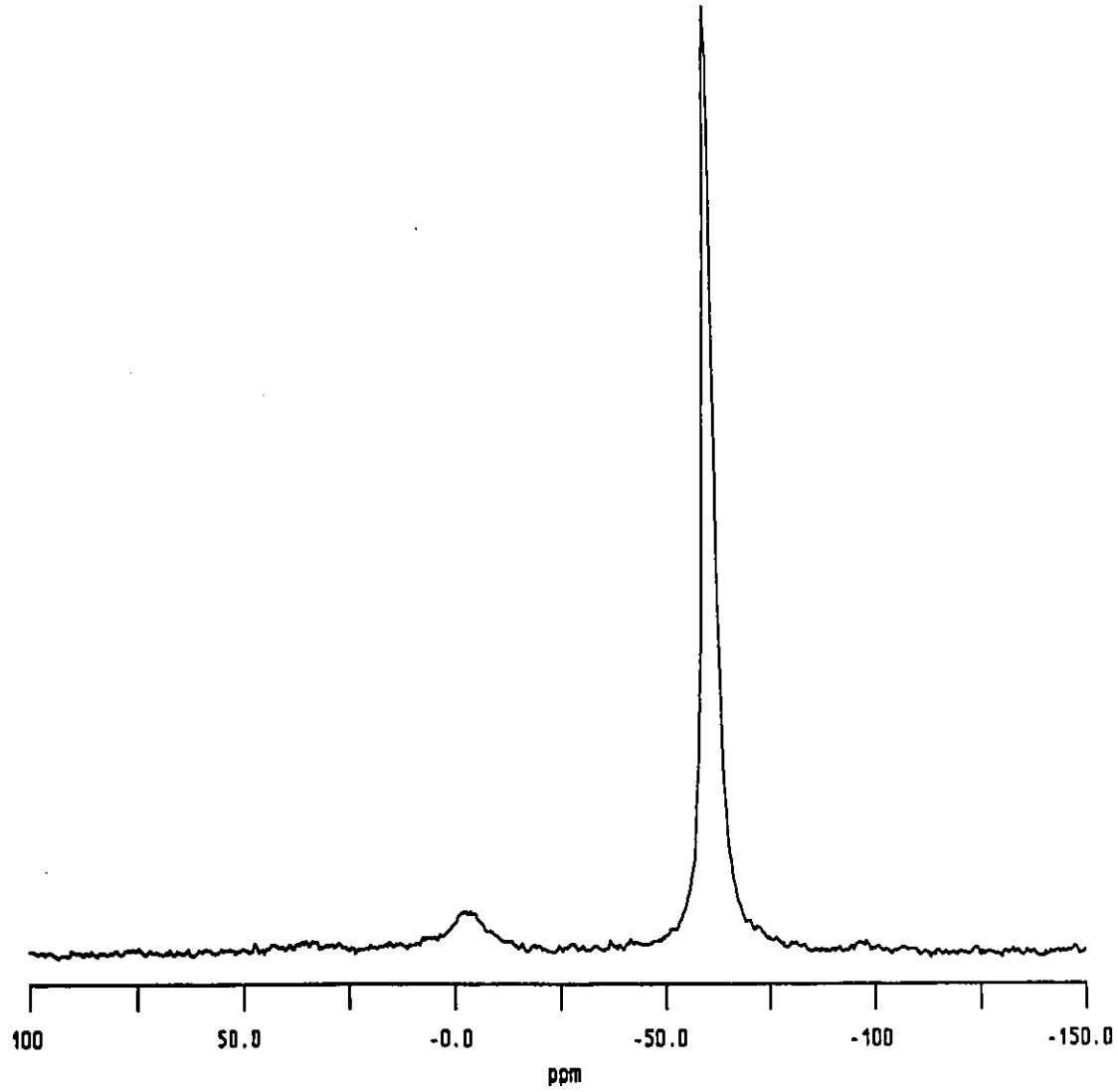

Fig 3-10: ^{31}P MAS NMR of PMe_3 on Al_2O_3(2%F, RT)

About 122mg Al_2O_3(2%F) was degassed at room temperature and 84 μmols of PMe_3 frozen in before the tube was sealed off.

given in [35] is used to attempt a correction to the number of Brønsted sites one would calculate that there are 85 μmols per gram of Brønsted sites on Al_2O_3(2%F, RT). Spectra would have to be obtained either at low temperature or as a function of coverage in order to decide if this small correction for chemical exchange is meaningful.

No attempt has been made to obtain quantitative NMR data for samples activated at higher temperatures. The spectra simply become too difficult to obtain. Presumably long T_1 values occur for these samples. ^{31}P T_1 values on the order of two seconds were observed when PMe_3 was adsorbed on chlorided Al_2O_3.[49] Sufficient signal was never obtained on fluorided Al_2O_3 samples degassed above 300°C for a meaningful estimate of T_1 to be made, but it was certainly longer than 2 seconds.

It is not difficult to demonstrate that some Brønsted acidity remains even after activation at fairly high temperatures. Fig. 3-11 shows the ^{31}P CPMAS spectra obtained after PMe_3 adsorption on Al_2O_3(2%F, 440). Lewis acid sites are evidenced by a very broad peak centred near -40 ppm. The resolved scalar coupling that was seen when PMe_3 was adsorbed on pure Al_2O_3 is not observed, possibly blurred out by an increase in the heterogeneity of the Lewis acid sites present. In agreement with infrared results (not shown) there is still some Brønsted acidity remaining after 440°C evacuation, as evidenced by the peak at -3 ppm. Fig. 3-11B illustrates that the species responsible for the peak at -3 ppm does indeed bear a directly bonded proton, as the signal from this species disappears if decoupling is delayed by 70 μs before the start of acquisition.

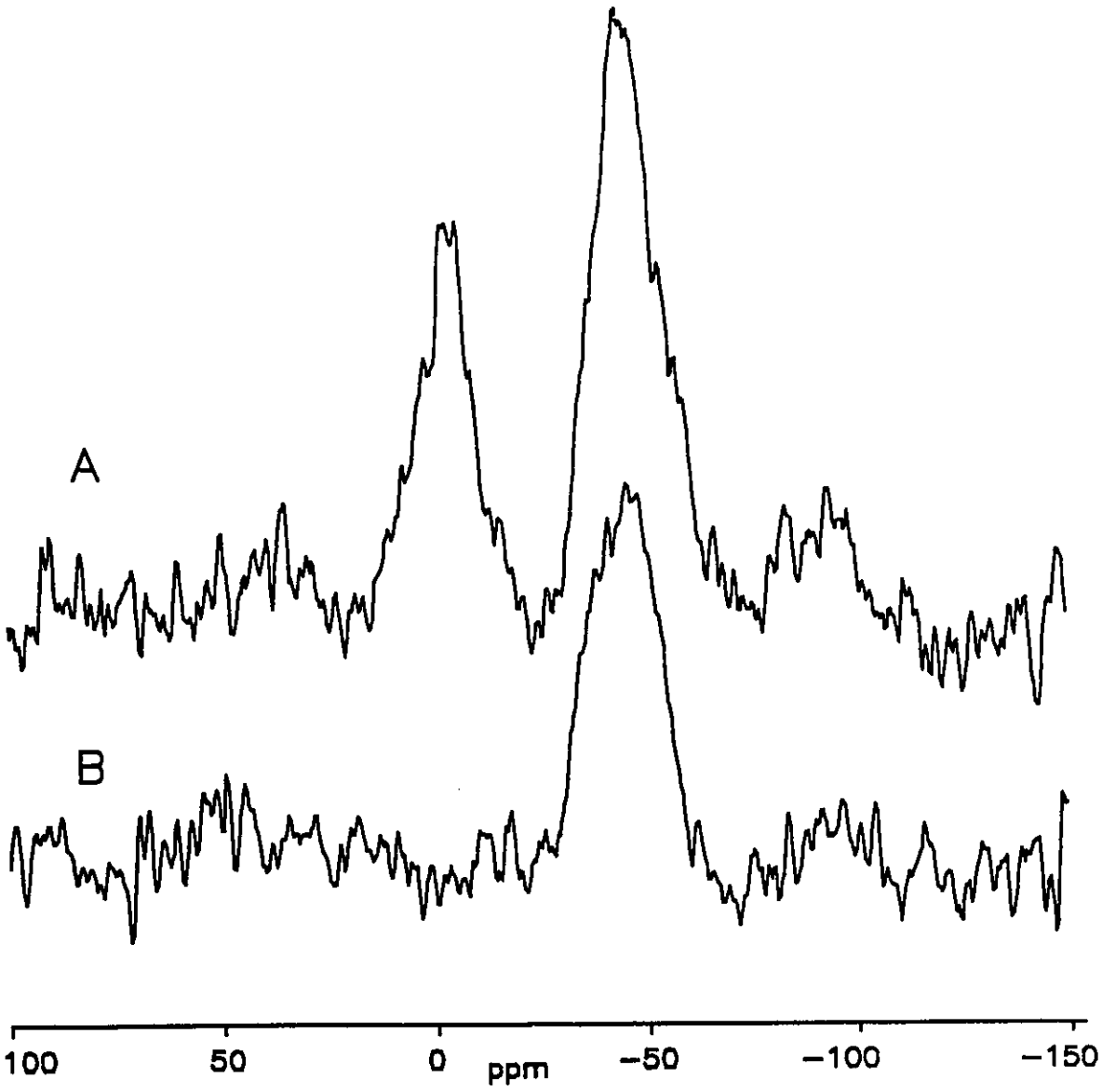

Fig. 3-11: ^{31}P CPMASNMR Spectra of PMe_3 on Al_2O_3(2%F, 450)

A- CPMAS NMR spectrum, 38 μmols PMe_3 frozen in on 138 mg Al_2O_3(2%F, 440)

B- CPMAS NMR spectrum with a 70 μs delay before decoupling.

Adsorption of PMe_3 on TiO_2 and Sulfated Titania

Infrared spectra of PMe_3 adsorbed on pure TiO_2 showed only the presence of coordinated PMe_3. The spectra were very similar to those already shown for PMe_3 adsorption on Al_2O_3, particulary in that there was no indication of the presence of different types of Lewis acid site. When PMe_3 was adsorbed on TiO_2(400) a composite peak centred at about 2970 cm^{-1} was observed in the $\nu_{as}(CH_3)$ region. This composite peak became slightly better resolved, showing components at 2974 and 2966 cm^{-1} when the sample was cooled to liquid nitrogen temperature. The region of $\nu_s(CH_3)$ showed only a single peak centred at about 2906 cm^{-1}, and cooling to liquid nitrogen temperature did not change the appearance of this peak. If there is no structure in the region of $\nu_s(CH_3)$, there is no evidence for multiple species in the infrared spectrum of Lewis bound PMe_3 on TiO_2. The structure in the region of $\nu_{as}(CH_3)$ can be due to a splitting of the degeneracy of this mode as discussed previously.

Solid state NMR spectroscopy of adsorbed PMe_3 did allow the differentiation of different Lewis acid sites, as shown in Fig. 3-12. In Fig. 3-12A, the coverage of PMe_3 is low compared to the other curves; about 0.55 PMe_3 molecules per nm^2 have been adsorbed. The main species present gives a ^{31}P resonance at about -33 ppm, and a shoulder near -25 ppm is clearly visible. In Fig 3-12B the activation temperature has been raised to 400°C, and the coverage has been increased to about 0.89 molecules per nm^2. The same two species are still detected, although at this higher coverage the shoulder at -25 ppm is less distinguishable. In Fig. 3-12C and 3-12D a TiO_2(300) sample is in contact with what amounts to 4.17 PMe_3 molecules per nm^2. Two peaks are present, one at about -30ppm, showing none of the structure that was present in this

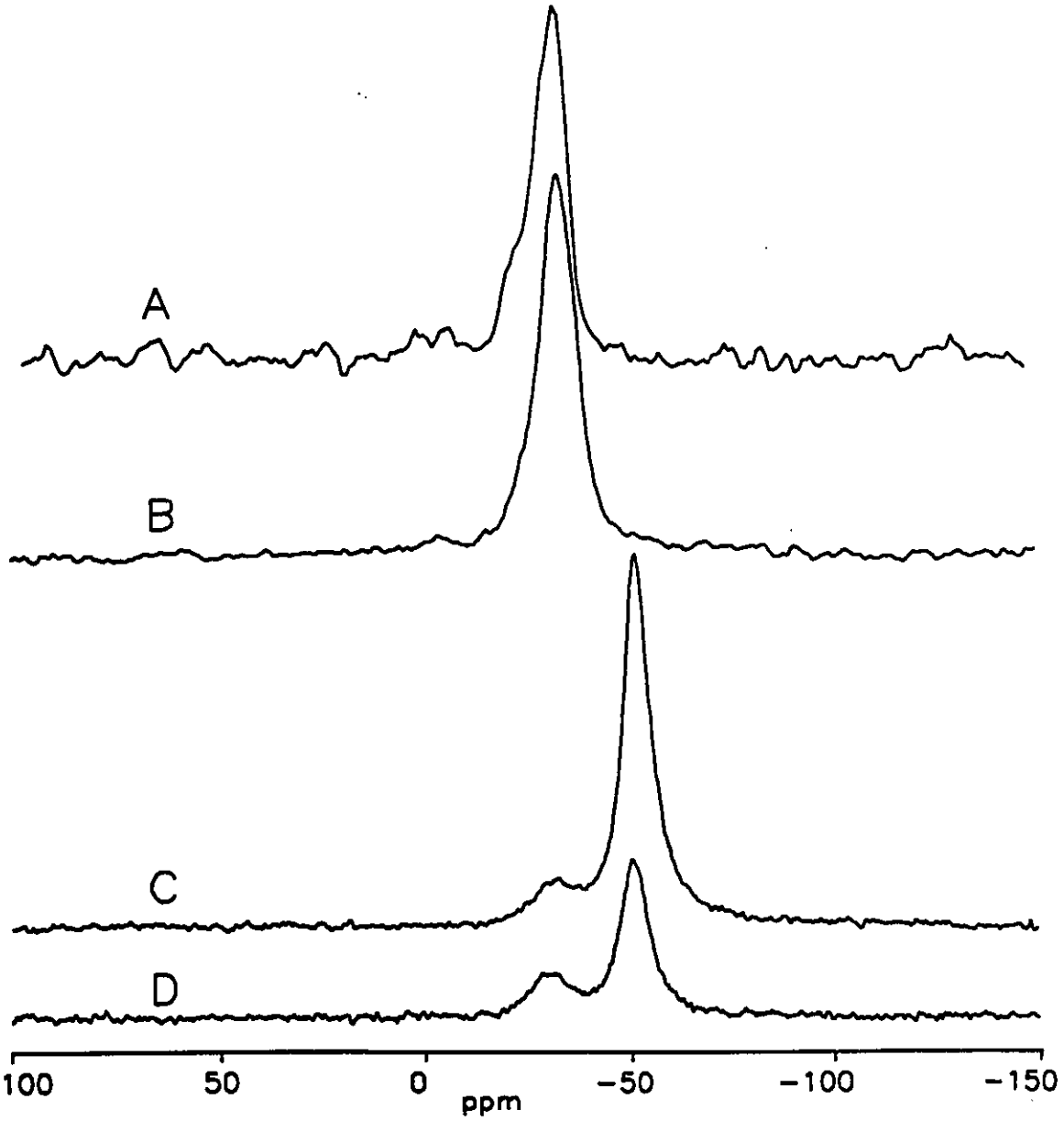

Fig. 3-12: ^{31}P MASNMR Spectra of PMe_3 Adsorbed on TiO_2

A- CP spectrum of 10 μmols of PMe_3 adsorbed on 200 mg TiO_2(235).

B- 90° pulse spectrum of 14.5 μmols of PMe_3 on 190 mg TiO_2(400).

C- 90° pulse spectrum of 61 μmols PMe_3 on 160 mg TiO_2(300).

D- CP spectrum of same sample as curve C.

region at lower coverage, and a second peak at about -51 ppm. This latter peak is relatively more intense in a 90° pulse spectrum than in a cross polarization spectrum. Therefore some or all of the PMe_3 responsible for the signal at -51 ppm is more mobile than that responsible for the -30 ppm peak. From the amount of PMe_3 added and the areas of the peaks in the 90° pulse spectrum, one calculates that the -30 ppm peak accounts for about 0.38 PMe_3 molecules per nm^2. This is a lower number of apparent Lewis acid sites than is observed on either of the other two samples studied, one of which was activated at lower temperature and the other at higher temperature. It thus seems likely that at high coverage some Lewis acid sites participate in chemical exchange, so that intensity in the -30 ppm region is being transferred to the -51 ppm peak.

If one assumes a diameter of 5.5 Å for the PMe_3 molecule as was done in [53], a maximum packing density of about 3.8 molecules per nm^2 would be predicted. Depending on the crystal plane considered, TiO_2 will have a surface cation density in the range of 11 to 14 per nm^2.[57] Potentially there are many more Lewis acid sites than could ever be probed with PMe_3. Most of these sites are probably only weakly Lewis acidic. Coordination of PMe_3 to these "normal" cation sites could give rise to ^{31}P intensity at -51 ppm. A resonance in this region has been observed when PMe_3 is coordinated to weak Lewis acid sites on chlorided Al_2O_3.[49] Since this peak is still quite strong in the cross-polarization spectrum it is reasonable to assign some of its intensity to PMe_3 coordinated to weak Lewis acid sites. Chemical exchange between the -30 ppm peak and the free liquid (δ=-62 ppm) can also be contributing to the -51 ppm signal. Maciel [47] found that even low temperature studies do not give an unambiguous indication of when to consider intensity in this region as being due to weakly coordinated PMe_3 or to the free

liquid. For this reason the authors of both [47] and [35] agree that there is no spectroscopic "end-point" to allow the quantification of weak Lewis acidity by NMR of adsorbed PMe_3, and the apparent number of Lewis acid sites deduced by this method must always be considered as a lower bound to the true number.

Adsorption of PMe_3 on Sulfated TiO_2

Fig. 3-13 shows infrared spectra of PMe_3 adsorbed on TiO_2 that has been doped to 200 μmols/g with H_2SO_4. In each case the cell has been evacuated at room temperature after exposure to the sample to a large excess of PMe_3, and spectra are shown for increasing activation temperature of the catalyst. By analogy with the results for fluorided Al_2O_3, the peaks at 3004 and 2924 cm^{-1} in Fig. 3-13A are due to protonated PMe_3, and those at 2906 and 2972 cm^{-1} are due to Lewis coordinated PMe_3. A peak at about 2485 cm^{-1} can be assigned to ν(P-H) of protonated PMe_3. As the activation temperature is raised the peaks due to protonated PMe_3 lose intensity while those due to coordinated PMe_3 become stronger. When the activation temperature is raised to 400°C, most of the sulfate decomposes [58], and the spectrum of adsorbed PMe_3 resembles that observed on pure TiO_2.

At lower activation temperatures the infrared spectrum of sulfated TiO_2 has a strong peak at about 1380 cm^{-1} due to sulfate species that bear no proton and hence cannot act as Brønsted sites [58]. This peak has been shown to be due to a single (ie vibrationally uncoupled) S=O oscillator. Several other strong peaks are observed in the 1200-1000 cm^{-1} region, and are due to the vibrations of coupled S-O oscillators, as well as surface hydrogenosulfate species.[58] The

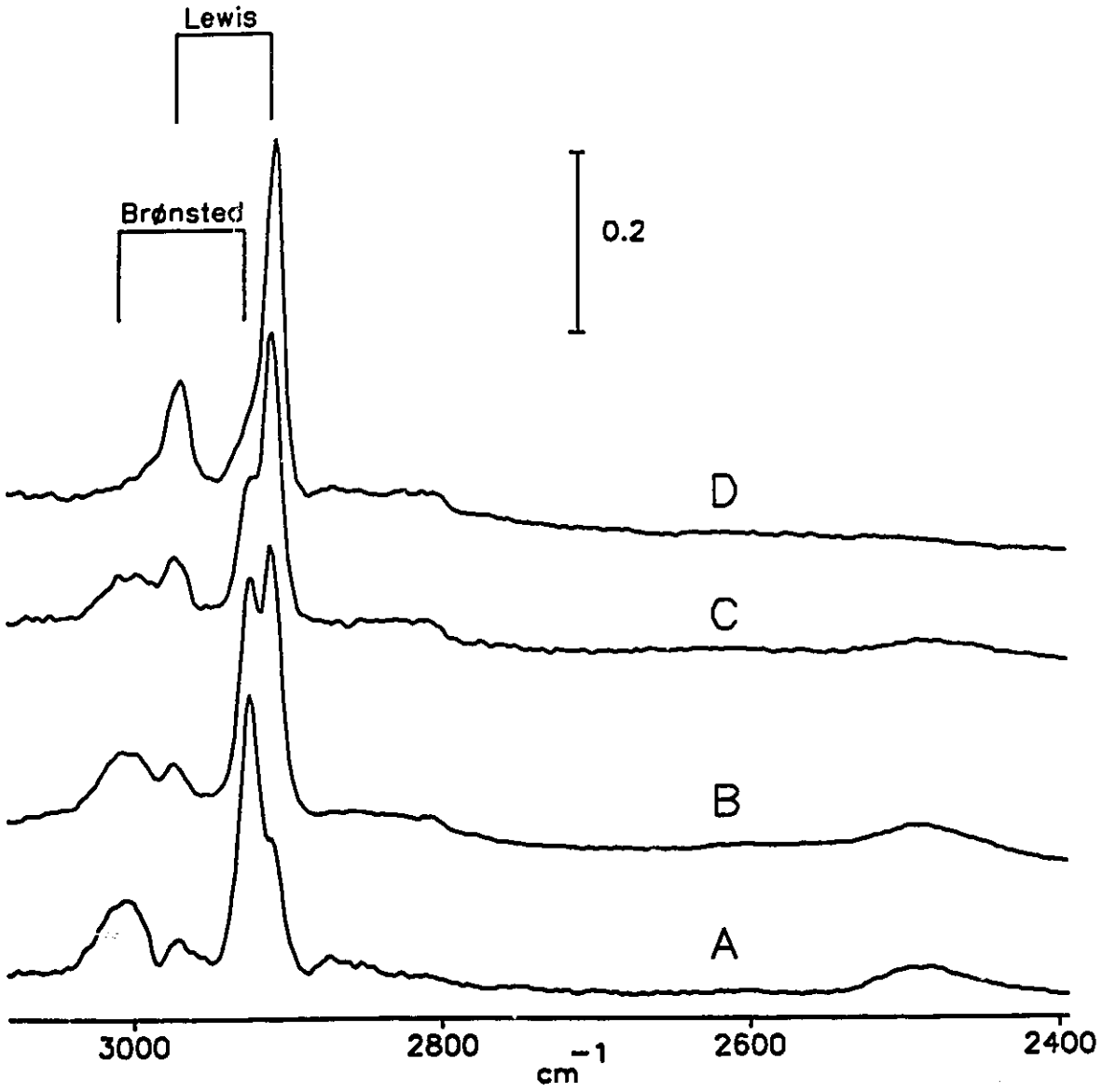

Fig. 3-13: PMe_3 Adsorption on TiO_2(200μmols/g H_2SO_4)

All samples have been exposed to excess PMe_3 and then evacuated at room temperature. The activation temperature were 100°C for curve A, 200°C for B, 300°C for C and 400°C for curve D.

1380 cm^{-1} peak is always strongly decreased in intensity when PMe_3 is adsorbed, being replaced by a strong and very broad band at about 1300 cm^{-1}. The spectra in the region 1300-1000 cm^{-1} were very complex, due to the presence of different sulfate bands. If sulfate were being reduced by PMe_3 a band due to ν(P=O) near 1180 cm^{-1} would be expected, but its presence would be difficult to establish due to the clutter in this spectral region. NMR spectroscopy shows that there is normally very little oxidation of PMe_3 when it is adsorbed on sulfated TiO_2. The reduction of intensity of the 1380 cm^{-1} peak is not solely due to reduction of sulfate by PMe_3. Surface sulfate groups either act as Lewis acid sites, or are perturbed by adsorption of PMe_3 on very nearby Lewis acid sites.

No fewer than four sets of samples of PMe_3 adsorbed on TiO_2(200μmols/g H_2SO_4) were prepared in Ottawa and sent to Vancouver for NMR analysis. In all of these samples oxidation of PMe_3 had occurred to some extent. In one sample the only peak observed was at 70 ppm, the chemical shift expected for Me_3P=O interacting with a strong Brønsted acid site.[56] PMe_3 is very readily oxidized to Me_3P=O, so that it might well be expected to reduce surface sulfate species, or even TiO_2 since Ti^{3+} is a fairly stable oxidation state. What was disturbing was that the spectra of all the sets of samples were different; it was impossible to obtain reproducible results on samples that were not run very shortly after preparation.

Fig. 3-14 shows the 90°-pulse MASNMR spectra of PMe_3 adsorbed on a set of sulfated TiO_2 samples that were prepared in Vancouver, so that the spectra could be obtained within a few hours of sample preparation. It is apparent that there is almost no oxidation of PMe_3 occurs in this case. The peak at about 26 ppm in Fig. 3-14D is not a spinning sideband. A weak peak at this chemical shift was also observed by Lunsford [53], but no assignment was given. It is still

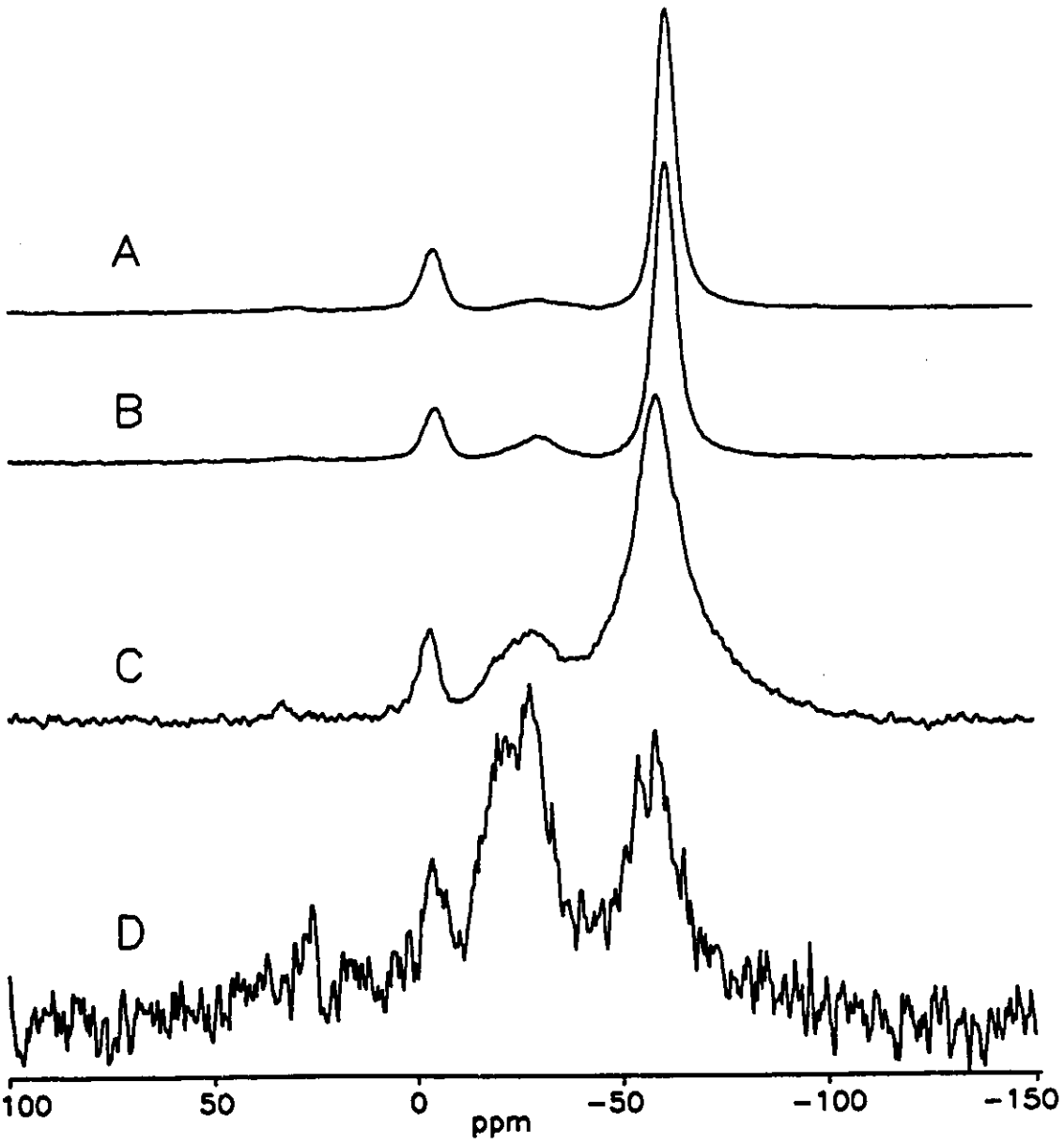

Fig. 3-14: ^{31}P MASNMR of PMe_3 adsorbed on TiO_2(200μmols/g H_2SO_4)

A- 101 μmols of PMe_3, 0.178g of sample activated at 100°C.

B- 102 μmols of PMe_3, 0.176g of sample activated at 200°C.

C- 102 μmols of PMe_3, 0.166g of sample activated at 300°C.

D- 93 μmols of PMe_3, 0.192g of sample activated at 400°C.

unclear to what species this peak is to be assigned. Dimethylphosphine oxide, $Me_2P(H)=O$, has a chemical shift of 21 ppm [59], but delayed decoupling showed that the species responsible for the 26 ppm peak in Fig. 3-14D does not have a proton directly bonded to the phosphorus atom. The residual peak at -3 ppm in Fig. 3-14D did disappear in a delayed decoupling experiment, so it is due to Me_3PH^+, and there really is a little residual Brønsted acidity remaining on this surface.

The ratios of the areas of the peaks at -3ppm to the total integrals in Fig. 3-14A 3-14B and 3-14C imply the presence of 93 μmols/g, 68 μmols/g and 42 μmols/g of non-exchanging Brønsted acid sites in each sample respectively. This seems like a credible quantity of Brønsted acidity, given that 200 μmol/g of H_2SO_4 was added, but that it reacts extensively with the surface. A curve-fitting procedure led to Lewis acid amounts of 30 μmols/g, 60 μmols/g and 103 μmols/g for the samples in 3-14A, 3-14B and 3-14C respectively. (These numbers are based on the total area of the peaks near -30 ppm.) The Lewis acidity of the samples increases as the Brønsted acidity decreases, as was observed in a more qualitative manner by infrared spectroscopy.

No attempt was made to quantify the data for the 400°C activated sample. As is apparent in Fig. 3-14D this would probably not be meaningful. It appears that the sample has been reduced by heating under vacuum at 400 °C, and signal is being lost due to interaction of PMe_3 with paramagnetic sites. The peaks in this spectrum are broadened substantially, and the signal has become rather weak compared to the other samples. All of these spectra represent roughly 1500 scans with a one second delay between scans. The higher noise level in Fig. 3-14D actually indicates a much weaker signal from this sample.

Adsorption of PMe_3 by ZrO_2 and Sulfated ZrO_2

As was the case for PMe_3 adsorption on TiO_2, the infrared study of the interaction of PMe_3 with ZrO_2 gave evidence for H-bonded and coordinated PMe_3, but there was no spectroscopic indication of the presence of different distinct Lewis acid sites. NMR spectroscopy was more effective for this purpose, as shown in Fig. 3-15.

It has been estimated that ZrO_2 will have a surface cation density of about 7.5 per nm^2.[57] In Fig. 3-15 only about one PMe_3 molecule per nm^2 has been allowed to absorb on a ZrO_2(450) sample. The 90°-pulse and cross-polarization spectra show the same peaks with the same relative intensities, so that all the species present at this coverage are rigidly held. Peaks due to PMe_3 coordinated to Lewis acid sites of different strength appear at -28, -36 and -42 ppm. A weak peak in Fig. 3-15B at about 34 ppm is possibly due to $Me_3P{=}O$.

In Fig. 3-16 excess PMe_3 has been added to a series of sulfated zirconia samples that have been activated at various temperatures. These catalysts have been doped with 200 μmols per gram of H_2SO_4, as was done for sulfated TiO_2. This corresponds to about 2.7 sulfate groups per nm^2. A simple estimate of the area required by a sulfate group based on the density of H_2SO_4 leads to a prediction of 4.5 sulfate groups per nm^2 for complete coverage of the surface.

As for sulfated TiO_2 samples, the only species present are protonated PMe_3 (- 3ppm), coordinated PMe_3 (composite peak centred near -35 ppm) and excess free PMe_3 (-62ppm). Fripiat *et. al.* [60] observed sharp peaks at 26ppm and 23ppm when PMe_3 was adsorbed on sulfated zirconia, and attributed these peaks to PMe_3 interacting with very strong Lewis acid sites. These peaks were not observed in the present study, for pure or sulfated zirconia, for any

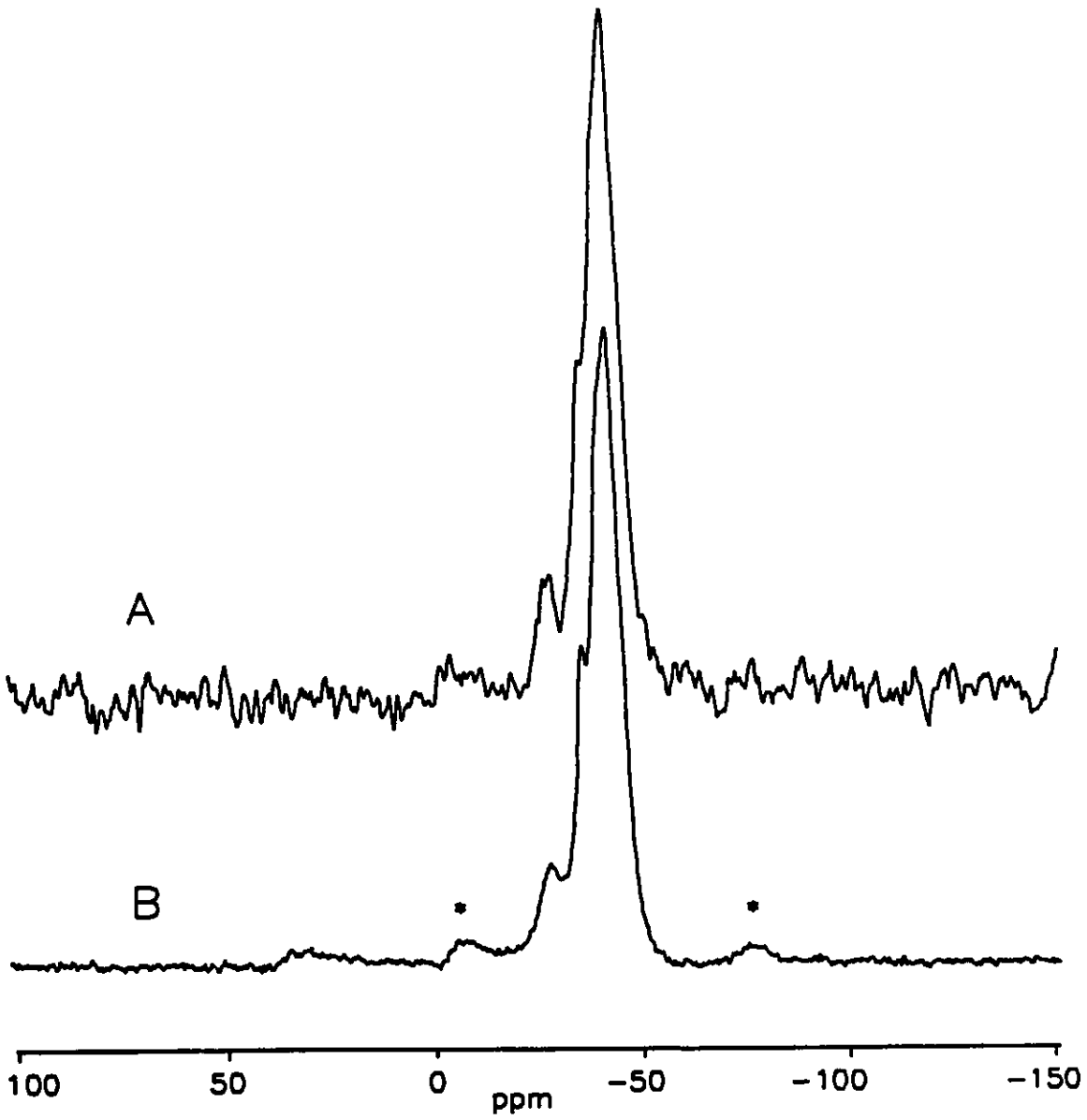

Fig. 3-15: ^{31}P MASNMR Spectra of PMe_3 Adsorbed on ZrO_2(450)

A- 90°-pulse spectrum.

B- Cross-polarization Spectrum.

Asterisks indicate spinning sidebands.

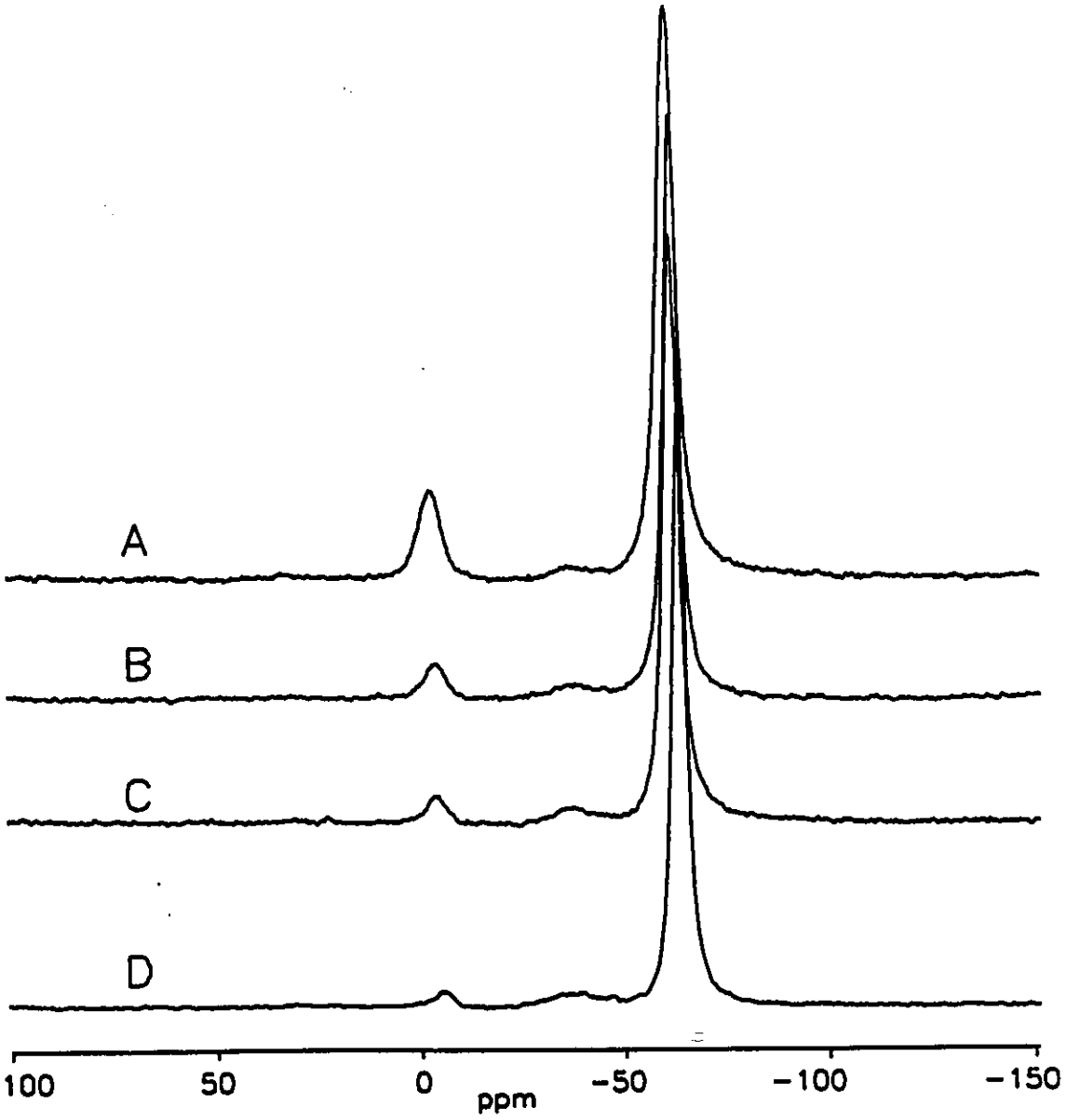

Fig. 3-16: 90°-Pulse MASNMR Spectra of PMe_3 Adsorbed on ZrO_2(200μmols/g H_2SO_4)

A- 143 μmols of PMe_3 interacting with 297 mg ZrO_2(200μmols/g H_2SO_4, 100)

B- 122 μmols of PMe_3 interacting with 187 mg ZrO_2(200μmols/g H_2SO_4, 200)

C- 122 μmols of PMe_3 interacting with 180 mg ZrO_2(200μmols/g H_2SO_4, 300)

D- 130 μmols of PMe_3 interacting with 190 mg ZrO_2(200μmols/g H_2SO_4, 400)

coverage or activation temperature. This would appear to corroborate the opinion of Lunsford [61], who maintains that peaks in this region are probably not due to Lewis bound PMe_3. The same peaks have sometimes been observed when PMe_3 is adsorbed on zeolites, although to what species they are to be assigned remains unclear.[53,61] The proposition that they are due to PMe_3 coordinated to super-acidic sites peculiar to sulfated zirconia seems untenable.

Integrals of the spectra in Fig. 3-16 lead to the following densities of non-exchanging Brønsted and Lewis sites:

Table 3-1: Apparent Site Densities on ZrO_2(200μmols/g H_2SO_4)

Activation Temperature °C	Brønsted Site Density μmols/g	Lewis Acid Site Density μmols/g
100	62	17
200	44	40
300	26	33
400	18	43

In [61] rather higher site densities were obtained; for example for activation at 100°C 160 μmols/g of Brønsted acid sites were observed. The specific area of the sulfated zirconia samples were not given, so the significance of the difference cannot be assessed. In common with [61] it is found that although the Brønsted site density decreases with increasing activation temperature, above 200°C there is no concomitant increase in the density of Lewis acid sites. Presumably as the surface is dehydrated and Brønsted acidity is lost, a zirconium sulfate surface

phase that weakly Lewis acidic compared to pure zirconia is generated. In the case of sulfated TiO_2, degassing at 400°C caused most of the surface sulfate to decompose, as evidenced by the near total disappearance of the 1380 cm^{-1} sulfate band.[58] The resulting surface shows increased Lewis acidity compared to lower outgassing temperatures. The 1380 cm^{-1} band observed in the infrared spectrum of sulfated zirconia loses only a small fraction of its intensity when the samples are degassed at 400°C.

For the quantitative interpretation of the NMR spectra of PMe_3, one must perform signal averaging with a delay between scans that is large compared to the phosphorus T_1.[35] For the sulfated TiO_2 samples and for most of the sulfated ZrO_2 samples no measurements were made of T_1. Instead spectra were recorded with a one second delay between scans, and it was checked for most samples that no significant change in relative intensities occurred when spectra were acquired with a two second delay between scans. For the ZrO_2(200μmols/g H_2SO_4, 400) sample a series of spectra allowing the determination of T_1 for each species present was acquired. In this experiment a first FID is acquired after a single 90°-pulse. After a delay long compared to T_1, a second FID is acquired after a 180°-pulse, a delay of τ milliseconds, and a final 90° pulse. The second FID is subtracted from the first. One obtains a series of spectra, one for each τ value. If longitudinal relaxation is exponential, the area of each peak decreases as $\exp(-\tau/T_1)$. T_1 is then given by the negative reciprocal of the slope of a plot of the natural logarithm of the signal area against τ. The resulting plots are shown in Fig. 3-17. The plots for free and protonated PMe_3 are quite linear, leading to T_1 values to 24 and 41 milliseconds respectively. For Lewis bound PMe_3 the plot is not as linear. This could be due to non-exponential relaxation, but could just as easily be due to inaccuracy in the assigned peak areas, as the separation of the

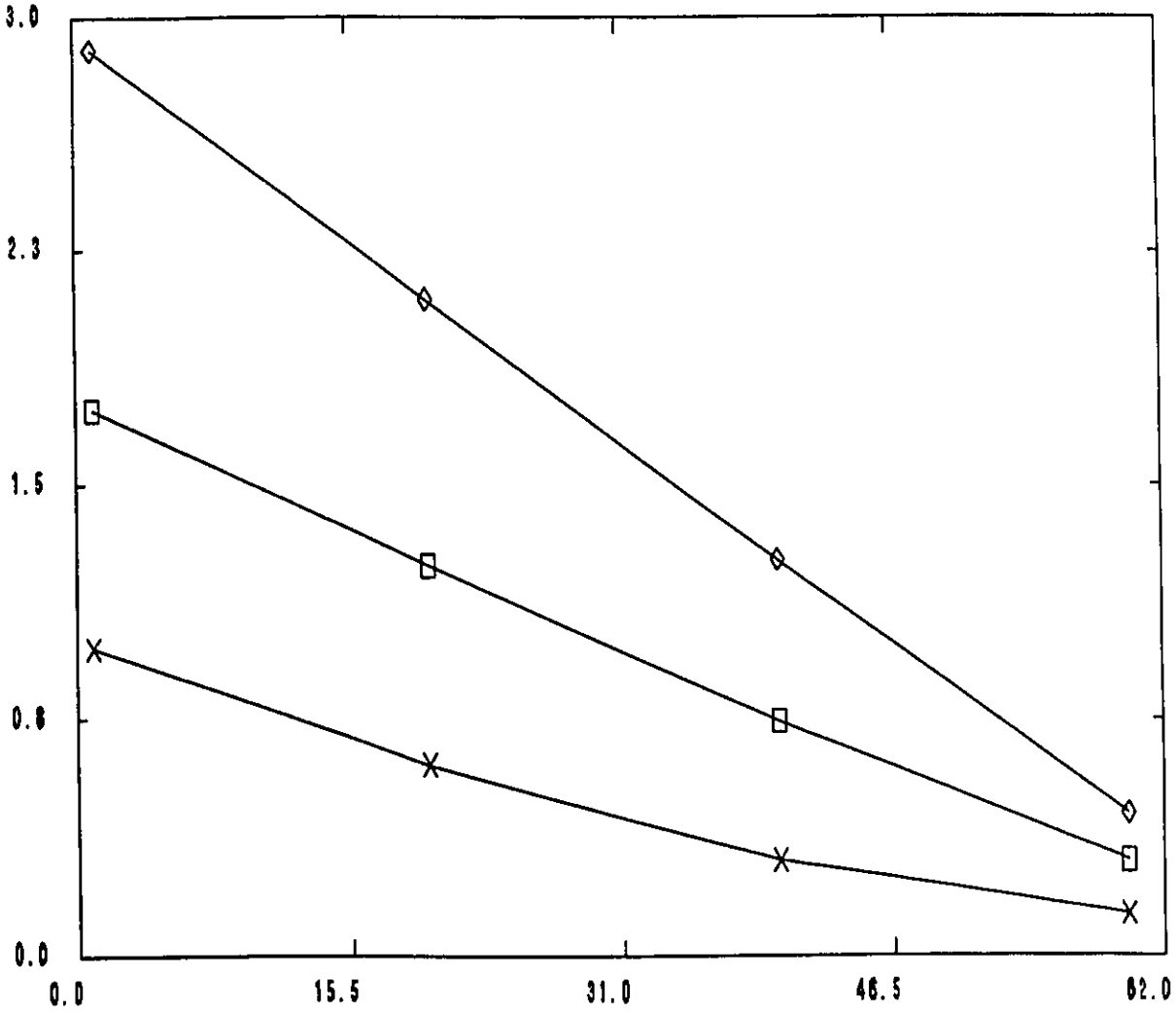

Fig. 3-17: Plot for ^{31}P T_1 Measurement of PMe_3 on ZrO_2(200μmols/g H_2SO_4, 400)

◇- Free PMe_3 (9)

□- Protonated PMe_3 (75)

x- Lewis bound PMe_3 (15)

For ease of presentation the peak areas were scaled by the values in parentheses before taking natural logarithms.

areas due to Lewis bound PMe_3 and the much more abundant free PMe_3 is a rather arbitrary and uncertain procedure. The least squares slope for this plot leads to a T_1 value of about 70 milliseconds, so that regardless of whether the relaxation is exponential or not, a delay of 1 second between scans is ample time to allow for relaxation.

The preparation of super-acidic sulfated zirconia catalysts has been shown to be rather complex, in that the acidity of the catalyst ultimately prepared is sensitive to many variables.[62] It is generally agreed that the surface sulfate density is an important parameter,[62,63] and that Brønsted acidity only becomes important at a surface sulfate density above about two per nm^2. Neither infrared nor NMR spectra of PMe_3 adsorbed on ZrO_2(200μmols/g H_2SO_4) showed any unusual features that might be related to the alleged super-acidity of sulfated zirconia. Therefore higher sulfate densities were investigated.

Fig. 3-18 shows NMR spectra of PMe_3 adsorbed on ZrO_2(1000μmols/g). This corresponds to a doping level of about 13.4 sulfate groups per nm^2, the equivalent of several monolayers. In Fig. 3-18A the spectrum has been acquired as soon as possible after the PMe_3 has been allowed to warm up from liquid nitrogen temperature and interact with the catalyst. (About 15 minutes were required to obtain this spectrum.) Three peaks are evident in this spectrum. The peak at -60 ppm is near the position of the free liquid, but its appearance in this spectrum indicates this resonance is due to a species immobile enough to be cross-polarized. The peak is also very broad compared to the free liquid. Perhaps this species is involved in chemical exchange. The peak at -3ppm is due to Me_3PH^+. This is the chemical shift expected for this species, and this peak disappears in a delayed decoupling experiment. The new very narrow peak at 1.5 ppm also disappears in delayed decoupling. It is therefore tempting to attribute the 1.5 ppm to a new

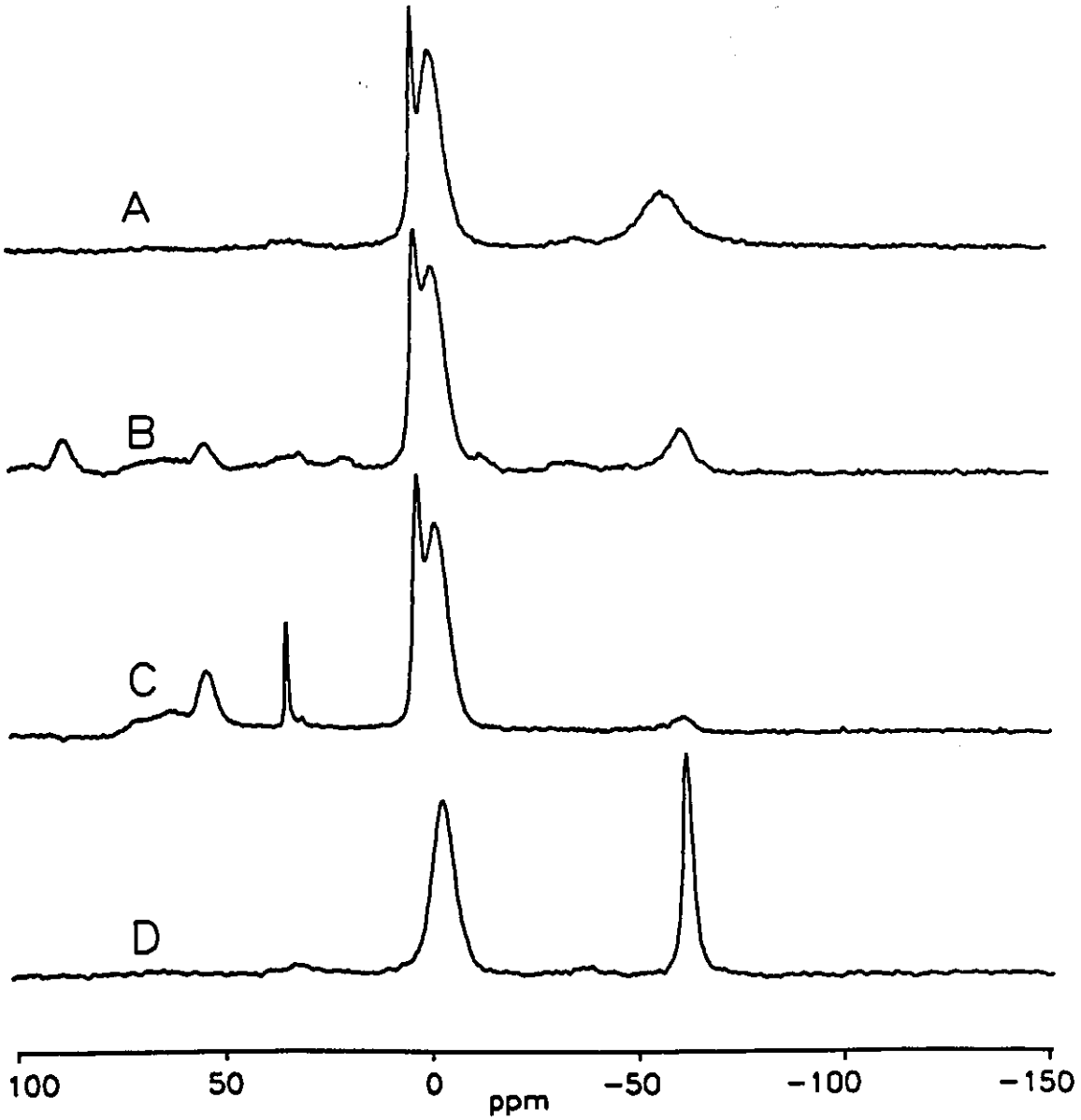

Fig. 3-18: ^{31}P MASNMR Spectra of PMe_3 Adsorbed on ZrO_2(1000μmols/g H_2SO_4)

A- 123 μmols PMe_3 on 201 mg of catalyst activated at 100°C. CP spectrum.

B- Same sample as in A. CP spectrum after 90 minutes reaction.

C- Same sample as in A. CPTOSS after 21 hours reaction.

D- 135 μmols PMe_3 on 200 mg catalyst activated at 190°C. CP spectrum.

Me_3PH^+ species, perhaps created by super-acidity of the sample. A chemical shift of 2.71 ppm has been reported for the CF_3SO_3H salt of PMe_3[64], so that as far as existing data indicate, increased chemical shift appears to be associated with increasing acid strength.

The spectrum in Fig. 3-18B was acquired about ninety minutes after that shown in Fig. 3-18A. It is evident that peaks due to pentavalent phosphorus species are growing with time. The CPTOSS spectrum in Fig. 3-18C was acquired after about twenty-one hours. Peaks due to P(V) species appear at 30, 34, 53, 62 and 69 ppm. The very sharp peak at 34 ppm has extensive spinning sidebands when these are not suppressed, and the stronger sidebands appear to low field. These facts and the peak's position suggest it is due to crystalline $Me_3P=O$, since this molecule has δ=34 ppm and principal shielding components 102, 102 and -96 ppm.[65] The peaks above 50 ppm can be due to different forms of Lewis bound $Me_3P=O$, as this gives multiple peaks in the 40 to 60 ppm region on zeolite HY, or also to protonated $Me_3P=O$, which is said to give peaks at 65 and 74 ppm on zeolite HY.[56] $Me_3P=S$ may also be present; its chemical shift is 59 ppm.[65] Assigning each peak to a definite species is difficult and probably unimportant, as the appearance of all the peaks due to P(V) species is probably due to reaction of PMe_3 with free H_2SO_4. When the sample is activated at 190°C prior to PMe_3 adsorption, droplets of liquid were observed on the inside of the glass just beyond the region heated by the furnace. This was probably H_2SO_4. When PMe_3 is adsorbed on this sample no P(V) species are observed. As shown in Fig 3-18D, the 1.5 ppm peak due to the new Me_3PH^+ species is not observed either. This suggests the 1.5 ppm species is simply PMe_3 in 100% H_2SO_4 that is adhering to the zirconia surface. This may be so, but the 1.5 ppm species could not be generated on Al_2O_3 that had been doped to the same surface sulfate density. ZrO_2 appears to be unusual in its ability to stabilize

the 1.5 ppm species.

Sample of ZrO_2(1000μmols/g H_2SO_4) degassed at higher temperatures showed decreased amounts of Brønsted acidity, but virtually no Lewis acidity developed.

Conclusions

PMe_3 adsorbs only weakly on silica via hydrogen bonding. After activation at extreme temperatures a Lewis acid base interaction with defect sites can be detected. PMe_3 can also interact with Al_2O_3 via hydrogen bonding. On activated Al_2O_3 a Lewis acid base complex is formed, and resolved scalar coupling is observed in the NMR spectrum. This demonstrates direct P-Al bonding. On fluorided Al_2O_3 this scalar coupling is unresolved. This probably indicates a more heterogeneous distribution of Lewis acid sites. A small population of Brönsted acid sites is observed on fluorided Al_2O_3. On sulfated titania and zirconia, strong Brönsted and Lewis acidity could be titrated with PMe_3. Weak acidity was impossible to quantify, both because of chemical exchange effects and because of the steric requirements of the PMe_3 as a probe.

On all oxides except silica, a portion of the PMe_3 was adsorbed strongly enough that it could not be desorbed without decomposition.

CHAPTER 4

An Infrared and ^{31}P MAS NMR Study of the Adsorption of PCl_3 and $OPCl_3$ on Silica

Introduction

The infrared spectrum of PCl_3 adsorbed on silica has been studied by Bogatyrev and Chuiko [70] who observed the appearance of two broad IR bands due to perturbed isolated surface silanols near 3650 and 3500 cm^{-1}. Although no specific attribution was specified for either band, they assumed that two different structures could result from the interaction between physically adsorbed PCl_3 and SiOH.

An additional IR band was reported at 605 cm^{-1} which was attributed to the antisymmetric PCl stretching mode of PCl_3 coordinated to SiOH. However, for pure PCl_3 the antisymmetric and symmetric PCl_3 stretching modes [71] lie between 515 and 487 cm^{-1} and such a large high wavenumber shift would not be expected for any molecular complex [72].

Because ^{31}P NMR spectroscopy can be additionally used to study the adsorption and reactions of this compound on silica, and because of the anomaly reported above, we have undertaken a re-investigation of this system using both IR and solid state NMR spectroscopy. In order to unravel some of the reaction paths of PCl_3, we have also studied the adsorption of

$O{=}PCl_3$, H_3PO_3 and H_3PO_4 on silica.

Experimental

The NMR spectra were recorded at either 1.4 or 3.5 T, giving ^{31}P resonance frequencies of 24.3 and 60.5 MHz respectively. The magic angle spinner has been described [73], and all spectra were proton decoupled. The spectra of PCl_3 treated SiO_2 were recorded at 24.3 MHz using either 90° pulse excitation or cross-polarization with a 2 ms contact time, with 2.5 kHz magic angle spinning. The spectra of H_3PO_4 treated SiO_2 were also obtained at 24.3 MHz, with 3kHz MAS. For higher activation temperatures extensive dehydroxylation of the H_3PO_4 treated SiO_2 samples made the acquisition of cross-polarization spectra impossible. Furthermore, for H_3PO_4 treated SiO_2 samples activated at 400°C, the ^{31}P T_1 was too long to permit 90° pulse spectra to be obtained without the addition of about 300 torr of O_2 to the sample tube. Addition of dry O_2 to these samples had no effect that could be observed by infrared spectroscopy. For lower activation temperatures spectra were acquired using 90° pulses but O_2 was not added. It is doubtful that any of the H_3PO_4 treated SiO_2 spectra are fully relaxed, and these spectra cannot be interpreted quantitatively. Since these spectra are only used for qualitative purposes this limitation is not important. The NMR spectra of H_3PO_3 treated SiO_2 were obtained at 60.5 MHz and about 2.5 kHz MASS. These samples could not be activated above 200°C without extensive decomposition, as shown by the loss of intensity of $\nu_{P\text{-}H}$ in the infrared. The spectra presented here were aquired using cross-polarization. The extensive sidebands present at this higher magnetic field were suppressed by using a TOSS sequence.

In the descriptions below, we will write SiOP=O(X,Y) for a structure

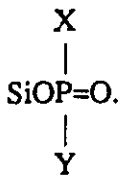

Results

(a) Short adsorption times:

The infrared spectrum of SiO_2 after vacuum activation is shown in Fig. 4-1. As explained in Chapter 1, the sharp peak at 3747 cm^{-1} is due to non-interacting surface silanol groups [SiOH or $Si(OH)_2$] and the broader features below 2000 cm^{-1} are due to fundamentals or combinations and overtones of SiO_2 modes of the substrate [15,16]. PCl_n stretching modes [71,74,75] lie between 700 and 400 cm^{-1} (however, silica is totally absorbing below 550 cm^{-1}), and P=O stretching vibrations are expected to lie between 1320 to 1100 cm^{-1}. In the latter spectral range, only higher wavenumber P=O vibrations would be expected to be observed in view of the steeply rising background absorption of silica, the practical limit of IR transmission being near 1275 cm^{-1}. The IR spectra shown in Fig. 4-2 and 4-3 are presented as difference spectra after subtraction of the silica background following adsorption of a given compound.

Fig. 4-2A shows the spectral changes observed in the OH stretching region following adsorption of PCl_3 on silica; there was a decrease in the intensity of the isolated silanol peak at 3747 cm^{-1} (the sharp band pointing down) accompanied by the appearance of two broader bands to lower wavenumber at 3650 and 3500 cm^{-1} (peaks pointing upward). Accompanying these changes, additional bands were observed at 605 and 1290 cm^{-1} (Fig. 4-3A). The spectral features in the OH region, and at 605 cm^{-1}, were similar to those previously reported by Bogatyrev and

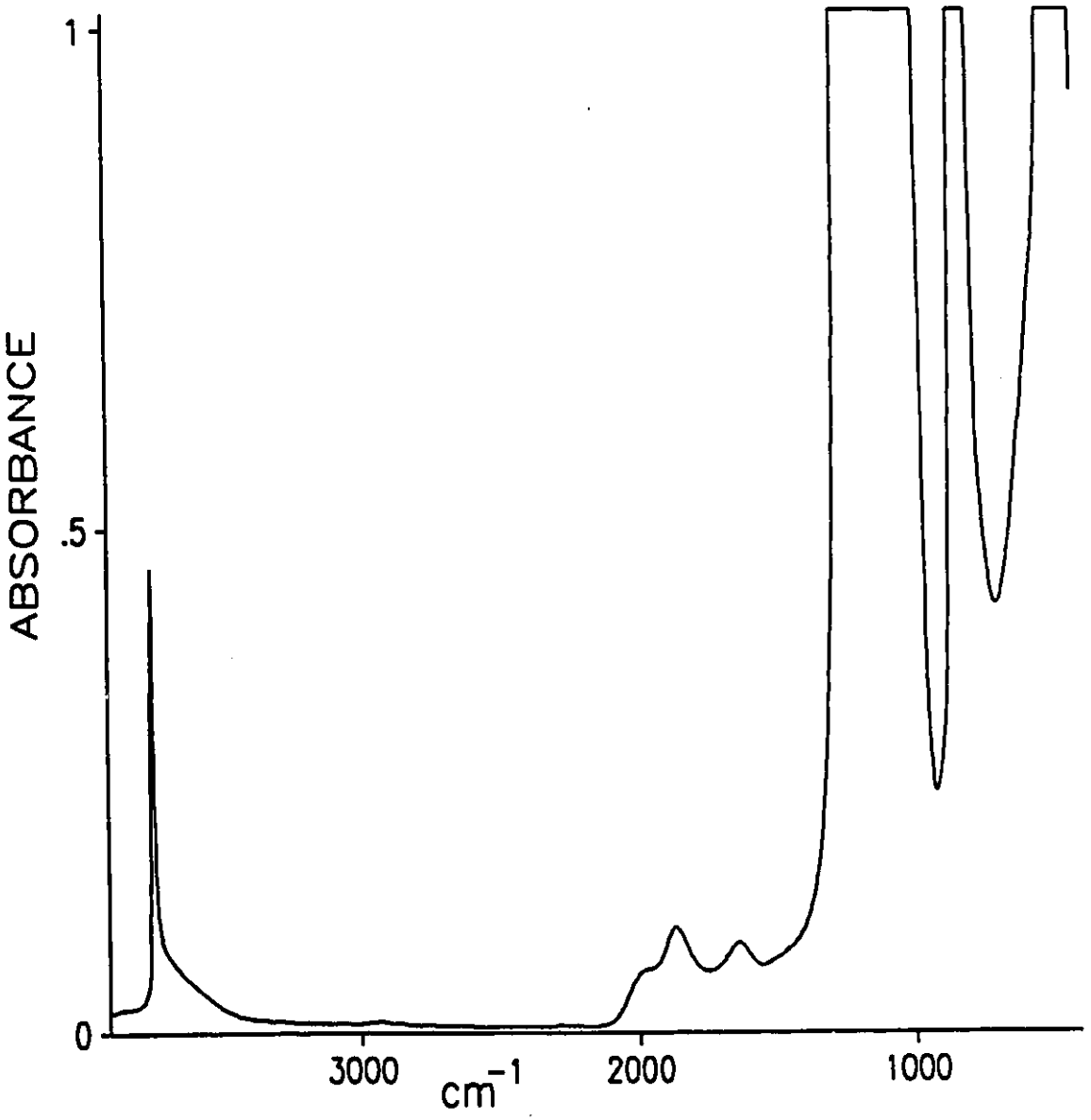

Fig. 4-1: Background infrared spectrum, at room temperature, of a silica disc after 1 hour activation at 450°C. The quantity of SiO_2 used was 4 mg/cm^2. Spectra shown in Fig.4-2 and Fig 4-3 are difference spectra obtained after subtraction of this background spectrum.

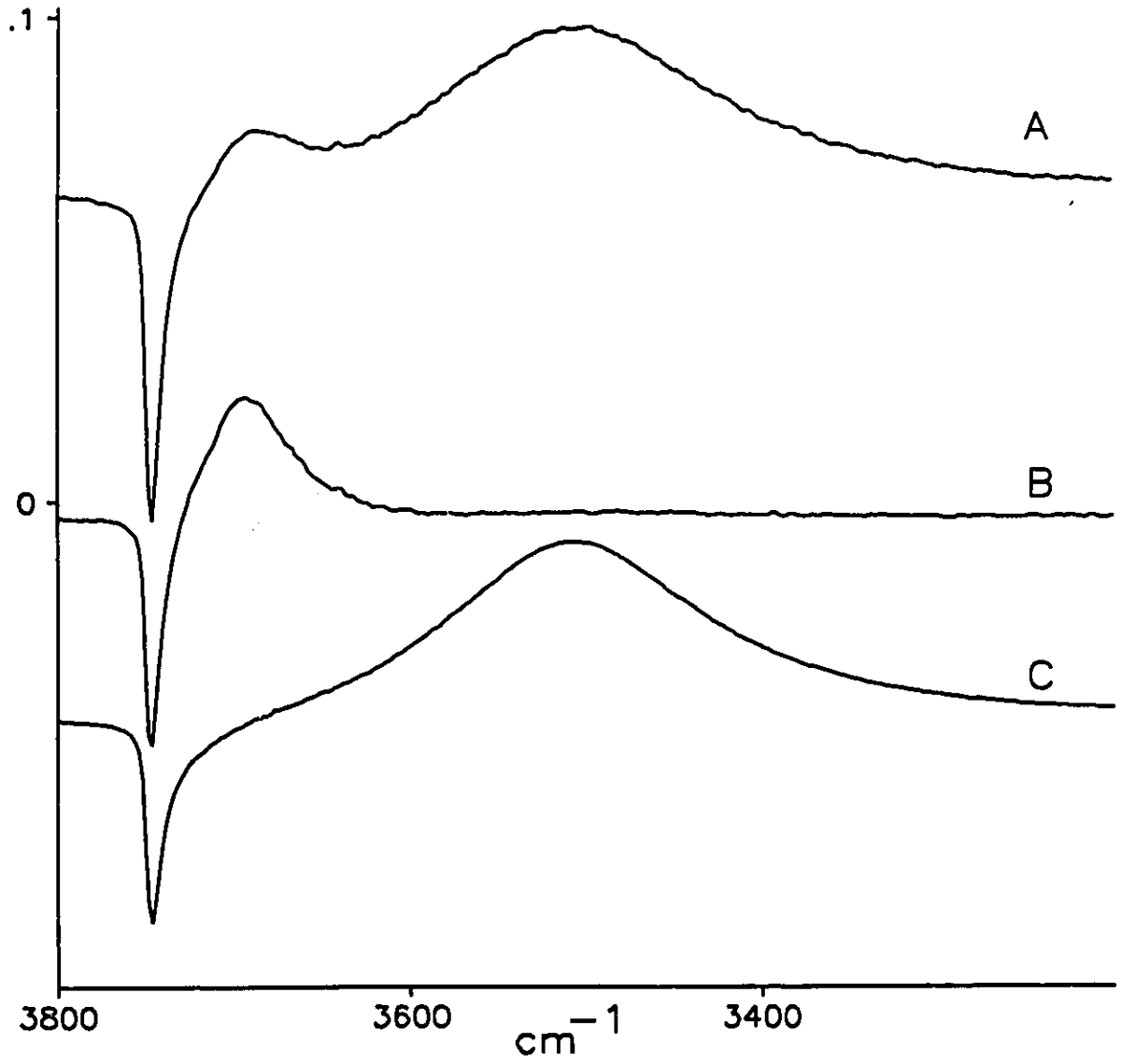

Fig. 4-2: A- IR spectrum after adsorption of an equilibrium pressure of 4.5 Torr of 'as received' PCl_3 on silica. B- As for (A), but with purified PCl_3 (see text). C- As for (A) but with 1 Torr of $OPCl_3$. The absorbance scale applies to curves A and B, curve C is five time more intense (multiply the absorbance scale by 5 for curve C).

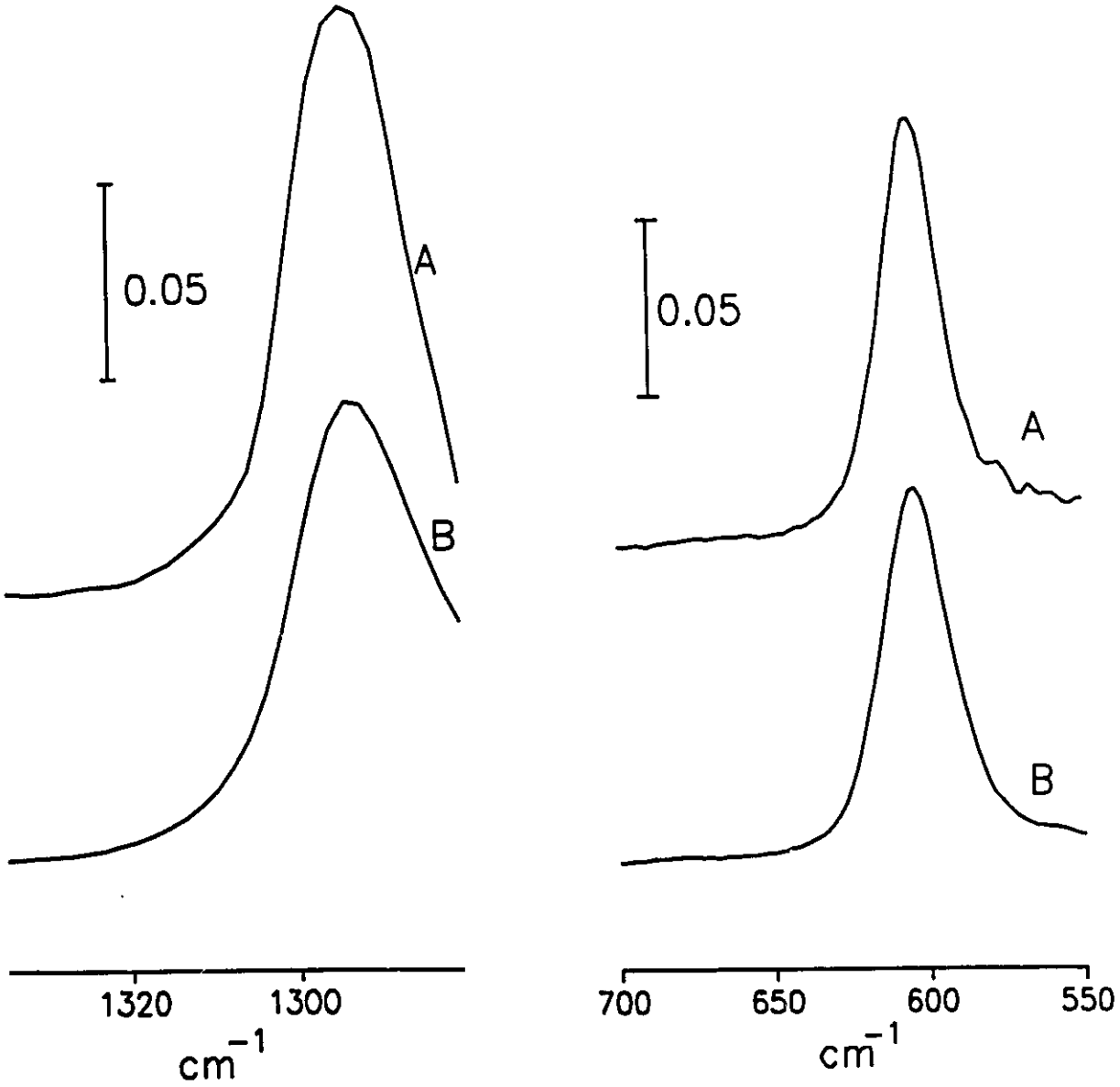

Fig. 4-3: A- Low wavenumber IR spectra of 'as received' PCl_3 adsorbed on silica. B- Similar spectra for pure $O{=}PCl_3$ adsorbed on silica. The intensity scale applies to curve A, the real intensities for curve B are five times greater.

Chuiko [70]. Although the 605 cm^{-1} band could be seen in the window of partial transparency without spectral subtraction, that at 1290 cm^{-1} could not be observed without subtraction because of the rapidly rising silica background in this region. Bogatyrev and Chuiko presumably missed this band because they did not have the ability to carry out background subtraction.

A ^{31}P NMR analysis of the commercially available PCl_3 solution indicated, in addition to a peak at 219 ppm due to PCl_3, a second peak at 3 ppm corresponding to about 1.6% of the total phosphorous. The 3 ppm peak is due to phosphoryl chloride, $OPCl_3$. Table 4-1 lists the vibrational frequencies of the stretching modes of PCl_3 and $OPCl_3$. The IR spectrum of the gaseous as received PCl_3 also revealed, in addition to the strong blended peak near 510 due to the two PCl_3 stretching modes of PCl_3, additional weak bands at 594 and 1323 cm^{-1}, clearly demonstrating that our sample was contaminated with $OPCl_3$.

Table 4-1

Infrared Frequencies (cm^{-1}) of PCl_3 and $OPCl_3$

	PCl_3[a]	$OPCl_3$ (gas)[b]	$OPCl_3$ (sol'n)[c]	PCl_3 (SiO_2)[b]	$OPCl_3$ (SiO_2)[b]
ν(P=O)	-	1323	1300-1310	-	1290
$\nu_{as}(PCl_3)$	515	594	586-594	n.o.*	605
$\nu_s(PCl_3)$	505	482	482-487	n.o.	n.o.

a = ref. [71a], *b* = this work, *c* = ref. [75]

* n.o. = not observed.

Phosphoryl cloride can be removed from PCl_3 by briefly contacting the mixture with dry $AlCl_3$. The IR bands due to $OPCl_3$ were removed, and an IR spectrum observed following adsorption of purified PCl_3 on silica did not show the 605 and 1290 cm^{-1} peaks. Further, the perturbed silanol band at 3500 cm^{-1} was also not observed; only that at 3650 cm^{-1} remained (Fig. 4-2B). Conversely, adsorption of pure $OPCl_3$ on the same silica sample gave IR bands at 3500 (Fig. 4-2C) 1290 and 605 cm^{-1} (Fig. 4-3B). The assignments for both compounds adsorbed on SiO_2 are shown in Table 4-1. Although it might seem surprising that $OPCl_3$ as such a low level impurity in PCl_3 could give IR bands of significant intensity, the phosphoryl group confers a significant basicity to this compound [76], and it would be selectively adsorbed by silica. Accordingly, the $OPCl_3$ perturbed silanol band is at a lower wavenumber than that which is perturbed by PCl_3. Finally, the shift of ν(P=O) to lower wavenumber and of $\nu_{as}(PCl_3)$ to higher wavenumber for adsorbed $OPCl_3$ relative to gaseous $OPCl_3$ is consistent with a P=O...HO hydrogen bonded interaction.[75]

Following evacuation at room temperature all of the spectral features noted above slowly decreased, and disappeared after about 1 hour evacuation. Therefore, all changes can be attributed to physical adsorption of PCl_3 or $OPCl_3$ on silica. Finally, NMR spectra which were obtained after PCl_3 had been in contact with SiO_2 for up to a few hours showed no additional peaks other than that due to physically adsorbed PCl_3 (see below regarding the formation of chemisorbed species after longer contact times).

(b) Long adsorption times:

If pure PCl_3 was left in contact with SiO_2 for 18 hours, new IR bands at 1290 and a doublet near 2490 cm^{-1} were observed, the latter spectral region being associated with PH stretching modes. These bands could not be removed by prolonged evacuation at room temperature, or even at 150°C. The NMR spectrum after 18 hours adsorption showed new weak peaks at 184 ppm, 24 ppm, -5 ppm and -16 ppm (Fig. 4-4).

By virtue of its chemical shift alone the 184 ppm peak can be assigned to $SiOPCl_2$. A NMR peak at 186 ppm was attributed to this species by Bogatyrev *et. al.* following reaction of PCl_3 with SiO_2 at 320°C [77]; they may also have observed a peak at 156 ppm attributable to $(SiO)_2PCl$. These assignments are reasonable given the following data for similar model compounds [78]:

	NMR	IR
$MeOPCl_2$	181	508/455 cm^{-1} for P-Cl_2
$(MeO)_2PCl$	169	496 cm^{-1} for PCl

The above vibrational frequencies [79] lie in a region of strong SiO_2 absorption and, being at the low wavenumber limit of our spectrometer, the infrared bands due to $SiOPCl_2$ or $(SiO)_2PCl$ would be virtually impossible to observe.

Insight into the nature of the lower frequency NMR signals can be obtained with reference to the NMR spectra of some known Si containing model compounds, and with reference to the

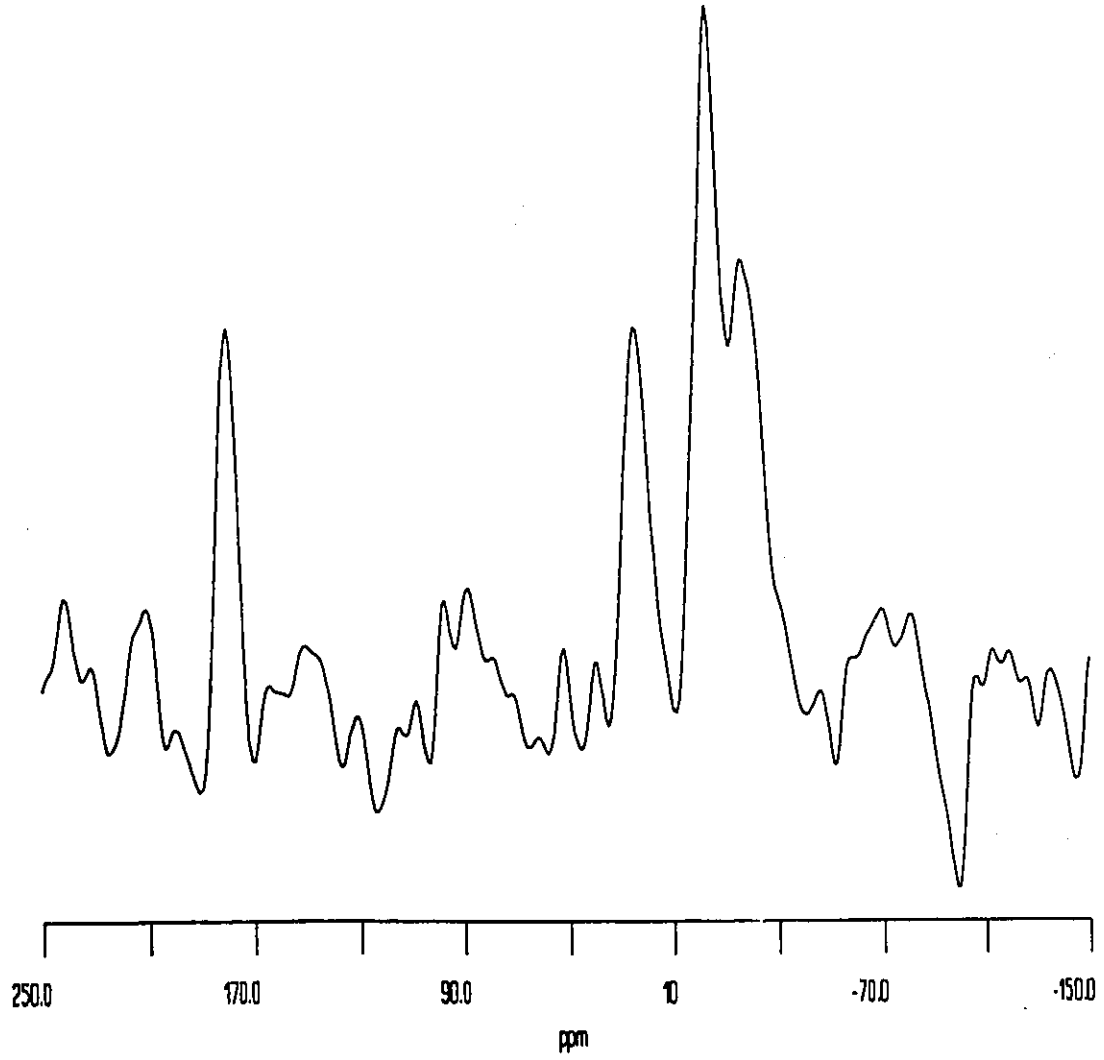

Fig. 4-4: Cross polarization ^{31}P MAS NMR spectrum of pure PCl_3 after 18 hours adsorption on silica.

NMR and IR spectra of H_3PO_3 and H_3PO_4 adsorbed on silica. Although the IR spectrum showed a doublet at 2490 cm^{-1}, the ratio of the intensities of the two components varied from experiment to experiment, suggesting that two P-H containing species were generated. Finally, the chemical shift of H_3PO_4 is 0 ppm; that of H_3PO_3 is 5 ppm in solution [80] and we found that this gave two lines at 8 and 13.2 ppm for the solid. As will be discussed below, the -5 ppm signal is most probably due to SiOP=O(H,OH), and that at -16 ppm is due to the di-adsorbed species, $(SiO)_2P=O(H)$.

Assuming that some of the species generated are chemically bonded to the surface via a SiOP linkage, we have examined the NMR spectra of a series of model compounds which contain varying numbers of Me_3SiO- groups bonded to phosphorus. These are listed below:

COMPOUND	^{31}P NMR SHIFT	REFERENCES
$Me_3SiOP=O(H,OH)$	-1	[81]
$(Me_3SiO)_2P=O(H)$	-14.9 , -14.3, -13.3	[82], [83], [81]
$(Me_3SiO)_3P=O$	-28.3	[84]

The value of the chemical shift need not concern us, but the trend is worth noting, namely an approximately 12-14 ppm shift to lower frequency with each additional SiO attachment to P.

A similar trend can be found in the NMR spectrum of phosphoric acid impregnated silica. Silica was impregnated with phosphoric acid (1.2 P/nm^2), dried in air at 110°C, and placed in an

NMR tube for vacuum treatment at room temperature or at 200 or 400°C prior to sealing the tube. The ^{31}P NMR spectrum of the room temperature evacuated sample gave three resonances at -10, -20 and -35 ppm, the -20 resonance being the most intense (Fig. 4-5A). The spectrum of the 200°C activated sample was similar to the room temperature sample whereas the 400°C activated sample had no resonance at -10 ppm and the -35 ppm resonance (now shifted to near -38 ppm) was more intense than that at -20 (Fig. 4-5B).

Mudrakovskii *et al.* [85] obtained the ^{31}P NMR spectra of H_3PO_4 impregnated SiO_2 samples containing 1.8 or 5.9 P/nm^2 after calcining in air at 100, 250 or 500°C. They convincingly argued that a NMR peak near -10 ppm was due to chemically attached $SiOP{=}O(OH)_2$. A signal near -25 to -31 ppm which was not present after roasting the 1.8 P/nm^2 sample at 100°C appeared after roasting at 250°C and was attributed to a bridging phosphate group. Finally, a peak to lower frequency (-42 to -46 ppm), which was only observed after roasting the 1.8 P/nm^2 sample at 500°C, was attributed to a silicon pyrophosphate phase.

Infrared spectra show that, with increasing evacuation temperatures (room temperature, 250 and 400°C studied here, see Fig. 4-6), there is a substantial decrease in the number of H-bonded SiOH/POH interactions with increasing temperature (broad band near 3100 cm^{-1}). Additionally, between 250 and 400°C, the number of isolated POH groups (sharp band, 3670 cm^{-1}) decreases. This *can* indicate that more surface SiOP bonds form, on average, for each adsorbed molecule, but does not of itself rule out the possibility that condensation to form P-O-P species also could occur.

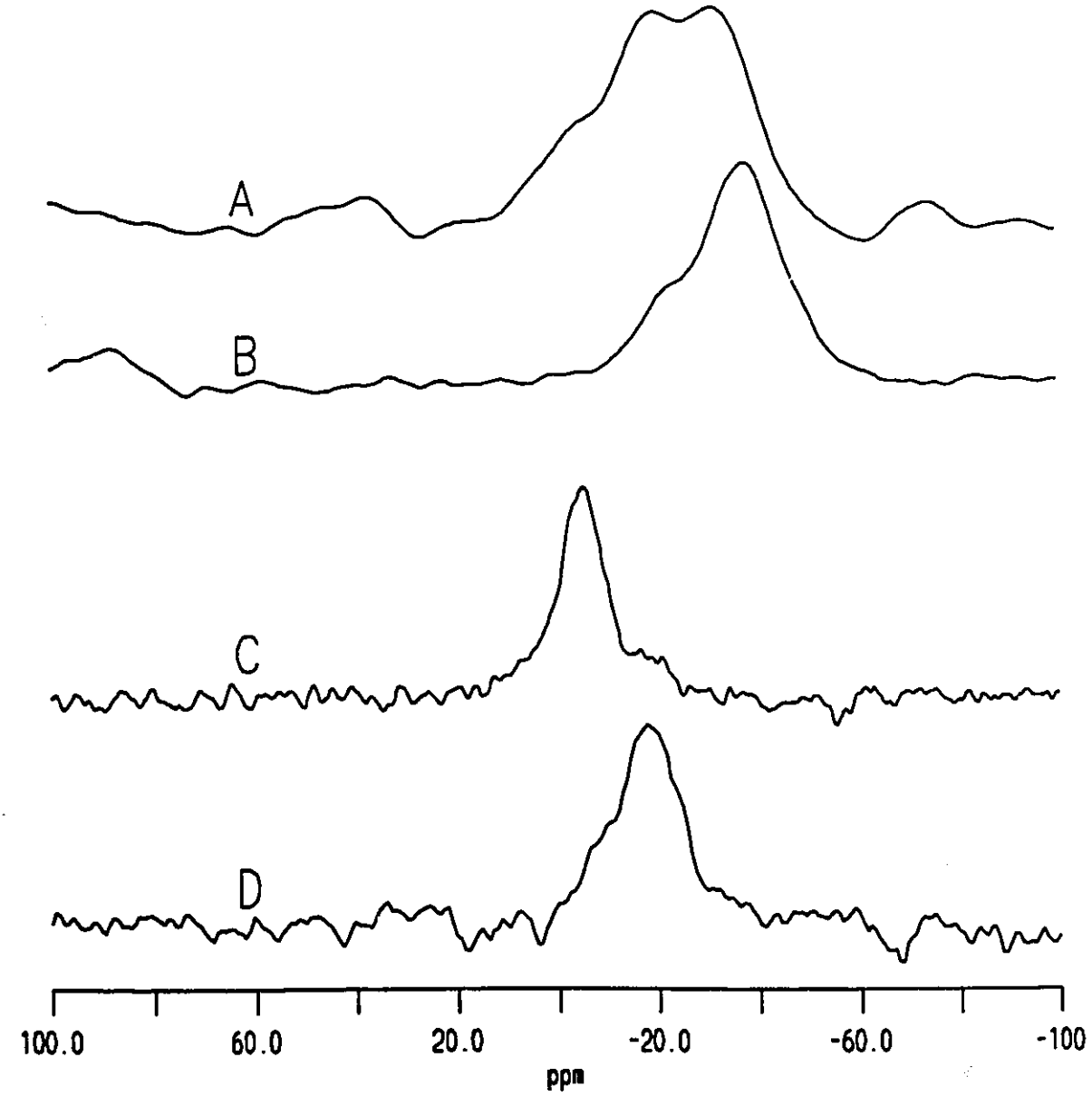

Fig. 4-5: ^{31}P MAS NMR spectra of H_3PO_4 (curves A, B; 90° pulses) and H_3PO_3 (curves C, D; cross polarization with TOSS) adsorbed via impregnation of silica (see text for details). Curves A and C were observed after room temperature evacuation of the impregnated samples. Curve B was observed after evacuation of A at 400°C and curve D was observed after evacuation of C at 150°C.

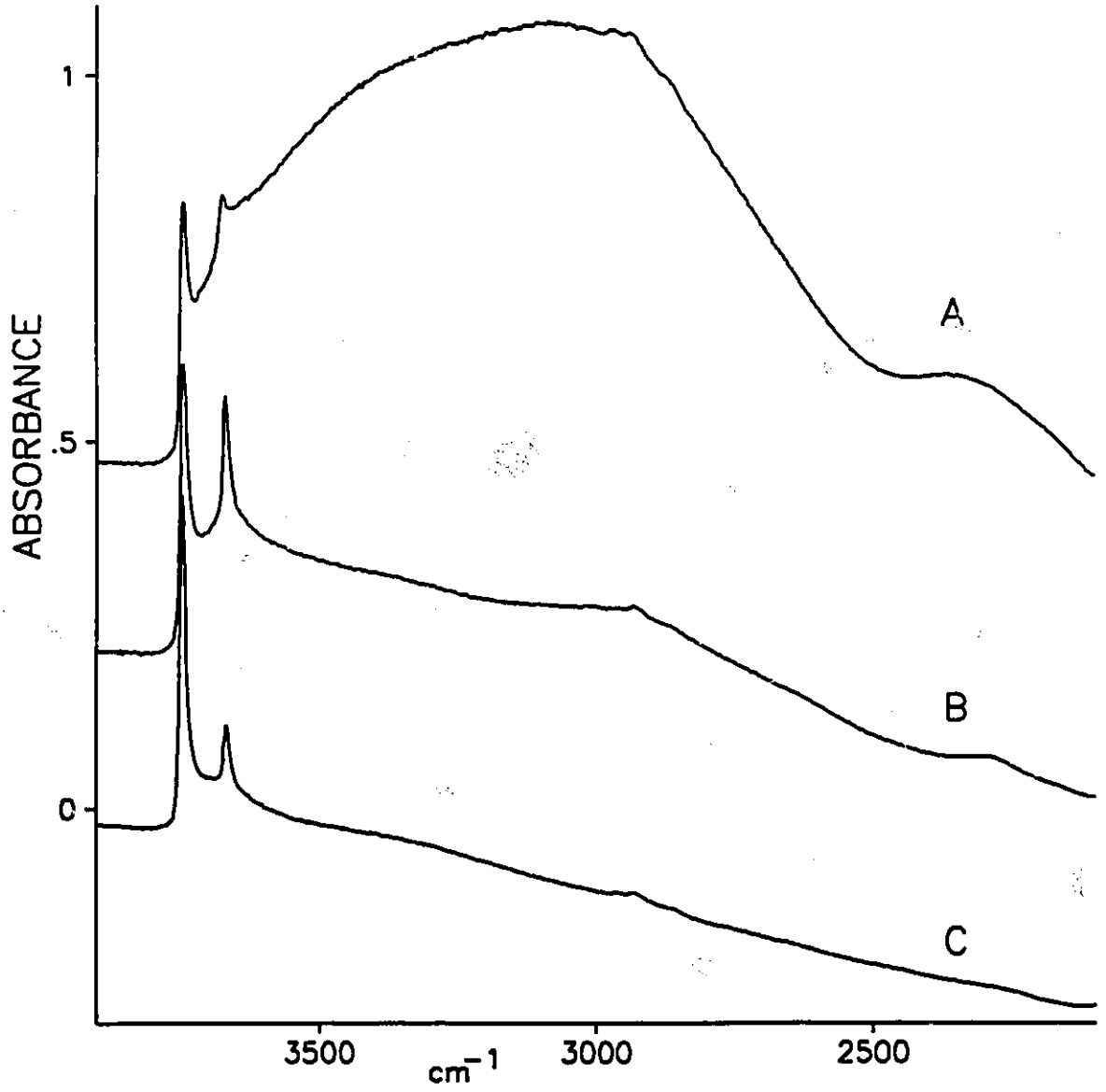

Fig.4-6: Infrared spectra of H_3PO_4 impregnated silica (800 μmol/g) after evacuation at (A) room temperature, (B) 250°C and (C) 400°C.

The weight of evidence from the IR and NMR experiments, when taken with the NMR data from the model compounds, would suggest that the two ^{31}P resonances for H_3PO_4/SiO_2 at -10 and -20 ppm can be attributed to $SiOP=O(OH)_2$ and $(SiO)_2P=O(OH)$ respectively. A similar trend, (a chemical shift to lower frequency leading to a greater number of surface P-O bonds when the temperature is increased), has been reported in a NMR study of phosphated TiO_2 and ZrO_2 [86]. The third peak near -35 to -38 ppm may be attributable to a triply bound species, $(SiO)_3P=O$, or to a polyphosphate species. However, the latter attribution is unlikely given a Si density [87] of 7-8/nm^2 and a P density of 1.2/nm^2, and in view of the appearance of the -35 ppm signal even in the absence of thermal activation.

Finally, further evidence of this trend (an increasing number of SiOP bonds as the temperature is increasd) also comes from a study of the IR and NMR spectra of phosphorus acid, H_3PO_3, on silica. As stated previously, the ^{31}P NMR spectrum of H_3PO_3 in solution has a single peak at 5 ppm, and as a solid there are two lines at 13.8 and 8 ppm. The NMR spectrum of silica doped with H_3PO_3, dried in air, and evacuated at room temperature prior to sealing the tube has a single peak at about -6 ppm with a slight asymmetry to lower frequency, Fig. 4-5C. If the sample was evacuated at 150°C instead of room temperature, the peak appeared near -18 ppm, with asymmetry to higher frequency, Fig. 4-5D. The IR spectrum in each case showed a characteristic P=O vibration at 1290 cm^{-1}, and a PH absorption near 2485 cm^{-1}. As with the H_3PO_4 impregnated sample, heating would be expected to lead to an increasing number of surface bonds, with a corresponding displacement of the chemical shift to lower frequency.

The NMR peaks observed from H_3PO_3 impregnated SiO_2 are very close to those observed for overnight adsorption of PCl_3 on silica, being at -5 and -16 ppm and the PH stretching frequency is the same as that observed for the adsorption of H_3PO_3 on SiO_2. The evidence suggests that these two surface species are SiOP=O(H,OH) (-5 ppm) and $(SiO)_2P$=O(H) (-16 ppm), the small shift from those observed from the doping of SiO_2 with H_3PO_3 presumably being due to the presence of other adsorbed species from PCl_3 adsorption, as already discussed.

Finally, the weak peak at 24 ppm only appeared in cross polarization spectra and it cannot be assigned at present. However, it disappeared after heating the NMR tube at 150°C for 2 h and the peaks formerly at -5 and -16 ppm merged into a single broad peak near -10 ppm.

Discussion

The reaction of PCl_3 on silica has produced some unexpected products and this has necessitated a study of the reactions of phosphoryl chloride, phosphorous acid and phosphoric acid on the same surface in order to determine the nature of the surface species formed.

It is apparent that PCl_3 is not particularly reactive with silica at room temperature and that the results previously reported in the literature can be attributed to the effects of $OPCl_3$ as a minor contaminant in PCl_3. $OPCl_3$ itself does not chemically adsorb on SiO_2 at room temperature although it relatively strongly H-bonds to surface SiOH groups. For short adsorption times, PCl_3 weakly H-bonds to SiOH groups.

For a longer adsorption time, one mode of the reaction of PCl_3 is a simple one step process involving surface SiOH;

$$PCl_3 + SiOH \rightarrow SiOPCl_2 + HCl$$

Although the above reaction is expected, we did not anticipate that all chlorine atoms could be stripped from PCl_3 to yield the surface species SiOP=O(H,OH) and $(SiO)_2P$=O(H). It is difficult to devise a mechanism for their formation, but given the propensity of P(III) to undergo oxidation to P(V) species, the first step of the reaction is probably

$$SiOH + PCl_3 \rightarrow SiCl + Cl_2POH$$

$$\downarrow$$

$$Cl_2P{=}O(H)$$

We have also found that a similar process is the first step in the reactions of PMe_2Cl and $PMeCl_2$ with SiO_2. Although we have no IR or NMR evidence for the generation of the intermediate Cl_2P=O(H), this is expected to be a reactive species and it presumably subsequently reacts further with one or two SiOH groups to generate SiOP=O(H,OH) or $(SiO)_2P$=O(H) and two or one HCl molecules respectively. Further speculation concerning the mechanism of reaction is unwarranted, particularly as one other unidentified species (+24 ppm NMR peak) was also present as a relatively minor product.

Conclusions

Phosphorus trichloride reacts with silica at room temperature to give surface $SiOPCl_2$, SiOP=O(H,OH) and $(SiO)_2P=O(H)$ species. The last two surface species are also produced from the adsorption of H_3PO_3, on silica at room temperature. Phosphoryl chloride does not chemically adsorb on silica at room temperature, but it strongly H-bonds with surface silanol groups.

CHAPTER 5

Infrared Spectra of Chlorinated Silica

Introduction

There has been considerable interest in the development of methods for the alkylation of silica surfaces in order to produce stationary phases for chromatographic purposes.[7,8,88] One common method for doing this involves first chlorinating the surface with agents such as $SOCl_2$, CCl_4, Cl_2, or $SiCl_4$, followed by a subsequent reaction with an alkylation agent such as LiR to produce a chemically modified SiR surface.[10,89,90] For example, using thionyl chloride, a proposed chlorination step involving a reaction with surface silanol is; SiOH + $SOCl_2$ $\rightarrow$ SiCl + HCl. However, McDaniel[91] concluded that siloxane sites were also implicated in the chlorination.

Evidence for chlorination has generally come from chemical analysis, and for chlorination at the gas-solid interface, the reaction conditions have been rather severe, at temperatures above 300°C.[10,89-94] A report of chlorination also emerges as a secondary objective in a study of the reactions of $TiCl_4$, BCl_3 and PCl_3 on silica.[95] Knözinger and Boehm [92] have summarized the work prior to 1983.

The purpose the the present work is to determine whether IR spectroscopy can be used

to monitor the chlorination of silica using $SOCl_2$ or other chlorinating agents. Apart from the chromatographic interest, this study has also been motivated by our IR and NMR studies of the reactions of chloroalkyl phosphines with silica, where we have only been able to account for mechanistic details of the reactions involved by invoking the idea of direct chlorination of silica.

To our knowledge there are only two published accounts of the use of IR spectroscopy to monitor the chlorination reaction.[93,94] This is probably due to the fact that SiCl stretching modes [96] generally lie in the range from about 640 to 425 cm^{-1} and self-supported silica discs only exhibit a limited transmission in the narrow range from about 750 to 550 cm^{-1} (Fig. 5-1A). Tripp and Hair [93] studied the adsorption of the chloromethylsilanes on silica and were able to detect SiCl stretching modes of various grafted species. Uniquely, an additional band near 625 cm^{-1} was observed following adsorption of $SiMe_3Cl$ which was attributed to a surface SiCl species. On the other hand, Fink and Plotzki [94] studied the chlorination of silica using $SiCl_4$ and CCl_4 and reported weak bands at 715 and 635 cm^{-1}; they attributed the former band to a surface SiCl species, and the latter to surface $SiCl_2$ as a result of the chlorination of geminal $Si(OH)_2$ groups.

Neither study provides convincing proof that these IR bands are due exclusively to direct chlorination of silica. In the study of Tripp and Hair [93], because the chlorination was carried out using an SiCl containing agent, it is possible that the unassigned band observed could be due to another grafted species of unknown structure. Regarding the study of Fink and Plotzki [94], the IR band at 715 cm^{-1} is well above the normal range associated with SiCl stretching

modes.[96]

This results of this study will demonstrate that the chlorination of silica is considerably more complex than has often been assumed.

Experimental

Samples were activated under vacuum for 1 h at temperatures ranging from 200 to 800°C prior to admitting reactant gases at pressures in the range from 10 to 40 Torr (see Results section for specific details). Chlorination was accomplished using a variety of Cl-containing reactants; $SOCl_2$ (J. T. Baker, 'purified' grade), Cl_2 (Air Products, 99.998%), CCl_4 (Fisher Scientific, 'spectranalyzed' grade), $SiCl_4$ (Aldrich, 99.999%, $OPCl_3$ (BDH Lab. reagent grade). All IR spectra were recorded at room temperature.

Results and Discussion

Thionyl chloride, $SOCl_2$, has been previously used to chlorinate silica, the reaction with single silanol groups being [89,92]:

$$SiOH + SOCl_2 \rightarrow SiCl + SO_2 + HCl$$

IR evidence for this reaction comes from an observed decrease in the intensity of the isolated SiOH band at 3747 cm^{-1} in the IR spectrum, and from the detection of the IR spectrum of

gaseous HCl and SO_2. Fig. 5-1A shows the background IR spectrum (1500 to 500 cm^{-1}) of silica after vacuum activation at 450°C (solid line), and after 'complete' reaction (SiOH totally removed) with $SOCl_2$ at 450°C (dashed line). The strong absorption features present initially from 1250-1000 cm^{-1}, near 800 cm^{-1}, and below about 530 cm^{-1}, are well known substrate modes of the underlying SiO_2 framework.[15,16]

The spectral changes can be more clearly seen after subtracting the background spectrum from the spectrum observed after reaction with $SOCl_2$; this is shown in Fig. 5-1B. Positive features going upward represent the creation of new IR bands, negative features going downward represent the destruction of IR bands present before reaction. For complete reaction, all initially present isolated SiOH groups were destroyed, as was evidenced by the removal of the 3747 cm^{-1} band (not shown). Elimination of SiOH is also shown in Fig. 5-1B by the observation of a negative feature at 980 cm^{-1} (Si-OH stretching mode) and the broad negative features near 860 and 770 cm^{-1} (SiOH deformation modes).[15] The new features observed after reaction include the peaks at 710 and 635 cm^{-1}, as well as a broad continuum absorption extending below 600 cm^{-1}. The features above 740 cm^{-1} were common to all subsequent spectra, and, hereafter, we will only show spectra for the region below 740 cm^{-1} as 'difference spectra' after background subtraction.

The 710/635 cm^{-1} bands could also be produced if chlorination was carried out using $SOCl_2$ at higher or lower temperatures, and if the silica had been preactivated at different temperatures. Fig. 5-2 shows spectra for some different reaction conditions (curve B corresponds

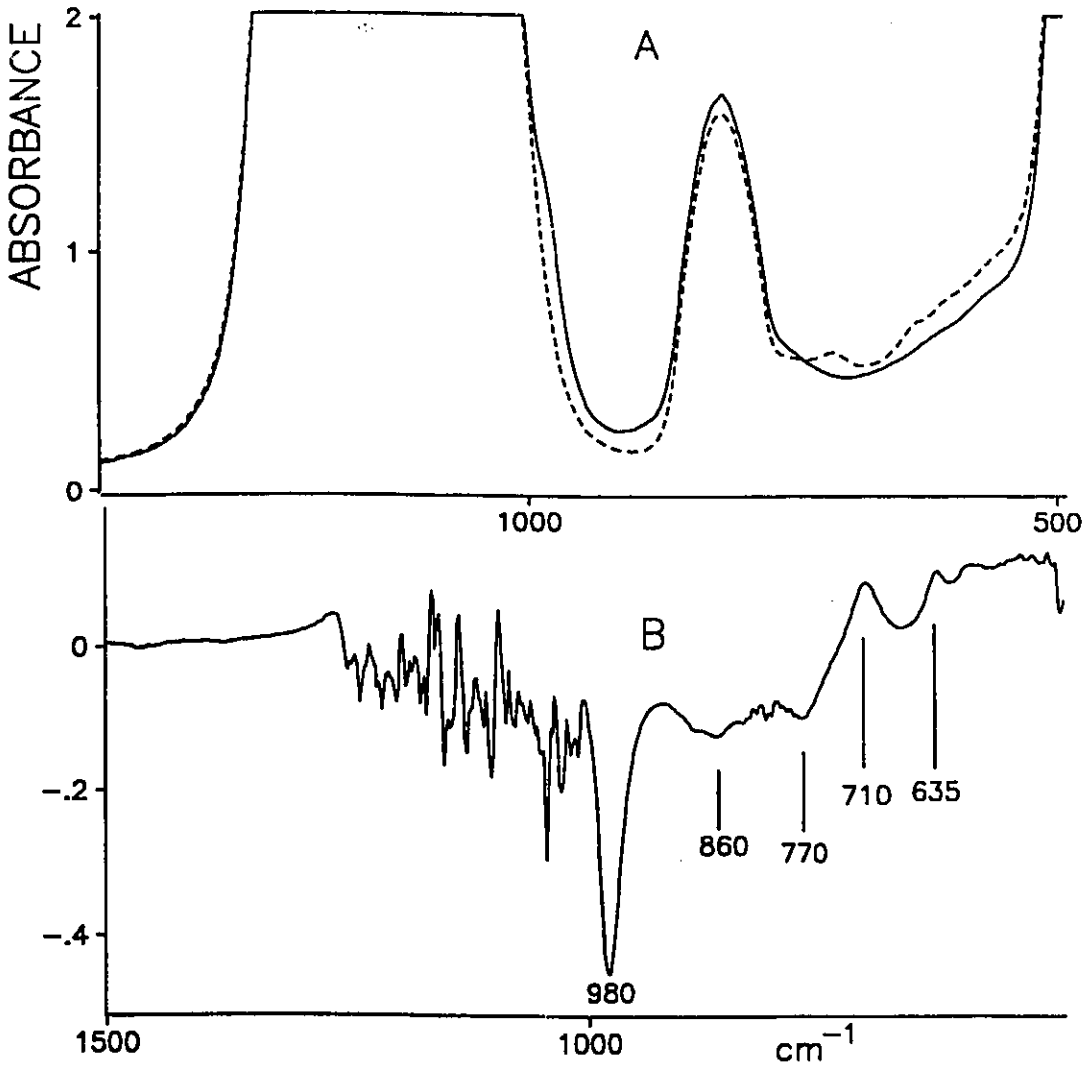

Fig. 5-1: A- Background infrared spectra of silica after vacuum activation for 1 h at 450°C (solid line) and after reaction with $SOCl_2$ for 1 hour at 450°C followed by evacuation of excess at 450°C (dashed line). B- Difference spectrum, after subtracting the background spectrum (solid line above) from the spectrum after reaction with $SOCl_2$ (dashed line).

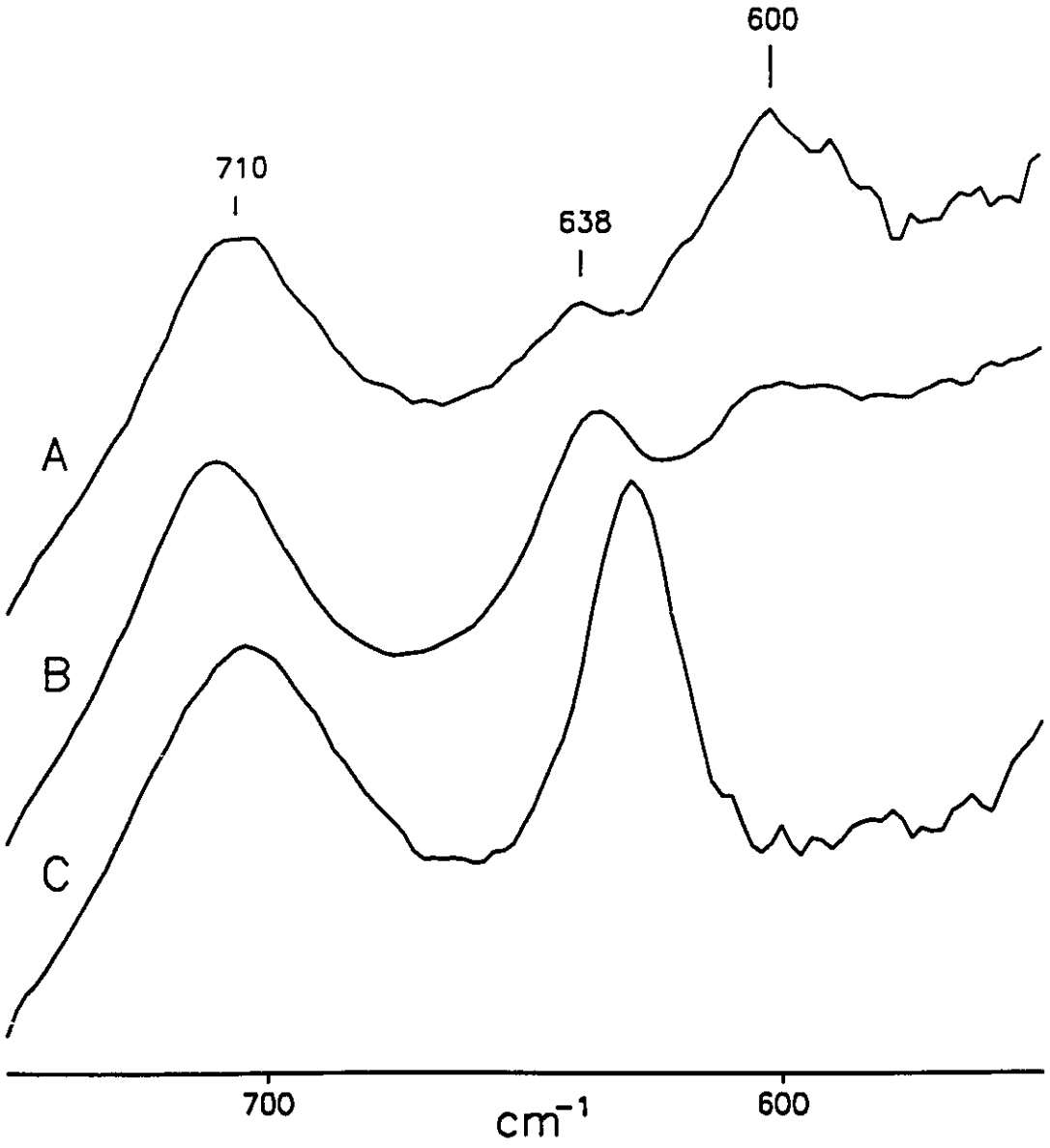

Fig. 5-2: Infrared spectra (after background subtraction) following reaction of silica with $SOCl_2$ under the following conditions: A- Silica activated at 800°C followed by 18 h reaction at 200°C. B- The same spectrum as shown in Figure 1B. C- Silica activated at 250°C followed by 18 h reaction at 200°C. All spectra have been normalized so as to have equal intensities for the band at 710 cm^{-1} (see text).

to that shown in Fig. 5-1B). Although the background is sloping upward to lower wavenumber, it can clearly be seen that the ratio of the intensities of the 710/635 cm^{-1} bands varies considerably, suggesting that at least two separate species have been generated. (Reaction with SiOH was not complete for the low temperature conditions used to obtain the spectra shown in curves 5-2A and 5-2C, and to facilitate comparison, the peak intensities at 710 cm^{-1} have been normalized so as to be approximately the same.) Two further aspects of these spectra are to be noted. Although the peak position of the 710 cm^{-1} band was always constant to within about ± 1 cm^{-1}, the peak position of the 635 cm^{-1} band varied somewhat, ranging from about 638 to 630 cm^{-1}; for convenience we will continue to refer to this as the '635' band. Secondly, there is a broad feature near 600 cm^{-1}, particularly evident in Fig. 5-2A; This feature only appeared sometimes, and then only when the silica had been activated at at least 450°C, and particularly if activated at 800°C, and appeared as a significant feature only when the intensity of the 710/635 cm^{-1} bands was low, as in Fig. 5-2A (the absolute peak intensity of the 710 band in Fig. 5-2A is about 20% of that for Fig. 5-2B). We will comment more on this feature later.

The 710/635 cm^{-1} IR bands could be generated if the chlorination was carried out using CCl_4 (600 to 800°C, reaction for several hours, Fig. 5-3A) or using Cl_2 at 800°C (Fig. 5-3B). For any reactant, if the reaction was carried out at higher temperatures, or if the silica had been previously activated at 800°C prior to reaction at lower temperatures, the 710 cm^{-1} band was relatively more intense than that at 635 cm^{-1}. This was partially associated with the destruction of the strained and highly reactive four-membered siloxane surface sites which give rise to the well known pair of characteristic IR bands at 908/888 cm^{-1} which are only created in significant

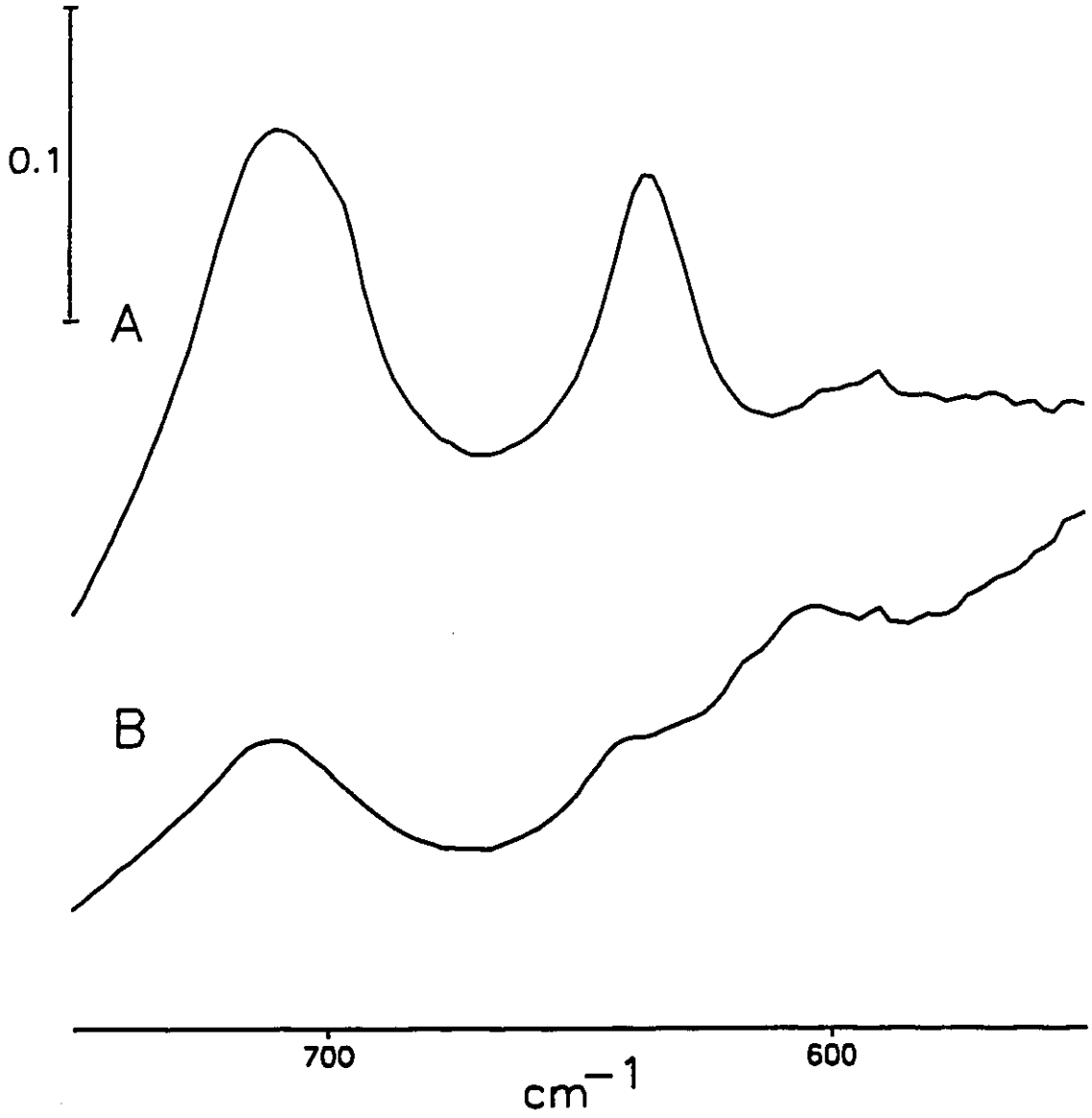

Fig. 5-3: A- IR spectrum after reacting silica (activated 1 h at 450°C) with CCl_4 at 800°C for 30 min. B- IR spectrum after reacting silica (activated at 800°C for 1.5 h) with Cl_2 at 800°C for 1.5 h. In both cases the excess reactant was evacuated at 800°C prior to cooling to room temperature.

concentration when the silica is heated at or above 800°C.[18,97] However, this is not the exclusive cause of the 710 cm^{-1} band; it can be observed even if the silica had only been activated at 250°C (in which case the strained site concentration is below detection limit) followed by reaction with $SOCl_2$ at 150 or 200°C.

The 710/635 cm^{-1} bands were also observed by Fink and Plotzki [94] following reaction of SiO_2 (activated at 800°C) with CCl_4 at 500°C (the 710 cm^{-1} being reported to be at 715 cm^{-1} in that study). These bands, and an additional one at 625 cm^{-1} could also be generated following the reaction of $SiCl_4$ with the same silica; however, the 625 cm^{-1} was generated first at low coverages. Fink and Plotzki attributed the 710, 635 and 625 cm^{-1} bands to SiCl, $SiCl_2$ and $SiCl_3$ species respectively. We have also studied this reaction on 800°C activated SiO_2. Fig. 5-4A shows the spectrum after reaction with excess $SiCl_4$ at 275°C under conditions where about 10% of the residual SiOH groups had reacted. Following evacuation of the reactant, a sharp feature at 624 cm^{-1} and a shoulder near 638 cm^{-1} were observed. After 'complete' reaction at 400°C (all SiOH removed), three bands appeared in the spectrum (Fig. 5-4B, gas phase evacuated), a doublet at 637/625 cm^{-1}, and a weaker feature near 710 cm^{-1}. Finally, after recording the spectrum shown in Fig. 5-4B, the furnace region of the sample cell was heated to 800°C under dynamic vacuum while the sample remained at room temperature in the optical region of the cell. Then, the sample was placed in the furnace region at 800°C for 5 min, returned to the optical region and the spectrum shown in Fig. 5-4C was recorded with the sample at room temperature. Note that the 625 cm^{-1} band disappeared and the usual 710/635 cm^{-1} bands were observed. The intensity of the peak at 710 cm^{-1} was comparable to that that shown in Fig. 5-2B.

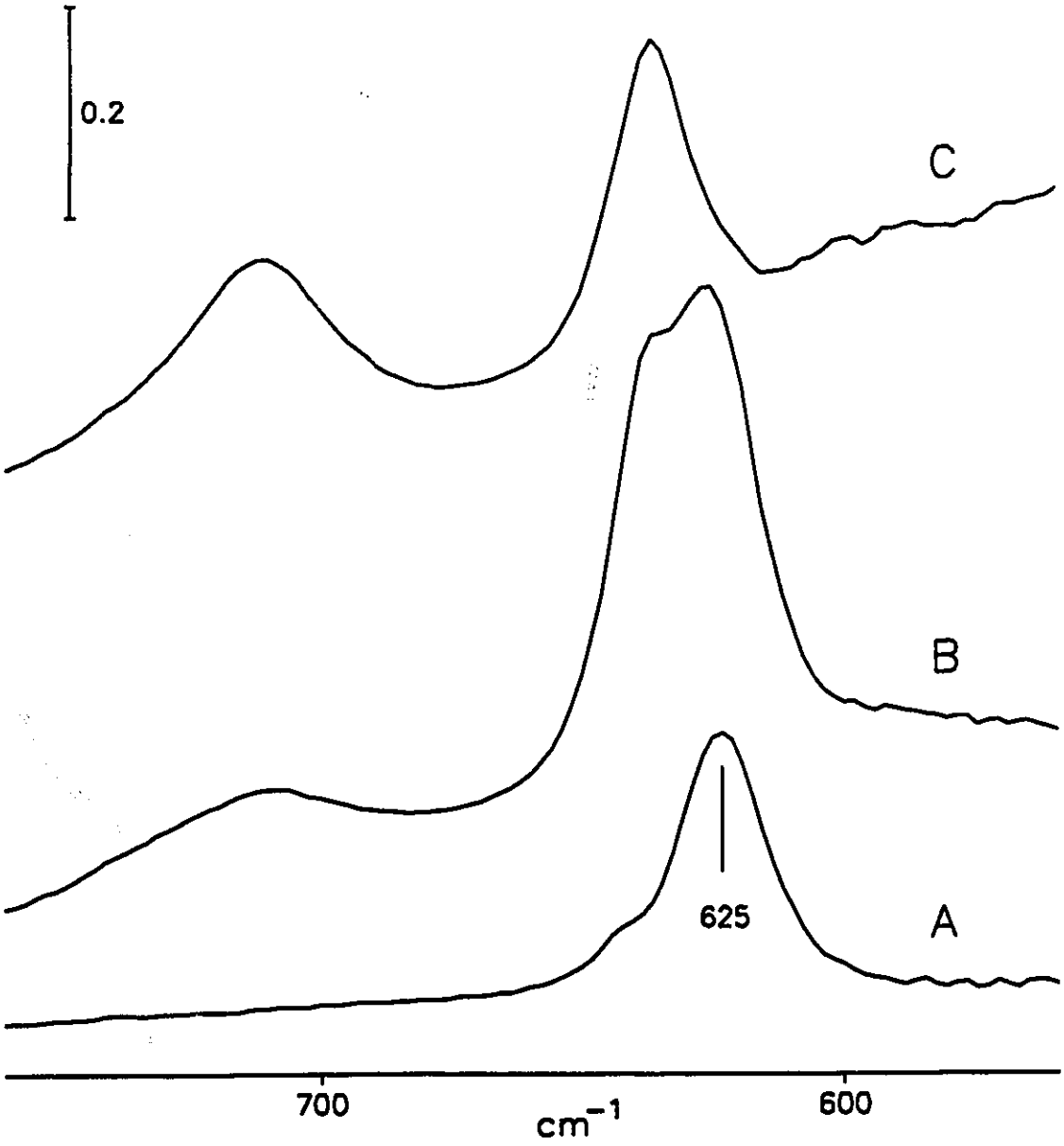

Fig. 5-4: A- IR spectrum of silica (activated at 800°C) after reaction with excess $SiCl_4$ at 275°C so as to remove 10% of the SiOH groups. B- After complete removal of silanol groups from A by reacting the silica with $SiCl_4$ at 400°C for 30 min. C- After 5 min reaction of B at 800°C (see text). In each of Curves A to C, the gas phase had been evacuated prior to recording the spectrum.

The spectra shown in Fig. 5-4A and 5-4B are similar to those shown by Fink and Plotzki [94] after reaction with $SiCl_4$ at 400°C for 5 min and 15 min respectively (they did not heat their sample at higher temperatures). Tripp and Hair [93] also reported a single IR band at 622 cm^{-1} following reaction with $SiCl_4$ at 300°C on a silica pre-activated at 450°C. Fink and Poletzki attributed the 625 cm^{-1} band to adsorbed $SiCl_3$ species, whereas Tripp and Hair attributed this to an SiCl species of unspecified structure (the reaction of $SiCl_4$ with SiO_2 was not the main purpose of the study of the latter group).

The assignment of the 625 cm^{-1} band to surface $SiCl_3$ seems reasonable based on its appearance at a relatively low temperature (Fig. 5-4A), particularly under conditions whereby only about 10% of the hydroxyl groups had reacted. The reaction is presumably SiOH + $SiCl_4$ -> $SiOSiCl_3$ + HCl. However, heating the $SiCl_4$ treated silica at temperatures above 400°C results in the appearance of the same spectral features at 710 and 635 cm^{-1} which were observed with the other non-silicon containing chlorinating agents. This shows that at sufficiently high temperatures, $OSiCl_3$ groups are thermodynamically unstable with respect to the species responsible for the 710 and 635 cm^{-1} bands. Possible assignments of these bands are discussed below.

The 710 cm^{-1} band is above the wavenumber range normally associated with SiCl containing species.[96] Therefore, we considered the possibility that it might be due to an SiOCl mode, or to some structural rearrangement of silica. However, if the chlorination was carried out on a highly ^{18}O exchanged silica (about 85% SiOH exchanged via repeated heating in multiple

doses of $H_2{}^{18}O$ at 450°C), no shift was observed, (a diatomic ^{16}OCl species having and IR band at 710 cm^{-1} should shift to 682 cm^{-1} for the ^{18}O containing species). Nor was there an ^{18}O shift of the 635 cm^{-1} band. Further, McDaniel showed that complete dehydroxylation and partial bromination of silica resulted from reacting silica with a 50:50 CO/Br_2 mixture at 800°C.[98] We also confirmed that complete dehydroxylation occurred under these conditions, but no IR bands were observed in the 750-550 cm^{-1} spectral region which could be attributed to unusual $(SiOSi)_n$ species.

Therefore, the available evidence suggests that at least two chlorine containing species are produced as a result of direct chlorination. In spite of the high wavenumber of the 710 cm^{-1} band for a SiCl species, we note in footnote 5 of ref. [99] that the polycyclic compound $Si_8Cl_8O_{12}$ reputedly has a strong IR band at 712 cm^{-1}. Further, Bärtch et al. recently reported [100] that the Raman active symmetric SiCl stretching mode for this compound was anomalously high relative to the SiCl stretching mode in $ClSi(OSiMe_3)_3$, 733 cm^{-1} and 588 cm^{-1} respectively. They attributed this to the imposed trans configuration for the SiOSiCl group demanded by the cubic silsesquioxane structure as opposed to the normal cis configuration imposed by steric interactions in non-cyclic silyl compounds.

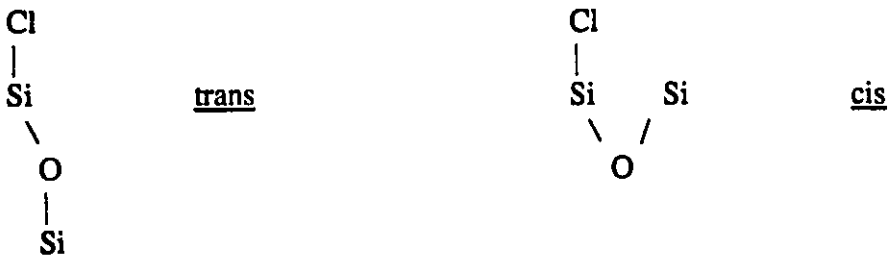

The trans configuration would also be expected to apply to a single SiCl group on chlorinated SiO_2. Therefore, our observation of an IR band at 710 cm^{-1} on this material need not be considered an anomaly.

The species responsible for the 710 and 635 cm^{-1} bands show the chemistry expected for a surface SiCl group which may contain one or more Cl groups.[92] Thus, they disappear if reacted with H_2O at moderate temperatures (100 to 150°C) liberating HCl. They also disappear if MeOH is added, giving HCl and SiOMe. With NH_3, the known $SiNH_2$ species is created [101] (IR bands at 3514, 3441, 1552 and 932 cm^{-1}), accompanied by strong bands due to the ammonium ion, the overall reactions being:

$$SiCl + NH_3 \rightarrow SiNH_2 + HCl$$

$$HCl + NH_3 \rightarrow NH_4Cl$$

We had hoped to be able to directly assign structures to the species responsible for each band. For example, if one could convert $SiCl_n$ to SiH_n species, one might be able to assign the original bands because, for example, SiH and SiH_2 species are well resolved and characterized.[102] Heating in H_2 only gave a reaction at a reasonable rate at 800°C, both bands disappeared, and only a single IR band due to an SiH species was generated at 2292 cm^{-1} (νSiH) and at 876 cm^{-1} (δ OSiH).[103] (SiH_2 is expected [102] to absorb nearer 2230 cm^{-1}.) Unfortunately, SiH_2 is not expected to be stable at 800°C, so this result is inconclusive. However, readdition of Cl_2 at 300°C regenerated both the 710 and 635 cm^{-1} bands. Both of the

710 and 635 cm^{-1} bands decreased uniformly after reaction with NH_3 at 20°C, or with H_2 at 800°C.

In spite of the above, we believe that the original assignments of Fink and Plotski [94] are correct (710 cm^{-1} - SiCl, 635 cm^{-1} - $SiCl_2$). The silsesquioxane results clearly show that a frequency in excess of 700 cm^{-1} is to be expected for a single SiCl group in a trans SiOSiCl configuration. Regarding the attribution of the 635 cm^{-1} peak to geminal surface $SiCl_2$ species, we cannot prove that this structure exists, but we do have indirect evidence that a species carrying more than one Cl atom might exist. When SiO_2 was first totally dehydroxylated by reaction with $OPCl_3$ at 450°C (which gave the 710 and 635 cm^{-1} bands), and then the reaction was continued for an additional 18 hours at 450°C, the 710/635 cm^{-1} bands continued to increase in intensity by about 30%, and a substantial IR band at 621 cm^{-1} due to gaseous $SiCl_4$ was detected. In a similar experiment using $SOCl_2$ at 500°C, $SiCl_4$ was also detected, only in this case there was no change in the intensity of the 710/635 cm^{-1} bands in the 18 hour second stage. Because $SiCl_4$ is formed, multiple chlorination of surface Si atoms must occur at some stage in the reaction. We have shown that $SiOSiCl_3$ species are thermally unstable with respect to dissociation into the species responsible for the 710 and 635 cm^{-1} bands, the former being surface SiCl, and an attribution of the 635 cm^{-1} band to $SiCl_2$ is not unreasonable. Given that about 15 to 20% of the surface silicon atoms of silica bear two hydroxyl groups [104], the rest being single silanols (and no trisilanol species), it is not unreasonable that single and geminal SiCl and $SiCl_2$ species are the only species formed on the chlorinated silica surface.

The chlorination reaction is not as simple are previously envisaged (solely a reaction with silanol groups) and it is apparent, in agreement with McDaniel [91], that siloxane groups are also implicated in the chlorination (i.e., chlorination continues even after removal of all SiOH groups). We have no clear attribution for the weak broad 600 cm^{-1} band. It only appeared when the silica was activated at 800°C or when reaction was carried out at temperatures at or above 450°C. Under high temperature conditions, we know that the silica surface is modified (IR bands [101] at 908/888 cm^{-1}), and we also know that reaction with surface siloxane groups occurs. Therefore, this band may be due to a chlorine containing surface species of unknown structure, or it may be due to the creation of surface sites of unusual geometry. For example, the well known [105,106] D_2 Raman defect band due to cyclic $(SiO\text{-})_3$ structures occurs at 608 cm^{-1}, and we note that strong SiOSi modes near this frequency are also observed in the IR spectra of cyclotrisiloxanes.[107] This species was not formed at reaction temperatures at or below 400°C as long as the silica had not been pre-activated at higher temperatrues and further speculation concerning its identity is not warranted.

Conclusions

The purpose of this work was to find spectroscopic evidence for surface chlorination which could be used to support mechanistic proposals when studying the reactions of other chlorine containing species with silica. Many of these hydrogen sequestering reactions occur at or near room temperature. The observation of IR bands near 635 or 710 cm^{-1} that cannot otherwise be accounted for by any other spectroscopic argument will in future be taken as evidence of chlorination of silica.

CHAPTER 6

Infrared and Solid State NMR Studies of the Adsorption of PMe_2Cl on Silica

Introduction

Trimethylphosphine has been successfully used as a ^{31}P NMR probe of the acid sites on oxide catalysts because the chemical shift of the Lewis coordinated form is very different from that of protonated PMe_3H^+ which results from its interaction with Brønsted acid sites.[35,60,66,53] Infrared spectroscopy can also be used to a limited extend for the same purpose, particularly with respect to the appearance of a PH stretching mode which is indicative of the presence of Brønsted acidity.[52,53]

As useful as PMe_3 is for detection of acidity, this molecule is not expected to react with other types of sites on oxide surfaces, particularly non-acidic hydroxyl groups. On the other hand, the chloromethylphosphines are expected to react with such sites in view of the susceptibility of the P-Cl bond to hydrolytic cleavage.[108] At the same time, molecules of this type might also be expected to react with Lewis and Brönsted acid sites as does PMe_3. In the present study, we have used ^{31}P solid state NMR and infrared spectroscopies to study the reaction of PMe_2Cl on silica; silica was chosen for this initial study because it does not possess

significant acidity at the gas-solid interface and, therefore, is a necessary baseline for studies on more complex surfaces.

The PMe_2Cl used was obtained from Strem Chemicals Inc. and contained no detectable ^{31}P NMR impurities. As before, SiOP=O(X,Y) is written to represent the structure

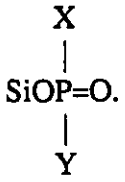

Results

The ^{31}P NMR spectrum observed following room temperature adsorption of 0.7 mmole of PMe_2Cl per gram of SiO_2, (about equal to the number of OH groups [16]) is shown in Fig. 6-1. With cross-polarization (CP), a single peak at 42 ±1 ppm was observed (Fig. 6-1A), but with 90° pulses there was an additional weak broad feature at -27 ppm (Fig. 6-1B). The species responsible for the 42 ppm peak was 'solid-like' as was shown by its appearance in CP, and its measurable chemical shift anisotropy of 150 ppm. Delayed decoupling showed that the species giving the 42 ppm peak did not have a direct PH bond. Finally, if the sample tube was evacuated, only the 42 ppm feature was observed using either 90 degree pulses or CP (Fig. 6-1C). The identical 42 ppm peak was observed regardless of the temperature of activation of the silica.

Table 6-1 lists the chemical shifts of some phosphorus containing model compounds which can aid us in the interpretation of the NMR spectrum of adsorbed PMe_2Cl on SiO_2. (Some

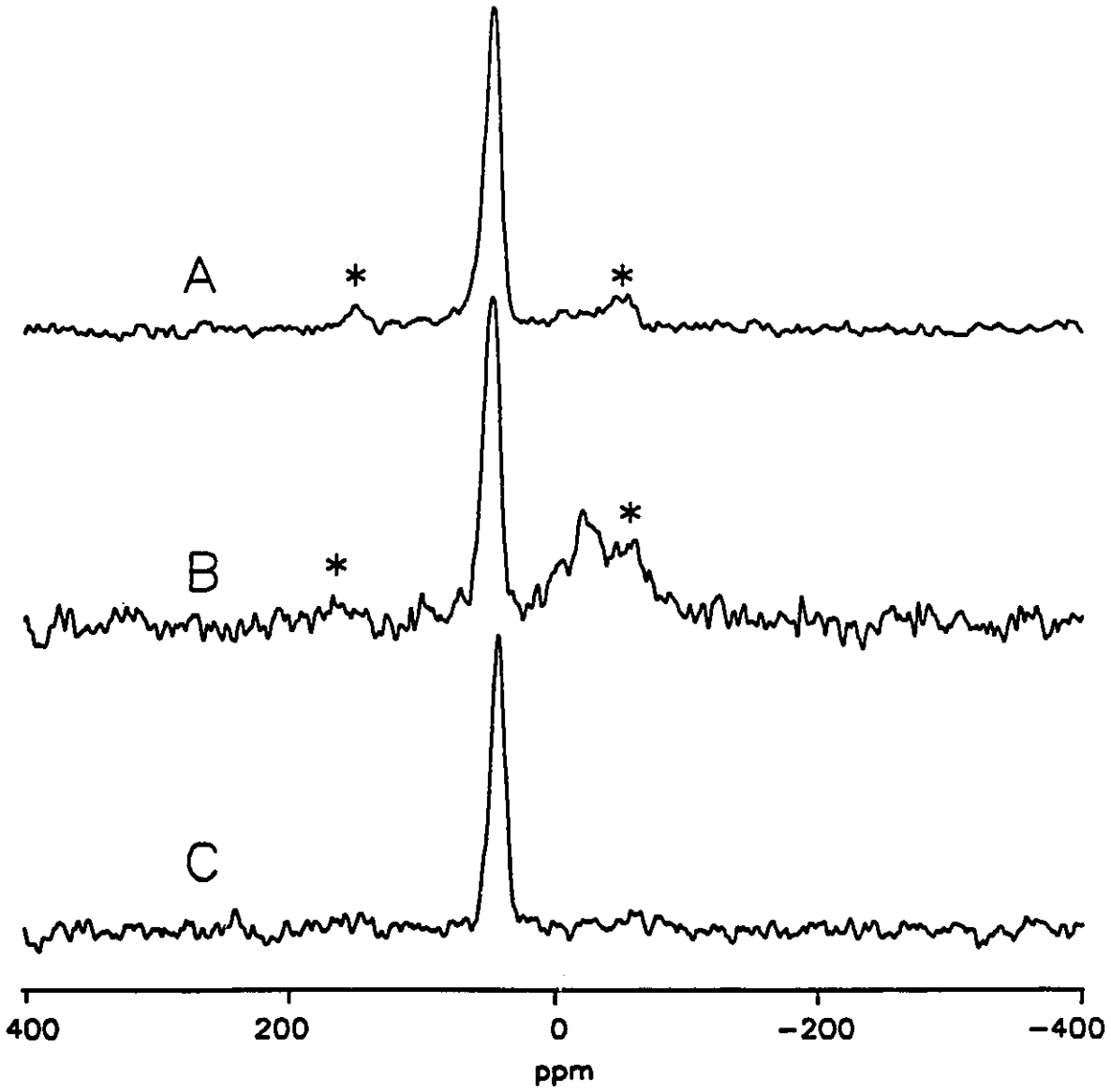

Fig. 6-1: ^{31}P MAS NMR spectra of PMe_2Cl adsorbed on 450°C vacuum activated silica (0.7 mmole/g of SiO_2). A - spectrum with cross-polarization (CP). B - spectrum with 90° pulses. C - CP spectrum after evacuation. Peaks marked with a * are spinning side bands.

additional compounds are listed, which will be discussed later in connection with the mechanism of the reaction of PMe_2Cl on SiO_2.) The only model compound having a shift close to that observed is $Me_3SiOP{=}O(Me_2)$ at 41.8; this suggests that the immobile species formed might be surface $SiOP{=}O(Me_2)$. Note that although $SiOPMe_2$ might be expected as a reaction product ($SiOH + PMe_2Cl \rightarrow SiOPMe_2 + HCl$), its chemical shift would be expected to be close to that of $MeOPMe_2$, 124 ppm. The origin of the -27 ppm peak, seen only with 90° pulses, will be discussed later.

Table 6-1

^{31}P Chemical Shifts of Some Model Phosphorus Compounds

Compound	Chem. Shift (ppm)	Reference
PMe_2Cl	94	[76] p. 717
$MeOPMe_2$	124	[59]
$(MeOPMe_2H)^+Cl^-$	78.2	[59]
$(Me_2PH_2)^+Cl^-$	-27.3	[59]
$Me_2P{=}O(H)$	21	[59]
Me_2PH	-99	[109]
$(Me_2P)_2$	-57.8	[109]
$Me_3SiOP{=}OMe_2$	41.8	[109]
$Me_2P{=}O(OH)$	55.3	[110]

The IR spectrum (3800 - 2400 cm^{-1}) of silica after activation at 450°C is shown in Fig. 6-2. The sharp feature near 3747 cm^{-1} is due to isolated non H-bonded silanol groups [≡SiOH or $=Si(OH)_2$]. The IR spectrum observed immediately following the addition of 1.7 mmol of PMe_2Cl per gram of SiO_2 is shown in Fig. 6-2B, and that observed after one hour reaction is shown in Fig. 6-2C. The most noticeable effect is the decrease and eventual elimination of the

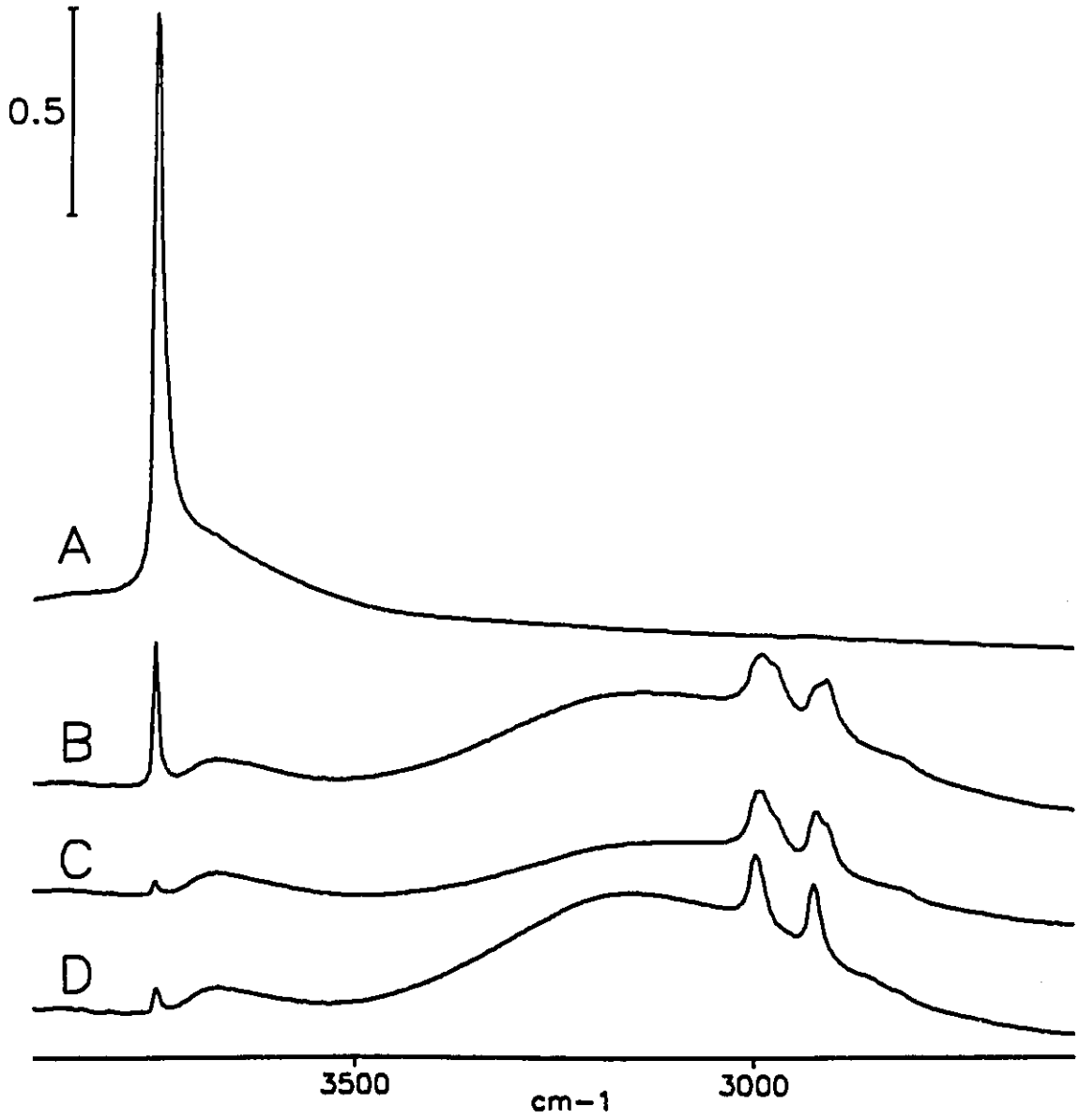

Fig. 6-2: A- infrared spectrum of SiO_2 after vacuum activation at 450°C. B- after addition of PMe_2Cl (1.7 mmole/g of SiO_2). C- after 1 h reaction. D- following evacuation of C for 14 hours.

3747 cm^{-1} silanol band and its replacement by a broad absorption at 3250 cm^{-1}, accompanied by sharper bands between 3000-2900 cm^{-1}. During the course of the reaction, IR bands due to gaseous HCl were clearly observed, but these have been subtracted from the spectra shown in Fig. 6-2. Finally, the spectrum observed after 14 h evacuation is shown in Fig. 6-2D.

Fig. 6-3 shows the 'difference' spectra in these regions which correspond to those shown in Fig. 6-2B to 6-2D.

Table 6-2 lists the infrared 'group frequencies' expected for organo-phosphorus compounds which are relevant to this study. Sharp IR bands observed in this study near 1425 and 1300 cm^{-1} are very diagnostic of the presence of PCH_3 containing species (CH_3 antisymmetric and symmetric angle deformation modes); that each of these lines is a doublet indicates there are two methyl oscillators. The bands near 930 and 870 cm^{-1} are the corresponding rocking modes whereas those at 2997 and 2924 cm^{-1} are antisymmetric and symmetric CH_3 stretching modes, and the broad band centered near 3250 cm^{-1} suggests that a strongly H-bonded species is present, either a POH containing species, or a species which is H-bonded to residual SiOH.

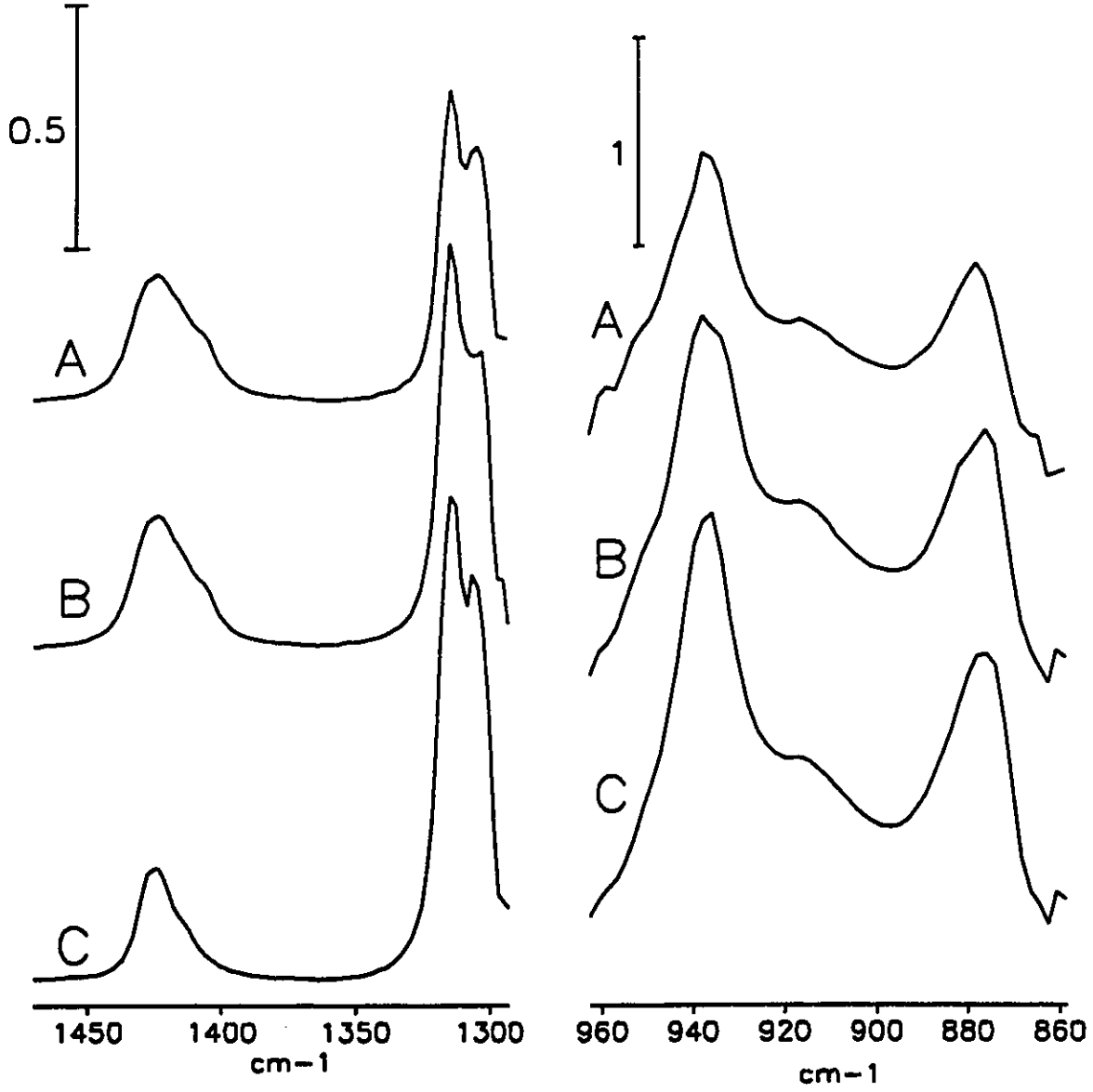

Fig. 6-3: A-C: Low wavenumber IR spectra, after subtraction of the SiO_2 background spectrum, corresponding to the conditions for Fig. 6-2 B, C, and D respectively.

TABLE 6-2

Group Frequencies (cm^{-1}) for Various P-X Functional Groups[a]

Vibration	Wavenumber	Assignment
$P(CH_3)$	3005 - 2995 (w)	antisym. CH_3 stretch
	2930 - 2920 (w)	sym. CH_3 stretch
$P(CH_3)$	1425 - 1415 (vw)	antisym. CH_3 deformation
	1325 - 1300 (m)	sym. CH_3 deformation
$P(CH_3)$	920 - 870 (s)	CH_3 rock
$P-C_n$	730 - 680 (w)	P-C stretch
P=O	1300 - 1140	P=O stretch
P-O	830 - 740 (s)	P-O stretch

a: From references [74,111]

The NMR results suggest that a P=O containing species is present, and its P=O stretching mode is expected to lie in the spectral region where SiO_2 is opaque, between 1300 and 1140 cm^{-1}. However, if a thin film of silica (0.1 to 0.4 mg/cm^2) is spread on an optically transparent ZnSe window, the spectral region between 1250 - 1000 cm^{-1} is not totally absorbing and, after spectral subtraction of the SiO_2 background, new peaks in this spectral region due to adsorbed species may be detected.[93,112] Fig. 6-4A shows such a difference spectrum in the 1500-800 cm^{-1} spectral region after reaction with PMe_2Cl. The strong band at 1244 cm^{-1} is characteristic of a free P=O containing species whereas the broad band near 1045 cm^{-1} would be due to an SiOP vibration. Adsorption of PMe_2Cl on ^{18}O exchanged SiO_2 (Fig. 6-4B) shows that both of these

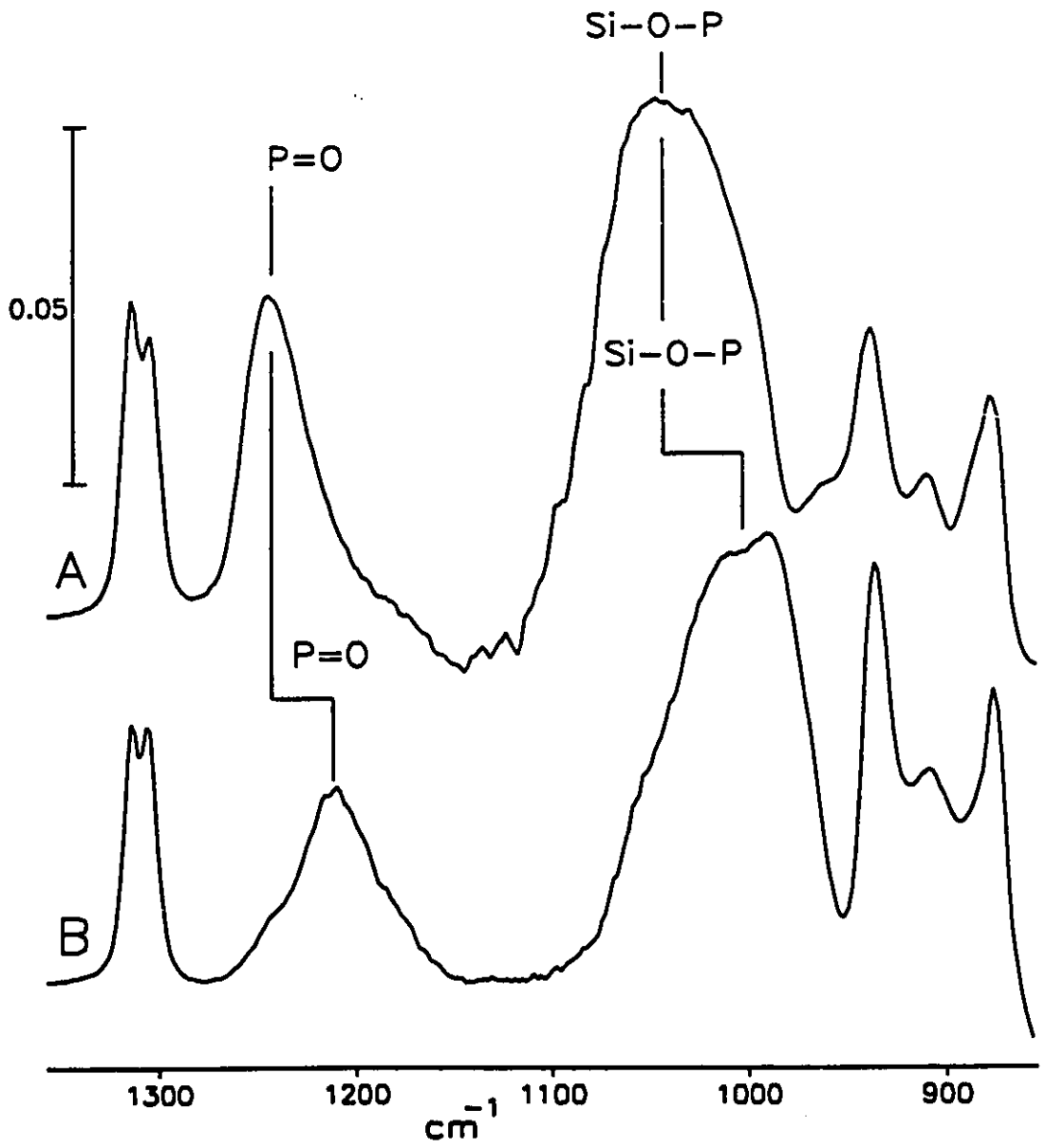

Fig. 6-4: IR spectra following adsorption and evacuation of excess PMe_2Cl on a thin film of silica, after subtraction of the background. A- on $Si^{16}O$. B- on $Si^{18}O$. In the case of the ^{18}O exchanged silica, the silica had been exchanged with ^{18}O to about 85 percent prior to adsorption.

bands undergo a significant shift of about 35-38 cm^{-1} to lower wavenumber for ^{18}O substitution [for a diatomic P=O species the calculated shift would be about 45 cm^{-1}]. Therefore, IR spectroscopy further supports the notion that the single P containing adsorbed species formed is $SiOP{=}O(Me_2)$. The IR frequencies are almost identical to those found for the model compound $Me_3SiOP{=}O(Me_2)$.[113]

The information in the spectral region between 750-550 cm^{-1} additionally supports this assignment and provides additional clues pertaining to the mechanism of the creation of this species. In this spectral region the vibrations characteristic of PC_x and SiCl stretching modes are found; PCl_x stretching modes generally lie below 600 cm^{-1}. We observed IR bands at 750, 705, 675 and 635 cm^{-1} (Fig. 6-5A). An $O\text{-}PC_2$ unit is expected to have a symmetric and antisymmetric P-C stretching mode and a P-O stretching mode near 750, 705 and 675 cm^{-1} (in reality these modes would be mixed and could not be described as pure PC_2 or P-O modes[114]). None of these modes would be expected to be as low as 635 cm^{-1}. On the other hand, we have previously established that chlorination of silica using SO_2Cl, Cl_2 or CCl_4 produces SiCl surface species which have IR absorptions at 710 and 635 cm^{-1}. The 635 cm^{-1} band can only reasonably be assigned to an SiCl containing species arising from direct chlorination of the surface, while the 710 cm^{-1} SiCl band would be masked by the 705 cm^{-1} due to the $O\text{-}PC_2$ unit.

Discussion

The IR and NMR evidence indicate that a single phosphorus containing chemisorbed species was formed, $SiOP{=}O(Me_2)$, accompanied by surface chlorination yielding SiCl. Given the propensity of trivalent P species to form pentavalent species whenever possible, the product

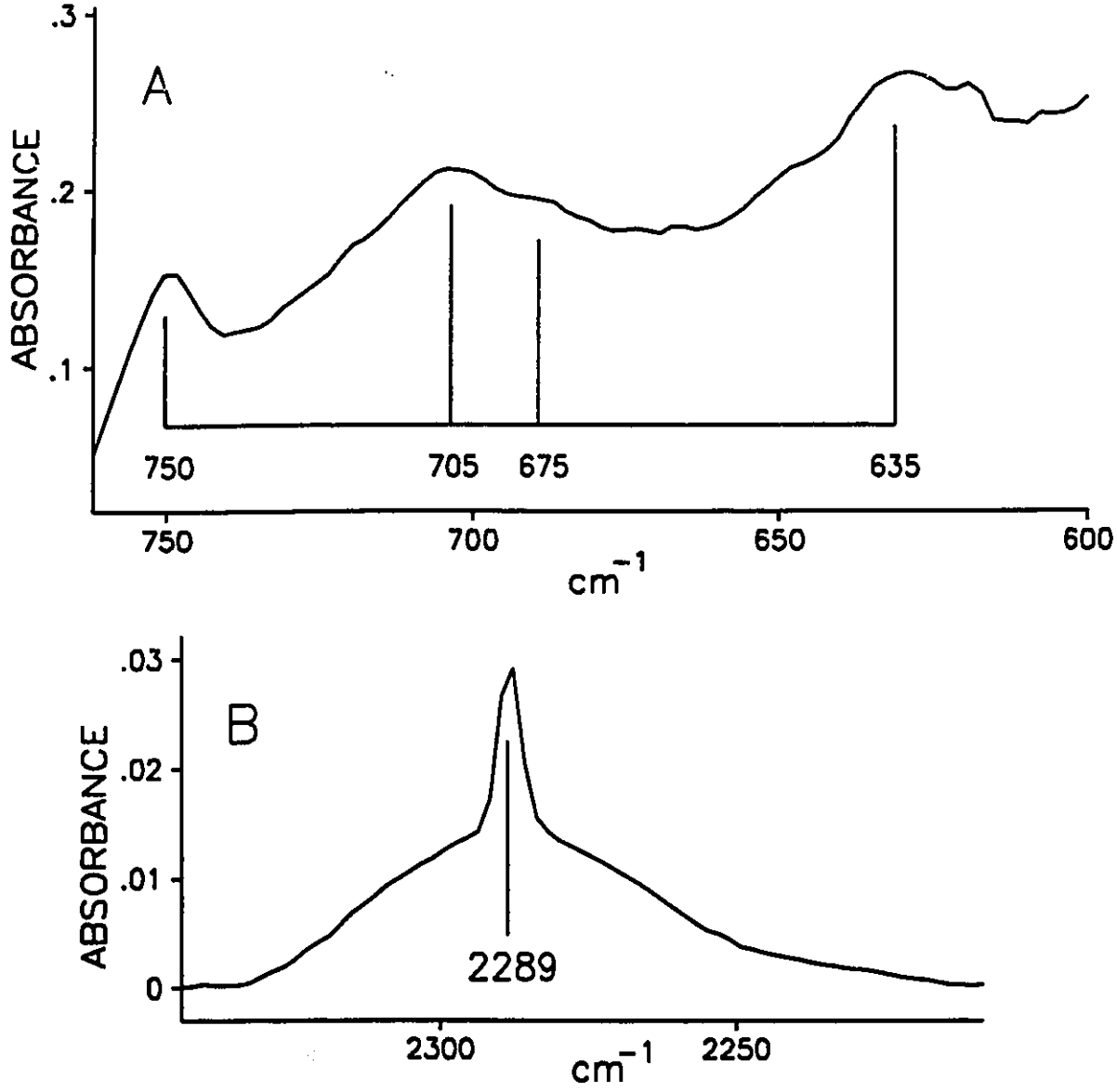

Fig. 6-5: A- IR spectrum, 770-600 cm^{-1}, following adsorption and evacuation of PMe_2Cl on SiO_2 (background subtracted). B- Gas phase spectrum in the PH stretching spectral region during the course of the reaction of PMe_2Cl on SiO_2.

was not unexpected (as has been found in our earlier studies of the adsorption of $P(OMe)_3$ and PCl_3 on SiO_2). It is known that MeOH and PMe_2Cl can react via a phosphonium salt (stable at -78°C) to give $Me_2P{=}O(H)$ and MeCl. We postulate the reaction:

$$SiOH + PMe_2Cl \rightarrow Si\text{-}O\text{-}\overset{\overset{+}{|}}{\underset{|}{P}}Me_2 + Cl^- \rightarrow Si\text{-}Cl + Me_2P(H){=}O$$
(H)

Dimethyl phosphine oxide was not detected (but see further below), but SiCl was detected, as evidenced by the band at 635 cm^{-1} which cannot otherwise be accounted for.

It has been shown that many products are formed when PMe_2Cl and $Me_2P{=}O(H)$ interact. All products are accounted for if the following reaction with excess PMe_2Cl is assumed to occur following generation of $Me_2P{=}O(H)$: [115,116]

$$PMe_2Cl + \overset{O}{\overset{\|}{H}}PMe_2 \rightarrow [Me_2P\text{-}O\text{-}\overset{\overset{+}{|}}{\underset{|}{P}}Me_2]Cl^- \rightarrow Me_2PH + Cl\text{-}\overset{O}{\overset{\|}{P}}Me_2$$
(H)

Followed by:

$$Me_2P(Cl){=}O + SiOH \rightarrow HCl + Si\text{-}O\text{-}\overset{O}{\overset{\|}{P}}Me_2$$

In this scheme, all intermediates except Me_2PH are consumed. However, the latter species has a characteristic PH vibration at 2289 cm^{-1}, and Fig. 6-5B shows the spectrum of the gas

phase during the course of this reaction. This is a typical gas phase IR spectrum showing a prominent Q-branch at 2289 cm^{-1} and is certainly due to Me_2PH. In addition, NMR with 90° pulses shows a broad line at -25 ppm and the dimethylphosphonium ion resonates at -27 ppm (Table 6-1). Given the small volume of the NMR tube compared with the IR cell, it is probable that the equilibrium $HCl + PMe_2H \rightharpoonup (Me_2PH_2)^+Cl^-$ is shifted to the right.

To conclude, we have evidence for surface SiCl, gaseous HCl and Me_2PH, and chemisorbed $SiOP{=}O(Me_2)$. The overall reaction apparently occurs via the mechanism given above, and the overall reaction is:

$$2\ SiOH + 2\ PMe_2Cl \rightarrow SiCl + Me_2PH + HCl + SiOP{=}O(Me_2).$$

Conclusions

PMe_2Cl reacts with silica to produce HCl and Me_2PH in the gas phase, and $\equiv$Si-O-P(O)Me_2 as a chemisorbed species. There is evidence that chlorination of the silica occurs during the reaction.

We set out to determine if PMe_2Cl might be a useful molecule for probing the surface structure of oxides. Established probes such as NH_3 [117,118], pyridine [119,120] or PMe_3 [66] interact with surface hydroxyl groups via H-bonds of varying strength, or, if the oxide is sufficiently acidic, may ultimately become protonated, revealing the presence of Brönsted acidity.

It may also coordinate to Lewis acid sites if present. Whether H-bonded, protonated or coordinated, IR and NMR spectroscopies can detect the mode of interaction with the surface.

The results of this study show that PMe_2Cl is very reactive on silica, an oxide which does not exhibit Lewis or Brönsted acidity at the gas solid interface. It removes surface protons as HCl and Me_2PH, and extracts surface oxygen atoms leading to the formation of P(V) species. Therefore, the protonic site is destroyed rather than probed. We conclude that PMe_2Cl will not be a useful molecule for probing the surface properties of oxides.

CHAPTER 7

An Infrared and Solid State ^{31}P NMR Study of the Adsorption of $P(CH_3)Cl_2$ and $P(CH_3)Cl_2/PCl_3$ Mixtures on Silica

Introduction

The surface chemistry of organophosphorus compounds is of interest in several important areas.[121] For example, the catalytic and stoichiometric decomposition of toxic phosphorus compounds has been studied extensively, using techniques ranging from those of classic catalytic studies to those of surface science.[122,123] In addition, surface phosphorus species are occasionally important components of industrial hydrotreating catalysts.[124] Several strategies for the immobilization of transition metal phosphine complex catalysts on oxide supports have been investigated.[125] In the latter two examples solid-state ^{31}P NMR has been particularly valuable in elucidating the state and role of the surface phosphorus species.

In the present work solid-state NMR and FTIR have been used to investigate the reaction of $PMeCl_2$ with a pyrogenic silica. It is shown that while the reaction of $PMeCl_2$ with silica is relatively simple, PCl_3 (present in ~5% amounts in commercial samples of $PMeCl_2$) reacts with the chemisorption products of $PMeCl_2$. This increases the apparent complexity of the reaction, and the combination of two spectroscopic techniques was essential to understanding the chemistry.

Experimental Section

For NMR studies of $PMeCl_2/SiO_2$, a 5 mm o.d. NMR tube was sealed to a pyrex vessel having a volume of 110 mL; pieces of the pressed discs about 1 to 3 mm in size were inserted into the large volume reactor where the thermal activation and chemical reactions were carried out; finally the reactor was detached from the vacuum line and it was tilted so as to slide the disc fragments into the small volume NMR tube. The NMR tube was then sealed and detached from the reactor with a glass blowing torch. Chemically doped NMR samples were activated directly in the NMR tube.

For the initial work, two $PMeCl_2$ samples were purchased (six months apart) from an established commercial supplier. Although both samples were apparently from different 'lots', a ^{31}P NMR analysis of the neat liquids revealed that both samples contained about 5% PCl_3 as the only P containing impurity. In the text we will nonetheless refer to this as $PMeCl_2$ where it is understood, unless explicitly stated, that this material was contaminated by about 5% PCl_3.

As will be detailed below, the presence of PCl_3 even as a minor contaminant proved to have a significant effect on the course of the reaction. Therefore, we synthesized two samples of $PMeCl_2$ which were free of PCl_3. The first of these involved the synthesis of ^{13}C $PMeCl_2$ (99% labelled) from pure PCl_3 and $^{13}CH_3I$ according to the procedure described by Colquhoun and McFarlane.[126] Sufficient material for 2 NMR experiments was obtained. In a second procedure, a $Cl_2MeP{=}S$ sample having no phosphorus containing impurities at greater than 0.1

mole percent was purchased from Alfa Inorganics. This was reacted with tri(n-butyl)phosphine according to the procedure of Ulmer *et al.* [127] to give $PMeCl_2$ which was free of PCl_3 (0.1 mole% detectability).

Phosphorous acid was Fisher Certified grade and no P containing impurities were detected by ^{31}P NMR. Methylphosphinic acid was prepared by the methanolysis of $PMeCl_2$ according to the procedure of Fiat *et al.* [110]

Results

The ^{31}P NMR spectrum observed after 45 minutes of adsorbing $PMeCl_2$ on SiO_2 which had been previously activated at 450°C showed a broad peak at 22 ± 2 ppm (Fig. 7-1A) whose width, using two different magnetic fields, was constant when expressed in ppm. Therefore, the peak width is probably due to a wide dispersion in isotropic chemical shifts rather than to dipolar coupling with quadrupolar Cl nuclei. If the proton decoupler was turned off for 70μs before the start of data asquisition, the signal at 22 ppm disappeared. This delayed decoupling shows that the species responsible for this peak bore at least one directly bonded proton. The same NMR spectrum could be generated, Fig. 7-1B, by doping SiO_2 with methylphosphinic acid, MeP=O(H,OH). After overnight reaction a second NMR peak appeared near -18 ppm with asymmetry to high frequency (Fig. 7-1C). Fig. 7-1D shows the ^{31}P spectrum of H_3PO_3 doped SiO_2. Aqueous H_3PO_3 has a chemical shift of 5 ppm; as a solid we found a doublet at 8 and 13.6 ppm indicative of the presence of two non-equivalent sites in the crystal. For a H_3PO_3 doped

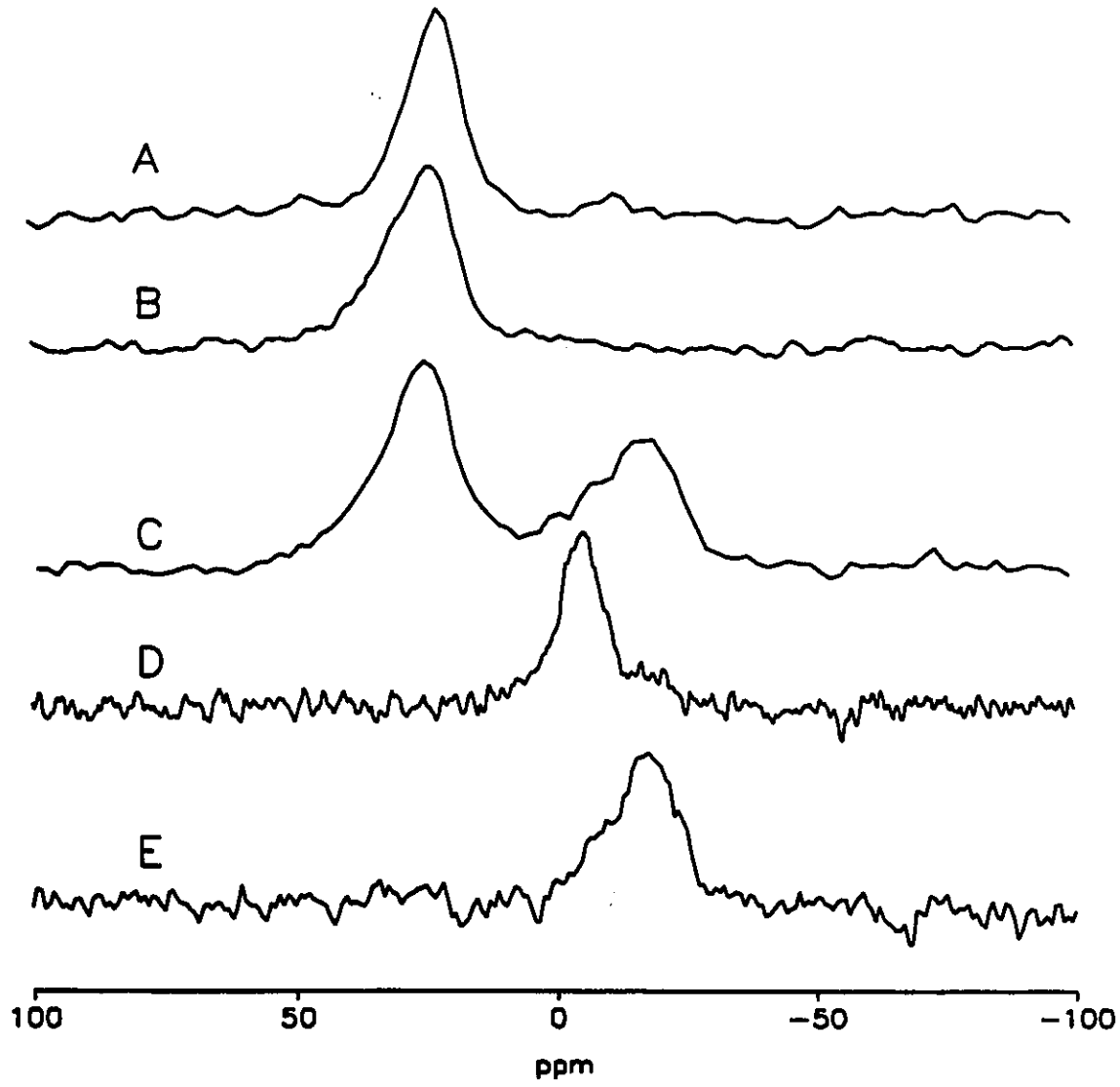

Fig. 7-1: ^{31}P CPMAS spectra. Spectra A to C were recorded at 24.3 MHz, D and E at 60.5 MHz. Sideband suppression (TOSS) was used with spectra D and E. A- 70mg SiO_2 activated at 175°C, put into contact with 50 Torr $PMeCl_2$ for 45 min., evacuated for 20 min. B- 100mg SiO2 doped to 500 µmoles/g MePH(O)OH from $HCCl_3$ solution, evacuated 3.5 h. C- 70 mg SiO_2 activated at 175°C, allowed to react with 50 Torr $PMeCl_2$ for 19 h., evacuated 20 min. D- 100mg SiO_2 doped to 310 µmoles/g with aqueous H_3PO_3, evacuated 2 hours. E- 100mg SiO_2 doped to 310 µmoles/g with aqueous H_3PO_3, evacuated 2 hours at 200°C.

SiO_2 sample evacuated at room temperature the peak maximum occurred near -8 ppm, with a shoulder at more negative shift. When this sample was degassed at 200°C (Fig. 7-1E), the peak maximum occurred at -18 ppm, with a shoulder to positive shift. The second peak which was observed from the $PMeCl_2/SiO_2$ reaction appears to be due to a combination of these two species.

Delayed decoupling showed that the second group of species obtained from the $PMeCl_2$ reaction (-8 to -18 ppm) had directly bonded protons. Delayed decoupling on the H_3PO_3/SiO_2 samples showed that no decomposition of PH had occurred under these mild degassing conditions; all of the P was still protonated.

The NMR evidence shows that two chemisorbed or immobile PH containing species were created during the $PMeCl_2$ reaction on SiO_2. For convenience in the following, we will designate the first species A (+22 ppm), and those created for longer reaction times, B (-8 to -18 ppm).

The progress of the reaction could be monitored continuously more easily by infrared spectroscopy. Fig. 7-2 shows two examples of the IR spectra recorded in the spectral region between 3800 and 2800 cm^{-1}, during the first several hours (see figure caption for details) of the reaction of $PMeCl_2$ with 450°C activated silica. Following addition of $PMeCl_2$ there was an immediate decrease in the intensity of the 3747 cm^{-1} peak due to isolated silanols (not shown in Fig. 7-2, but the intensity of the 3747 cm^{-1} peak was about 1.5 absorbance units initially). This was accompanied by the appearance of a broad band at 3650 cm^{-1}. Over the next several hours, both the 3747 and 3650 cm^{-1} bands decreased in intensity as a very broad band at 3250 cm^{-1} grew

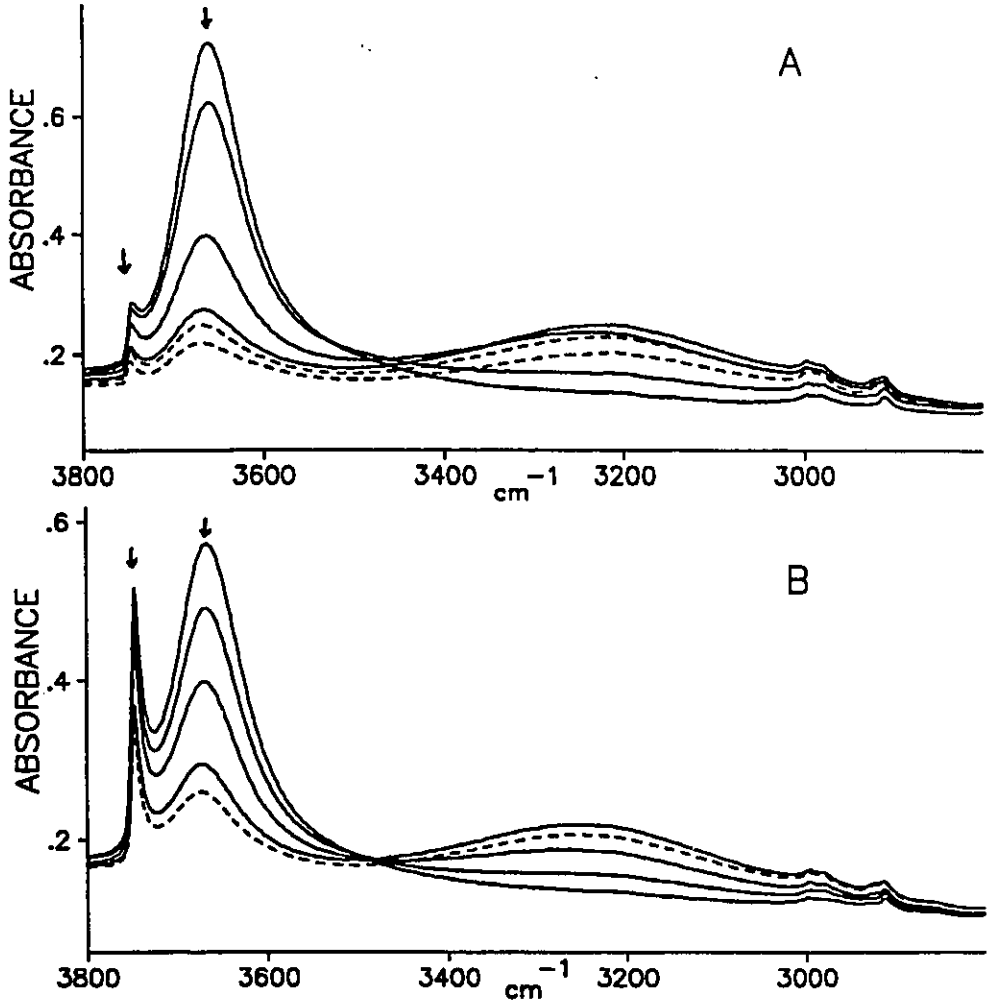

Fig. 7-2: Infrared spectra (3800 - 2800 cm^{-1}) as a function of time following the addition of 73 Torr (A) or 44.6 Torr (B) of $PMeCl_2$ to silica. For each set of spectra, the arrows indicate that the intensity of the IR bands at 3747 and 3650 cm^{-1} decrease continuously, the first curve (maximum intensity) is the spectrum observed immediately after addition of $PMeCl_2$. The remaining spectra were recorded at the following times after addition of $PMeCl_2$. A - 15min, 75min, 2.5 h, 3.5h, 5h. B - 30min, 1h, 2.5, 3.5h. The intensity at 3250 cm^{-1} increases steadily for the solid curves, then starts to decrease for the dashed curves.

in intensity and then decreased in intensity. Throughout all of these changes the spectrum of gaseous HCl was observed and its intensity increased with the time of reaction (the HCl bands have been subtracted from the curves in Fig. 7-2). If a lower pressure of $PMeCl_2$ was added, the decrease in the intensity of the 3747 cm^{-1} was lower initially but the accompanying spectral changes were qualitatively similar.

Accompanying the above spectral changes, a new band at 2390 cm^{-1} appeared in the spectral region associated with PH_x stretching vibrations.(Fig. 7-3A) This reached its maximum intensity after about 3 to 5 hours, depending on the pressure used (generally from 10 to 80 Torr), then slowly started to decrease in intensity with longer reaction times as a second PH band developed at 2490 cm^{-1} (Fig. 7-3B). The latter band was asymmetric to low wavenumber. Upon reacting $PMeCl_2$ with a deuterated silica, the 2390 and 2490 cm^{-1} bands appeared at 1705 and 1805 cm^{-1}, a low wavenumber shift by a factor of 1.40 and 1.38 respectively, demonstrating that both bands were indeed due to PH/PD stretching modes. Finally, the extent of growth of either PH band did not exactly correlate with the increase or decrease in the intensity of the broad 3250 cm^{-1} feature.

Therefore, in agreement with the NMR results, at least two proton containing species were formed following adsorption of $PMeCl_2$ on SiO_2, species A for shorter periods of reaction, and then species B. Neither A or B were removed following evacuation at room temperature and the growth of the PH band of species B ceased.

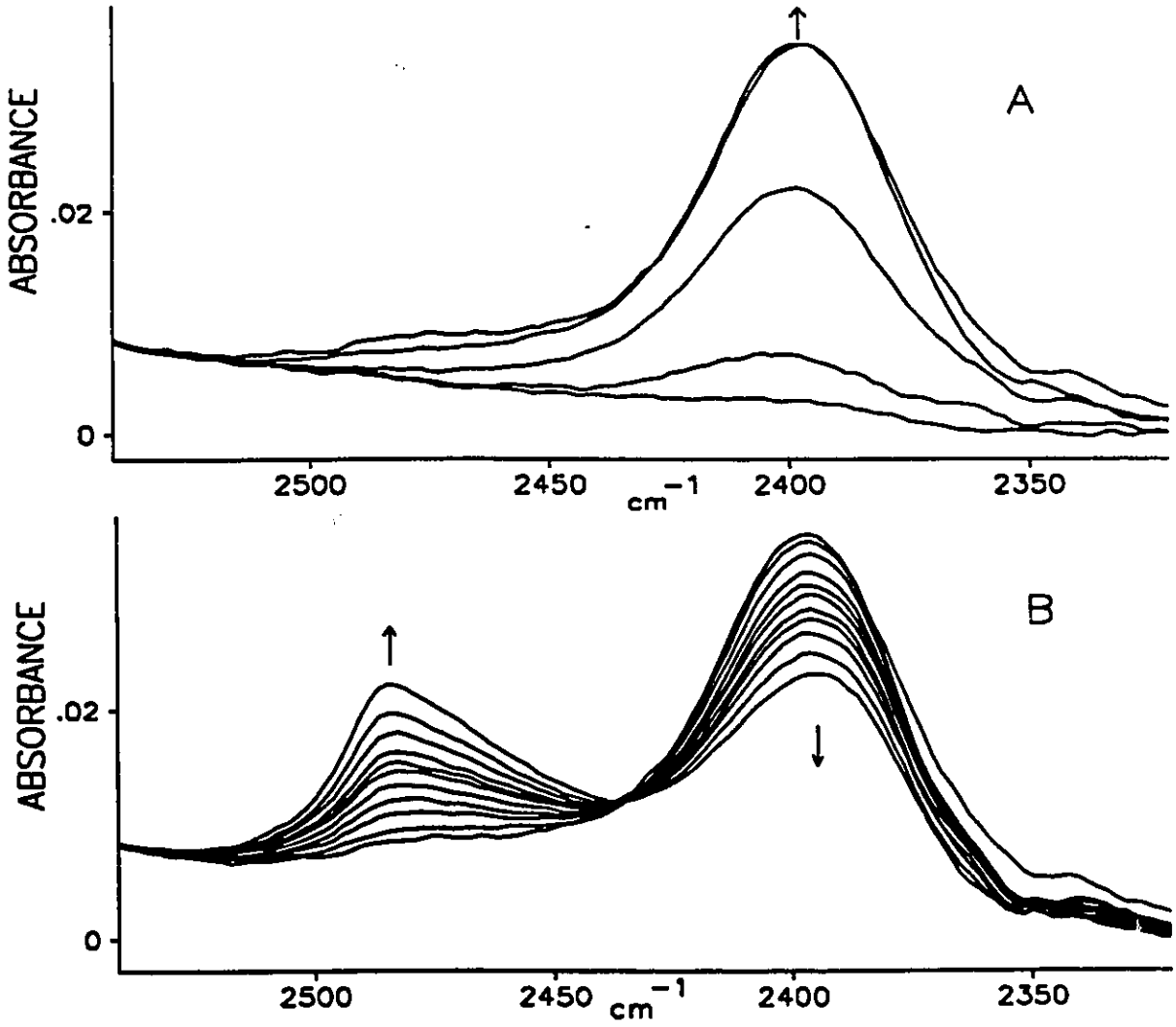

Fig. 7-3: IR spectra in the PH stretching region as a function of time for the addition of 73 Torr of $PMeCl_2$ to silica (corresponding initially to the spectra shown in Figure 2A). A - the intensity at 2390 cm^{-1} is increases with time, the bottom spectrum being that observed immediately after addition of $PMeCl_2$, the remaining spectra being recorded after 15min, 75min, 2.5h, 3.5h. B - the arrows indicate the direction of the spectral changes after 3.5h, 4h, 5h, 6h, 7h, 8h, 9h, 10h, 12h, 15h, and 20h.

Some additional insights into the nature of the products formed can be gleaned from the low wavenumber spectral region. Sharp IR bands near 1410 and 1300 cm^{-1} are diagnostic of the presence of a PCH_3 containing species. [74a] These are the CH_3 antisymmetric and symmetric angle deformation modes. For the parent compound, these bands are at 1412 and 1284 cm^{-1} respectively. During the early course of the reaction the growth of a new IR band at 1306 cm^{-1} could be correlated uniquely with the appearance of species A (Fig. 7-4). These spectra correspond to those shown in Fig. 7-2B for up to 3.5 h reaction. Brief evacuation (not shown) removed most of the contribution from physically adsorbed $PMeCl_2$ revealing that the antisymmetric CH_3 deformation mode of species A was nearly coincident with the same mode of the parent.

At low wavenumber, a pair of weak IR bands was always observed near 700 and 635 cm^{-1} (Fig. 7-5 shows several examples). It has been shown in chapter 5 that IR bands at these wavenumbers are due to the direct chlorination of silica (SiCl and $SiCl_2$ respectively). On the other hand, the P-CH_3 stretching mode is also expected to lie near 700 cm^{-1} and part of the intensity at 700 cm^{-1} many also have a contribution from this mode.[74a] Finally, the reactions described above proceeded at a reasonable rate only if the silica had been activated at temperatures below about 500°C. For higher temperatures of activation, the OH concentration diminishes,[128] it being very low when the activation is carried out at 800°C or higher. We found that the reaction rate was about three times slower if the silica had been activated at 700°C whereas for 1100°C activation there was insignificant reaction with the few residual surface silanol groups after 3.5 h.

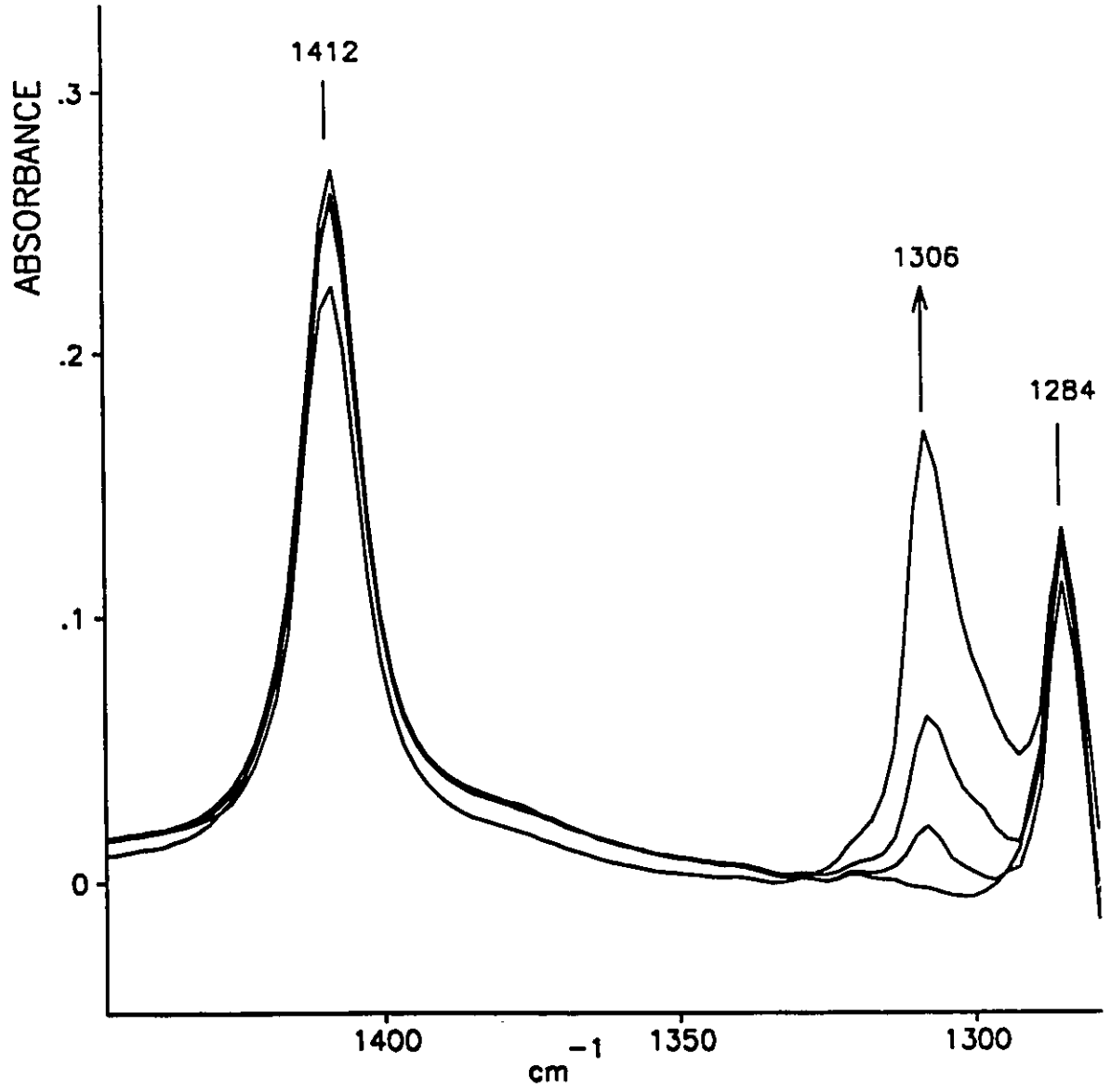

Fig. 7-4: IR spectra (1450 - 1360 cm^{-1}) for addition of 44.6 Torr $PMeCl_2$ to silica as a function of time. The bands at 1284 and 1412 cm^{-1} are due to the parent $PMeCl_2$. The only significant spectral changes correspond to the growth of a new band at 1306 cm^{-1} (as indicated by the arrow, see text) and the spectra are recorded after initial addition of reactant (zero intensity at 1306 cm^{-1}) and after 30min, 1h, and 3.5h.

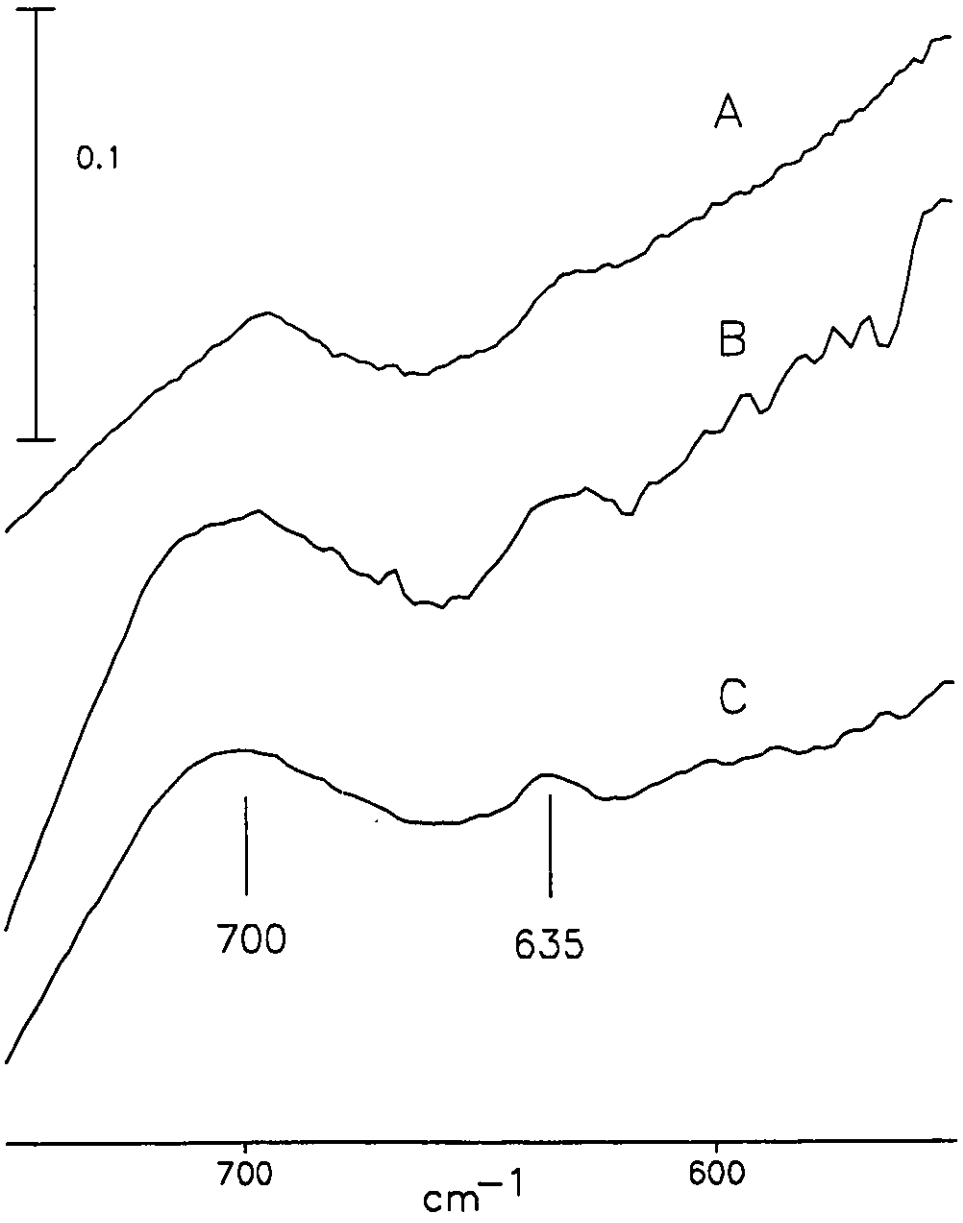

Fig. 7-5: IR spectra (740 - 550 cm^{-1}) recorded as follows: A - 2 mg/cm^2 disk, 47 Torr $PMeCl_2$ after 3.5h. B - 6 mg/cm^2 disc, 150°C activation, 43 Torr $PMeCl_2$ after 18h. C - 4 mg/cm^2 disk, 37 Torr $PMeCl_2$ after 20h. In all cases the gas phase had been evacuated for 15 min.

Discussion

(a) *Identity of species A:*

The NMR and IR results have shown that species A can be produced by the adsorption of methylphosphinic acid on silica. This species is immobile, and is probably:

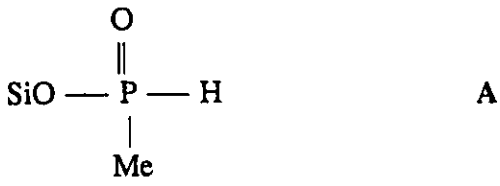

A

This is assignment is supported by the following:

(1) IR bands at 1306/1412 cm^{-1} guarantee that there is a PMe group.

(2) A PH band at 2390 cm^{-1} for A is close to 2386 cm^{-1} found for methylphosphinic acid, MeP=O(H,OH), and the PH frequency is not expected to change significantly for replacement of the OH group by 'OSi'

(3) The ^{31}P shift for $Me_3SiOP=O(H,Me)$ is 30.4 ppm[82] compared with 22 ppm found for A.

The generation of this species requires the presence of SiOH, the reaction rate being very slow for a highly dehydroxylated surface which contains few SiOH species, and being faster when the SiOH concentration is higher. We have evidence that there is chlorination of the surface to yield SiCl, and HCl is generated in the gas phase. Therefore we postulate the following basic two step process;

$$SiOH + PMeCl_2 \rightarrow MeP{=}O(H,Cl) + SiCl \quad (1)$$

$$SiOH + MeP{=}O(H,Cl) \rightarrow SiOP{=}O(Me,H) + HCl \quad (2)$$

the complete reaction being;

$$2\ SiOH + PMeCl_2 \rightarrow SiOP{=}O(Me,H) + SiCl + HCl \quad (3)$$

The intermediate methylphosphinic chloride [MeP=O(H,Cl)] was not detected via IR or NMR spectroscopy; the other products were. We assume that it is only present as an intermediate in low concentration and that it readily reacts with SiOH.

The immediate decrease in the intensity of the free SiOH peak at 3747 cm^{-1} and the appearance of a broader new peak at 3650 cm^{-1} following addition of $PMeCl_2$ is due to its physical adsorption and its weak perturbing influence on the free SiOH groups. A similar effect was found for the physical adsorption of PCl_3 on silica.

As the reaction proceeds, the 3650 cm^{-1} band slowly decreases in intensity as a very broad 3250 cm^{-1} band appears, accompanied by the growth of the PH band of species A at 2390 cm^{-1}. In the early stages of the reaction, and particularly for lower pressures of $PMeCl_2$, the 3250/2390 cm^{-1} peaks grew in unison, but after about 2 to 3 hours, the rate of growth of the 3250 cm^{-1} band decreased relative to the PH band, and eventually it started to decrease in intensity (Fig. 7-2A, 7-2B). As will be discussed below, the decrease in the intensity of the 3250 cm^{-1} band was not

related to the formation of species B. A similar broad band was found from the adsorption of trimethyphosphite or dimethylmethylphosphonate on silica,[129] but its intensity was about eight times greater. The 3250 cm^{-1} band is due to a strong H-bonding interaction between A and some OH groups. The eventual decrease in the intensity of the 3250 cm^{-1} occurs because the SiOH groups are continually being consumed by the reactant.

(b) *Identity of species B:*

The assignment of species B is more problematic. The IR and NMR results suggest that B can arise from the deposition of phosphorus acid, H_3PO_3, on silica. The species is protonated, as evidenced by the 2490 cm^{-1} IR band and ^{31}P delayed decoupling. Further, in chapter 4 it was shown that the reaction of PCl_3 with SiO_2 also gave species B, but never in such a large quantity and only on a longer time-scale. The two peaks at -8 and -18 ppm must be due to SiOP=O(H,OH) and $(SiO)_2P$=O(H) respectively. Because the parent compound has a P-CH_3 group and this is never removed in any chemical reaction at room temperature,[130] we were forced to assume that species B must have been generated from an interaction between PCl_3 and the products of the $SiO_2/PMeCl_2$ reaction.

In order to address this problem we synthesized two $PMeCl_2$ samples that were free of PCl_3. The first was 99% enriched in ^{13}C, but only enough material for two NMR experiments was obtained. At short reaction times, ^{31}P MAS-NMR showed that only species A occurred, as anticipated. For long reaction times species A was also formed, but species B could not be observed. The ^{13}C MAS-NMR of both these samples showed a doublet centered at 15 ppm with

a $J_{P\text{-}C}$ coupling constant of about 85 Hz. These observations further support the assignment of the structure SiOP=O(H,Me) to species A, since the analogous values were found to be 14.6 ppm and 90 Hz in the model compound MeOP=O(H,Me).[131]

The second sample, not ^{13}C enriched, was used for IR experiments. Again only species A was generated, even after 20 hours of reaction time. As with the PCl_3 contaminated sample, the broad 3250 cm^{-1} band initially increased in intensity and then decreased. When PCl_3 was added to the gas phase after 2 hours of reaction, species B formed with a concomitant decrease in the amount of species A, as was found with commercial $PMeCl_2$ samples (Fig. 7-6).

The above results show clearly that the formation of species B is an artefact due to the presence of PCl_3 in the 'as received' samples of $PMeCl_2$.

There is an isosbestic point in Fig. 7-3B showing that there is a correlation between the disappearance of species A and the creation of B. Now it is known that PCl_3 reacts with phosphinic acids as follows: [132]

$$2PCl_3 + 3RP{=}O(H,OH) \rightarrow 3PRCl_2 + 2H_3PO_3 \qquad (4)$$

When silica was doped with MeP=O(H,OH), only the parent acid and species A were observed by NMR and IR. When PCl_3 was allowed to react with the doped SiO_2, species B formed rapidly, and species A was consumed. In this reaction the formation of $PMeCl_2$ was

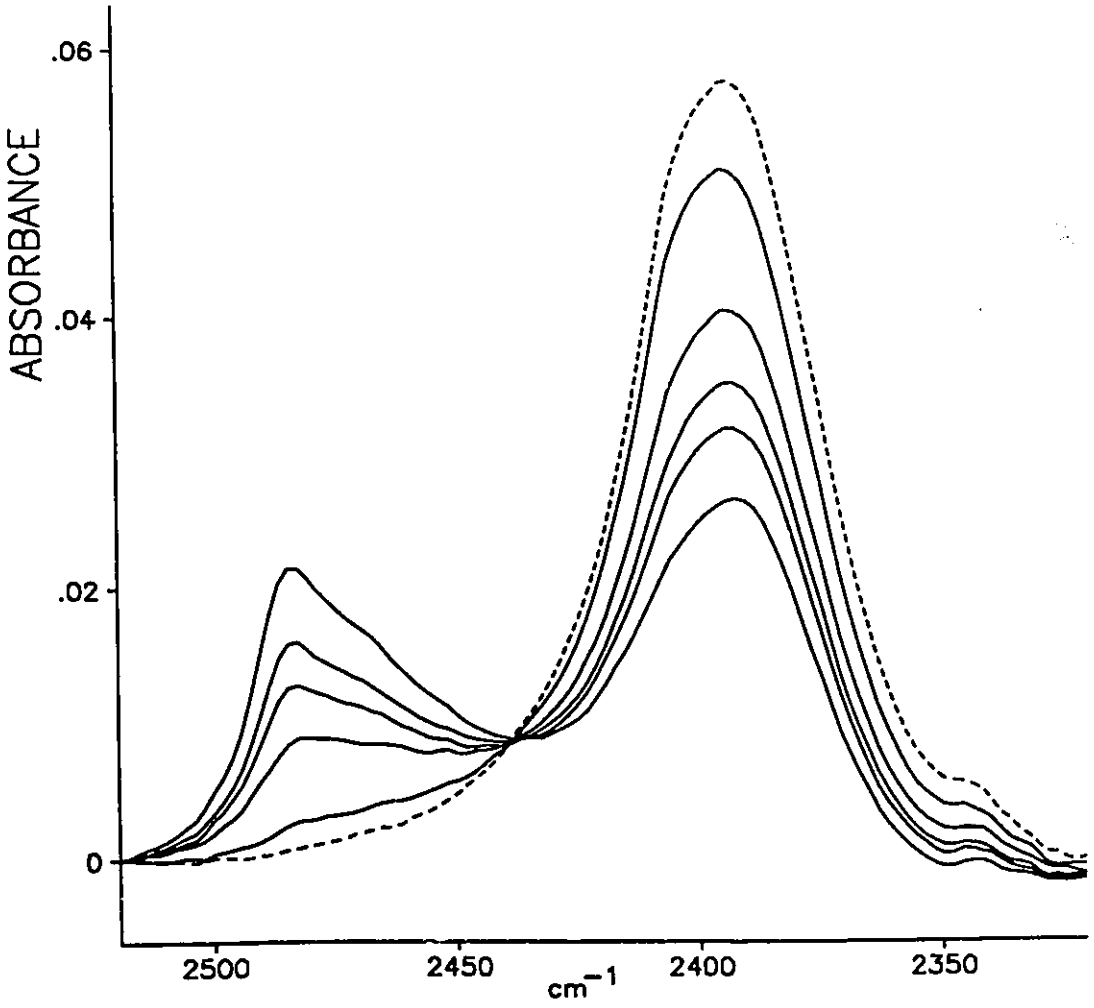

Fig. 7-6: Dashed (----) curve - IR spectrum observed in the PH stretching region after exposure to 21 Torr of pure $PMeCl_2$ (free of PCl_3 as an impurity). The gas phase was then condensed in liquid nitrogen in a separate compartment from the sample and PCl_3 equivalent to 7% of total P was added to the condensate. This was then warmed to room temperature and was re-added to the reaction cell. The subsequent spectra showing a decrease at 2390 cm^{-1} and an increase at 2490 cm^{-1} were recorded at the following times after admission of the 'mixture' to the cell; 0.3, 2.3h, 4.3h, 6.3h and 12.3h.

observed by both NMR and IR. This shows that a reaction similar to equation (4) can occur on silica. If it is assumed that gaseous HCl present in the ambient gas can participate in equilibria involving the chemisorbed species, the following scheme can rationalize the formation of species B from species A:

$$3HCl + 3SiOP{=}O(Me,H) \rightleftharpoons 3MeP{=}O(H,OH) + 3Si\text{-}Cl \quad (5a)$$

$$2PCl_3 + 3MeP{=}O(H,OH) \rightleftharpoons 3PMeCl_2 + 2H_3PO_3 \quad (5b)$$

$$2H_3PO_3 + 3Si\text{-}Cl \rightleftharpoons (SiO)_2P{=}O(H) + SiOP{=}O(H,OH) + 3HCl \quad (5c)$$

$$3SiOP{=}O(H,Me) + 2PCl_3 \rightleftharpoons (SiO)_2P{=}O(H) + SiOP{=}O(H,OH) + 3PMeCl_2 \quad (5d)$$

Equation (5d) would lead one to predict equal amounts of mono and di-functionally chemisorbed phosphorous acid should be formed. In fact ^{31}P NMR shows that the di-functionally adsorbed form, $(SiO)_2P{=}O(H)$, predominates at least at the late stages of the reaction between SiO_2 and $PMeCl_2/PCl_3$ mixtures. The scheme outlined in equations (5) does not account for all of the subtleties of the observed reactions, and it cannot be expected to do so. There are simply too many possibilities for competing reactions to occur. For example, since SiOH groups are low in concentration at the late reaction times during which species B appears, it is tempting to invoke the participation of siloxane bridges in the formation of species B:

$$SiOP{=}O(H,Me) + PCl_3 + SiOSi \dashrightarrow (SiO)_2P{=}O(H) + SiCl + PMeCl_2 \quad (6)$$

Unfortunately, a large number of reaction equations can be written to explain the observed products, but since distinguishing between them experimentally is very difficult, further speculation is not warranted. Whatever the exact mechanism, the generation of species B is an artefact due to the presence of PCl_3. In spite of being present in only 5 mol% amounts, the presence of PCl_3 manifested itself due to the high pressures of $PMeCl_2$ required for the reaction to proceed at a reasonable rate. Thus, a 25 to 50 torr pressure of reactant in a 300mL volume would contain 20 to 40 μmols of PCl_3. A 50 mg silica disk of area 325 m^2/g and containing 1.2 OH groups/nm^2 contains 32 μmols of OH.[16] Therefore the quantity of PCl_3 present is in fact comparable to the number of OH groups available. We have verified that with PCl_3 as an intentionally added impurity to $PMeCl_2$, at levels between 2 and 15 mol%, the same product distribution is observed.

Conclusions

The reaction of pure $PMeCl_2$ with SiO_2 produces SiOP=O(H,Me), SiCl and HCl and a likely reaction mechanism has been deduced. If the reactant is contaminated with small quantities of PCl_3 in the range from 2 to 15 mole percent, then the above species reacts with the mixture after long (several hours reaction) to produce two secondary phosphorus containing chemisorbed products, SiOP=O(H,OH) [minor product] and $(SiO)_2P$=O(H) [major product] and some plausible reaction sequences have been discussed.

CHAPTER 8

Chemisorption of $P(OMe)_3$ on Al_2O_3

Introduction

Morrow, McFarlan and Gay have previously studied the interaction of trimethyl phosphite with silica [129]. Motivation for this study came from several sources. Firstly, phosphorus is an essential surface component in several types of catalyst, ranging from acidic phosphates [85,133-136,121a-b] to immobilized transition metal phosphine complexes [125a-c]. Secondly there is a pressing need for understanding of the environmental fate of organophosphorus pesticides and chemical warfare agents.[121a,122a-b,137-140]

Silica was chosen for this initial study because it lacks Lewis acid or base sites [112], so that the chemistry of interaction with trimethyl phosphite should be simpler than with more active oxides. In that study the combination of IR and NMR spectroscopies led to a rather clear and complete understanding of the system.

Alumina is the logical choice for extension of the previous work on silica. It is among the most common industrial catalytic materials, both as a catalyst and as a catalyst support.[5] Phosphorus containing species constitute an essential surface component of several alumina based catalysts, including phosphates [133,141-2], hydrotreating catalysts [124a-b], and silico-aluminophosphates [143]. The results of the present study are also related to much previous work using alumina based materials to cause the heterogeneous decomposition of toxic organophosphorus compounds [144,122d,123c].

The chemistry of this system may be expected to be complex. Dimethyl phosphite (DMP) and dimethyl methylphosphonate (DMMP) might be expected as initial products [129], but these compounds will also be expected to interact strongly with the alumina surface [122d,144]. This will lead to complicating secondary reactions, but will also provide an opportunity. There has been extensive study of the adsorption of DMMP [122b,121c] and DMP [145,146] on aluminum oxidized by oxygen subjected to a dc-glow discharge, using inelastic electron tunnelling spectroscopy (IETS). It will prove interesting to compare the results of the present study, using more conventional spectroscopic techniques, as well as more conventional alumina samples, to these previous results.

Before the results for $P(OMe)_3$ adsorption are presented, it will be necessary to discuss the adsorption of DMMP and then DMP. This will provide a great deal of required chemical and spectroscopic background information.

Adsorption of DMMP [$CH_3P{=}O(OCH_3)_2$] on Alumina

Introduction and Some Notation

The adsorption of dimethyl methylphosphonate (DMMP) an Al_2O_3 was the most readily understood reaction system found in this study. It will be seen that DMMP adsorbs on alumina in three main forms. The first is as molecular DMMP. By this it is meant that DMMP has not lost either of its methoxy groups. This state will be indicated by the symbol DMMP(0). This

symbol is intended to include DMMP that interacts only weakly with the surface, for example via hydrogen-bonding of the phosphoryl oxygen with surface hydroxyl groups, as well as stronger interactions such as those involving Lewis acid-base adduct formation between the phosphoryl oxygen and surface Lewis acidic Al atoms:

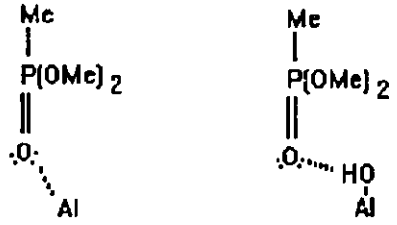

After fairly mild treatment the predominant species on a DMMP treated surface appear to be those with one methoxy group split off, denoted DMMP(1). It will be seen that if the alumina has been activated at temperatures above 400°C, DMMP(1) has no discrete P=O group. The P=O group is so strongly coordinated to the surface that it can be said to have become part of a surface metal-phosphonate phase. The π-bond order can be expected to be distributed over the two surface P-OAl bonds. In Al_2O_3 activated at 150°C DMMP(1) species that have a discrete P=O bond seem to exist:

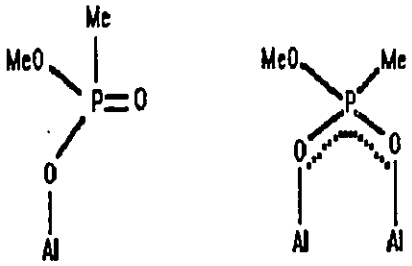

Finally, after higher temperature treatment, the second methoxy group is lost giving DMMP(2), This species never shows a discrete P=O group:

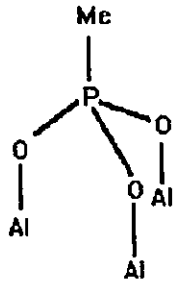

Throughout this chapter, the activation temperature of a sample will be given in degrees Celsius in parentheses after the oxide. For example, alumina activated at 150°C will be denoted $Al_2O_3(150)$. The discussion of the DMMP/Al_2O_3 system is most conveniently started with adsorption on $Al_2O_3(900)$. For this high an activation temperature there are so few surface hydroxyl groups that they are not a factor in the chemistry.[23]

Adsorption of DMMP on Dehydroxylated Alumina

When $Al_2O_3(900)$ is exposed to an excess of DMMP and the sample evacuated briefly at room temperature, the spectrum of the adsorbed species shown in Fig. 8-1A is dominated by that of DMMP(0). This is in contrast to the behavior observed by Weinberg on his samples, where DMMP(1) was the major species for adsorption temperatures between 25°C and 200°C.[122b] It is much more similar to the behavior of Sarin and diisopropyl methylphosphonate on

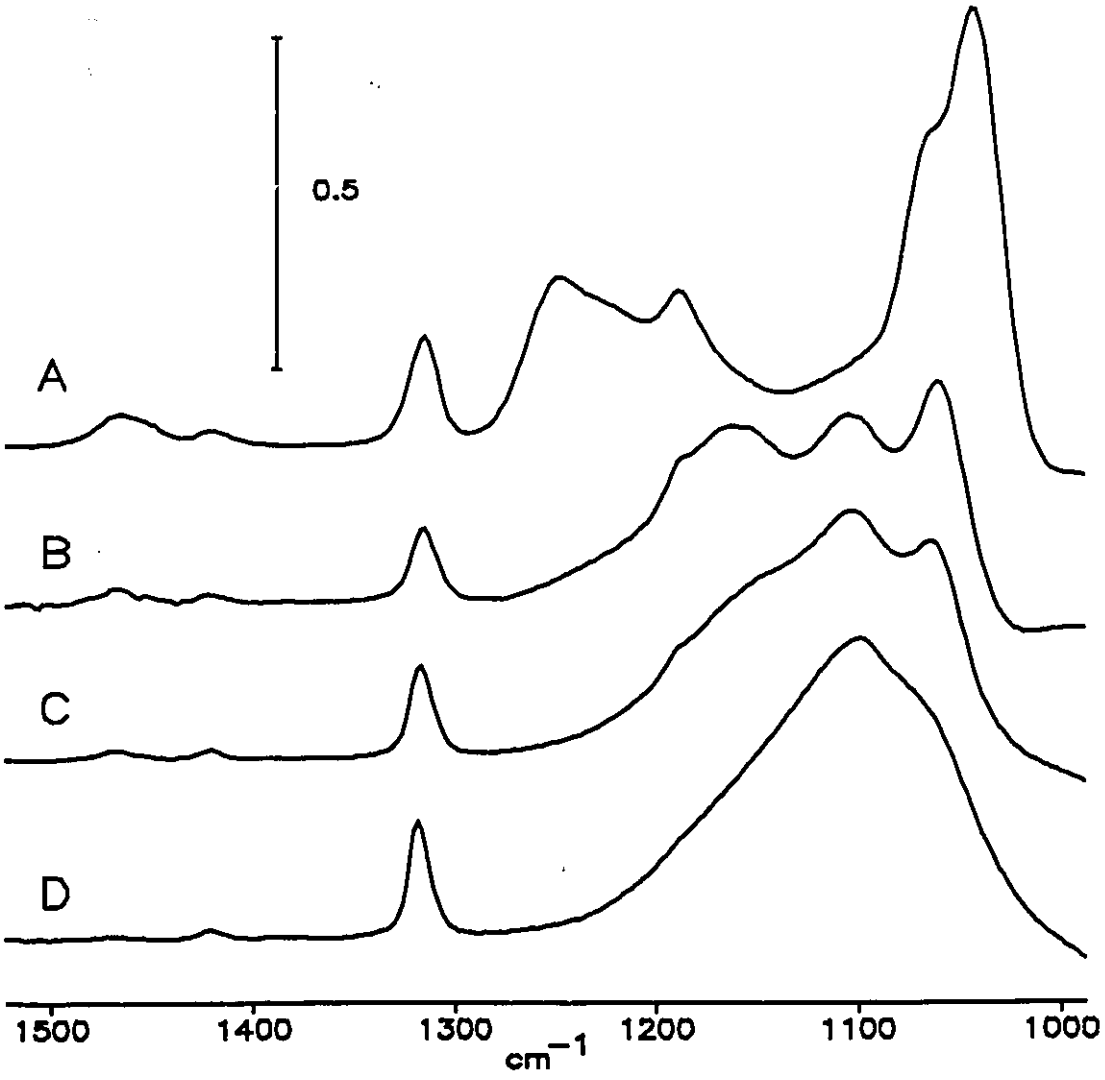

Fig 8-1: DMMP on Al_2O_3(900)

A-Adsorption of excess DMMP followed by 2 minutes evacuation at room temperature

B-Evacuation for 1 hr. at 100°C

C-Evacuation for 1 hr. at 200°C

D-Evacuation over night at 320°C

The spectrum before adsorption has been subtracted from those shown.

conventional Al_2O_3 samples observed by Kuiper *et. al.* [144]. The bands shown in the 1450-1000 cm^{-1} region in Fig. 8-1 are the most diagnostic available, and are assigned in a straightforward manner in accordance with the literature.[147]

The weak, broad peak centred at 1450 cm^{-1} is due to $\delta_s(CH_3)$ and $\delta_{as}(CH_3)$ of methoxy groups. These are mainly $POCH_3$ groups, but they are probably overlapped by a small contribution from $AlOCH_3$ groups as discussed below. The bands at 1410 cm^{-1} and 1314 cm^{-1} are the analogous modes arising from PCH_3 groups. The band at 1246 cm^{-1} is due to P=O groups that interact only weakly with the surface, since there is only a small low-wavenumber shift from the observed gas phase frequency of 1278 cm^{-1}. A shoulder due to more strongly coordinated P=O groups appears at 1220 cm^{-1}. The appearance of multiple P=O bands due to adsorption sites of different strength is consistent with the known extreme heterogeneity of transition Al_2O_3 surfaces.[144,148] The sharper band at 1188 cm^{-1} is $\rho(CH_3)$ due to OCH_3 groups. None of the above features give any indication as to whether or not DMMP has lost any methoxy groups on chemisorption. The doublet consisting of a band at 1040 cm^{-1} with a shoulder at 1060 cm^{-1} is due to C-O stretching modes, and indicates that most of the surface DMMP still has two attached methoxy groups.

If one considers rotation about the P-O axes, it is evident that there are three most probable angular orientations in which a methoxy group could be found. Two of these are gauche to the phosphoryl group and one is trans to the phosphoryl group:

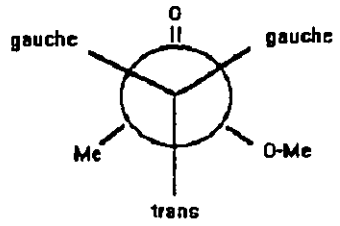

It is thought that the most stable conformer of DMMP has one gauche and one trans methoxy group, giving rise to the 1040 cm^{-1} and 1060 cm^{-1} bands respectively.[147] The implication of observing the same two bands with the same relative intensity when DMMP is adsorbed on Al_2O_3(900) is that not only are the two methoxy groups still intact and attached to the phosphorus atom, they exist in approximately the same conformation as they would in the free molecule. The interaction with the surface is primarily via the phosphoryl group. If the methoxy group oxygen atoms interact with surface Lewis acid sites at all they do so without any conformational change being induced.

In agreement with Kuiper [144], very slow changes occur in the spectrum when the sample is allowed to continue reacting at room temperature. The 1246 cm^{-1} and 1040 cm^{-1} bands due to DMMP(0) decrease in intensity slowly with time, while features at 1160 cm^{-1} and 1100 cm^{-1} due to the $\nu_{as}(PO_2)$ and $\nu_s(PO_2)$ modes of DMMP(1) slowly increase in intensity. The identification of these modes with DMMP(1) was first made in [149,150] from the infrared spectra of the polymeric model compound $Al(CH_3P(OCH_3)O_2)_3$, as well as related compounds. These modes were also observed in [144] after adsorption of other phosphonates on Al_2O_3.

Heating the sample at 100°C under either a static or dynamic vacuum essentially completes this process, as shown in Fig. 8-1B. The 1040 cm^{-1} band is gone, indicating that all

of the adsorbed DMMP has lost at least one methoxy group. There is no longer any distinct band in the 1200-1300 cm^{-1} region, showing that discrete P=O groups are completely absent. The C-O band at 1060 cm^{-1} is unchanged in intensity, implying that each surface DMMP has retained one of its methoxy groups. The two peaks at 1160 cm^{-1} and 1100 cm^{-1} due to $P(OAl)_2$ groups are very conspicuous in Fig. 8-1B. This is in contrast to the IETS studies where the weak electron-vibration coupling constant of these modes made them difficult to observe.[122b] These bands are the most diagnostic of the state of the adsorbed species, and in this case they are more readily observed in a conventional infrared experiment. The above evidence indicates that after 100°C evacuation, the predominant species on the surface of DMMP saturated $Al_2O_3(900)$ is the bridging form of DMMP(1):

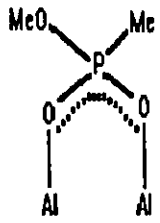

In Fig. 8-1A the predominant species is DMMP(0). The slow time dependence of the spectrum at this point indicated that some DMMP(1) was forming, but the bands due to DMMP(1) were all but undetectable in the presence of the strong, broad peaks of the more abundant DMMP(0) species. Similarly in Fig. 8-1B, the presence of some DMMP(2) cannot be ruled out.

In Fig. 8-1C it is apparent that as the evacuation temperature is increased the peaks at 1460 cm^{-1}, 1188 cm^{-1} and 1060 cm^{-1} due to methoxy groups decrease continuously in intensity.

Except for residual traces, methoxy groups are eliminated by prolonged evacuation at 300°C, as shown in Fig. 8-1D. After this treatment, the only bands that remain are those at 1420 cm^{-1} and 1310 cm^{-1} due to PCH_3 groups (as well as the associated bands in the C-H stretching region at 3008 cm^{-1} and 2935 cm^{-1}, not shown) and a very broad, intense asymmetric band peaked at about 1100 cm^{-1}. This must be the spectral signature of DMMP(2):

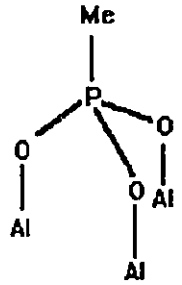

The spectrum in Fig. 8-2C can then reasonably be interpreted as a superposition of the spectra of DMMP(1) and DMMP(2). The reaction sequence can then be schematized:

$$\text{DMMP(0)} \xrightarrow{100°C} \text{DMMP(1)} \xrightarrow{300°C} \text{DMMP(2)}$$

although it has to be recognized that before 300°C multiple species probably exist.

Evacuating the sample for one hour at 450°C and then for one hour at 600°C caused very little change in the spectrum. This is in agreement with Weinberg, who also found that the DMMP(2) species were very stable thermally.[122b] In the IETS apparatus, temperatures greater than 475°C cannot be obtained, so that the upper limit to the thermal stability of DMMP(2) could

not be investigated. After evacuation of the sample for 1 hr. at 800°C, 80% of the intensity of the 1310 cm^{-1} band disappeared, and a weak band at 3678 cm^{-1} due to PO-H groups [133,141] appeared. The only change to the band at 1100 cm^{-1} was a slight shift to higher wavenumber, and the spectrum then resembled that of H_3PO_4 doped Al_2O_3 after similar activation.[eg. 141]

The Fate of the Methoxy Groups

It has been established that adsorbed DMMP loses its methoxy groups sequentially. The question naturally arises as to whether they remain adsorbed, desorb as methanol or dimethyl ether, or otherwise decompose. This question proves to be impossible to answer completely by infrared spectroscopy alone. In Fig. 8-2 the spectra after adsorption and 100°C outgassing of DMMP (Fig. 8-2A) and methanol (Fig. 8-2B) on Al_2O_3(900) are compared. Note that the $\nu_s(CH_3)$ mode at about 2840 cm^{-1} in Fig. 8-2B consists of at least two components. According to [151] the peak at 2844 cm^{-1} may be attributed to methoxide ions and very strongly coordinated methanol, and the peak at 2824 cm^{-1} is attributable to less strongly coordinated methanol. Both peaks have lower frequency than that produced by DMMP adsorption under similar conditions, which would tend to indicate that under these conditions most of the surface methoxy groups are bound to phosphorus. The peak at 2856 cm^{-1} in Fig. 8-2A is asymmetric to low wavenumber, and hence may contain a small contribution from the 2844 cm^{-1} surface methoxide species.

This may seem like a satisfactory interpretation, but unfortunately 2844 cm^{-1} may not be the correct frequency to expect for a surface AlOMe species derived from DMMP adsorption. In methoxy groups the frequency of this band is determined by the extent of weakening of the

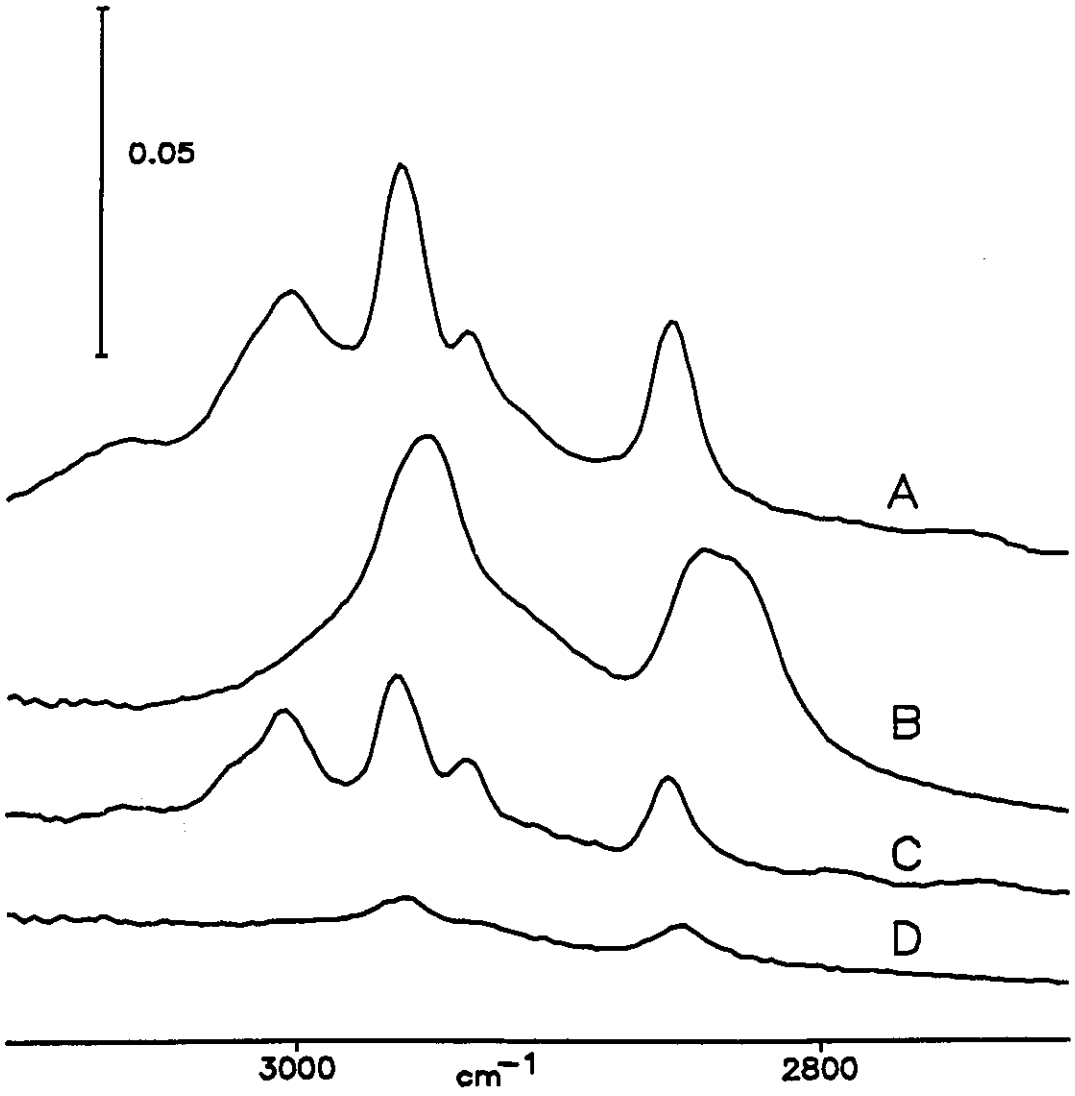

Fig. 8-2: Adsorption of DMMP and Methanol on Al_2O_3(900)

A-DMMP on Al_2O_3(900) degassed at 100°C

B-Methanol on Al_2O_3(900) degassed at 100°C

C-DMMP on Al_2O_3(900) degassed at 200°C

D-Methanol on Al_2O_3(900) degassed at 200°C

C-H bonds by the oxygen atoms' lone pairs.[33] If the methoxide group is placed in an environment that withdraws electron density, higher C-H stretching frequencies result. This effect has been used to distinguish between singly coordinated and bridging methoxide groups on ZrO_2.[152] The frequency of the $\nu_s(CH_3)$ mode of alumina bound methoxy groups will depend on the site at which it is found, and particularly on the coordination number. This will in turn depend on the method used to generate the methoxy groups. A frequency as high as 2852 cm^{-1} has been reported for this band when methoxy groups are generated by chemisorption of chloromethane on Al_2O_3.[153] If this were the frequency for the surface AlOMe groups formed after DMMP adsorption, their spectrum would overlap and be indistinguishable from those due to DMMP(0) and DMMP(1).

After the sample has been degassed at 200°C it appears unlikely that there is a significant number of surface methoxy groups, as shown in Fig. 8-2C and 8-2D. Before this evacuation temperature infrared spectra cannot definitively confirm or rule out the presence of AlOMe groups. As shown in Fig. 8-3 the other infrared active methoxy group modes ($\delta(CH_3)$ at 1460 cm^{-1}, $\rho(CH_3)$ at 1190 cm^{-1} and ν(C-O) at 1095 cm^{-1}) are also overlapped and overwhelmed.

One might attempt to determine whether or not AlOMe groups exist in this system by following the evolution of the relevant bands as a function of conditions, but this is only done with great uncertainty. In Fig. 8-4 the behavior of the $\delta_s(CH_3)$ mode of the PCH_3 groups is shown as a function of degassing temperature. When the sample is evacuated at 100°C the intensity of this band decreases by about one third, but one cannot tell if this is due to desorption of DMMP or to a decrease in extinction coefficient that might occur during the transformation DMMP(O) $\rightarrow$ DMMP(1). When degassing is continued to 300°C this band completely regains

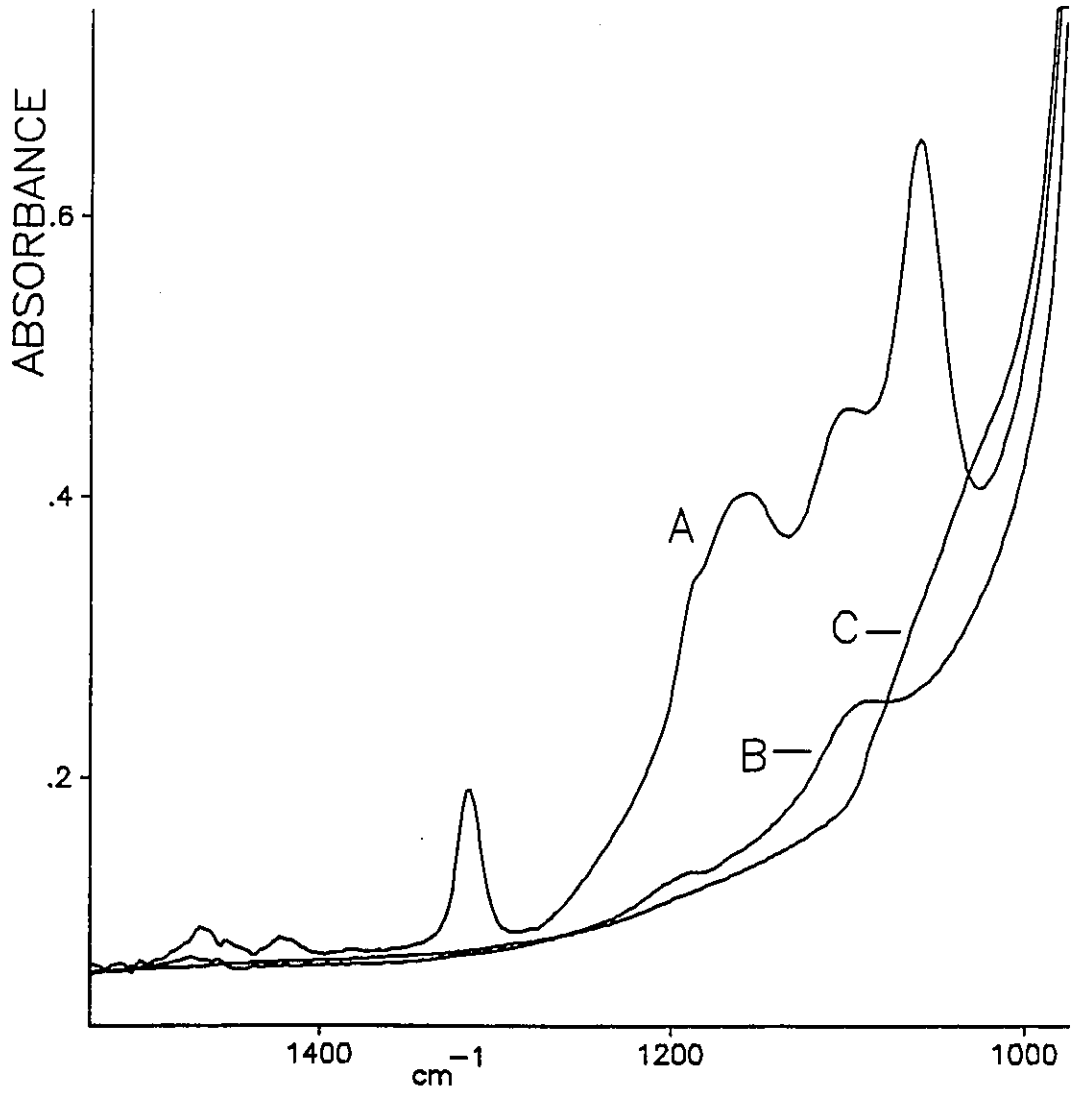

Fig. 8-3: Adsorption of DMMP and Methanol on Al_2O_3(900)

A-DMMP on Al_2O_3(900) degassed at 100°C

B-Methanol on Al_2O_3(900) degassed at 100°C

C-Typical Al_2O_3(900) background before adsorption

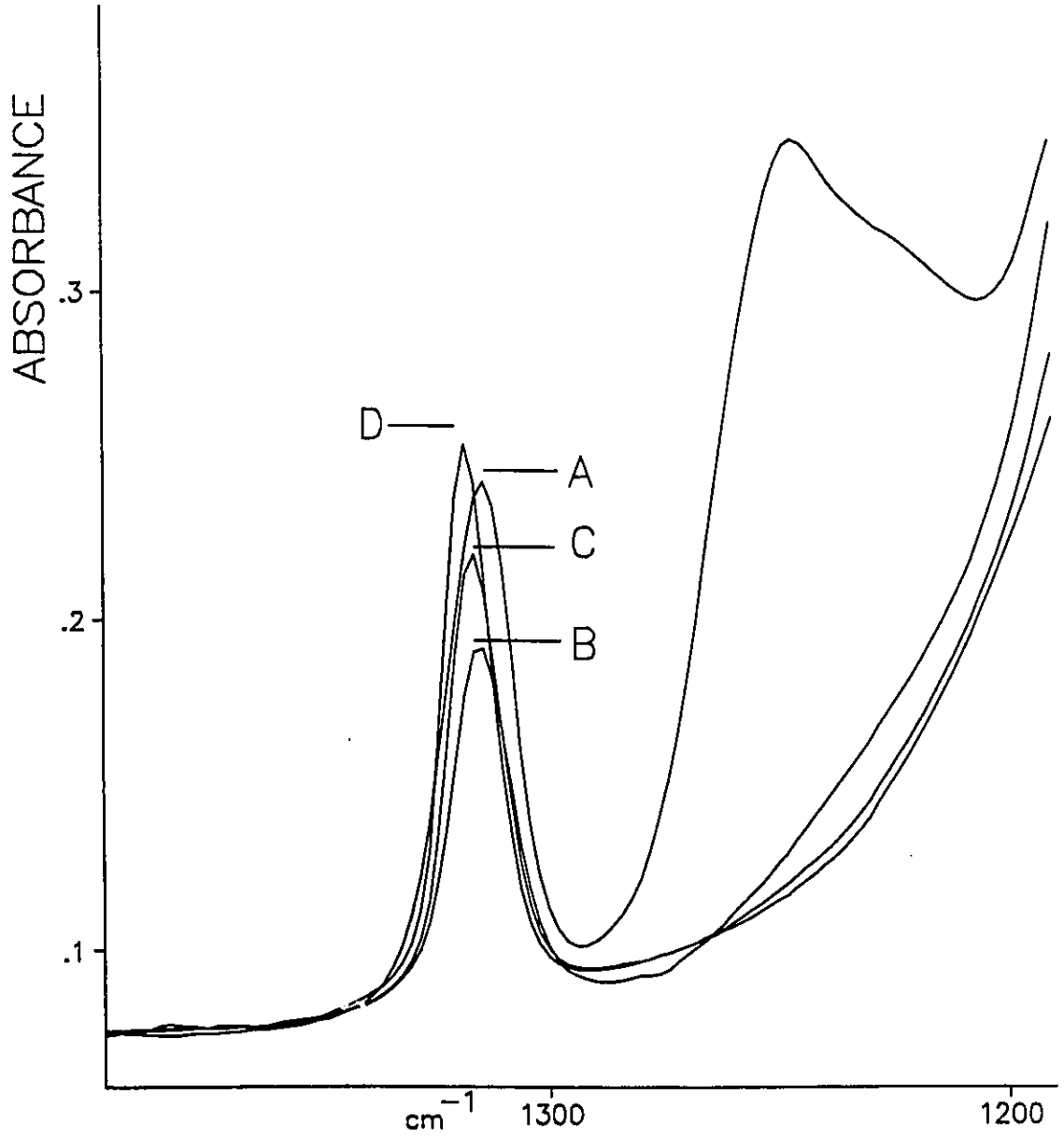

Fig. 8-4: DMMP on Al_2O_3(900)

A-DMMP on Al_2O_3(900) degassed 2 minutes at room temperature

B-Degas 1 hour at 100°C

C-Degas 1 hour at 200°C

D-Degas 1 hour at 300°C

its intensity. This must be due to an increase in extinction coefficient, and shows that interpretation of the intensities of bands that are due to more than one species are bound to be incorrect unless some subsidiary quantitative data can be obtained.

Digression on the Adsorption of DMMP on Other Oxides

When DMMP is adsorbed on activated MgO or ZrO_2 the existence of surface methoxide species is easily established, as shown in Fig. 8-5 and Fig. 8-6 respectively. On these more basic oxides the C-H stretching frequencies of the surface methoxide species are lower than on alumina.[152,154] In both Fig. 8-5 and Fig. 8-6, peaks appear at around 2820 cm^{-1} immediately upon adsorption of DMMP at room temperature , as well as a peak near 2845 cm^{-1}, which is closer to the position of $\nu_{as}(CH_3)$ for methoxy groups found after DMMP adsorption on Al_2O_3. The species responsible for the peaks near 2820 cm^{-1} when MgO or ZrO_2 is treated with DMMP prove to be quite resistant to thermal desorption.

While caution must be exercised in generalizing results obtained with other oxides to the DMMP/Al_2O_3 system, the appearance of two peaks in the $\nu_s(CH_3)$ region for both oxides strengthens the attribution of most of the intensity of the 2856 cm^{-1} band that appears on Al_2O_3 to $POCH_3$ groups, and makes it seem likely that some surface methoxide groups exist on DMMP treated Al_2O_3.

The infrared spectrum of the gases that were trapped after DMMP saturated Al_2O_3(900) was heated at 300°C only showed the presence of DMMP and dimethyl ether. Klabunde also found dimethyl ether as the primary degradation product of DMMP over MgO.[155] In that paper it was considered that the main species left after evacuation at 500°C was DMMP(1). In

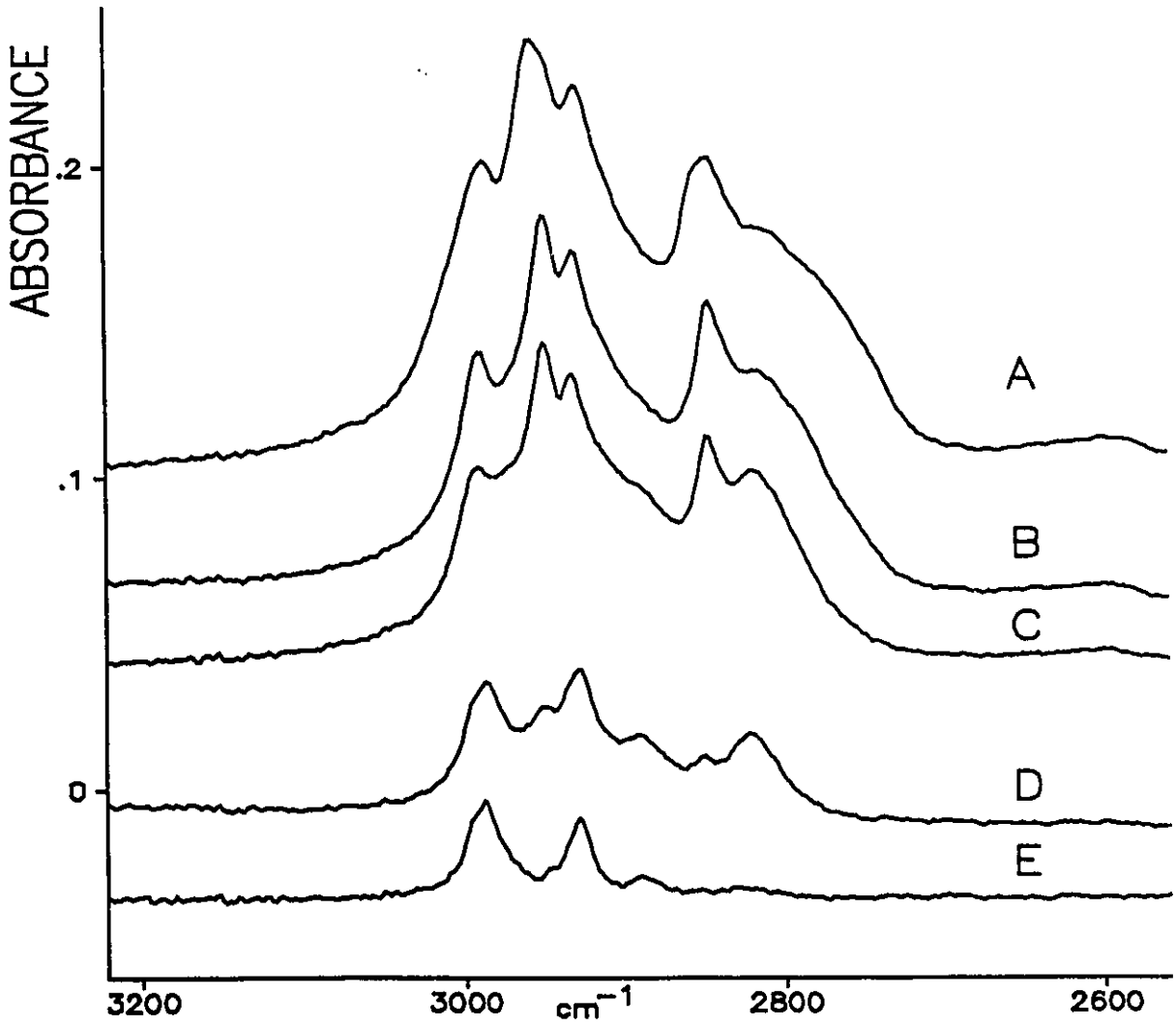

Fig. 8-5: Adsorption of DMMP on MgO(1000)

A-Add excess DMMP at room temperature

B-Evacuated 1 hour at 100°C

C-Evacuated 1 hour at 200°C

D-Evacuated 1 hour at 300°C

E-Evacuated 1 hour at 450°C

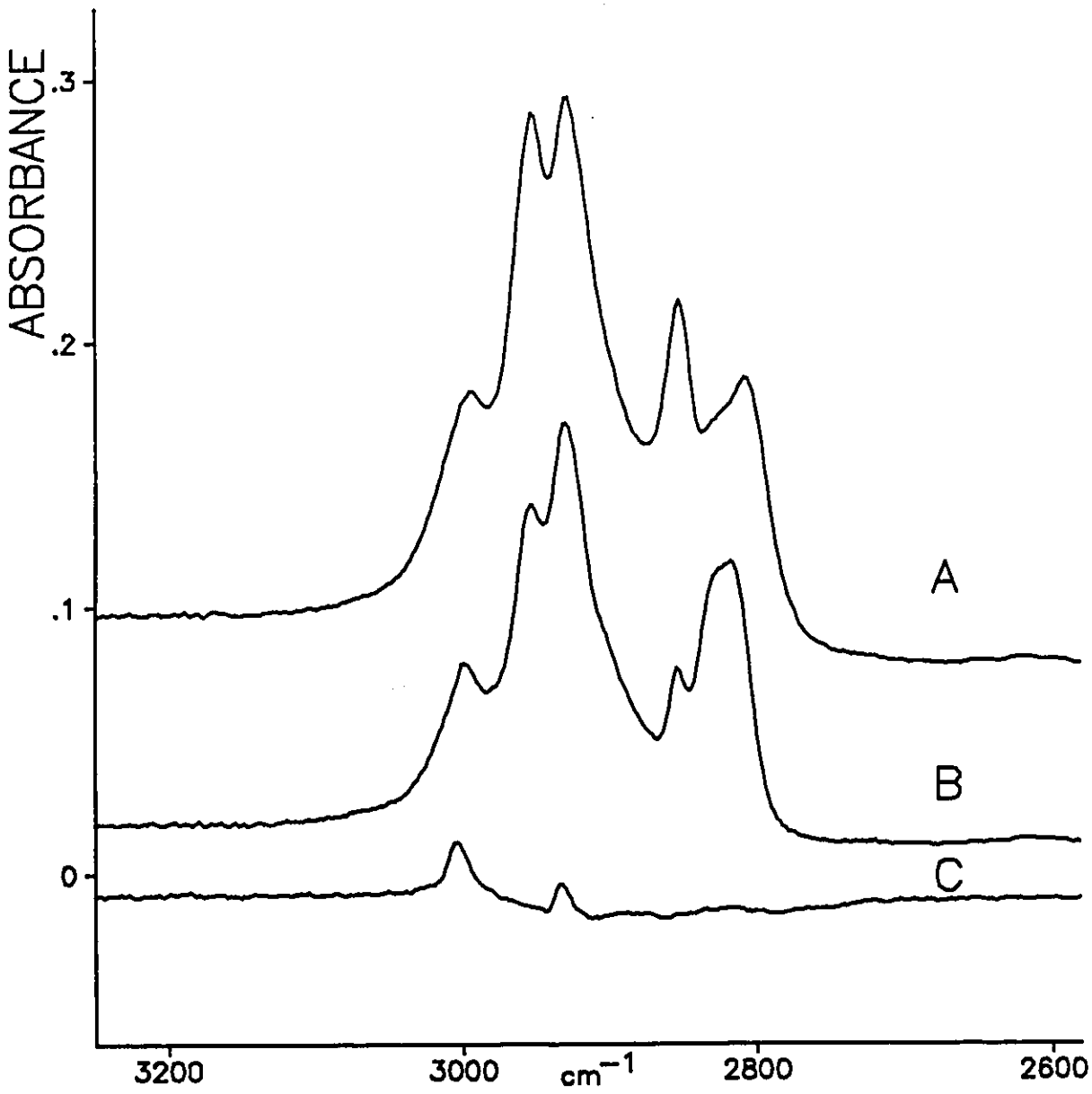

Fig 8-6: Adsorption of DMMP on ZrO_2(450)

A-Excess DMMP added and evacuated at room temperature

B-Evacuated at 150°C

C-Evacuated at 400°C

From the spectrum shown in Fig. 8-5E it is clear under the conditions of these experiments all of the methoxy groups have been removed by evacuation at 450°C. After this treatment only the much weaker bands at 2990 and 2928 cm^{-1} remain. These are due to the $\nu_{as}(CH_3)$ and $\nu_s(CH_3)$ modes of P-CH_3 groups, and indicate that the phosphorus then exists as DMMP(2).

The Nature of DMMP(2)

Returning to Fig 8-1D, it is noticeable that in the region of the P-O stretches around 1100 cm^{-1}, the appearance is different from that sometimes observed in the literature for metal phosphonates. In cases where the three P-O bonds have threefold symmetry and the sample is well crystallized the three vibrational degrees of freedom associated with the three P-O bonds give rise to two well resolved bands. The high wavenumber band is assigned to the doubly degenerate $\nu_{as}(PO_3)$ mode, and the lower wavenumber band to the the singly degenerate $\nu_s(PO_3)$ mode. These appear at 1100 cm^{-1} and 980 cm^{-1} in the case of Na_2MePO_3 [156], and at 1077 cm^{-1} and 1024 cm^{-1} in the case of $Zr(HPO_3)_2$.[157]

On Al_2O_3 it is doubtful the PO_3 groups have threefold symmetry. The ^{31}P MAS NMR spectrum of a sample degassed at 300°C shows a single peak at 27 ppm. The principal components of the chemical shielding tensor were found by the method of Herzfeld and Berger [158] to be 111±4, 35±4 and -53±4. If the local environment of the phosphorus nucleus has threefold symmetry two of these components would be expected to be the same.[159]

If the local symmetry is not more than twofold, three bands will be expected in the PO_3 stretching region of the infrared spectrum. Given that the alumina surface is very heterogeneous,

or even amorphous [148], each of the three bands will be quite broad. If they overlap sufficiently a broad unresolved peak with only a hint of asymmetry would result. This would be entirely consistent with the observed infrared spectrum of DMMP(2).

Effects of Lower Activation Temperatures

For the DMMP/Al_2O_3 system the effects of varying the activation temperature are rather modest, as shown in Fig. 8-7. The most obvious trend is that there is a relatively small but continuous increase in the uptake of DMMP as the temperature of activation is increased. In all the spectra shown there is only one C-O stretching peak present, at 1060 cm^{-1}, showing that for any activation temperature the predominant species after evacuation at 100°C is DMMP(1). For a sample activated at 150°C there is still a distinct P=O mode present in the spectrum after the sample has been evacuated at 100°C. This indicates that highly activated aluminas coordinate P=O bands more avidly, so that the formation of a surface metal phosphonate phase in which the P=O bond has lost its distinct identity occurs at lower temperatures.

^{31}P CPMAS NMR Spectra

NMR spectra have been recorded for a few sets of sample preparation conditions in order to obtain data to aid in the interpretation of the spectra of adsorbed $P(OMe)_3$. Unfortunately these samples were prepared in Ottawa and run in Vancouver. There is therefore some ambiguity in the interpretation of the spectra, as the delay of several days between preparation and data acquisition means that these samples have been treated in a manner not easily duplicated in infrared experiments.

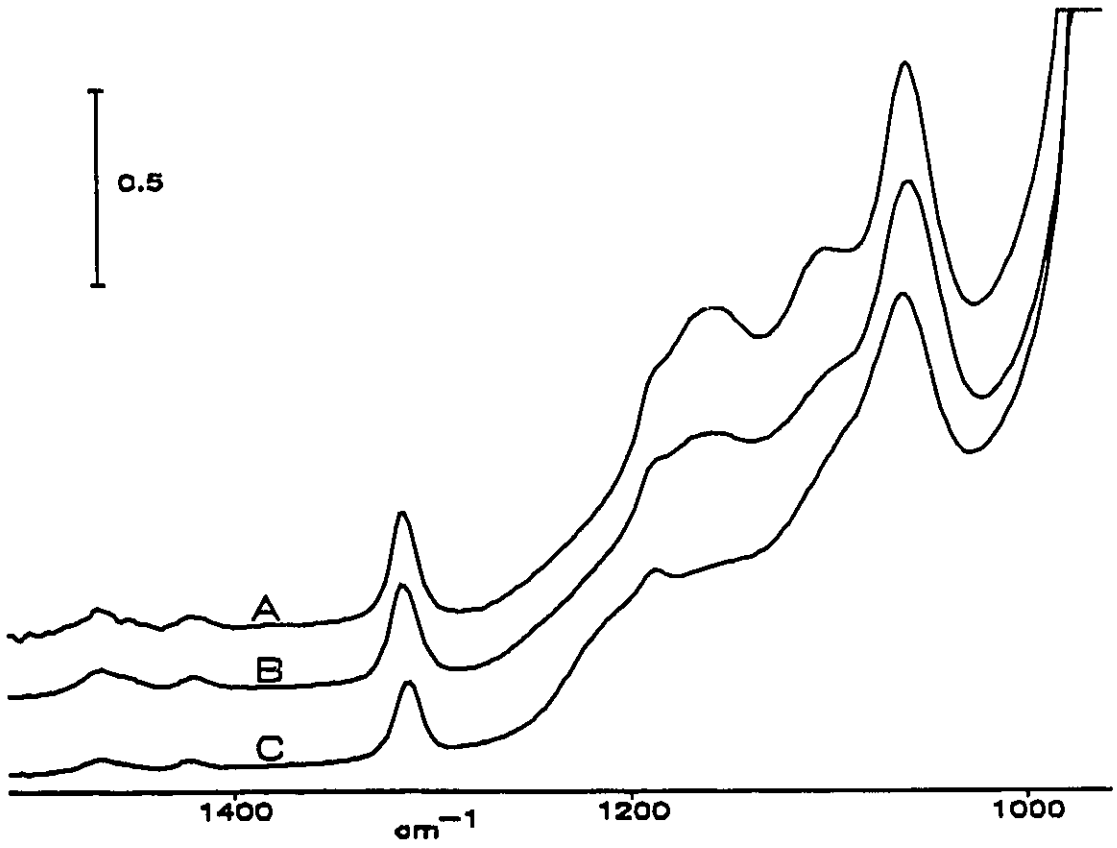

Fig. 8-7: DMMP on Al_2O_3 Activated at Different Temperatures

A-Al_2O_3(900) saturated with DMMP and evacuated at 100°C

B-Al_2O_3(450) saturated with DMMP and evacuated at 100°C

C-Al_2O_3(150) saturated with DMMP and evacuated at 100°C

Fig. 8-8C shows the ^{31}P NMR spectrum of a sample subjected to the mildest conditions tried, room temperature evacuation of DMMP saturated Al_2O_3(150). There are two main peaks present, at 32 and 23 ppm. (There is also a minor peak at about -16 ppm. This is the region associated with $AlPO_4$ phases.[160] It is puzzling that this peak appears for mild sample treatments and not for more severe treatments. It could be that in this particular sample the torch used to seal off the sample pyrolysed some DMMP.) Infrared spectra show that after room temperature adsorption the major species is DMMP(0) with a little DMMP(1). Since 32 ppm is exactly the chemical shift of the neat liquid DMMP,[129] one is tempted to assign the 32 ppm peak to DMMP(0) and the 23 ppm peak to DMMP(1). The obvious problem with this assignment is that DMMP(0) on a fully hydroxylated Al_2O_3 sample would be expected to be a mobile species, and therefore be difficult to observe in the cross-polarization spectrum. The spectrum is more intense in cross-polarization than in 90° pulses, indicating at least that the majority of surface DMMP molecules are not very mobile. It appears that some of the intensity at 32 ppm in Fig 8-8C is due to DMMP(1). Perhaps the long delay between sample preparation and data acquisition has led to the formation of some DMMP(2) in sample 8-8C, and DMMP(2) is responsible for the 23 ppm peak. In Fig 8-8B the sample has been outgassed at 100°C, so that there can no longer be any DMMP(0) species present. The high frequency peak has shifted to 30 ppm, but it is still very strong. It cannot be due to DMMP(0). Attributing the peak at 30 ppm to DMMP(1) and the peak at 22 ppm to DMMP(2) now seems attractive. Fig. 8-8A shows that this is an over-simplification. After evacuation at 450°C there can only be DMMP(2) species present. In the spectrum of this sample there is a single peak at 25 ppm but, the width of this peak is as large as the combined widths of the two peaks in Fig. 8-8C or 8-8B. Note that the

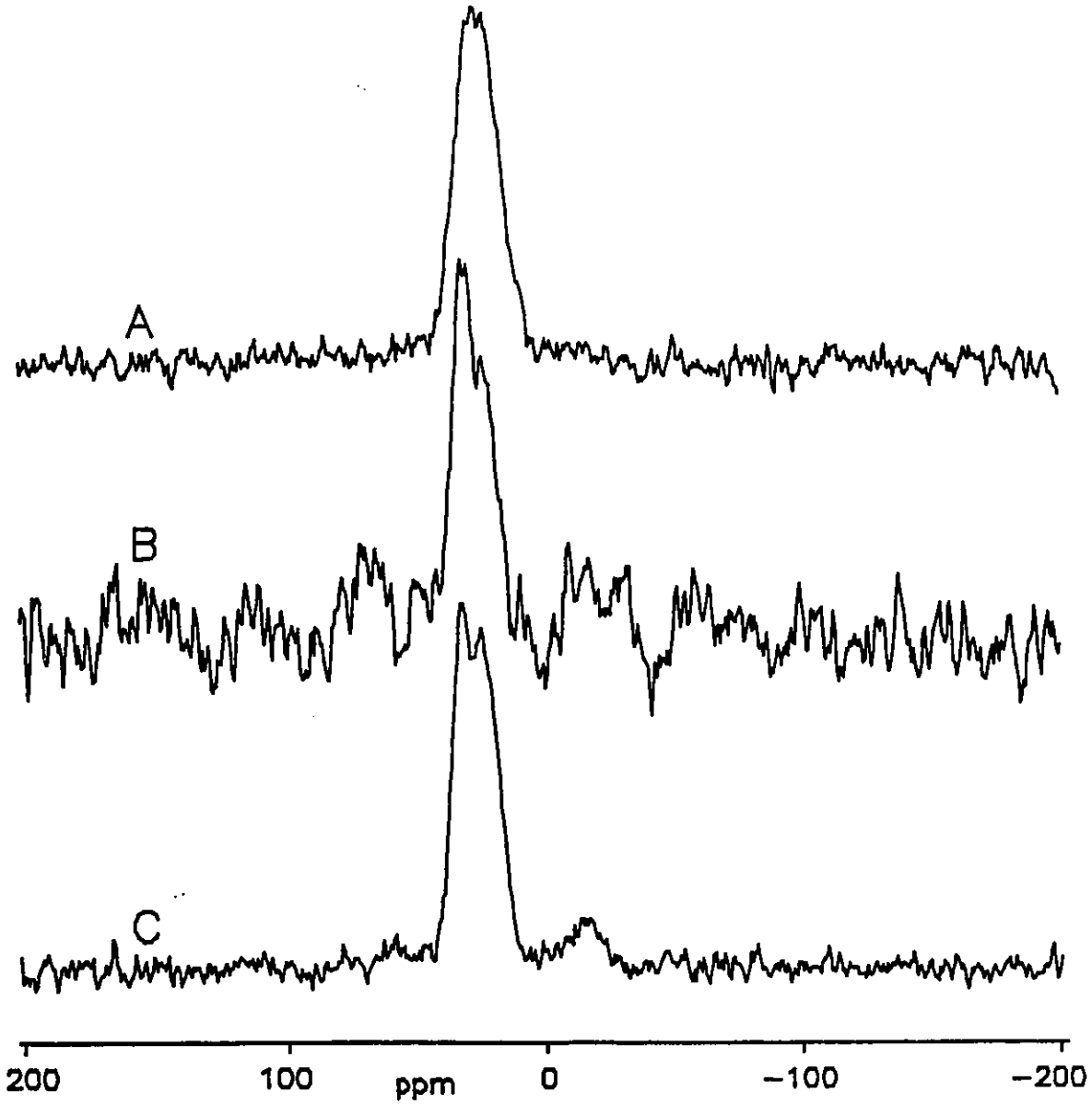

Fig 8-8: ^{31}P CPMAS Spectra of DMMP on Al_2O_3

A-DMMP on Al_2O_3(450), evacuated at 450°C, CPTOSS

B-DMMP on Al_2O_3(100), evacuated at 100°C, CPMAS

C-DMMP on Al_2O_3(150), evacuated at RT, CPTOSS

^{31}P chemical shift of $Zr(MePO_3)_2$ is 27 ppm.[161]

Because of the extreme heterogeneity of alumina, DMMP(2) species can make a substantial contribution to the spectral intensity at 30 ppm. Similarly DMMP(1) species probably make a strong contribution to the intensity at 23 ppm. It may even be that the probability distribution function for the chemical shift of DMMP(1)-type species has two maxima, at 32 and 23 ppm.

Further work would be needed to clarify the spectral assignments. Assigning the peaks at 30 ppm and 22 ppm to DMMP(1) and DMMP(2) respectively seems the most reasonable conclusion, but these attributions are tentative.

Conclusions

In agreement with previous work it is found that DMMP de-alkylates stepwise on Al_2O_3 surfaces.[122b,144] Unlike the materials prepared by Weinberg *et. al.* [122b] conventional Al_2O_3 samples de-alkylate DMMP only to a slight extent in a short room temperature exposure. Higher temperature behavior is more similar to that seen in [122b]. Both methyl groups are lost only after evacuation at or above 300°C. The resulting DMMP(2) species are very thermally stable.

While the ability to see the intense P-O stretching modes directly in an infrared experiment makes infrared spectroscopy seem like the proper tool to use for these studies, it must

be remembered that the IETS technique offers access to the entire frequency range. Low frequency information can be quite useful in some cases. For example, when H_3PO_3 is adsorbed on Al_2O_3, $\delta(PO_3^{2-})$ bands at 460 and 550 cm^{-1} due to HPO_3^{2-} groups appear,[121b] showing that both acidic protons react on adsorption. This spectral region is difficult to study by conventional infrared methods, due to the strong absorption of Al_2O_3 in this region.

Adsorption of DMP [$HP{=}O(OCH_3)_2$] on Alumina

The adsorption of $P(OMe)_3$ on Al_2O_3 is expected to lead to the formation of DMP as well as DMMP.[129] Adsorption of DMP on Al_2O_3 has been studied using IETS by Higo *et. al.*[145-6] These authors found that room temperature adsorption of DMP on their Al_2O_3 samples produced both DMP(1) and DMP(2) species. This notation is the same as was used for surface species derived from DMMP adsorption, ie DMP(O) has not lost either of its methoxy groups, and may exist in various forms, such as:

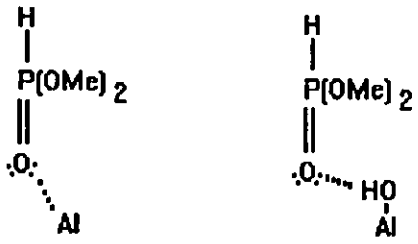

DMP(1) refers to DMP which has lost one methoxy group. DMP(1) may also exist in different forms, for example:

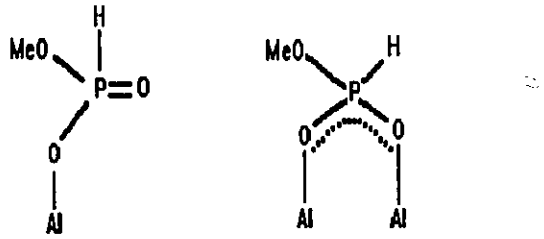

DMP(2) refers to DMP that has lost both methoxy groups:

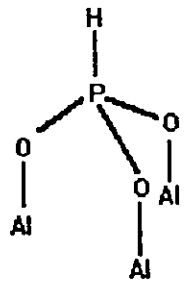

In the present study, other reactions were also found to occur, particularly if the Al_2O_3 was activated at temperatures greater than 150°C.

Fig. 8-9 shows ^{31}P CPTOSS spectra of DMP adsorbed on Al_2O_3 for various sample treatments. In Fig 8-9A the sample has been treated as mildly as possible. As for DMMP under similar conditions, two peaks are observed. The most intense peak is at 2.5 ppm, and a shoulder is observed at 8 ppm. The peak at 8 ppm is very close to the chemical shift of 11 ppm observed for neat DMP.[129] The peak at 2.5 ppm is probably attributable to demethoxylation products. The spectrum in Fig. 8-9A is virtually identical in appearance to that obtained when the spectrum is excited using 90° pulses. This indicates that the 8 ppm peak is due to an immobile species, quite possibly DMP(1), and DMP(2) might be responsible for the peak at 2.5 ppm. As for DMMP, this type of assignment is difficult to verify. In Fig. 8-9B the sample has been evacuated at 150°C so that no DMP(0) should be present, and a mixture of DMP(1) and DMP(2) is anticipated. In this spectrum it appears that the two peaks in Fig 8-9A have broadened and coalesced into a single peak, centred at about 5 ppm. This would be reasonably consistent with the attribution of the 8.5 ppm peak to DMP(1) and the

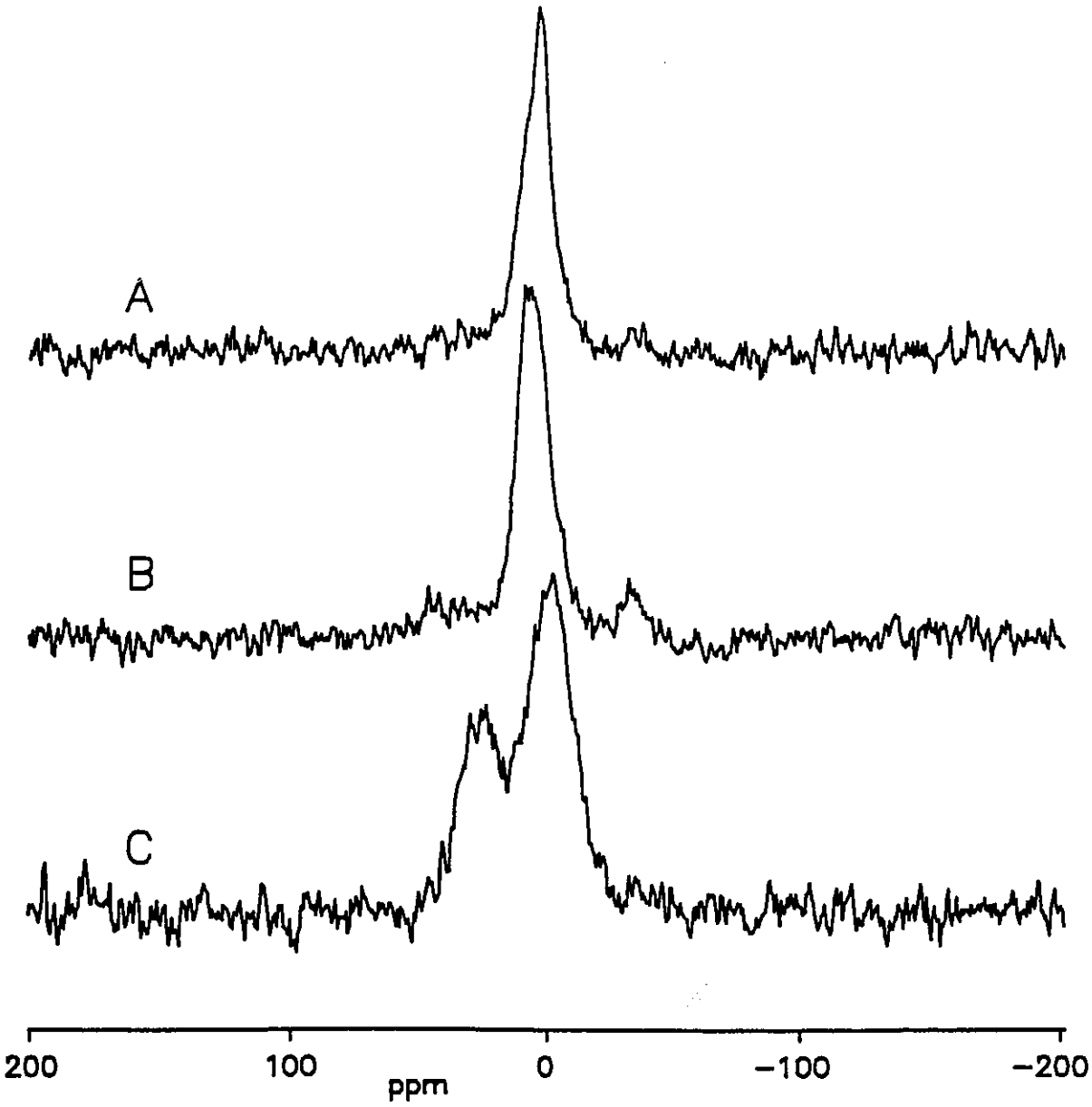

Fig. 8-9: ^{31}P CPTOSS Spectra of DMP on Al_2O_3

A-Excess DMP on Al_2O_3(RT)

B-Excess DMP on Al_2O_3(150), evacuated at 150°C

C-Excess DMP on Al_2O_3(450), evacuated at 450°C

2.5 ppm peak to DMP(2).

In Fig. 8-9C an $Al_2O_3(450)$ sample has been saturated with DMP and then evacuated at 450°C. The peak due to DMP(2) has shifted to -2 ppm. Al_2O_3 doped with 200 μmols/g H_3PO_3 show only a single ^{31}P resonance at -2 ppm for samples activated at room temperature, 200°C or 400°C. In Fig. 8-9C a there is also a strong peak at 24 ppm, the region where one expects DMMP(2) ^{31}P resonances to occur. The occurrence of DMMP derived species under these harsh conditions might have been anticipated, as it is known that DMP is thermally unstable.[162] When DMP is heated under inert atmosphere, DMMP and phosphine are among the main products of the complicated decomposition reactions.

When DMP is heated over $SiO_2(450)$ at 220°C, no DMMP derived surface species were observed. When the reaction temperature was raised to 450°C, a strong sharp peak at 1320 cm^{-1} due to the methyl group in species such as $MeP{=}O(OSi)_2$ was observed. Thus under the conditions of these experiments, the thermal decomposition of DMP becomes important at temperatures above 220°C. If the reaction of DMP with Al_2O_3 at temperatures lower than 200°C gives DMMP derived species, Al_2O_3 can be said to catalyze the decomposition of DMP.

IR Study of the Adsorption of DMP on $Al_2O_3(150)$

For the sake simplicity the discussion of the infrared results is started with conditions where almost no DMMP derived species form. In Fig. 8-10 the spectra upon adsorption of

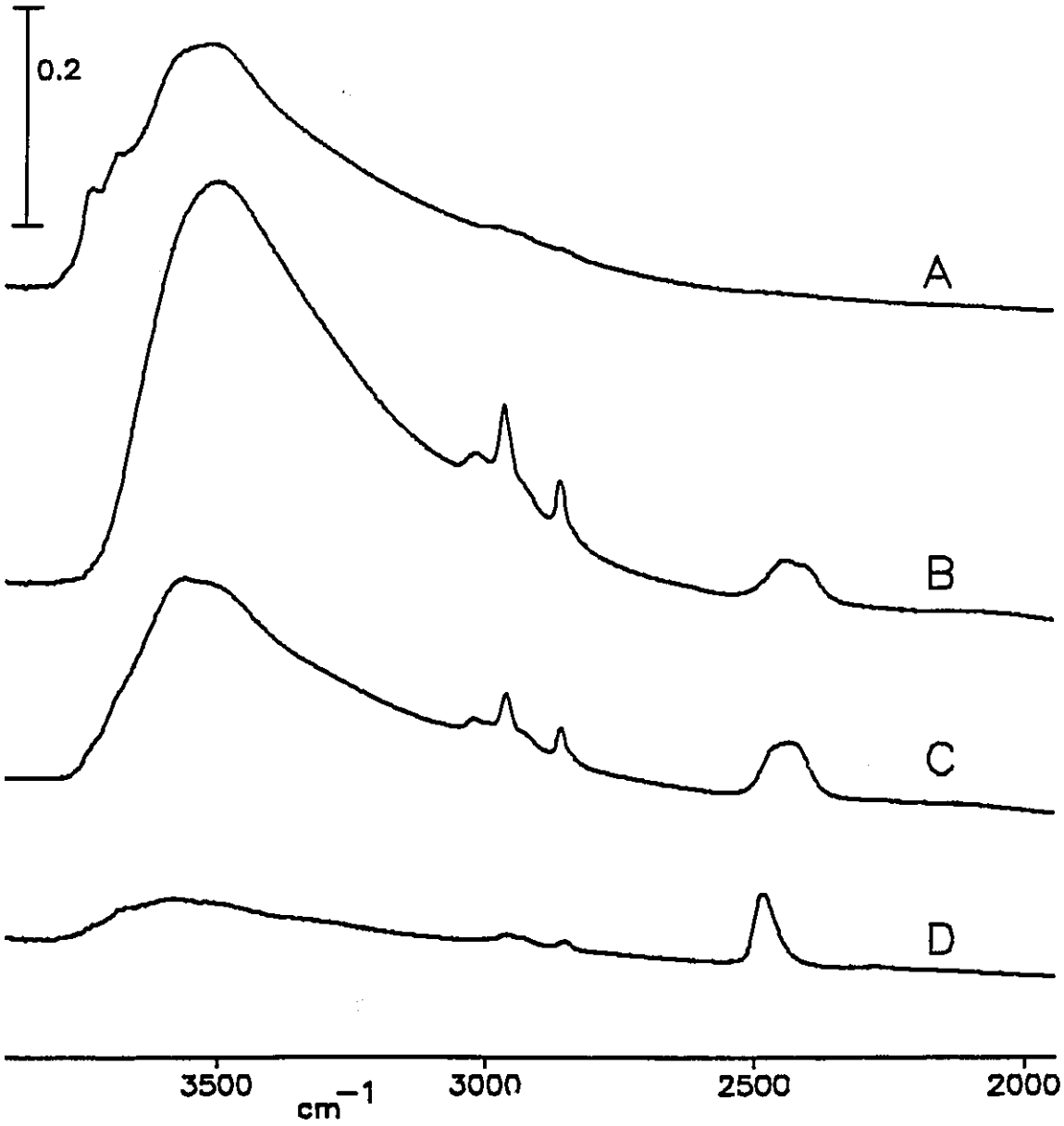

Fig. 8-10: Adsorption of DMP on Al_2O_3(150)

A-Al_2O_3(150) before adsorption

B-Add excess DMP and then evacuate two minutes at RT

C-Evacuate 200°C for 40 minutes

D-Evacuate 350°C for 30 minutes

DMP on Al_2O_3(150) in the 3900-2000 cm^{-1} region are shown. Fig. 8-10A is a typical Al_2O_3(150) background. In Fig. 8-10B shows the spectrum after exposure to the vapour pressure to DMP for 5 minutes and then evacuation for 2 minutes. The peaks at 3780, 3735 and 3680 cm^{-1} due to isolated AlOH groups are completely gone. This might be due to dissociative chemisorption:

$$H\text{-}P{=}O(OMe)_2 \quad + \quad HOAl \rightarrow \quad H\text{-}P{=}O(OMe)\text{-}O\text{-}Al \quad + \quad MeOH$$

There is a large increase in the intensity of the peak at 3450 cm^{-1} due to H-bonded Al-OH groups. This would argue against extensive dissociative chemisorption and in favour of a simple H-bonding interaction, as was observed with DMMP. In the case of DMMP the spectrum on adsorption in the C-O stretching region was clearly resolved and showed that at room temperature most of the adsorbate was present as DMMP(0). In the case of DMP the spectrum in this region is less well resolved. The C-O stretches have been assigned at 1042 and 1079 cm^{-1} in the liquid phase.[163] In this study a strong broad peak at 1070 cm^{-1} with a shoulder at 1095 cm^{-1} is observed in the gas phase. The rest of the infrared data for this experiment is shown in Fig. 8-11. The room temperature adsorption spectrum (one of the solid curves) shows a broad peak at 1050 cm^{-1} with a just discernable shoulder at 1085 cm^{-1}. This poorly resolved spectrum does not show that most of the adsorption was non-dissociative as definitively as was the case for DMMP. Nevertheless the chemistry of the two molecules may be expected to be similar under these mild conditions, and it is a good assumption that

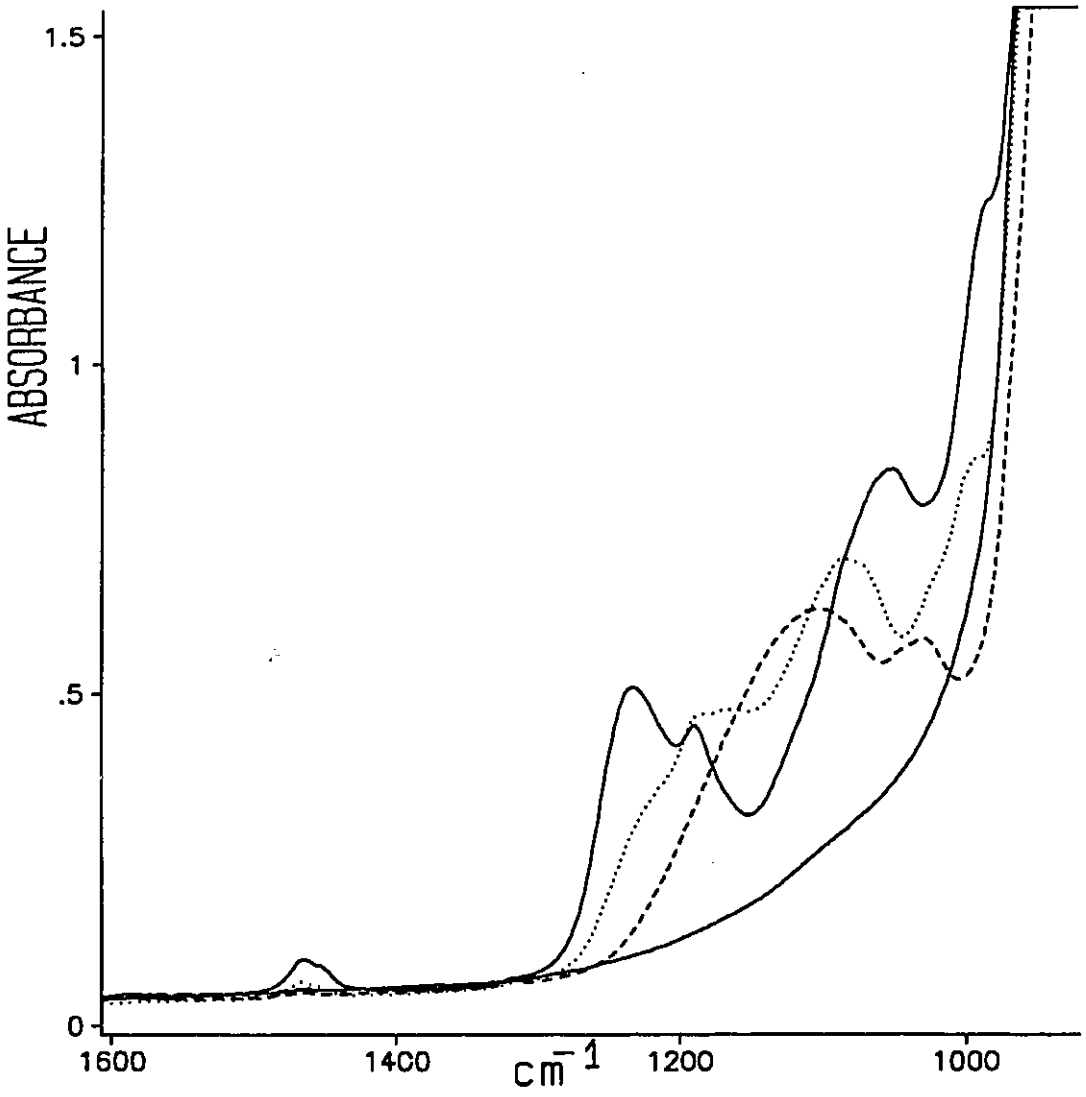

Fig. 8-11: Adsorption of DMP on Al_2O_3(150)

Solid curves correspond to Fig. 8-10A and 8-10B, Al_2O_3(150) before and after room temperature reaction with DMP respectively.

Dotted curve: evacuation at 200°C as for Fig. 8-10C

Dashed curve: evacuation at 350°C as for Fig. 8-10D

in Fig. 8-10B most of the DMP is present as DMP(0).

Comparison of Fig. 8-10A and 8-10B suggests that a large proportion of the AlOH groups, those which were already involved in H-bonding interactions before DMP was adsorbed, do not interact with DMP. This suggests that these AlOH groups are inaccessible to DMP. This can be explained by assuming that the "hydration-layer" of a weakly activated Al_2O_3 sample may be several layers deep. There are probably AlOH groups one or more cation layers below the surface. This is a reasonable assumption, because it is known that if η-Al_2O_3 is heated at 37 °C in the vapour pressure of water for several weeks, one can detect the formation of bulk hydroxide phases by X-ray diffraction.[164]

There is a puzzling feature in Fig 8-10B. The P-H stretching band appears as a doublet, with components at 2438 and 2409 cm^{-1}. On silica,[129] the P-H stretching band for adsorbed DMP(0) was also found to be a doublet with peaks at 2457 and 2440 cm^{-1}. The 2457 cm^{-1} peak was shown to be due to DMP(0) H-bonded to SiOH groups, and the 2440 cm^{-1} peak was assumed to be due to physisorbed DMP(0) not involved in a specific H-bonding interaction. (Gas phase DMP has a P-H stretching peak at 2443 cm^{-1} that is asymmetric to low wavenumber.) This interpretation does not apply to DMP(0) on Al_2O_3. Al_2O_3 is amphoteric, whereas SiO_2 is classified as an acidic oxide. The OH groups on Al_2O_3 are less acidic than those on SiO_2. Fig. 8-10B shows that AlOH groups are too weakly acidic to form a strong enough H-bond with DMP to give rise to a P-H band at as high a frequency as 2457 cm^{-1} after room temperature adsorption. Furthermore, the higher wavenumber component cannot be due to hydrogen bonded species. It will be seen shortly that when

DMP is adsorbed at room temperature on a totally dehydroxylated Al_2O_3 sample, there is a single ν(P-H) peak at 2443 cm^{-1}. This is similar to the position of the peak observed for non H-bonded DMP(0) species on SiO_2. The question then is how to explain the appearance of a band at such a low frequency as 2409 cm^{-1} in Fig. 8-10B.

It has been shown that the P-H frequencies of dialkyl phosphites are strongly dependent on the conformations of the alkoxy groups.[165,166] In Fig. 8-12 the notation for the conformations of dialkyl phosphites is explained.

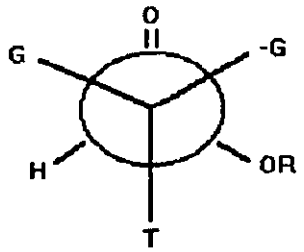

Fig. 8-12A

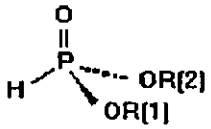

Fig. 8-12B

In Fig. 8-12A one sights along a P-O single bond. The alkyl group may be trans to the P=O group (T), or gauche to the P=O group. The two gauche positions are differentiated by giving them different labels, G and -G, as shown in Fig. 8-12A. To specify a conformation one orients the molecule as in Fig 8-12B. Two symbols separated by a comma are given, specifying the orientation of OR(1) and then OR(2).

The lowest energy conformation is considered to be the G,G (equivalent to -G,-G) conformation.[165-167] This conformer has a P-H stretching frequency of 2439 cm^{-1}. At slightly higher energy is the -G,T conformer. This conformer has a P-H frequency of 2405

cm^{-1}, very close to that of the low frequency peak on Al_2O_3. The -G,T conformer has been shown to increase in concentration relative to other conformers when the solvent polarity is increased, and is thus assumed to be the more polar conformer. The fact that a P-H stretching band at 2409 cm^{-1} appears when DMP is adsorbed on Al_2O_3(150), but not on Al_2O_3(900), suggests that the more polar conformers of DMP are more stable on a hydroxylated Al_2O_3 than on a dehydroxylated Al_2O_3. There is no obvious reason why this should be so.

Fig. 8-10C shows the spectrum after evacuation at 200°C. A mixture of DMP(1) and DMP(2) species is expected for these conditions if the DMMP results are a suitable guide. One still observes two peaks in the ν(P-H) region, now at 2455 and 2426 cm^{-1}. DMP(2) is expected to exist in a conformation that most resembles the -G,G conformation of DMP, as this conformation allows all three P-O bonds to be directed downward into the Al_2O_3 surface. This conformation has ν(P-H) at 2470 cm^{-1}. The 2455 cm^{-1} peak may have a contribution from DMP(2) species, but it is also possible that DMP(1) exists in different conformations, giving rise to two ν(P-H) peaks. If the sample is degassed at 350°C as in Fig. 8-10D, only DMP(2) species should be present. Except for residual traces, all peaks in the C-H stretching region have been eliminated. This is consistent with the expectation that only DMP(2) should now be present. A single peak in the P-H stretching region at 2482 cm^{-1}, due to the conformationally rigid DMP(2) species, is now observed.

The spectra shown in Fig. 8-11 are very similar to the analogous spectra for DMMP

on Al_2O_3 except for two details. As discussed already, the ν(C-O) region is less well resolved than it is for DMMP. The second feature is the presence of intense bands due to δ(P-H) modes. In the solid curve for room temperature adsorption this band is at 987 cm^{-1}, the same position as for gaseous DMP. In the dotted curve for evacuation at 200°C, this band has shifted to 991 cm^{-1}. In this curve there seem to be shoulders at higher wavenumber. When the sample is degassed at 350°C (dashed curve) P-H bending motions give rise to a doublet centered at 1032 cm^{-1}. These bands are not seen in DMMP adsorption, and can be reproduced exactly by doping Al_2O_3 with 200 μmols/g H_3PO_3 and degassing at 400°C. This proves this doublet is due to P-H bending motions of DMP(2). In the dotted curve one can attribute the 991 cm^{-1} band to DMP(1) and the higher wavenumber shoulders to DMP(2). Finally, if the dashed curve in Fig. 8-11 were to be expanded, a very weak band at 1320 cm^{-1} can be detected. This is due to $\delta_s(CH_3)$ of P-CH_3 groups. Only a minuscule amount of DMMP derived surface species have formed after interaction of DMP with Al_2O_3(150), even after degassing at 350°C.

Adsorption of DMP on Al_2O_3(900)

Fig. 8-13 shows spectra during the first stages of the reaction between Al_2O_3(900) and DMP. Immediately upon adsorption a weak peak at 1320 cm^{-1} is observed. Some DMP is converted to a DMMP derived species at room temperature by activated Al_2O_3. The other feature in Fig. 8-13 that has not yet been seen is a peak at 2831 cm^{-1}. When the sample continues to react at room temperature the 2831 cm^{-1} peak decreases in intensity, and peaks due to POMe groups (and possibly AlOMe groups) at 2858 and 1460 cm^{-1} also decrease in

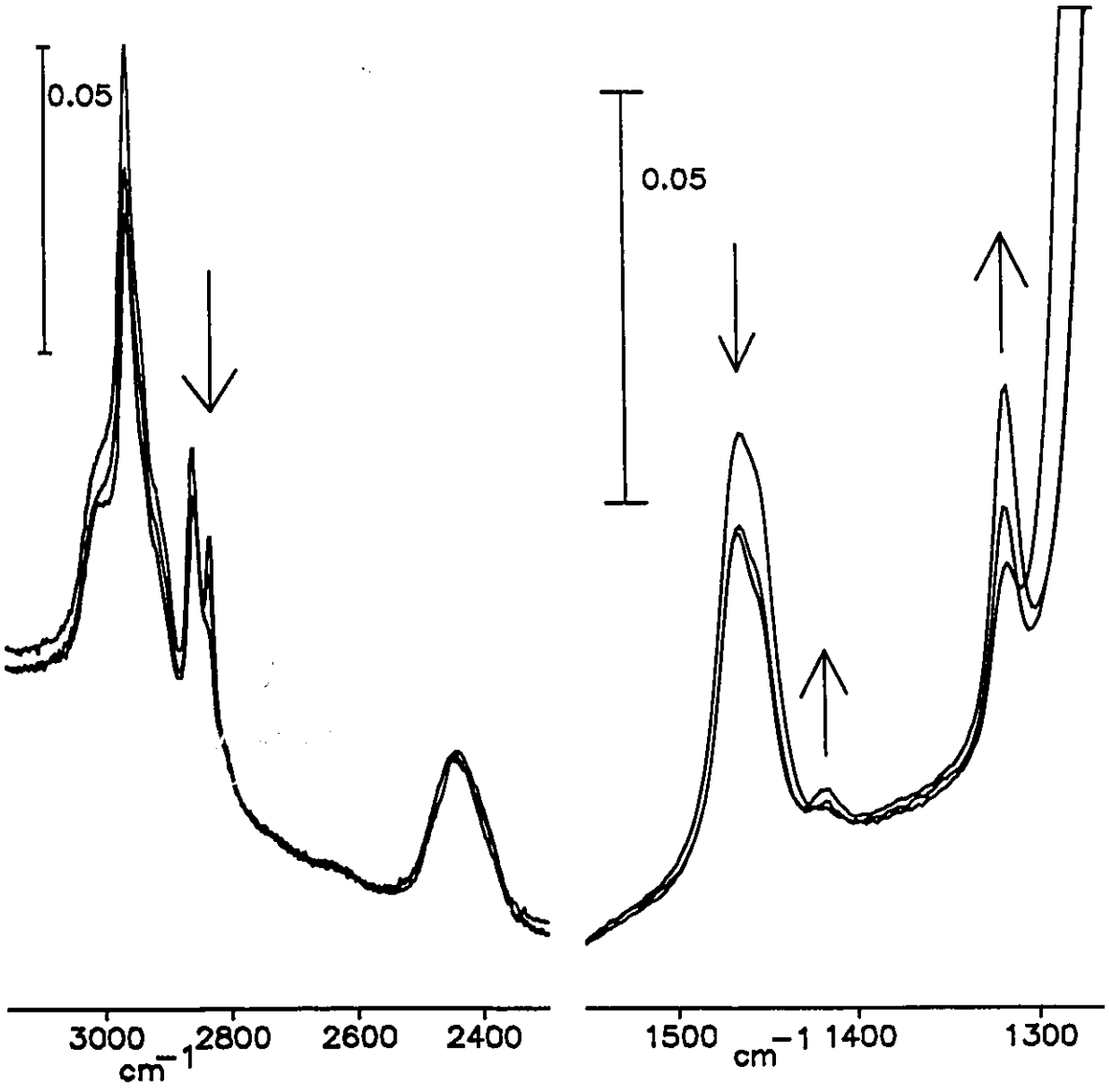

Fig. 8-13: DMP on Al_2O_3(900)

The first spectrum was recorded as quickly as possible after 0.5 torr of DMP was allowed into the IR cell. The gas phase was subtracted from this spectrum. The second spectrum was recorded after four minutes room temperature evacuation. The final spectrum was recorded after the sample was then allowed to react under static vacuum for 2.5 hours. The arrows show the direction of spectral changes with time.

intensity. The 1320 cm^{-1} band gains intensity in parallel to the decrease in intensity of the 2831 cm^{-1} band. This suggests that the 2831 cm^{-1} band, which is in a frequency region associated with methoxy groups with at least a partially anionic character, is due to a species that is a precursor to the formation of new P-C bonds.

One cannot claim to identify an intermediate on the basis of one infrared band, but speculation that is consistent with known chemistry can be offered. Strong bases such as NaH can deprotonate dialkyl phosphites, giving rise to anionic species:

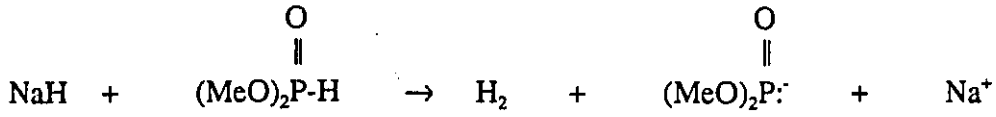

When these species are used as nucleophiles to form new P-C bonds, the reaction is known as the Michaelis-Becker reaction.[168]

A variant of the Michaelis-Becker reaction could produce surface P-Me groups:

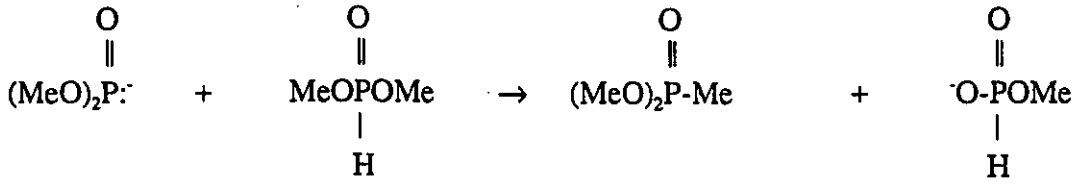

When one starts to consider all of the reactions that are possible one realizes that all of the reactions of this system will never be completely sorted out, at least not on the basis of the observation of a single unusual infrared band. The literature on the infrared spectra of

metal salts of dialkyl phosphites [169,170] is very scarce and of little help in the present area. Nevertheless it can be concluded that Al_2O_3 activated at temperatures higher than 450°C acts as a catalyst for the formation of P-C bonds at room temperature, and that a precursor species can be observed by infrared.

When the sample used in Fig. 8-13 was degassed at increasing temperatures, the 1320 cm^{-1} band continued to grow, even after the 2831 cm^{-1} band was no longer observable. By the time the sample was degassed at 400°C the 1320 cm^{-1} band had obtained fully one half the intensity that was observed when pure DMMP was adsorbed on Al_2O_3(900) and the sample subsequently degassed at 400°C. This is consistent with the substantial DMMP(2) peak seen in the ^{31}P CPTOSS spectrum in Fig. 8-9C.

Adsorption of TMP [$P(OCH_3)_3$] on Al_2O_3

In previous work [129] it was found that DMP and DMMP were the only P containing species produced when $P(OMe)_3$ reacted with silica at room temperature. Surface Si-O-Me groups were the only chemisorbed product found after room temperature reactions. These observations were explained by invoking some reaction mechanisms very similar to the well known Arbusov rearrangement. No trivalent phosphorus species were found, nor was any species that might be considered a precursor to the formation of the observed "Arbusov-rearranged" products detected.

One might have envisioned two possible initial reactions between DMP and surface SiOH groups:

$$P(OMe)_3 + SiOH \rightarrow DMP + SiOMe \quad (1)$$

$$P(OMe)_3 + SiOH \rightarrow DMP(1) + MeOH \quad (2)$$

At room temperature, reaction (2) did not occur to a detectable extent, and DMP was the initial product of the interaction. The DMP thus produced diffused to residual surface SiOH groups, and hydrogen bonded with them strongly enough so as to prevent them from reacting with $P(OMe)_3$. At later stages of the reaction (after 2 or 3 hours) as available SiOH groups became scarce, isomerization of $P(OMe)_3$ to DMMP was the main reaction.

For SiO_2 activated at or above 450°C, the surface SiOH groups can be virtually quantitatively converted to either SiOMe groups or $SiOSiMe_3$ groups, by reaction with methanol or hexamethyldisilazane respectively. A silica surface treated in either fashion did not cause $P(OMe)_3$ to isomerize to DMMP, indicating that SiOH groups catalyze this

isomerization.

For higher activation temperatures, leaving fewer surface Si-OH groups, the ratio of DMMP to DMP ultimately produced was higher. Reaction at 100°C produced some DMP(2), and reaction at 400°C for example produced significant amounts of both DMP(2) and DMMP(2).

These results can now be compared to those found for $P(OMe)_3$ adsorption on Al_2O_3.

Adsorption of $P(OMe)_3$ on $Al_2O_3(150)$

$Al_2O_3(150)$ will have a surface OH group density of about $10/nm^2$, and no significant Lewis acid or base properties.[23] One may then expect the chemistry of $P(OMe)_3$ adsorption on $Al_2O_3(150)$ to be dominated by interactions with surface hydroxyl groups, as was the case for silica.

Fig. 8-14 shows that this is largely the case. Immediately on adsorption of $P(OMe)_3$ the isolated AlOH peaks at 3726 cm^{-1} and 3676 cm^{-1} completely disappear. They are replaced by a strong broad peak at 3500 cm^{-1}, which overlaps the peak due to hydrogen bonded AlOH groups that were present before adsorption. The $\nu_s(CH_3)$ band initially appears at 2843 cm^{-1}, exactly the position observed for gas phase $P(OMe)_3$. This indicates that the initial interaction of $P(OMe)_3$ with the surface of $Al_2O_3(150)$ is mainly via hydrogen bonding of molecular $P(OMe)_3$ with surface AlOH groups. A weak P-H peak has developed (cf Fig. 8-10B, note the factor of two difference in absorbance scales) showing that a small amount of $P(OMe)_3$ has already undergone Arbusov rearrangement.

After fourteen hours, the hydrogen bonded OH band has shifted to lower frequency

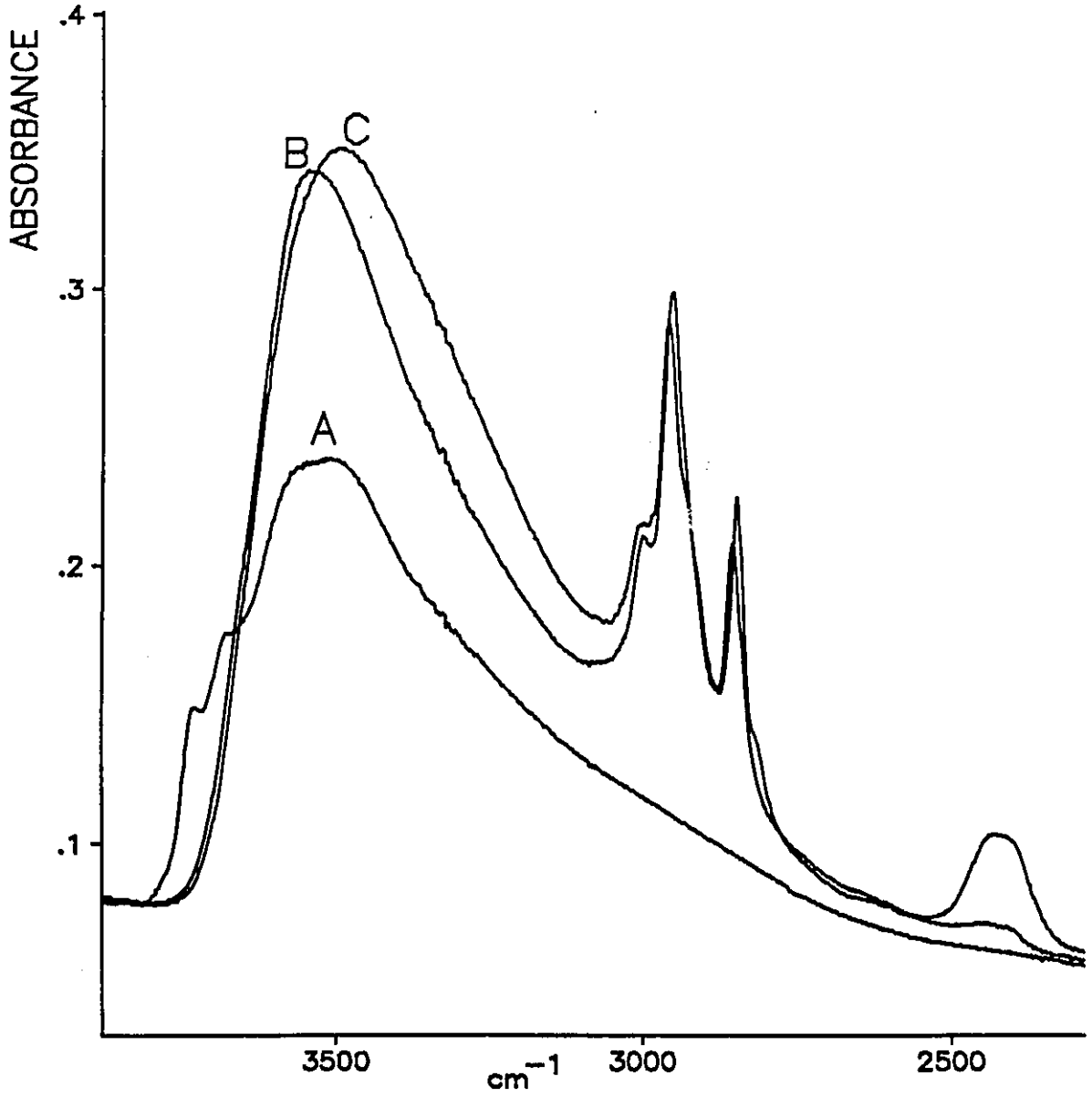

Fig. 8-14: $P(OMe)_3$ on Al_2O_3(150)

A-Background

B-Two torr $P(OMe)_3$ in cell, the gas phase has been subtracted.

C-After fourteen hours reaction, the gas phase has been subtracted.

and gained a little intensity. This might indicate that weak hydrogen bonds between $P(OMe)_3$ and surface AlOH groups are disappearing, while some stronger hydrogen bonds between AlOH groups and phosphoryl groups are forming, leading to a more intense band at lower wavenumber.

The $\nu(CH_3)$ band at 2843 cm^{-1} continuously decreased in intensity, being replaced by a new band at about 2851 cm^{-1}. This is consistent with the above interpretation of the changes in the position of the hydrogen bonded peak. The 2843 cm^{-1} band is due to molecular $P(OMe)_3$, and decreases in intensity as $P(OMe)_3$ reacts to give pentavalent phosphorus species. The new 2851 cm^{-1} peak is probably due to methoxy groups attached to pentavalent phosphorus species, with a small contribution due to AlOMe groups. The P-H band grows and becomes clearly recognizable as a doublet, having components near 2434 cm^{-1} and 2405 cm^{-1}. This doublet resembles that produced immediately produced on DMP adsorption on $Al_2O_3(150)$ very closely, except that the 2405 cm^{-1} component has a slightly higher relative intensity. DMP(0) appears to be present, as was the case for reaction with silica.

Fig. 8-15 shows the rest of the accessible infrared data for this experiment. Fig. 8-15B shows some intensity at 1220 cm^{-1}, showing that immediately on adsorption some $P(OMe)_3$ undergoes Arbusov rearrangement to give species containing phosphoryl groups. The other features in this figure, at 1188 cm^{-1} ,1060 cm^{-1} and 1010 cm^{-1} are mainly due to physisorbed $P(OMe)_3$. After fourteen hours reaction and brief evacuation the curve in Fig. 8-15C is obtained. (The only change on evacuation was the elimination of the 1010 cm^{-1} band due to $P(OMe)_3$.) The 1220 cm^{-1} peak has continued to grow; there is only a broad peak

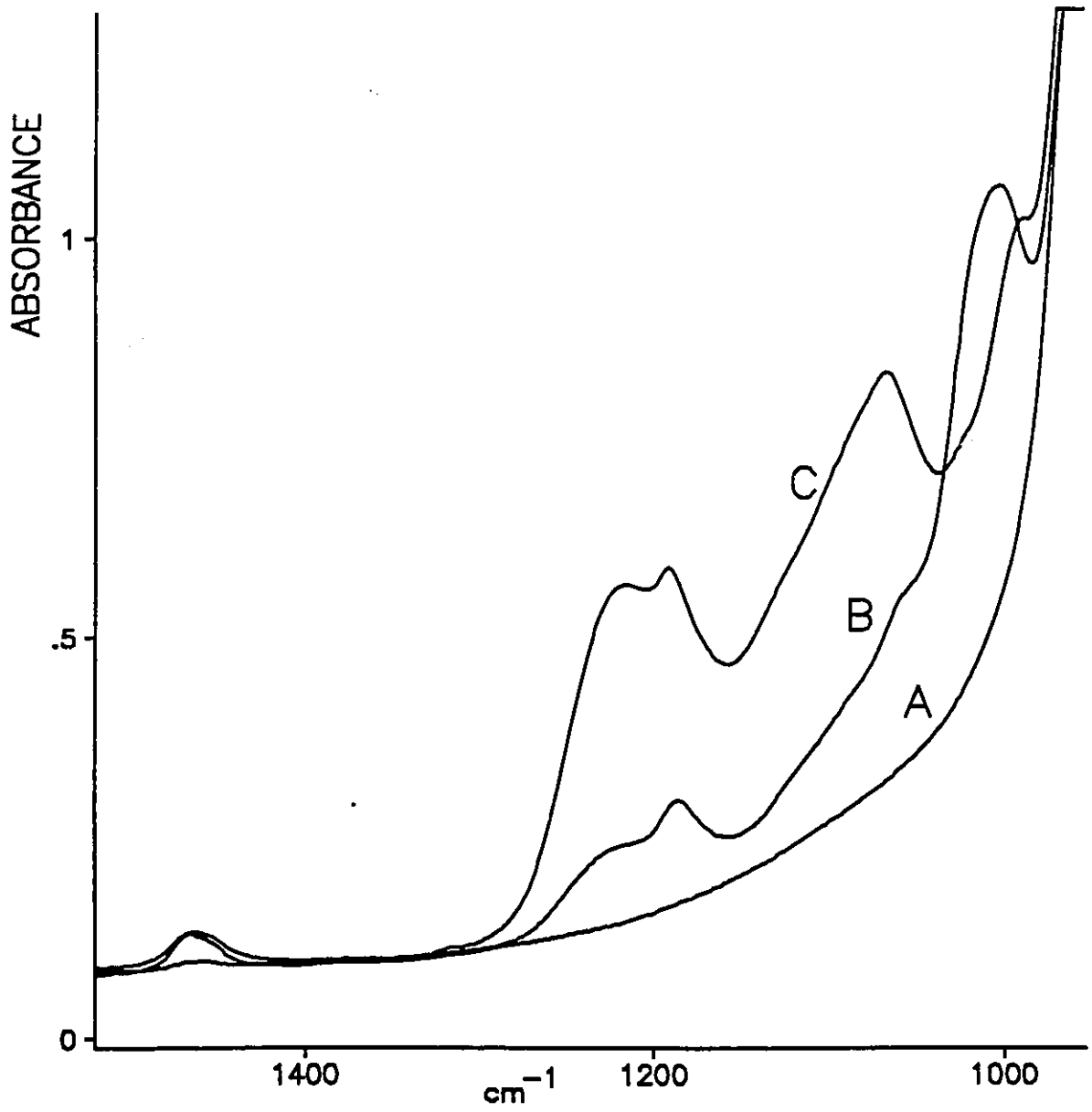

Fig. 8-15: $P(OMe)_3$ on $Al_2O_3(150)$

A-Background

B-Two torr $P(OMe)_3$ in cell, the gas phase has been subtracted

C-Fourteen hours reaction, the gas phase has been evacuated to remove the 1010 cm^{-1} $P(OMe)_3$ band

at about 1064 cm^{-1} in the C-O stretching region, and a narrow peak at 989 cm^{-1} has developed. There is only a minuscule peak at 1315 cm^{-1}, indicating that almost no DMMP has formed. The 989 cm^{-1} peak is a P-H bending mode, which can be due to either DMP(0) or DMP(1). The main peak in the C-O stretching region on DMP adsorption on Al_2O_3(150) occurred at 1047 cm^{-1}. This, together with the considerable intensity at 1100 cm^{-1}, the region associated with DMP(1) or DMMP(1) P-O stretches, indicates that some of the DMP has been dealkylated to give DMP(1).

It thus appears that unlike silica, reaction of $P(OMe)_3$ with Al_2O_3(150) at room temperature produces both DMP(0) and DMP(1). This conclusion is substantiated by solid-state ^{31}P NMR, as shown in Fig. 8-16. In this experiment approximately two $P(OMe)_3$ molecules per OH group have been allowed to react with Al_2O_3(150) overnight. Curve 8-16A shows the spectrum obtained with 90° pulses. The intense, narrow peak at 143 ppm is due to unreacted $P(OMe)_3$. In Fig 8-14 it was apparent that many of the Al-OH groups are unaffected by $P(OMe)_3$ at room temperature. This is consistent with the large intensity of the peak due to unreacted $P(OMe)_3$ in Fig. 8-16A. The inset in Fig. 8-16A shows the peaks present in the region for pentavalent phosphorus species on an expanded scale. They have a FWHM about eight times that for a liquid $P(OMe)_3$ under the same conditions, and show extensive spinning side-bands. This indicates that these are immobile species. Curve 8-16B shows the CPMAS spectrum. The peak at 143 ppm due to liquid $P(OMe)_3$ is greatly attenuated, indicating that only a small fraction of the adsorbed $P(OMe)_3$ is held rigidly enough for its phosphorus atoms to be cross-polarized. This peak may actually be due to a

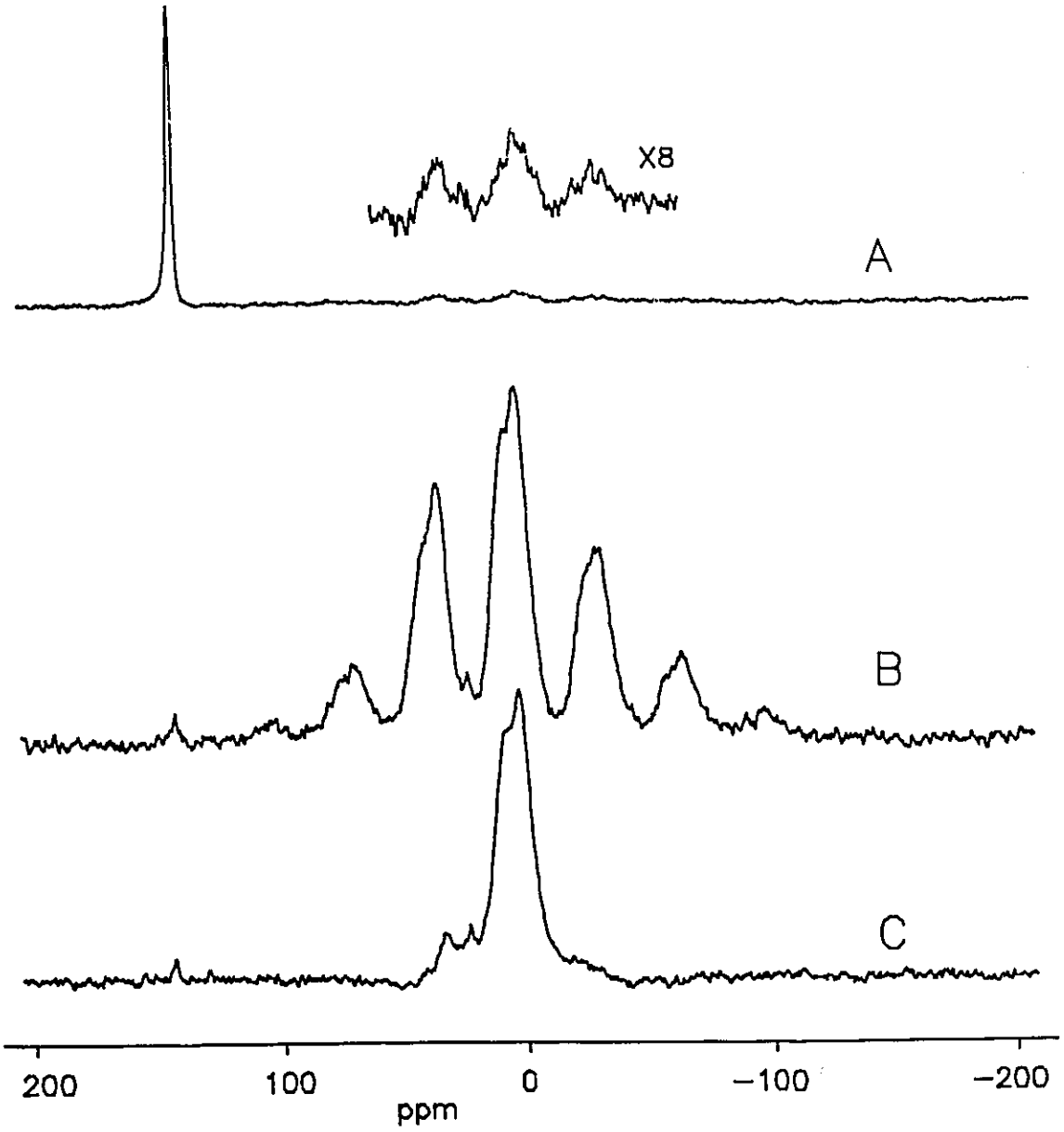

Fig. 8-16: ^{31}P MASNMR Spectra of $P(OMe)_3$ on $Al_2O_3(150)$

Spectra recorded after over night reaction at room temperature.

A-90° pulse spectrum

B-CP spectrum

C-CPTOSS spectrum

species such as Al-O-$P(OMe)_2$, but it seems unlikely this species would have exactly the same chemical shift as $P(OMe)_3$. There are two main peaks near zero ppm, at 7 and 2 ppm. This is seen more clearly in Fig 8-16C, which is a CP spectrum with the side-bands suppressed. These peaks are similar to those seen when DMP was adsorbed on Al_2O_3 (Fig. 8-9A), except that the 7 ppm component is stronger, probably indicating the presence of more DMP(0). The small peaks at 33 and 24 ppm in Fig 8-16C are due to a small amount of DMMP and its dealkylation products, as can be seen by comparison with Fig. 8-8C.

$P(OMe)_3$ on $Al_2O_3(450)$

Fig. 8-17 shows spectra following the reaction of $P(OMe)_3$ with $Al_2O_3(450)$. The evolution of the spectra in the 4000-2000 cm^{-1} region are quite similar to those shown for the reaction with $Al_2O_3(150)$, except for two small differences. The 2405 cm^{-1} component of the P-H stretching band is much less intense. This is to be expected, as it has already been shown that this band is much less intense when DMP is added to a dehydroxylated Al_2O_3 surface. The second difference is the presence of a shoulder at 2820 cm^{-1}, in addition to the band at 2843 cm^{-1} due to methoxy groups in $P(OMe)_3$, and that at 2852 cm^{-1} due to methoxy groups attached to pentavalent phosphorus. This band can be observed in Fig. 8-14, but in this experiment it disappeared after about two hours reaction. For $Al_2O_3(450)$ or Al(900) this band maintains a nearly constant intensity after the first exposure to $P(OMe)_3$. It is a fairly stable species, not disappearing completely until evacuation at 300°C, when all of the methoxy groups are gone. Yates [171] has assigned a peak at 2820 cm^{-1} to molecular

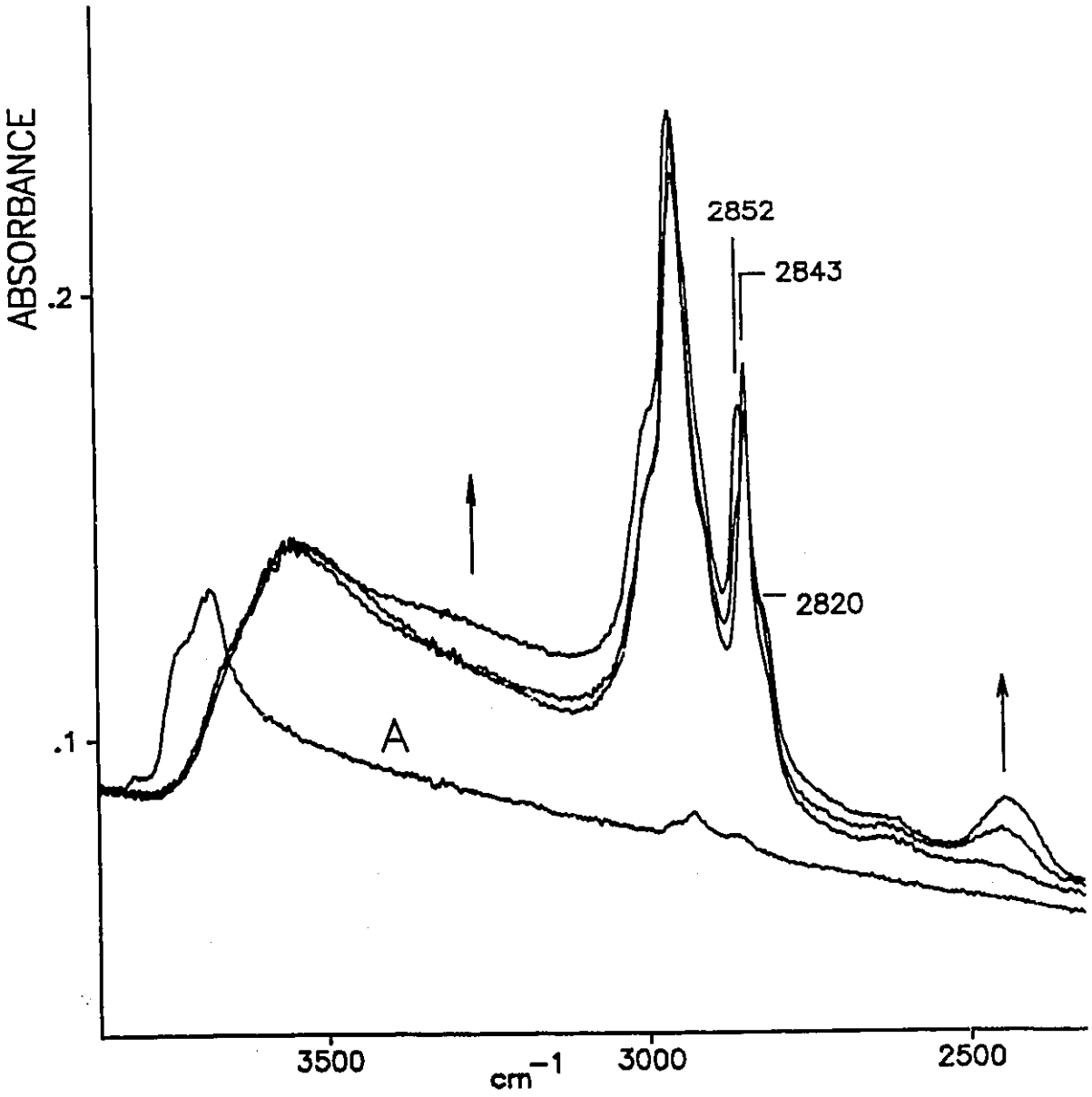

Fig. 8-17: $P(OMe)_3$ on Al_2O_3(450)

A-Background

Subsequent spectra were recorded on addition of $P(OMe)_3$, after two hours and after 19 hours. The gas phase has been subtracted from these spectra. The arrows indicate the direction of spectral change with time.

dimethyl ether adsorbed on Al_2O_3. Dimethyl ether has been detected as a desorption product after $P(OMe)_3$ treated Al_2O_3 is degassed at 300°C, but it has been found difficult to reproduce this peak very closely by adsorbing dimethyl ether on Al_2O_3. It is unclear at this time whether this peak is due to dimethyl ether, coordinated $P(OMe)_3$, or to an unusual type of surface AlOMe group.

Fig. 8-18 shows the 1500-1000 cm^{-1} region of the spectrum during this experiment. Again most features are similar to those on $Al_2O_3(150)$. The most important difference is the presence of a fairly strong band at 1320 cm^{-1} due to DMMP derived species. There is structure in the C-O stretching region, with maxima at 1040 and 1060 cm^{-1}, suggesting some DMMP(0) is present. The intensity at 1100 cm^{-1} grows continuously, suggesting DMMP(1) and/or DMP(1) is forming. Even on $Al_2O_3(450)$ there is a peak at about 1220 cm^{-1}, showing that discrete P=O groups still form. Mild heating seems to be required to form DMMP(1) or DMP(1) groups with no discrete P=O group. This band disappears on heating to 100°C, as was the case for DMP and DMMP.

In Fig. 8-19 two ^{31}P CPTOSS NMR spectra of a similarly treated sample are shown. Comparison with Fig. 8-16C shows that a much higher relative proportion of DMMP derived species is formed on samples activated at higher temperatures, as was the case for silica. In the case of silica, the DMMP and DMP formed were quite mobile, leading to relatively easy acquisition of quantitative data, even as a function of time. In the case of reactions with $Al_2O_3(450)$, the species are very immobile. The sidebands are so broad and so intense that

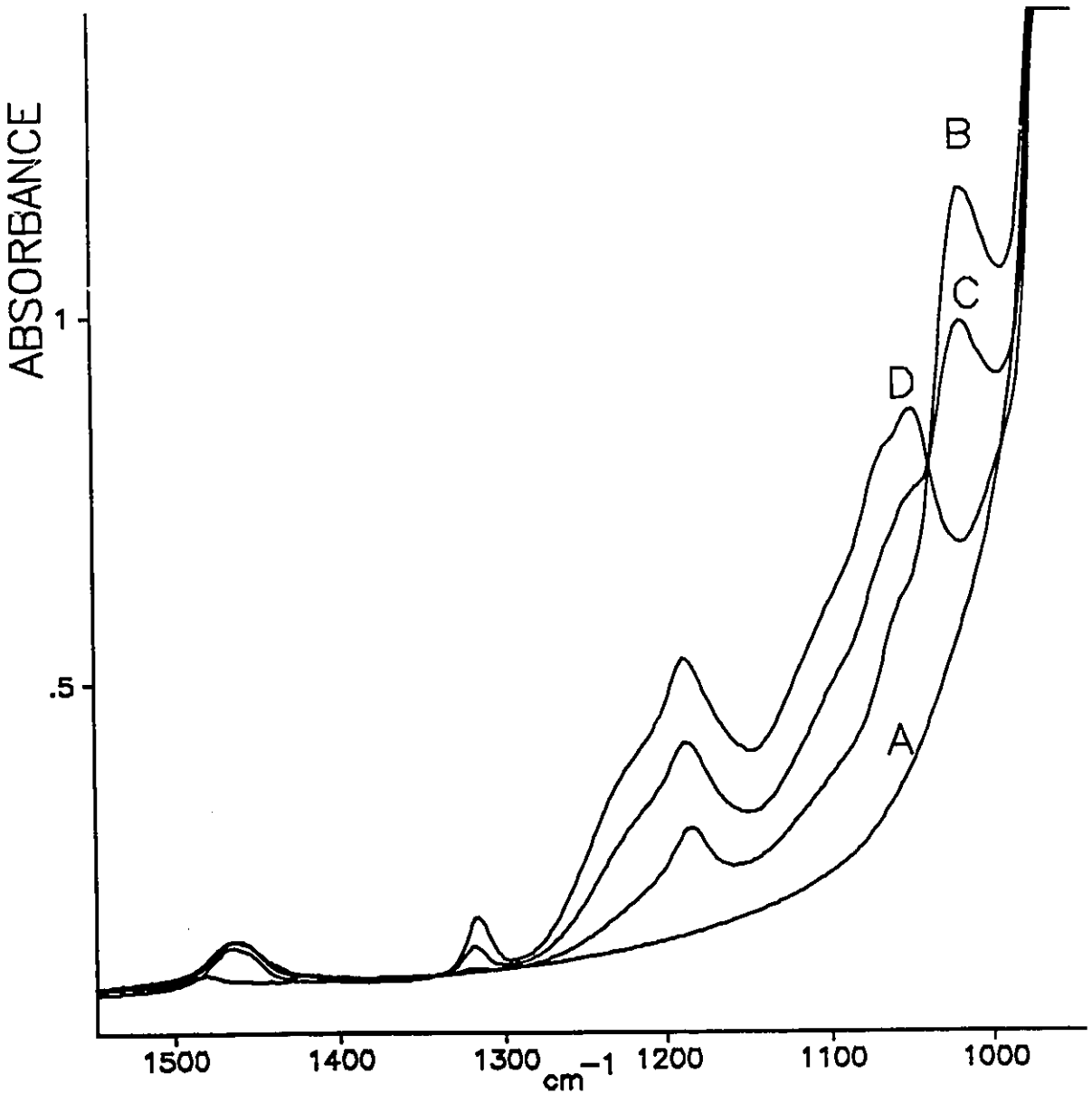

Fig. 8-18: $P(OMe)_3$ on $Al_2O_3(450)$

A-Background

B-Add $P(OMe)_3$, the gas phase has been subtracted.

C-Two hours reaction, the gas phase has been subtracted.

D-Nineteen hours reaction, the gas has been pumped out for fifteen minutes.

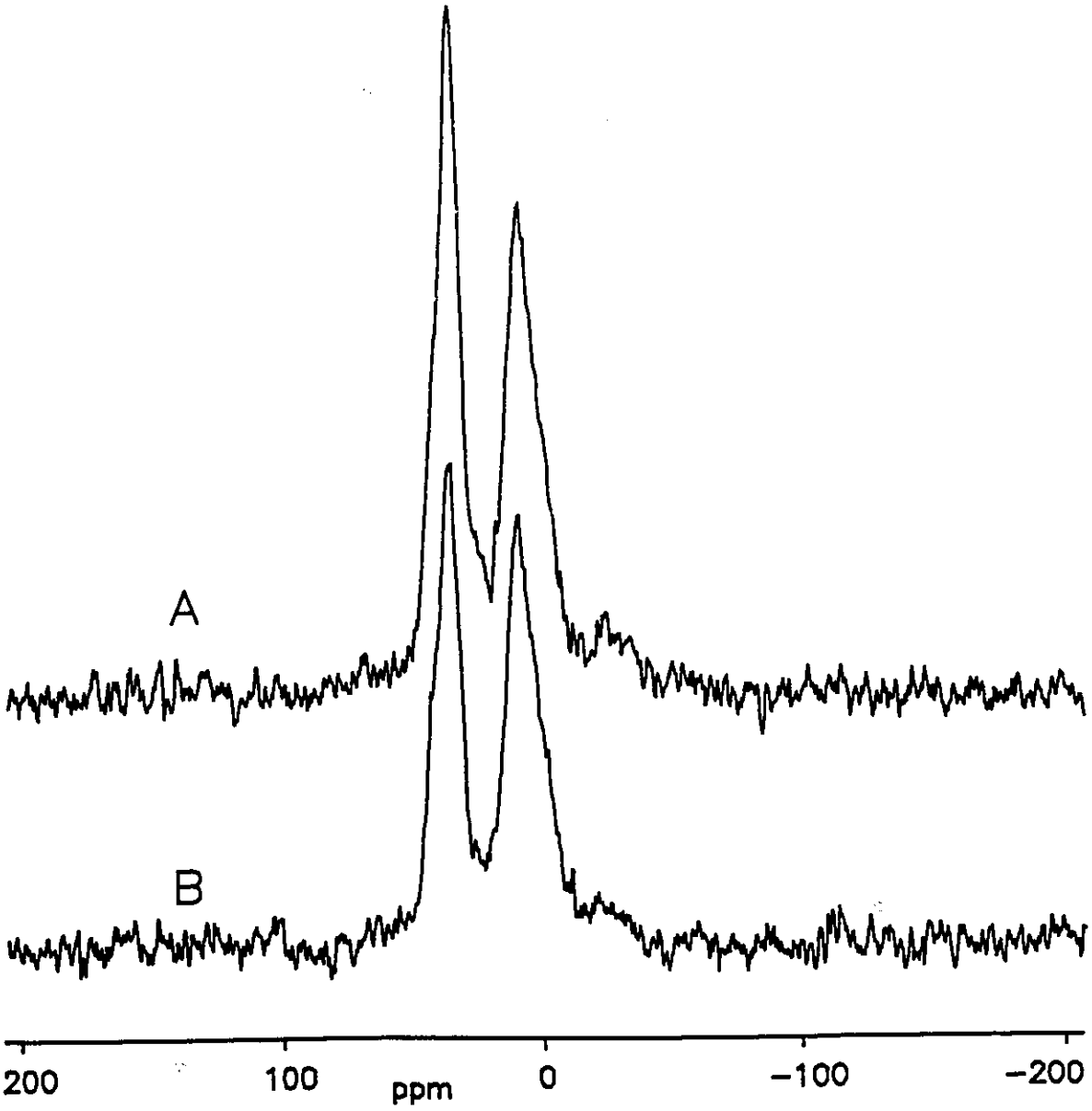

Fig. 8-19: ^{31}P CPTOSS Spectra of $P(OMe)_3$ on $Al_2O_3(450)$

A-Two hour acquisition after thirteen hours reaction.

B-Two hour acquisition after two hours reaction.

one cannot even tell how many isotropic peaks there are without running a TOSS spectrum. Unfortunately a TOSS spectrum is not to be interpreted quantitatively, ie. relative peak areas do not necessarily equate to relative populations. Nevertheless it can be noted in Fig. 8-19 that, as was the case for silica, the production of DMP derived species ceases fairly early in the reaction, while DMMP production continues. No peak due to a trivalent phosphorus species can be observed in cross polarization. In 90° pulse mode only unreacted $P(OMe)_3$ can be observed.

Increasing the activation temperature decreased the amount of DMP derived species formed, but their formation could not be totally suppressed, even though Al_2O_3 can be totally dehydroxylated by activation at 900°C. Despite numerous attempts at this reaction, a P-H band with 15 to 20 % of the intensity of that found for reaction on Al_2O_3(150) always formed. This could be a real effect, the protons arising from the decomposition of methoxy groups. Klabunde has claimed that such reactions do occur when DMMP is adsorbed on activated MgO[155], but it is generally believed such reactions don't occur to a large extent at room temperature on Al_2O_3.[151,171] It seems more likely that the protons that end up forming surface P-H groups come from water adsorbed on the walls of the vacuum system, as these samples are simply too hygroscopic to keep dry for the long duration of these experiments.

Conclusions

Trimethyl phosphite reacts with Al_2O_3 to produce DMP and DMMP, much as it does

with silica. Al_2O_3(150) leads to almost no DMMP, and the amount of DMMP formed increases with activation temperature. This indicates that AlOH groups are poor catalysts for the $P(OMe)_3$ to DMMP rearrangement compared to the more acidic SiOH groups on silica. Aprotic centres created on higher temperature activation do catalyze this reaction. Unlike silica, the DMP and DMMP produced as primary products are reactive towards Al_2O_3, and DMP(1) and DMMP(1) are definitely produced at room temperature. Al_2O_3 activated at temperatures above 450°C catalyzes the transformation of hydrogen-phosphonates to alkyl-phosphonates.

CHAPTER 9

Manipulating Magic-Angle-Spinning NMR Spectra With 180° Pulses

Introduction:

In a very influential paper, Dixon [172] has suggested three experiments aimed at simplifying magic angle spinning solid state NMR spectra. These experiments are mainly expected to be useful in the case of spin-½ nuclei influenced only by the chemical shielding, heteronuclear dipolar, and Zeeman interactions. All three of the experiments considered are relatively simple to implement, as they involve only the application of a small number of 180° pulses to the sample after excitation of the spectrum.

Perhaps the most important, and certainly the most used and discussed of the three, is the TOSS (total suppression of side-bands) experiment. In its original form this experiment used four 180° pulses applied at specific times, synchronously with the sample rotor. The result of a TOSS experiment is a spectrum that is free of spinning side-bands, with the isotropic line intensity scaled by a factor that depends on the magnitude of the chemical shift anisotropy.[173] Four is the minimum number of pulses that can be used, as will shortly be evident, although larger numbers of pulses can be used advantageously.[174,181] As has been seen in the experimental work in this thesis, the ability to remove the spinning side-bands is virtually indispensable in NMR studies of solid surfaces.

A second parameter that is useful in chemical solid state NMR is the chemical shift anisotropy. There are several methods to determine this parameter,[175] but the most convenient of these is probably the method of Herzfeld and Berger.[158] This method requires measurement of the relative intensities of a few spinning side-bands, so that elimination of the side-bands using a TOSS sequence is also eliminating a source of information. Short trains of 180° pulses can also be used to introduce well defined phase shifts between the side-bands and centre bands, allowing selective editing of spectra. By taking appropriate linear combinations of spectra with different phase relationships information on centre and sideband intensities can be suppressed or recovered as necessary, and no information is lost. This is the phase-adjusted spinning side-band experiment.(PASS)

The third experiment is the solid state analogue of Hahn echoes. This experiment would be particularly useful for spectra with very broad lines, as in this case the FID decays quickly, and the loss of data points during receiver dead time leads to significant distortion of spectra. As is well known, the application of a 180° pulse at an arbitrary time to a rotating sample does not lead to full echo, as the individual spins have time dependant frequencies. If the chemical shift anisotropy is large enough compared to the rotation frequency it may be that no echo at all is observed. For 180° pulses applied at a time corresponding to a single rotor period a full echo is observed after another rotor period has elapsed. This occurs because under magic angle rotation each spin has its frequency averaged to its isotropic frequency over one rotor period. The ability to form a Hahn echo before two rotor periods have passed would be an advantage for samples with a short T_2.

To analyze these experiments, the transverse magnetization may be treated as a classical vector.[176] In the case of experiments using four 180° pulses it will be seen that deriving the pulse times for the three types of experiments requires the solution of four equations in four unknowns. In all three cases the equations can be solved exactly, and the choice of the pulse times for a given experiment can be systematically optimized.

The expression for the frequency of a given spin-packet in a sample rotating at the magic angle is well known.[173,177,178]

$$\omega_i(t)=\omega_{oi}+g_{1i}\cos(\omega_R t+X_i)+g_{2i}\cos(2\omega_R t+Y_i) \qquad [9\text{-}1]$$

In this expression ω_{oi} is the isotropic frequency of the i^{th} spin and ω_R is the angular frequency at which the sample is spinning. The parameters g_{1i}, g_{2i}, X_i and Y_i are functions of the magnitudes of the chemical shielding anisotropy, the chemical shielding asymmetry parameter, and the Euler angles that define the orientation of the chemical shielding principal axis system relative to a coordinate system fixed to the sample rotor.[173,176] These parameters are not within the control of the experimenter, and a distribution of values of each parameter will exist in any sample. Experiments must therefore be designed to work no matter what the values of g_{1i}, g_{2i}, X_i and Y_i are.

The phase in the transverse plane of a precessing spin is given by the integral of Eq[9-1].

$$\phi_i^o(t)=\omega_{oi}t+\frac{g_{1i}}{\omega_R}\sin(\omega_R t+X_i)+\frac{g_{2i}}{2\omega_R}\sin(2\omega_R+Y_i)+c^0 \qquad [9\text{-}2]$$

The superscript zero on ϕ_i indicates that this expression applies when zero 180° pulses have been applied. The constant of integration c^0 must be evaluated by imposing the appropriate initial condition for the case of zero applied 180° pulses. This condition is of course $\phi_i^0(0)=0$. When this condition is imposed the expression for the phase of a given spin can be rewritten:

$$\phi_i^0(t)=\omega_{oi}t+\frac{g_{1i}}{\omega_R}[cosX_i\sin\omega_R t+sinX_i(\cos\omega_R t-1)] +\frac{g_{2i}}{2\omega_R}[cosY_i sin2\omega_R t+sinY_i(\cos2\omega_R t-1)] \qquad [9\text{-}3]$$

This equation shows clearly the origin of rotational echoes.[179] The terms proportional to g_{1i} and g_{2i} both become zero at integral multiples of the rotor period, $t=nT_R$. Every spin with a given isotropic frequency therefore has the same phase at $t=nT_R$, and a strong signal is observed for these times. The effect of the rotor frequency on the FID is then to produce rotational echoes, and the appearance of rotational echoes in an FID necessitates the appearance of spinning sidebands in the transformed spectrum. The key to suppressing or manipulating spinning sidebands is therefore the ability to manipulate rotational echoes. This can be achieved using 180° pulses, as can be seen when the effect of one 180° pulse on the FID is considered. Some changes in notation are now made to simplify writing the equations. The terms g_{1i}/ω_R and $g_{2i}/2\omega_R$ will simply be set equal to unity, as the equations derived here do not depend on their values.

Secondly, ω_R is also set equal to unity. Lastly the subscripts "i" will be dropped. It must be remembered that there is a distribution of the quantities X and Y in a powder sample. With these changes the expression for the phase of a given spin at time "A" can be written:

$$\phi^0(A)=\omega_o A+\cos X\sin A+\sin X(\cos A-1)+\cos Y\sin 2A+\sin Y(\cos 2A-1) \qquad [9\text{-}4]$$

If a 180° pulse is now applied $\phi^1(A)=-\phi^0(A)$. (One may prefer to write $\pi-\phi^0$ if the pulses are not phase shifted relative to the spectral excitation pulse, but the difference is immaterial for the pulse sequences considered here, which will all contain an even number of pulses.) The application of a 180° pulse does nothing to the precession frequency of the spin. This will still be given by Eq.[9-1]. The phase will therefore be given by Eq.[9-2], but the constant of integration, now denoted c^1, must be evaluated so that the phase satisfies the new boundary condition, $\phi^1(A)=-\phi^0(A)$. The expression for the phase of a spin for t>A is then:

$$\phi^1(t)=\omega_o(t-2A)+\cos X(\sin t-2\sin A)+\sin X(\cos t+1-2\cos A)$$
$$+\cos Y(\sin 2t-2\sin 2A)+\sin Y(\cos 2t+1-2\cos 2A) \qquad [9\text{-}5]$$

The four terms involving X and Y are now multiplied by expressions containing the pulse time, over which the experimenter has control. Repeating the steps that led to Eq.[9-5] three more times, with later pulse times B, C and D, will give enough freedom to simultaneously eliminate all four terms. The expression for the phase for t>D will then be:

$$\phi^4(t)=\omega_o(t\text{-}2D+2C-2B+2A)+\cos X(\sin t\text{-}2\sin D+2\sin C-2\sin B+2\sin A)$$
$$+\sin X(\cos t\text{-}2\cos D+2\cos C-2\cos B+2\cos A-1)$$
$$+\cos Y(\sin 2t\text{-}2\sin 2D+2\sin 2C-2\sin 2B+2\sin 2A)$$
$$+\sin Y(\cos 2t\text{-}2\cos 2D+2\cos 2C-2\cos 2B+2\cos 2A-1) \qquad [9\text{-}6]$$

The term proportional to ω_o in Eq.[9-6] shows that at all isotropic frequencies refocus at t=2(D-C+B-A). To avoid the need for large linear phase corrections in spectra containing more than one isotropic frequency, spectral acquisition must begin at this time. This time, denoted AQ, is the time a Hahn echo would occur in a liquid if four 180° pulses were applied. The other terms represent the effect of the anisotropic part of the chemical shift interaction on the precession of the spin. If the pulse times are such that the expressions multiplying sinX etc. all become zero at t=AQ, the anisotropic part of the chemical shift is refocused at the same time as the isotropic part. This case will be referred to as a solid Hahn echo. Examination of Eq.[9-5] shows that a solid Hahn echo can be achieved only if $A=nT_R$ when only a single 180° pulse is applied. AQ is then $2nT_R$. It will be of interest to see if solid Hahn echoes can be generated at shorter times by using more than one pulse. If all the terms in sinX etc. simultaneously become zero at some time later than AQ the result is a delayed rotational echo. This delayed echo means that the sidebands have different phases from the isotropic line, as discussed by Dixon.[172] This would be a PASS sequence.

Suppose the pulse times are chosen to satisfy the following equations.

$$\sin A-\sin B+\sin C-\sin D=0 \qquad [9\text{-}7a]$$

$$\cos A-\cos B+\cos C-\cos D=\tfrac{1}{2} \qquad [9\text{-}7b]$$

$$\sin 2A-\sin 2B+\sin 2C-\sin 2D=0 \qquad [9\text{-}7c]$$

$$\cos 2A-\cos 2B+\cos 2C-\cos 2D=\tfrac{1}{2} \qquad [9\text{-}7d]$$

In this case Eq.[9-6] will reduce to:

$$\phi^4(t)=\omega_o(t-AQ)+\sin(t+X)+\sin(2t+Y) \qquad [9\text{-}8]$$

Now it must be recalled that each spin has its own values of X and Y, and that the detected FID will represent the average over all spins of $e^{i\phi(t)}$. Since the terms sin(t+X) and sin(2*t*+Y) no longer become zero at $t=nT_R$, and since these terms will not all come to zero simultaneously because different spins have different values of X and Y, it is apparent that the rotational echoes are attenuated by this type of sequence. Using explicit expressions for X and Y, Raleigh [176] has shown that the average of $e^{i\phi(t)}$ contains no modulation at the rotor frequency. The spinning sidebands are removed from the spectrum. Solution of Eqs.[9-7] to determine all four-pulse TOSS sequences is of interest, since it was not previously known if all such sequences had been discovered.[180]

Analytical Expressions for TOSS Sequences

With high-field magnets becoming very common, techniques for side-band suppression for simplification and presentation of NMR spectra are becoming more necessary. The originally published sequences for the total suppression of side-bands (TOSS) experiment [172] suffer from two problems.[174] Firstly the late acquisition times decrease sensitivity for samples with a short T_2. Secondly the minimum delay between pulses is never larger than $0.0773T_R$, where T_R is the rotor period. Two 4-pulse sequences meant to address these difficulties have been determined using numerical search techniques,[180] but it is not known whether better ones exist. An analytical solution to the 4-pulse problem is presented here. While some new sequences are found it is shown that there are no new 4-pulse sequences that are substantial improvements on those previously known.

In the 4-pulse TOSS experiment a transverse magnetization is prepared by either a 90-degree pulse or by cross-polarization. The sample, spinning at the magic angle, is subjected to four π-pulses at specific times, corresponding to rotor rotation through the angles A, B, C and D after the preparation step. Acquisition begins at the angle AQ, the rotor angle at which all isotropic lines have zero phase regardless of their resonance offset.

More flexibility is expected using 6-pulse sequences, eg. [174,180]. Discovering whether or not other useful 4-pulse sequences exist requires the solution of four equations in four unknowns and is thus a completely determined problem, unlike the 6-pulse case. The equations to be solved are written explicitly in [174], and are rewritten as Eqs.[9-9a] to [9-9d] below. They

are expressed in the notation of Dixon.[172] All angles are expressed in revolutions, as is customary.

$$\cos A - \cos B + \cos C - \cos D = \tfrac{1}{2} \qquad [9\text{-}9a]$$

$$\sin A - \sin B + \sin C - \sin D = 0 \qquad [9\text{-}9b]$$

$$\cos 2A - \cos 2B + \cos 2C - \cos 2D = \tfrac{1}{2} \qquad [9\text{-}9c]$$

$$\sin 2A - \sin 2B + \sin 2C - \sin 2D = 0 \qquad [9\text{-}9d]$$

$$AQ=2(D-C+B-A) \qquad [9\text{-}9e]$$

Using standard trigonometric relations the set of Eqs.[9-9] may be rewritten as the set of Eqs.[9-10].

$$l\cos\theta - m\cos\phi = \tfrac{1}{2} \qquad [9\text{-}10a]$$

$$l\sin\theta - m\sin\phi = 0 \qquad [9\text{-}10b]$$

$$(l^2-2)\cos 2\theta - (m^2-2)\cos 2\phi = \tfrac{1}{2} \qquad [9\text{-}10c]$$

$$(l^2-2)\sin 2\theta - (m^2-2)\sin 2\phi = 0 \qquad [9\text{-}10d]$$

$$\theta=\tfrac{1}{2}(C+A),\ \phi=\tfrac{1}{2}(D+B),\ l=2\cos\tfrac{1}{2}(C-A),\ m=2\cos\tfrac{1}{2}(D-B),\ AQ=4(\phi-\theta)$$

Eq.[9-10b] can be satisfied by taking $\theta=k/2$ and $\phi=(n+k)/2$ with n and k positive integers, since by definition $\phi>\theta>0$. Eqs.[9-10] then reduce to two equations that can be solved for l and m. The resulting equations for TOSS sequences are given as Eqs.[9-11].

$$AQ=2n \qquad n=1,2,3... \tag{9-11a}$$

$$A=\frac{1}{2}k-\cos^{-1}[\frac{3}{8}(-1)^k] \qquad k=1,2,3...3n-1 \tag{9-11b}$$

$$B=\frac{1}{2}(n+k)-\cos^{-1}[\frac{1}{8}(-1)^{n+k}] \tag{9-11c}$$

$$C=\frac{1}{2}k+\cos^{-1}[\frac{3}{8}(-1)^k] \tag{9-11d}$$

$$D=\frac{1}{2}(n+k)+\cos^{-1}[\frac{1}{8}(-1)^{n+k}] \tag{9-11e}$$

Another set of solutions remains to be derived. The combinations $\sin\theta$ times Eq.[9-10a] minus $\cos\theta$ times Eq.[9-10b] and $\sin\phi$ times Eq.[9-10a] minus $\cos\phi$ times Eq.[9-10b] yield the relations given in Eq.[9-12].

$$l\ \sin(\phi-\theta) = \tfrac{1}{2}\ \sin\phi \qquad m\ \sin(\phi-\theta) = \tfrac{1}{2}\ \sin\theta \tag{9-12}$$

Squaring these relations and multiplying Eq.[9-10c] and Eq.[9-10d] by $\sin^2(\phi-\theta)$ allows l and m to be eliminated from Eq.[9-10c] and Eq.[9-10d]. Introducing $P=\phi-\theta$ and $Q=\phi+\theta$ for

compactness, Eq.[9-10c] and Eq.[9-10d] become Eq.[9-13a] and Eq.[9-13b] respectively.

$$sinP\ \{\ sinQ(16\sin^2P-1)+2sinP\ \}\ =\ 0 \qquad [9\text{-}13a]$$

$$sinP\ \{\ cosQ(16\sin^2P-1)+cosP\ \}\ =\ 0 \qquad [9\text{-}13b]$$

Setting sinP equal to zero in Eqs.[9-13] gives the solution given in Eqs.[9-11] again. Any further TOSS sequences must result from setting the quantities in large brackets in Eqs.[9-13] equal to zero. Another set of solutions results from doing so, although it is somewhat more cumbersome to express. It is given as Eqs.[9-14] and Eqs.[9-15].

Let P be any positive number satisfying:

$$P=\tan^{-1}\pm\sqrt{\frac{35}{221}} \qquad [9\text{-}14a]$$

For a given value of P a discrete set of values of the quantity Q is defined by:

$$Q=\tan^{-1}(2tanP)+\frac{j}{2} \qquad [9\text{-}14b]$$

The integer j must be chosen such that P<Q<8P, and be such that cosQ has the opposite sign to cosP and sinQ has the opposite sign to sinP. For each pair of angles P and Q, Eqs.[9-15] determine TOSS sequences.

$$AQ=4P \qquad [9\text{-}15a]$$

$$A=\frac{1}{2}(Q-P)-\cos^{-1}\left[\frac{\sin\tfrac{1}{2}(Q+P)}{4\sin P}\right] \qquad [9\text{-}15b]$$

$$B=\frac{1}{2}(Q+P)-\cos^{-1}\left[\frac{\sin\tfrac{1}{2}(Q-P)}{4\sin P}\right] \qquad [9\text{-}15c]$$

$$C=\frac{1}{2}(Q-P)+\cos^{-1}\left[\frac{\sin\tfrac{1}{2}(Q+P)}{4\sin P}\right] \qquad [9\text{-}15d]$$

$$D=\frac{1}{2}(Q+P)+\cos^{-1}\left[\frac{\sin\tfrac{1}{2}(Q-P)}{4\sin P}\right] \qquad [9\text{-}15e]$$

Two types of solution to the equations defining TOSS sequences have been derived. The first set of solutions, given by Eqs.[9-11], come from setting $\sin\theta$ and $\sin\phi$ equal to zero in Eq.[9-10b]. The second set, given in Eqs.[9-14] and [9-15], is derived by assuming that in Eq.[9-10b] $\sin\theta$ and $\sin\phi$ may have non-zero values. Examination of Eqs.[9-13] shows that there are no other possibilities. All possible 4-pulse TOSS sequences are given either by Eqs.[9-11] or by Eqs.[9-14] and [9-15].

The results of Eqs.[9-11] and Eqs.[9-14] and [9-15] are rather tedious to work out. Since inverse trigonometric functions are multivalued, a given set of the indices k and n, or a given index j may lead to multiple solutions. A sequence may occur for more than one set of values of the indices. For values of n and j inconsistent with the restrictions given it is certain that one or more pulses occur at negative times or after AQ. Nevertheless, for some values of the indices consistent with the restrictions, the required time ordering, $0<A<B<C<D<AQ$, cannot be achieved. For these reasons all solutions up to AQ=4, that cannot be derived from other

sequences by simply adding whole numbers of revolutions to one or more pulse times, are collected in Table 9-1.

It is seen that the earliest value of AQ at which a viable TOSS sequence exists is about 1.75 revolutions. For AQ values less than 3, the fifth sequence in Table 9-1 has the largest minimum delay between pulses, although for this sequence the separation between D and AQ will be inconveniently small at high spinning speeds. When spinning rates are very fast a minimum delay on the order of $0.077T_R$ may not be acceptable. In this case however, the use of larger values of AQ becomes more feasible. Sequences occurring at AQ=3.75 or AQ=4 offer much improved minimum inter-pulse delays. Should more flexibility than is available in Table 9-1 be required 6-pulse TOSS sequences may have to be used.

(An alternate derivation of the timings for four-pulse TOSS sequences has appeared in ref. [186].)

TABLE 9-1

A	B	C	D	AQ
0.576077	0.799757	0.877211	1.532973	1.758883[a]
0.188821	0.230053	0.811179	1.769947	2.000000[b]
0.188821	0.769947	0.811179	1.230053	2.000000
0.122789	0.200243	0.423923	1.467027	2.241117[b]
0.122789	0.467027	1.423923	2.200243	2.241117
0.423923	0.467027	1.122789	2.200243	2.241117[b]
0.576077	1.532973	1.877211	2.799757	3.758883[a]
0.877211	1.532973	1.576077	2.799757	3.758883
0.877211	1.799757	2.576077	3.532973	3.758883
0.811179	1.769947	2.188821	3.230053	4.000000
0.811179	1.230053	2.188821	3.769947	4.000000

[a] previously published in Ref.[180].

[b] previously published in Ref.[172].

PASS and Hahn Echo Sequences

The next problem to be solved is to determine pulse times that make the coefficients of sinX etc. in Eq.[9-6] on the introduction simultaneously vanish. As explained in the introduction this will lead to the determination of Hahn echo and PASS sequences. It is shown below that no 4-pulse Hahn echo sequences exist with AQ less than 2 revolutions. This is a rather disappointing result as there would be an immediate interest in any sequence that forms Hahn echoes at shorter times. A method to determine what PASS sequences are available for a given AQ is also presented. As the PASS sequences seem to be little used in the literature, this derivation is presented mainly for the sake of completeness. A complete solution to the 4-pulse echo problem may be of some future interest however, as the effects of echo producing sequences and how to use them in for example 2-dimensional solid-state NMR is an ongoing area of research.[175,182,183]

The equations to be solved can be read from Eqs.[9-6], and are explicitly:

$$\cos A-\cos B+\cos C-\cos D=\tfrac{1}{2}(1-\cos t) \qquad [9\text{-}16a]$$

$$\sin A-\sin B+\sin C-\sin D=-\tfrac{1}{2}\sin t \qquad [9\text{-}16b]$$

$$\cos 2A-\cos 2B+\cos 2C-\cos 2D=\tfrac{1}{2}(1-\cos 2t) \qquad [9\text{-}16c]$$

$$\sin 2A-\sin 2B+\sin 2C-\sin 2D=-\tfrac{1}{2}\sin 2t \qquad [9\text{-}16d]$$

Using the same variable changes as was used in the section on TOSS sequences these

equations are rewritten:

$$l\cos\theta - m\cos\phi = \tfrac{1}{2}(1-\cos E) \qquad [9\text{-}17a]$$

$$l\sin\theta - m\sin\phi = -\tfrac{1}{2}\sin E \qquad [9\text{-}17b]$$

$$(l^2-2)\cos 2\theta - (m^2-2)\cos 2\phi = \tfrac{1}{2}(1-\cos 2E) \qquad [9\text{-}17c]$$

$$(l^2-2)\sin 2\theta - (m^2-2)\sin 2\phi = -\tfrac{1}{2}\sin 2E \qquad [9\text{-}17d]$$

The character "E" has been substituted for "*t*" in the set of Eqs.[9-17] in order to emphasize that this quantity is no longer a continuous parameter over which the FID is collected. Rather, in Eqs.[9-17] "E" is the particular time at which the rotational echo will occur for a given pulse sequence. Taking the same combinations of Eq.[9-17a] and Eq.[9-17b] as were taken in the TOSS derivation gives:

$$m\sin(\phi-\theta) = \sin(\tfrac{1}{2}E)\cos(\tfrac{1}{2}E-\theta) \qquad [9\text{-}18a]$$

$$l\sin(\phi-\theta) = \sin(\tfrac{1}{2}E)\cos(\tfrac{1}{2}E-\phi) \qquad [9\text{-}18b]$$

These equations can now be used to eliminate "l" and "m" in Eqs.[9-17c] and [9-17d], again by following steps used in the TOSS section:

$$\{\sin^2(\tfrac{1}{2}E)\cos^2(\tfrac{1}{2}E-\phi)-2\sin^2(\phi-\theta)\}\cos 2\theta-\{\sin^2(\tfrac{1}{2}E)\cos^2(\tfrac{1}{2}E-\theta)-2\sin^2(\phi-\theta)\}\cos 2\phi$$
$$=\tfrac{1}{2}\sin^2(\phi-\theta)(1-\cos(2E)) \qquad [9\text{-}19a]$$

$$\{\sin^2(\tfrac{1}{2}E)\cos^2(\tfrac{1}{2}E-\phi)-2\sin^2(\phi-\theta)\}\sin 2\theta-\{\sin^2(\tfrac{1}{2}E)\cos^2(\tfrac{1}{2}E-\theta)-2\sin^2(\phi-\theta)\}\sin 2\phi$$
$$=-\tfrac{1}{2}\sin^2(\phi-\theta)\sin 2E \qquad [9\text{-}19b]$$

Introducing $P=\phi-\theta$ and $Q=\phi+\theta$ again, after some manipulation, these equations become:

$$\sin Q\sin P(1-\cos E-8\sin^2 P)=\sin E\sin P(2\sin E\sin P-\cos P+\cos P\cos E) \qquad [9\text{-}20a]$$

$$\cos Q\sin P(1-\cos E-8\sin^2 P)=\cos E\sin P(2\sin E\sin P-\cos P+\cos P\cos E) \qquad [9\text{-}20b]$$

As was the case in the TOSS derivation, when $\sin P=0$ ($AQ=2n$ revolutions) these equations are satisfied, but give no information on "Q" or "E". The case $AQ=2n$ will have to be treated separately by studying the properties of Eqs.[9-17] for the case $\phi-\theta=\tfrac{1}{2}n$.

Consideration of Eqs.[9-20] shows that these equations can only be satisfied if $\sin P=0$ or if:

$$1-\cos E-8\sin^2 P=\pm(2\sin E\sin P-\cos P+\cos E\cos P) \qquad [9\text{-}21]$$

There are thus two "branches" of solutions to investigate. If the "+" sign in Eq.[9-21] holds Eqs.[9-20] show $Q=E+m$, ($m=0,1,2..$). Similarly if the "-" sign applies $Q=E+\tfrac{1}{2}m$,

(m=0,1,2..).

The method to examine PASS sequences is now clear. One can choose a value of P, which is equivalent to choosing a value of AQ, and then determine all possible values of Q and E using Eq.[9-21]. One then must calculate the pulse times from Eqs.[9-22]:

$$A=\frac{1}{2}(Q-P)-\cos^{-1}[\frac{\sin(\frac{1}{2}E)\cos\frac{1}{2}(E-Q-P)}{2\sin P}] \qquad [9\text{-}22a]$$

$$B=\frac{1}{2}(Q+P)-\cos^{-1}[\frac{\sin(\frac{1}{2}E)\cos\frac{1}{2}(E-Q+P)}{2\sin P}] \qquad [9\text{-}22b]$$

$$C=\frac{1}{2}(Q-P)+\cos^{-1}[\frac{\sin(\frac{1}{2}E)\cos\frac{1}{2}(E-Q-P)}{2\sin P}] \qquad [9\text{-}22c]$$

$$D=\frac{1}{2}(Q+P)+\cos^{-1}[\frac{\sin(\frac{1}{2}E)\cos\frac{1}{2}(E-Q+P)}{2\sin P}] \qquad [9\text{-}22d]$$

Since there is a continuum of values of P that are allowed, it is not possible to discuss the possibilities given by Eq.[9-21] in as complete a manner as could be done for TOSS sequences. It is possible to put the two branches of Eq.[9-21] into a more readily examinable form. For the positive branch one has:

$$\cos E(1+\cos P)+\sin E(2\sin P)=1+\cos P-8\sin^2 P \qquad [9\text{-}23]$$

Let $U^+=\{(1+\cos P)^2+4\sin^2 P\}^{1/4}$, a positive quantity. Let V^+ be the angle that satisfies:

$$U^{+}\cos V^{+}=1+\cos P \quad \text{and} \quad U^{+}\sin V^{+}=2\sin P$$

The angle "V^{+}" is then unambiguous. The relation between "E" and "P" for the positive branch of Eq.[9-21] is then:

$$E = V^{+} + \cos^{-1}((1+\cos P-8\sin^{2}P)/U^{+}) \qquad [9\text{-}24]$$

Similarly for the negative branch of Eq.[9-21] one has:

$$E = V^{-} + \cos^{-1}((1-\cos P-8\sin^{2}P)/U^{-}) \qquad [9\text{-}25]$$

where $U^{-}=\{(1-\cos P)^{2}+4\sin^{2}P\}^{1/2}$, and V^{-} must be chosen to satisfy:

$$U^{-}\cos V^{-}=1-\cos P \quad \text{and} \quad U^{-}\sin V^{-}=-2\sin P$$

Since the inverse cosine of a quantity greater than unity does not exist, there are some values of "P" for which neither PASS nor Hahn-echo sequences exist. Using Eqs.[9-24] and [9-25] it is straightforward to show that no sequences exist for $0.494196<AQ<1.505804$, and also for $2.494196<AQ<3.506164$. (Only sequences with AQ values up to 4 revolutions have been considered. For later times there will also be such "forbidden" regions.)

There is some interest in sequences that produce echoes at low values of AQ, regardless

of what happens to the phases of the phases of the spinning sidebands. No viable sequence could be found at AQ=0.494196. At AQ=1.505804 a sequence exists with A=0.614095, B=0.776808, C=0.900357, D=1.490546 and E=2.390903. This is not a very useful sequence, as AQ is not much earlier than 2 revolutions, which can be achieved with only a single pulse, and because the time "D" of the last pulse is inconveniently close to AQ.

The analysis of the AQ=2n case is straightforward but surprisingly tedious. Only the conclusions are given, and then only for the case AQ=2. At AQ=2 only two types of sequence are possible. One may generate a Hahn-echo, which is not interesting, or one may generate a sequence in which the rotational echo comes at AQ+½. This sequence gives all odd order spinning sidebands 180° out of phase with the isotropic line. The pulse times are A=0.209785, B=0.290215, C=0.790215 and D=1.709785. This sequence has been demonstrated in ref. [172].

It remains to show that there are no 4-pulse Hahn-echo sequences with AQ<2. For a Hahn-echo one must set E=AQ=4P. For the positive branch of Eq.[9-21] this means:

$$(1+\cos 4P)(1+\cos P)=2\sin P(4\sin P+\sin 4P) \qquad [9\text{-}26]$$

This equation can be rearranged to:

$$\sin^4 P(1-\cos P)=0 \qquad [9\text{-}27]$$

If sinP=0, P=½n and AQ=4P=2n. If cosP=1, P=n and AQ=4n.

For the negative branch of Eq.[9-21] the analogue of Eq.[9-27] is:

$$\sin^4 P(\cos P+1)=0 \qquad [9\text{-}28]$$

If cosP=-1, P=n+½ and AQ=4n+2. Therefore it can be concluded there are no 4-pulse Hahn-echo sequences with AQ<2.

Hahn-Echo Sequences Using More Than Four Pulses

It has been shown that with four 180° pulses one cannot form a solid Hahn-echo at earlier times than can be achieved with a single pulse. It has also been mentioned that the use of 6-pulse TOSS sequences allows greater flexibility than is available with 4-pulse sequences. It is therefore natural to investigate whether or not a useful 6-pulse Hahn-echo sequence exists. It will be shown that Hahn-echoes can be produced in rotating solids at times much earlier than previously reported in the literature.[182]

Since this is an under-determined problem, making complete analysis difficult, analysis is restricted to the case of rotational echoes occurring at t=1 revolution. The extension to 6-pulses of Eqs.[9-16] for t=1 is:

$$\cos A-\cos B+\cos C-\cos D+\cos E-\cos F=0 \qquad [9\text{-}29a]$$

$$\sin A-\sin B+\sin C-\sin D+\sin e-\sin F=0 \qquad [9\text{-}29b]$$

$$\cos 2A-\cos 2B+\cos 2C-\cos 2D+\cos 2E-\cos 2F=0 \qquad [9\text{-}29c]$$

$$\sin 2A-\sin 2B+\sin 2C-\sin 2D+\sin 2E-\sin 2F=0 \qquad [9\text{-}29d]$$

For a 6-pulse sequence:

$$AQ=2(F-E+D-C+B-A) \qquad [9\text{-}29e]$$

Such a symmetrical set of equations suggests that a solution with equally spaced pulses might exist. A trial solution is attempted with the space between pulses given by τ. Adding Eq.[9-29a] to "i" times Eq.[9-29b] gives:

$$e^{iA}(1-e^{i\tau}+e^{i2\tau}-e^{i3\tau}+e^{i4\tau}-e^{i5\tau})=0 \qquad [9\text{-}30]$$

Multiplying by $1-e^{i\tau}$ gives:

$$e^{iA}(1-e^{i6\tau})=0 \quad \text{or}$$

$$6\tau=2n\pi \quad n=1,2... \qquad [9\text{-}31]$$

The only acceptable solution given by Eq.[9-31] is τ=1/6 revolutions. The pulse time "A" is completely arbitrary, but is most conveniently chosen to be 1/12 revolutions. The complete sequence is then:

A=1/12, B=1/4, C=5/12, D=7/12, E=3/4, F=11/12

It is easily verified that these pulse times also satisfy Eq.[9-29c] and Eq.[9-29d]. Since AQ=1, as given by Eq.[9-29e], and is equal to the time at which the pulses lead to the formation of a rotational echo, this represents a solid Hahn-echo sequence.

Since the pulse time "A" was arbitrary in the last pulse sequence, one is tempted to set "A" equal to zero. This is equivalent to dropping the first pulse and employing five pulses to generate a solid Hahn-echo. Eqs.[9-29] above are only valid for 6-pulse sequences. For the 5-

pulse case the equations analogous to Eqs.[9-29] can be written in complex exponential form as:

$$e^{iA} - e^{iB} + e^{iC} - e^{iD} + e^{iE} = 1 \qquad [9\text{-}32a]$$

$$e^{2iA} - e^{2iB} + e^{2iC} - e^{2iD} + e^{2iE} = 1 \qquad [9\text{-}32b]$$

It is easily verified that these equations are satisfied by the following sequence:

$$A=1/6,\ B=1/3\ ,\ C=1/2,\ D=2/3,\ E=5/6$$

AQ for this 5-pulse sequence is 2(E-D+C-B+A)=1. Thus it is verified that the above sequence is a 5-pulse solid Hahn-echo sequence.

The previous two solid Hahn-echo sequences have been experimentally verified to give Hahn-echoes in spinning solid samples, and to do so without introducing phase shifts in the spinning sidebands. In Fig. 9-1 an example of a 6-pulse solid Hahn-echo is shown. Note in Fig. 9-1C the intensity of the spectrum is largely destroyed when one attempts to produce a Hahn echo in a spinning solid under conditions incompatible with the principles discussed in this section. Note also in Fig. 9-1C the phases of the spinning sidebands have been altered by the experiment. In Fig 9-1D the spinning sidebands have been returned to their proper phases, and most of the intensity has been restored.

The intensity of the isotropic peak in Fig. 9-1D is nearly the same as in Fig. 9-1B. If pulse non-ideality was unimportant in this experiment, the isotropic peak in Fig. 9-1D should be somewhat larger than in Fig. 9-1B, and somewhat less than in Fig. 9-1A. It is apparent that

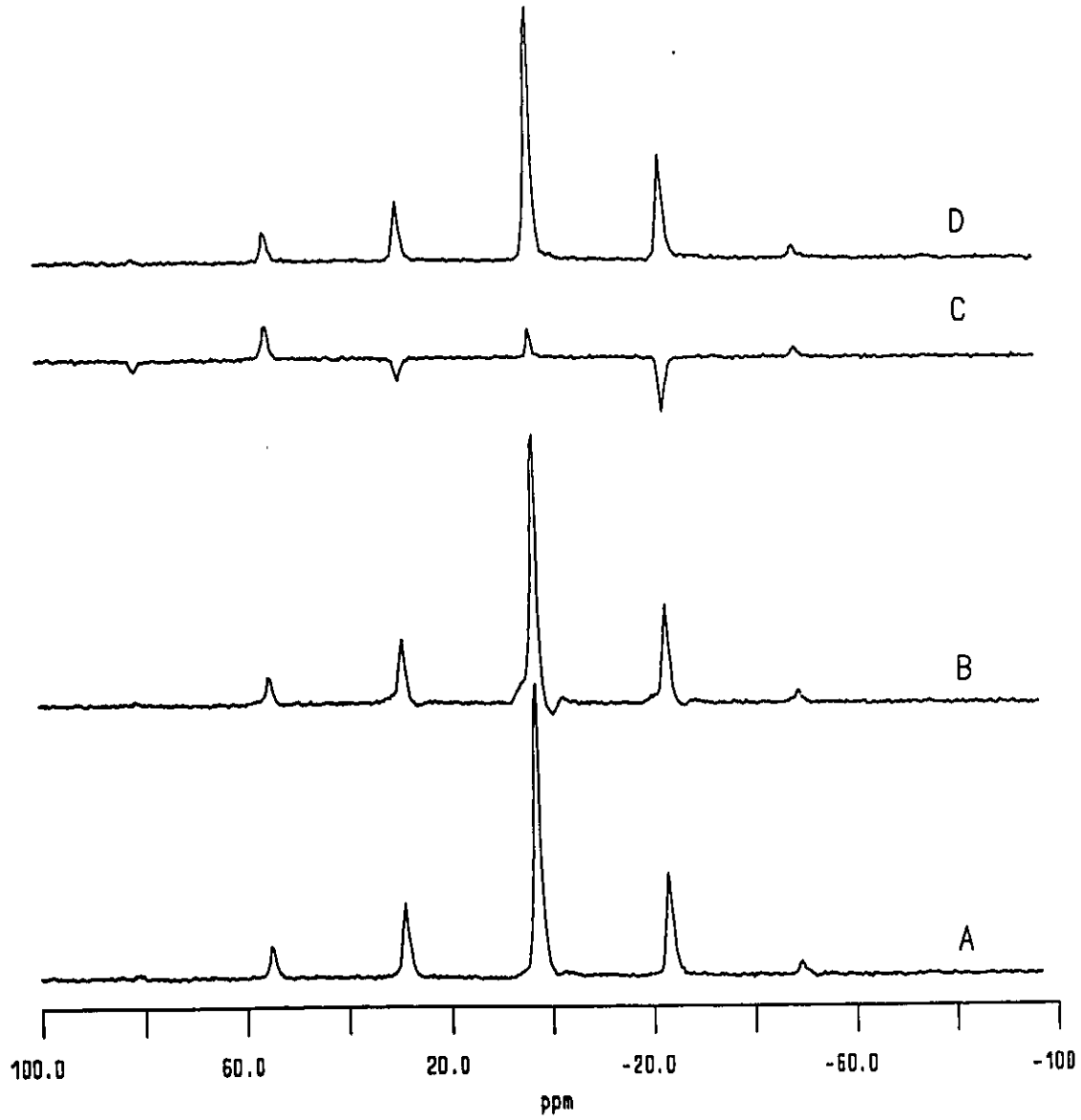

Fig. 1: ^{31}P CPMAS spectra of Diammonium Phosphate.

All spectra recorded at 60.5MHz with 1.6kHz sample spinning.

The same phase adjustment parameters have been used in processing all four spectra.

A:CP-MASS spectrum, B: single pulse Hahn echo with AQ=2

C:single pulse Hahn echo with AQ=1, D: 6-pulse Hahn echo with AQ=1

pulse non-ideality is causing some signal loss in the 6-pulse Hahn-echo experiment.

The spectrum in Fig. 9-1D was acquired using 180° pulses with the same phase as the Hartman-Hahn contact pulses. If the spins in the sample precessed at constant frequency this sequence would produce six Hahn echoes. Since this is an even number, pulse length errors would cancel out in the same manner as in the Meiboom-Gill method of producing spin echoes. In the case studied here however the spins do not precess at constant frequency, and the sequence is not necessarily as effective at compensating pulse length errors as it would be for a liquid sample. Using 180° pulses phase shifted by 90° with respect to the initial phase (Carr-Purcel phases) has been found to cause a much greater signal loss than is found using 180° pulses with Meiboom-Gill phases. Thus using Meiboom-Gill phases is at least better for preventing the accumulation of pulse length errors than using Carr-Purcel phases, where one expects such errors to have a strong cumulative effect. Using a sequence with Carr-Purcell phases of alternating phase (eg if the magnetization is initially prepared along the y-axis, the phase of the 180° pulses is alternated between the positive and negative x-axis) gives a signal of comparable strength to the Meiboom-Gill case. The phase alternated Carr-Purcell type sequence should compensate pulse length errors much more effectively than the Carr-Purcell type sequence without phase alternation. Therefore it can be said that the phase alternated Carr-Purcell type sequence and the Meiboom-Gill type sequence are at least partially effective at compensating for pulse-length errors in the 6-pulse solid Hahn-echo sequence.

Even though the isotropic line is near zero frequecy in Fig. 9-1, the spins do not

necessarily have zero frequency when the 180° pulse is applied. Offset Hamiltonian errors are inevitably present when the sample is in the "slow-spinning" regime considered here. Composite pulses such as the 90_x-270_y-90_x pulse suggested by Levitt [184] may be more useful than any phase alternation scheme in reducing the combined effects of pulse length errors and offset errors on the performance of the 6-pulse solid Hahn-echo sequence. The substitute for the 180° pulse suggested above has the effect (to first order) of an ideal 180° pulse applied with a phase angle of 45° in the x-y plane relative to the phase of a nominal 180° pulse. For the 6-pulse sequence no effect of this phase shift should be seen. For the 5-pulse sequence, a constant phase shift should be introduced to the entire spectrum. It is known [185] that the use of composite pulses can be beneficial in TOSS sequences.

References

1. J. M. Thomas, K. I. Zamaraev "Perspectives in Catalysis", Blackwell Scientific Publications, London (1992) p2.

2. P. B. Venuto, E. T. Habib Jr. "Fluid Catalytic Cracking With Zeolite Catalysts", Marcel Dekker Inc., New York (1979).

3. J. Scherzer, "Octane-Enhancing Zeolite FCC Catalysts", Marcel Dekker Inc., New York (1990)

4. M. C. Oballa, S. S. Shih "Catalytic Hydroprocessing of Petroleum and Distillates", Marcel Dekker Inc., New York (1993).

5. C. N. Satterfield "Heterogeneous Catalysis in Industrial Practice" 2nd ed., McGraw Hill, New York (1991).

6. E. P. Pluddeman, "Silane Coupling Agents" 2nd ed., Plenumm Press, New York (1991).

7. D. E. Leyden (ed.), "Silanes, Surfaces and Interfaces", Gordon and Breach, New York (1986).

8. K. K. Unger, "Porous Silica: Its Properties and Use as Support in Column Chromatography", Journal of Chromatography Library Volume 16, Elsevier, New York (1979).

9. A. V. Kiselev "Infrared Spectra of Surface Compounds" Wiley, New York (1975).

10. M. L. Hair "Infrared Spectroscopy in Surface Chemistry", Marcel Dekker Inc., New York (1967).

11. L. M. Little "Infrared Spectra of Adsorbed Species", Academic Press, London (1966).

12. A. A. Davydov "Infrared Spectroscopy of Adsorbed Species on the Surface of Transition Metal Oxides", Wiley, New York (1990).

13. J. T. Yates Jr., T. E. Madey "Vibrational Spectroscopy of Molecules on Surfaces", Plenum Press, New York (1987).

14. A. T. Bell, A. Pines (eds.) "NMR Techniques in Catalysis", Marcel Dekker Inc., New York (1994).

15. B. A. Morrow, A. J. McFarlan *J. Phys. Chem.* **96**, 1395 (1992).

16. B. A. Morrow, A. J. McFarlan *Langmuir* **7**, 1695 (1991).

17. B. A. Morrow, I. A. Cody *J. Phys. Chem.* **80**, 1995, (1976).

18. B. A. Morrow, I. A. Cody *J, Phys. Chem.* **80**, 1998, (1976).

19. B. A. Morrow, I. A. Cody, Lydia S. M. Lee *J. Phys. Chem.* **80**, 2761, (1976).

20. L. Marchese, S. Bordiga, S. Coluccia, G. Martra, A. Zecchina *J. Chem. Foc Faraday Trans.* **89**, 3483 (1993).

21. B. C. Lippens, J. J. Steggerda, in "Physical and Chemical Aspects of Adsorbants and Catalysis", B. G. Linsen ed., Academic Press, London (1970). p171.

22. C. Morterra, V. Bolis, G, Magnacca *Langmuir* **10**, 1812 (1994).

23. H. Knözinger, P. Ratnasamy *Catal. Rev.-Sci. Eng.* **17**, 31 (1978).

24. J. Datka, M. Boczar, P. Rymarowicz *J. Catal.* **114**, 368 (1988).

25. G. Busca, V. Lorenzelli, V. S. Escribano, R. Guidetti *J. Catal.* **131**, 167 (1991).

26. A. Zecchina, S. Coluccia, C. Morterra *Appl. Spectrosc. Rev.* **21**, 259 (1985).

27. G. Busca, H. Saussey, O. Saur, J. C. Lavalley, V. Lorenzelli *Appl. Catal.* **14**, 245 (1985).

28. K.-H. Jacob, E. Knözinger, S. Benfer *J. Mater. Chem.* **3**, 651 (1993).

29. E. Knözinger, K.-H. Jacob, S. Singh, P. Hofmann *Surf. Sci.* **290**, 388 (1993).

30. B. A. Morrow, P. Ramamurthy *J. Phys. Chem.* **77**, 3052, (1973).

31. K. Kim *Bull. Korean Chem. Soc.* **11**, 396, (1990).

32. D. C. McKean, G. P. McQuillan, W. F. Murphy, F. Zerbetto *J. Phys. Chem.* **94**, 4820 (1990).

33. D. C. McKean *Chem. Rev.* **7** 399, (1978).

34. D. C. McKean, G. P. McQuillan *J. Mol. Str.* **49**, 275, (1978).

35. T.-C. Sheng, I. G. Gay *J. Catal.* **145**, 10, (1994).

36. V. R. Baumgartner, W. Sawadny, J. Goubeau *Z. anorg. allg. Chem.* **333**, 171, (1964).

37. J. A. Creighton, G. B. Deacon, J. H. S. Green *Aust. J. Chem.* **20**, 583, (1967).

38. L. J. Bellamy "The Infra-red Spectra of Complex Molecules", Chapman and Hall, London (1975) p15.

39. J. E. Drake, J. L. Hencher, B. Rapp *Inorg. Chem.* **16**, 2289, (1977).

40. G. A. Olah "Friedel-Crafts Chemistry", John Wiley & Sons Inc., New York (1973) p250.

41. H. H. Sisler, M. A. Mathur *J. Inorg. Nucl. Chem.* **39**, 1745, (1977).

42. M. Arshad, A. Beg, M. S. Siddiqui *Can. J. Chem.* **43**, 608, (1965).

43. N. N. Greenwood, E. J. F. Ross, A. Storr *J. Chem. Soc.* 1400, (1965).

44. P.-J. Chu, A. de Mallman, J. H. Lunsford *J. Phys. Chem.* **95**. 7362, (1991).

45. P.-J. Chu, J. H. Lunsford, D. J. Zalewski *J. Magn. Reson.* **87**, 68, (1990).

46. C. Morterra, A. Chiorino, G. Ghioti, E. Garrone *J. Chem. Soc. Faraday Trans. 1* **75**, 271, (1979).

47. L. Baltusis, J. S. Frye, G. E. Maciel *J. Am. Chem. Soc.* **109**, 40, (1987).

48. J. A. Ripmeester *J. Am. Chem. Soc.* **105**, 2925, (1983).

49. H. Sang, H. Y. Chu, J. H. Lunsford *Catal. Lett.* **26**, 235, (1994).

50. J. C. Lavalley, M. Benaissa *J. Chem. Soc. Chem Comm.* 908, (1984).

51. P. O. Scokart, S. A. Selim, J. P. Damon, P. G. Rouxhet *J. Colloid Interface Sci.* **70**, 209, (1979).

52. R. A. Schoonheydt, D. Van Wouwe, H. Leeman *Zeolites* **2**, 109, (1982).

53. J. H. Lunsford, W. B. Rothwell, W. Shen *J. Am. Chem. Soc.* **107**, 1540, (1985).

54. R. Minkwitz, G. Medger, H. Preut *Z. anorg. Allg. Chem.* **614**, 102, (1992).

55. J. H. S. Green, H. A. Lauwers *Bull. Soc. Chim. Belges* **79**, 571, (1970).

56. D. J. Zalewski, P.-J. Chu, P. N. Tutunjian, J. H. Lunsford *Langmuir* **5**, 1026, (1989).

57. M. Niwa, N. Katada, Y. Murakami *J. Catal.* **134**, 340, (1992).

58. O. Saur, M. Bensitel, B. Mohammed Saad, J. C. Lavalley, C. P. Tripp, B. A. Morrow *J. Catal.* **99**, 104, (1986).

59. F. Seel, K. D. Velleman *Chem. Ber.* **105**, 406, (1972).

60. D. J. Coster, A. Bendada, F. R. Chen, J. J. Fripiat *J. Catal.* **140**, 497, (1993).

61. J. H. Lunsford, H. Sang, S. M. Campbell, C.-H. Liang, R. G. Anthony *Catal, Lett.* **27**, 305, (1994).

62. C. Morterra, G. Cerrato, E. Emanuel, V. Bolis *J. Catal.* **142**, 349, (1993).

63. M. Waqif, J. Bachelier, O. Saur, J.-C. Lavalley *J. Mol. Catal.* **72**, 127, (1992).

64. J. R. Bleeke, M. K. Hays *Organometallics* **6**, 486, (1987).

65. J. B. Robert, I. WeisenFeld *Mol. Phys.* **44**, 319, (1981).

66. J. H. Lunsford, P. N. Tutunjian, P.-J. Chu, E. B. Yeh, D. J. Zalewski *J. Phys. Chem.* **93**, 2590 (1989).

67. S. Sato, T. Sodesawa, F. Nozaki, H. Shoji *J. Molec. Catal.* **66**, 343 (1991).

68. A. Bendada, E. F. DeRose, J. J. Fripiat *J. Phys. Chem.* **98**, 3838 (1994).

69. P.-J. Chu, R. R. Carvajal, J. H. Lunsford *Chem. Phys. Lett.* **175**, 407 (1990).

70. V. M. Bogatyrev, A. A. Chuiko *Soviet Prog. in Chem.* **50**, 50, (1984).

71. (a) Nakamoto, K, "Infrared and Raman Spectra of Inorganic and Coordination Compounds", 4th Edition, John Wiley & Sons, New York, (1986). (b) S. G. Frankiss, F. A. Miller *Spectrochim. Acta* **21**, 1235, (1965). (c) R. A. Nyquist, *Appl. Spectrosc.*, 272, (1987).

72. H. G. M. Edwards, L. A. Woodward *Spectrochim. Acta* **26A**, 1077, (1970).

73. I. D. Gay *J. Magn. Reson.* **58**, 413, (1984).

74. (a) L. C. Thomas "Interpretation of the Infrared Spectra of Organophosphorus Compounds", Heydon, London, (1974). (b) D. E. C. Corbridge "Topics in Phosphorus Chemistry" **6**, 235, (1969).

75. R. A. Nyquist, C. W. Puehl, *Appl. Spectrosc.* **46**, 1552, (1992).

76. D. E. C. Corbridge, Studies in Inorganic Chemistry, vol. 6, "Phosphorous, an Outline of its Chemistry, Biochemistry and Technology", Elsevier, Amsterdam, (1985).

77. V. M. Bogatyrev, V. V. Brei, A. A. Chuiko *Theor. Expt. Chem.* (Eng. Ed.) **24**, 603, (1988).

78. V. Mark, C. H. Dungan, M. M. Crutchfield, J. R. Van Wazer, "Topics in Phosphorus Chemistry" **5**, 227, (1967).

79. V. N. Fritzowsky, A. Lentz, J. Goubeau *Z. Anorg. Allg. Chem.* **386**, 203, (1971).

80. T. Berenstein, P. Fink, V. M. Mastikhin, A. A. Shubin *J.C.S. Faraday I* **82**, 1879, (1986).

81. Recorded in $CDCl_3$ solution as part of this study; the compounds were prepared by an adaptation of the methods described in reference 83.

82. M. V. Livantsov, A. A. Prishchenko, I. F. Lutsenko *Zhur. Obshchei Khimii* (Eng. Ed.) **55**, 1976, (1985).

83. J. F. Brazier, D. Houalla, R. Wolf *Bull. Soc. Chim. France* 1089 (1970).

84. Ref. 78, page 321.

85. I. L. Mudrakovskii, V. M. Mastikhin, N. S. Kotsarenko, V. P. Shmachkova *Kin. i Kataliz* (Eng. Trans.) **29**, 165, (1988).

86. S. B. Randarevich, V. V. Strelko, V. N. Belyakov, Y. Y. Korovin, A. I. Bortun *Theor. Exptl. Chem.* (Eng. Ed.) **24**, 607, (1988).

87. G. E. Berendsen, L. de Galan *J. Liq. Chromatog.* **1**, 403, (1978).

88. J. Nawrocki, B. J. Buszewski *J. Chromatogr. Rev.* **449**, 1, (1988).

89. J. J. Pesek "Chemically Modified Oxide Surfaces", D. E. Layden and W. T. Collins (eds), Gordon and Breach Sc. Pub. New York, (1990), page 93.

90. J. E. Sandoval, J. J. Pesek *Anal. Chem.* **61**, 2067, (1989).

91. M. P. McDaniel *J. Phys. Chem.* **85**, 532, (1981).

92. H. Knözinger, H. P. Boehm "Catalysis-Science and Technol." (J. R. Anderson, M. Boudart eds.) **4**, 39, (1983). and references therein.

93. C. P. Tripp, M. L. Hair *Langmuir* **7**, 923, (1991).

94. P. Fink, I. Plotzki *Wiss. Z. Friedrich-Schiller-Univ. Jena, Math.-Naturwiss.* **29**, 809, (1980).

95. M. L. Hair, W. J. Hertl *J. Phys. Chem.* **77**, 2070, (1973).

96. A. Lee Smith *Spectrochim. Acta* **16**, 87, (1960); *ibid* **19**, 849, (1963).

97. B. C. Bunker, D. M. Haaland, K. J. Ward, T. A. Michalske, W. L. Smith, J.S. Binkley, C. F. Melius, C. A. Balfe *Surf. Sci.* **210**, 406, (1989).

98. M. P. McDaniel *J. Phys. Chem.* **85**, 537, (1981).

99. V. W. Day, W. G. Klemperer, V. V. Mainz, D. M. Millar *J. Am. Chem. Soc.* **107**, 8262, (1985).

100. M. Bärtsch, G. Calzaferri, C. Marcolli *Res. Chem. Intermediates*, in press.

101. B. A. Morrow, I. A. Cody, L. S. M. Lee *J. Phys. Chem.* **79**, 2405, (1975).

102. M. J. D. Low *J. Catal.* **103**, 496, (1987).

103. M. Bartsch, P. Bornhauser, H. Burgy, G. Calzaferri *Spectrochim. Acta* **47A**, 1627, (1991).

104. A. P Legrand, H. Hommel. A. Tuel, A. Vidal, H. Balard, E. Papirer, P. Levitz, M. Czernichowski, R. Erre, H. Van Damme, J. P. Gallas, J. F. Hemidy, J. C. Lavalley, O. Barres, A. Burneau, Y. Grillet *Adv. Colloid Interf. Sci.* **33**, 91, (1990).

105. T. A. Michalske, B. C. Bunker *J. Appl. Phys.* **56**, 2686, (1984).

106. C. J. Brinker, R. J. Kirkpatrick, D. R. Tallant, B. C. Bunker, B. Montez *J. Non-Cryst. Solids* **99**, 418, (1988).

107. A. Lee Smith, D. R. Anderson *App. Spectrosc.* **38**, 822, (1984).

108. H. Staendeke, H.-J. Kleiner Angew Chem. Internat. Ed. **11**, 877, (1973).

109. J. C. Tebby " Methods in Stereochemical Analysis 8: Phosphorus-31 NMR Spectroscopy in Stereochemical Analysis: Organic Compounds and Metal Complexes", (J. G. Verkade, L. D. Quin eds.) VCH Publishers, Deerfield Beach, U.S.A., (1987).

110. D. Fiat, M. Halman, L. Kugel, J. Reuben *J. Chem. Soc.* 3837, (1962).

111. D. Lin-Vien, N. B. Coltup, W. G. Fateley, J. G. Grasselli "The Handbook of Infrared and Raman Characteristic Frequencies of Organic Molecules", Academic Press Inc. New York, (1991).

112. B.A Morrow, A. J. McFarlan *J. Non-Cryst. Solids* **120**, 61, (1990).

113. Y. V. Kolodyazhnyi, I. A. Lapin, A. P. Sadimenko, O. A. Osipov *J. Gen. Chem. USSR* (Eng. Transl.) *Zh. Obshch. Khim.* **51**, 655 (1981).

114. B. J. Van Der Veken, R. L. Odeurs, M. A. Herman, J. R. Durig *Spectrochim. Acta* **40A**, 563, (1984).

115. F. Seel, K.-D. Vellemann *Chem. Ber.* **104**, 2972, (1971).

116. J. A. Miller in "Organophosphorus Chemistry, Volume 4, Specialist Perodical Reports", (S. Trippett ed.), Chemical Society, London, (1973). p54.

117. A. A. Tsyganenko, D. V. Pozdnyakov, V. N. Filimonov, *J. Mol. Structr.* **29**, 299, (1975).

118. E. H. Teunissen, R. A. van Santen, A. P. J. Jansen, F. B. van Duijneveldt *J. Phys. Chem.* **97**, 203 (1993).

119. L. M. Parker, D. M. Bibby, G. R. Burns *J. Chem. Soc. Faraday Trans.* **87**, 3319, (1991).

120. C. Morterra, G. Cerrato *Langmuir* **6**, 1810, (1990).

121. (a) J. G. Ekerdt, K. J. Klabunde, J. R. Shapley, J. M. White, J. T. Yates Jr. *J. Phys. Chem.* **92**, 6182, (1988). (b) R. D. Ramsier, P. N. Henriksen, A. N. Gent *Surf. Sci.* **203**, 72 ,(1988). (c) M. K. Templeton, W.H. Weinberg J. Am. Chem. Soc. **107**, 774, (1985).

122. (a) M. A. Henderson, T. Jin, J. M. White *J. Phys. Chem.* **90**, 4607, (1988). (b) M. K. Templeton, W. H. Weinberg *J. Am. Chem. Soc.* **107**, 97, (1985). (c) K. Y. Lee, M. Houalla, D. M. Hercules, W. K. Hall *J. Catal.* **145**, 223, (1994). (d) T. Z. Tzou, S. W. Weller *J. Catal.* **146**, 370, (1994).

123. (a) L.-F. Rao, J. T. Yates Jr. *J. Phys. Chem.* **97**, 5341, (1993). (b) X. Zhang, A. Linseigler, U. Heiz, J. T. Yates Jr. *J. Phys. Chem.* **97**, 5074, (1993). (c) D. K. Paul, L.-F. Rao, J. T. Yates Jr. *J. Phys. Chem.* **96**, 3446, (1992).

124. (a) E. C. Decanio, J. C. Edwards, T. R. Scalzo, D. A. Storm, J. W. Bruno *J. Catal.* **132**, 498, (1991). (b) O. H. Han, C. Y. Lin, N. Sustache, M. Mcmillan, J. D. Carruthers, K. W. Zilm, G. L. Haller *Appl. Catal. A* **98**, 195, (1993).

125. (a) S. Shinoda, K. Nakamura, Y. Saito, *Chem. Lett.* 1449, (1983). (b) B. N. Choudry, K. R. Kumar, M. L. Kantam *J. Catal.* **130**, 41, (1991). (c) J. Blumel *Inorg. Chem.* **33**, 5050, (1994).

126. I. J. Colquhoun, W. McFarlane *J. Label. Comp. Radiopharmaceuticals* **13**, 535, (1977).

127. H. E. Ulmer, L. C. D. Groenweghe, L. Maier *J. Inorg. Nucl. Chem.* **20**, 82, (1961).

128. L. T. Zhuravlev *Langmuir* **3**, 316, (1987).

129. I. D. Gay, A. J. McFarlan, B. A. Morrow *J. Phys. Chem.* **95**, 1360, (1991).

130. K. Weissermel, H.-J. Kleiner, M. Finke, M.; U.-H. Felcht *Angew. Chem. Int. Ed. Engl.* **20**, 223, (1981).

131. Synthesized by us as a by-product of the methanolysis of $PMeCl_2$, natural abundance ^{13}C NMR.

132. A. W. Frank in "Organic Phosphorus Compounds", (G. M. Kosolapoff, L. Maier eds.) Vol. 4, Wiley-Interscience, New York, (1972).

133. G. Busca, G. Ramis, V. Lorenzelli, P. R. Rossi, A. L. Genestra, P. Patrono *Langmuir* **5**, 911, (1989).

134. K. I. Hadjiivanov, D. G. Klissurski, A. D. Davydov *J. Catal.* **116**, 498, (1989).

135. A. Munnour, C. Ecolivet, D. Comet, J. F. Hemidy, J.-C. Lavalley *Mater. Chem. Phys.* **19**, 301, (1988).

136. J. B. Moffat *Catal. Rev.-Sci. Eng.* **8**, 199, (1978).

137. V. S. Smentkowski, P Hagans, J. T. Yates Jr. *J. Phys. Chem.* **92**, 6351, (1988).

138. B. Aurian-Blajeni, M. M. Boucher *Langmuir* **5**, 170, (1989).

139. S. T. Lin, K. J. Klabunde *Langmuir* **1**, 600, (1985).

140. M. P. Nadler, R. A. Nissan, R. A. Hollins *Appl. Spectrosc.* **42**, 634, (1988).

141. F. Abbatista, A. Delmastro, G. Gozzelino, D. Mazza, M. Vallino, G. Busca, V. Loernzelli *J. Chem. Soc. Faraday Trans.* **86**, 3653, (1990).

142. J. M. Lewis, R. A. Kydd *J. Catal.* **132**, 465, (1991).

143. E. M. Flanigen, R. L. Patton, S. T. Wilson "Innovations in Zeolite Materials Science", P. J. Grobet *et. al.* eds., Stud. Surf. Sci. Catal., Vol. 37, Elsevier, Amsterdam (1988), p. 13.

144. A. E. T. Kuiper, J. J. G. M. van Bokhoven, J. Medema *J. Catal.* **43**, 154, (1976).

145. M. Higo, S. Kamata *J. Phys. Chem.* **94**, 8709, (1990).

146. M. Higo, Y. Owaki, S. Kamata *Chem. Lett.* 2009, (1987).

147. R. M. Moravie, F. Froment, J. Corset *Spectrochim. Acta.* **45A**, 1015, (1989).

148. S. Blonski, S. H. Garofalini *Surf. Sci.* **295**, 263, (1993).

149. C. M. Mikulski, N. M. Karayannis, L. L. Pytlewski *J. Inorg. Nucl. Chem.* **8**, 971, (1974).

150. N. M. Karayannis, C. M. Mikulski, L. L. Pytlewski *Inorg. Chem. Acta Rev.* **5**, 69, (1971).

151. G. Busca, P. F. Rossi, V. Lorenzelli, M. Benaissa, J. Travert, J.-C. Lavalley *J. Phys. Chem.* **89**, 5433, (1989).

152. M. Bensitel, V. Moravek, J. Lamotte, O. Saur, J.-C. Lavalley *Spectrochim Acta* **43A**, 1487, (1987)

153. T. F. Beebe, J. E. Crowell, J. T. Yates Jr. *J. Chem. Phys.* **92**, 5119, (1990).

154. M. Bensitel, O. Saur, J.-C. Lavalley *Mater. Chem. and Phys.* **28**, 309, (1991).

155. Y.-X. Li, J. R. Schlup, K. J. Klabunde *Langmuir* **7**, 1394, (1991).

156. B. Dupuy, C. Garrigou-Lagrange *J. Chim. Phys.* **65**, 632, (1968).

157. B.-Z. Wan, S. Cheng, R. G. Anthony, A. Clearfield *J. Chem. Soc. Faraday Trans.* **87**, 1419, (1991).

158. J. Herzfeld, A. E. Berger *J. Chem. Phys.* **73**, 6021, (1980).

159. T. M. Duncan, D. C. Douglass *Chem. Phys.* **87**, 339, (1984).

160. W.F. Bleam, P. E. Pfeffer, J. S. Frye *Phys. and Chem. of Min*er. **16**, 455, (1989).

161. K. Segawa, A. Sugiyama, Y. Kurusu "Chemistry of Micoporous Crystals", B. Delmon J. T. Yates eds., Stud. Surf. Sci. Catal., Vol. 60, Elsevier, Tokyo (1991) p73.

162. G. O. Doak, L. D. Freedman *Chem. Rev.* **61**, 31, (1961).

163. R. A. Nyquist *Spectrochim. Acta.* **25A**, 47, (1969).

164. B. Imelik, P. Pascal *Comptes Rendus* **233**, 1284, (1951).

165. S. A. Katcyuba, N. I. Monakhova, L. K. Ashrafullina, R. R. Shagidullin *J. Mol. Str.* **269**, 1, (1992).

166. N. I. Monakhova, S. A. Katsyuba, L. K. Ashrafullina, R. R. Shagidullin *Russ. Appl. Spectrosc.* (English Translation) **51**, 1276, (1990).

167. J. R. Van Wazer, C. S. Ewig *J. Am. Chem. Soc.* **108**, 4354, (1986).

168. R. Engel "Synthesis of Carbon-Phosphorus Bonds:", CRC Press, Boca Raton (1988) p.7.

169. L. W. Dasch *J. Am. Chem. Soc.* **80**, 5301, (1958).

170. T. D. Smith *J. Inorg. Nuc. Chem.* **15**, 95, (1960).

171. J. G. Chen, P. Basu, T. H. Ballinger, J. T. Yates *Langmuir* **5**, 352, (1989).

172. W. T. Dixon *J. Chem. Phys.* **77**, 1800, (1982)

173. E. T. Olejniczak, S. Vega, R. G. Griffin *J. Chem. Phys.* **81**, 4804, (1984)

174. D. P. Raleigh, E. T. Olejniczak, S. Vega, R. G. Griffin *J. Magn. Reson.* **72**, 238, (1987).

175. N. J. Clayden Annual Reports on NMR Spectroscopy, **24**, 1, (1992).

176. D. P. Raleigh, E. T. Olejniczac, R. G. Griffin *J. Chem. Phys.* **89**, 1333, (1988).

177. E. R. Andrew Progress in NMR Spectroscopy, **8**, 1, (1978).

178. C. P Slichter " Principles of Magnetic Resonance", 3rd Edn. Springer-Verlag, (1990).

179. M. M. Maricq, J. S. Waugh *J. Chem. Phys.* **70**, 3300, (1979).

180. N C. Nielsen, H. Bildsoe, H. J. Jakobsen *J. Magn. Reson.* **80**, 149, (1988).

181. S. Zhiyan, O N. Antzutkin, X. Feng, M H. Levitt *Solid State Nucl. Magn. Reson.* **2**, 143, (1993).

182. A. C. Kolbert, D. P. Raleigh, R. G. Griffin *J. Magn. Reson.* 82, 483, (1989).

183. D. P. Raleigh, A. C. Kolbert, T. G. Oas, M. H. Levitt, R. G. Griffin *J. Chem. Soc. Faraday Trans. 1* **84**, 3691, (1988).

184. M. H. Levitt, R. Freeman *J. Magn. Reson.* **43**, 65, (1981).

185. A. Hagemeyer, D. Van Der Putten, H. W. Spiess *J. Magn. Reson.* **92**, 628, (1991).

186. O. N. Antzutkin, Z. Song, X. Feng, M. H. Levitt *J. Chem. Phys.* **100**, 130, (1994).

Conclusions

PMe_3 adsorption has been studied as a means to characterize catalysts. Infrared spectra structure correlations have been developed that give useful qualitative information on the nature of surface acid sites. It has been shown that ^{31}P MAS NMR studies complement the infrared studies, since the presence of oxidized species is often more readily established by NMR than by IR, and with appropriate care useful quantitative information can be obtained. This work can be extended to many other systems, and its correlation with the catalytic behaviour of different materials remains to be explored.

The reactions of PMe_nCl_{3-n} (n=0 to 3) with silica have been studied. With the exception of PCl_3 which leads to the formation of some $\equiv$Si-O-PCl_2, all of these compounds give chemisorbed species containing phosphoryl groups. The formation of these functional groups requires the extraction of oxygen from the silica surface, and the breaking of very strong Si-O bonds. Phosphoryl bonds are very strong, and their formation could provide the thermodynamic driving force for the observed reactions. Stoichiometrically, it is necessary that the Si-Cl bonds be formed in place of the broken Si-O bonds. The study of the reactions of a number of chlorinating agents with silica was necessary to show that silica is indeed chlorinated by reactions with the methylchlorophosphines. The chemistry of the interactions all of the methylchlorophosphines with silica was much more complex that might have been assumed a priori, and many interesting reaction pathways of interest in surface chemistry have been deduced.

The reactions of $P(OMe)_3$ and related compounds with Al_2O_3 have been studied. These reactions are relevant as models for the catalytic destruction of organophosphorus poisons, as well as the environmental degradation of phosphorus based pesticides and fertilizers. Al_2O_3 is a much more catalytically active material than silica. Although the formation of pentavalent phosphorus species dominated the chemistry of $P(OMe)_3$ on Al_2O_3, as it did during the analogous reactions with silica, Al_2O_3 caused other reactions to become energetically feasible. For example, the Michaelis-Becker reaction was observed to occur at room temperature on activated Al_2O_3 samples. Another difference between silica and Al_2O_3 is that Al_2O_3 reacts avidly with phosphonates to give very stable surface metal phosphonate phases. This makes Al_2O_3 very useful for adsorbing organophosphorus compounds, but limits the use of Al_2O_3 based materials for the ***catalytic*** destruction these compounds.

Exact expressions for the pulse timings in TOSS sequences have been developed. It was shown that all useful 4-pulse sequences are already known in the literature. PASS and Hahn-echo sequences were analyzed similarly. Two new solid state Hahn-echo sequences were demonstrated.

List of Publications

1. An Infrared and Solid State ^{31}P NMR Study of the Adsorption of $P(CH_3)Cl_2$ and $P(CH_3)Cl_2/PCl_3$ Mixtures on Silica
   S. J. Lang, I. D. Gay, B. A. Morrow
   Langmuir in press

2. An Infrared and ^{31}P Magic Angle Spinning Nuclear Magnetic Resonance Study of the Adsorption of PCl_3 and $OPCl_3$ on Silica
   B. A. Morrow, S. J. Lang
   Langmuir **10**, 756, (1994)

3. Structure of SiO_2 on Al_2O_3 Monolayer Catalysts: Investigation by Infrared Spectroscopy and ^{29}Si MAS NMR
   T.-C. Sheng, S. Lang, B. A. Morrow, I. D. Gay
   J. Catal. **148**, 341, (1994).

4. Infrared Spectra of Chlorinated Silica
   S. J. Lang, B. A. Morrow
   J. Phys. Chem. **98**, 13314, (1994).

5. Infrared and Solid-State NMR Studies of the Adsorption of PMe_2Cl on Silica
   B. A. Morrow, S. J. Lang
   J. Phys. Chem. **98**, 13319, (1994).

6. Analytical Expressions for TOSS Sequences
   S. J. Lang
   J. Magn. Reson. **104A**, 345, (1993)